MDC G4722

INVESTIGATION OF HIGH-PERFORMANCE INSULATION APPLICATION PROBLEMS

Final Report

AUGUST 1973

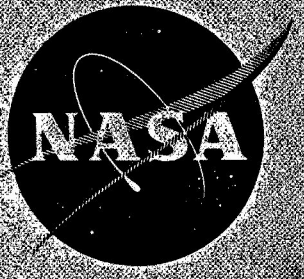

Prepared under Contract No. NAS8-21400
Advance Propulsion Department
McDonnell Douglas Astronautics Company – West
Huntington Beach, California
for
NATIONAL AERONAUTICS AND SPACE ADMINISTRATION

INVESTIGATION OF HIGH-PERFORMANCE INSULATION APPLICATION PROBLEMS

Final Report
AUGUST 1973

G. O. FREDRICKSON

Prepared under Contract No. NAS8-21400
Advance Propulsion Department
McDonnell Douglas Astronautics Company – West
Huntington Beach, California
for
NATIONAL AERONAUTICS AND SPACE ADMINISTRATION

FOREWORD

The McDonnell Douglas Astronautics Company—West (MDAC-W) is submitting this final report in partial fulfillment of the requirements of Contract NAS8-21400, Investigation of High Performance Insulation Application Problems. Mr. G. O. Fredrickson was the MDAC Project Manager and Mr. E. H. Hyde was the NASA-Marshall Space Flight Center Project Manager.

ACKNOWLEDGMENTS

Although too numerous to list individually, the work reported herein represents the contributions of a large number of MDAC personnel. Major contributions were made by J. N. Castle, M. C. Coes, J. R. Cook, J. Hutmacher, R. D. Saunders, J. M. Solontai, R. Spier, G. J. Tiezzi, and R. Yeaman.

CONTENTS

FIGURES

TABLES

Section 1

SUMMARY

The goal of this program was to design, demonstrate fabricability, and experimentally determine the performance of a practical, flightworthy, multilayer insulation (MLI) system for a Modular Nuclear Vehicle (MNV) LH_2 propellant tank.

As a result of the program effort, these goals were achieved and such an MLI system is now available. It may be applied to the MNV or any other space vehicle requiring MLI for thermal control. To date, the design concept has been adapted for an MLI installation that covered and was successfully flown on the Skylab forward dome.

1.1 SUMMARY OF MLI SYSTEM CHARACTERISTICS

Tests of the insulation system, developed in the program, applied in typical vehicle full-thickness MLI panels on a 105-in.-diameter LH_2 tank, Figure 1-1, indicated that the applied thermal performance represents a state-of-the-art advancement. This is illustrated by Figure 1-2, where test results are superimposed upon a NASA (TMX-64561) technology summary curve. The Test 1 data point should be compared to the other systems shown because a common test procedure (MLI evacuation prior to tank loading) was used. Test 2, performance during a simulated mission, demonstrated system structural integrity during launch decompression, as well as thermal performance from ground hold to orbit equilibrium. Structural integrity in a launch dynamic environment was demonstrated with separate tests of representative insulation panel segments.

The insulation composite was applied to the tank utilizing a modular installation concept developed in the study. In this concept, applicable to any MLI installation, the MLI system is built up from a number of similar, standardized, prefabricated insulation panel assemblies. The basic panel design, illustrated in Figure 1-3, stresses structural integrity and practical fabricability.

Figure 1-1. Installed Insulation System

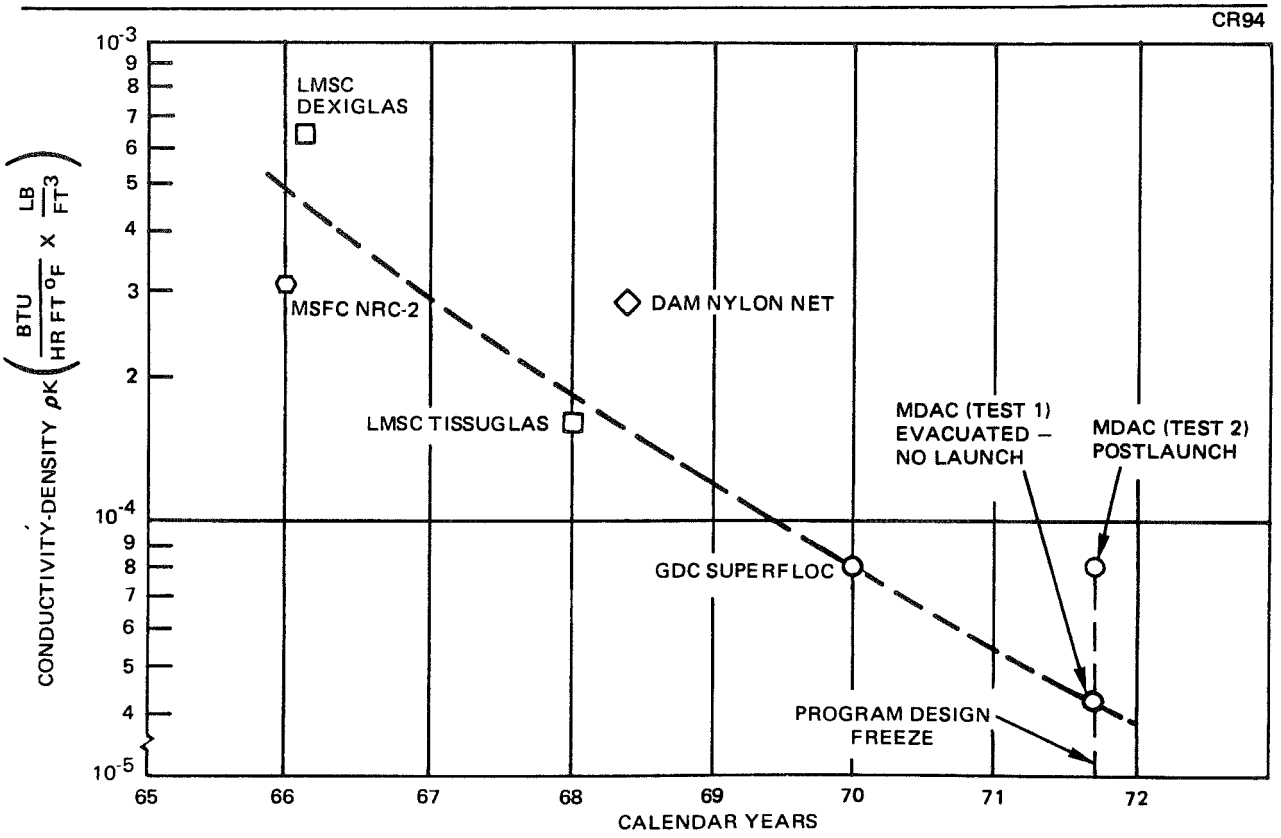

Figure 1-2. Large-Tank MLI System Performance Evolution

As shown in Figure 1-3, the insulation composite (reflectors and separators) is assembled between reinforced face sheets, which provide handling protection and built-in load-carrying members. Assembly is accomplished with nylon fasteners that penetrate through the panel. Two layers of panels, the outer offset from the inner, were used in the test system. Panels are attached to the structure at their upper end with grommets, which fit over studs mounted on the tank. All panel joints are butt type and fastened together with lacing and Velcro tabs on their exterior and interior, respectively. It should be noted that this design concept is insensitive to the choice of insulation composite materials, yielding complete flexibility for future composite development.

Components of the insulation system selected in the study and applied to the 105-in. tank are listed in Table 1-1. Vendor ordering data for the basic composite, perforated 15-gage double-aluminized Mylar (DAM) reflectors and Type B4A Dacron net separators, as well as for the other panel

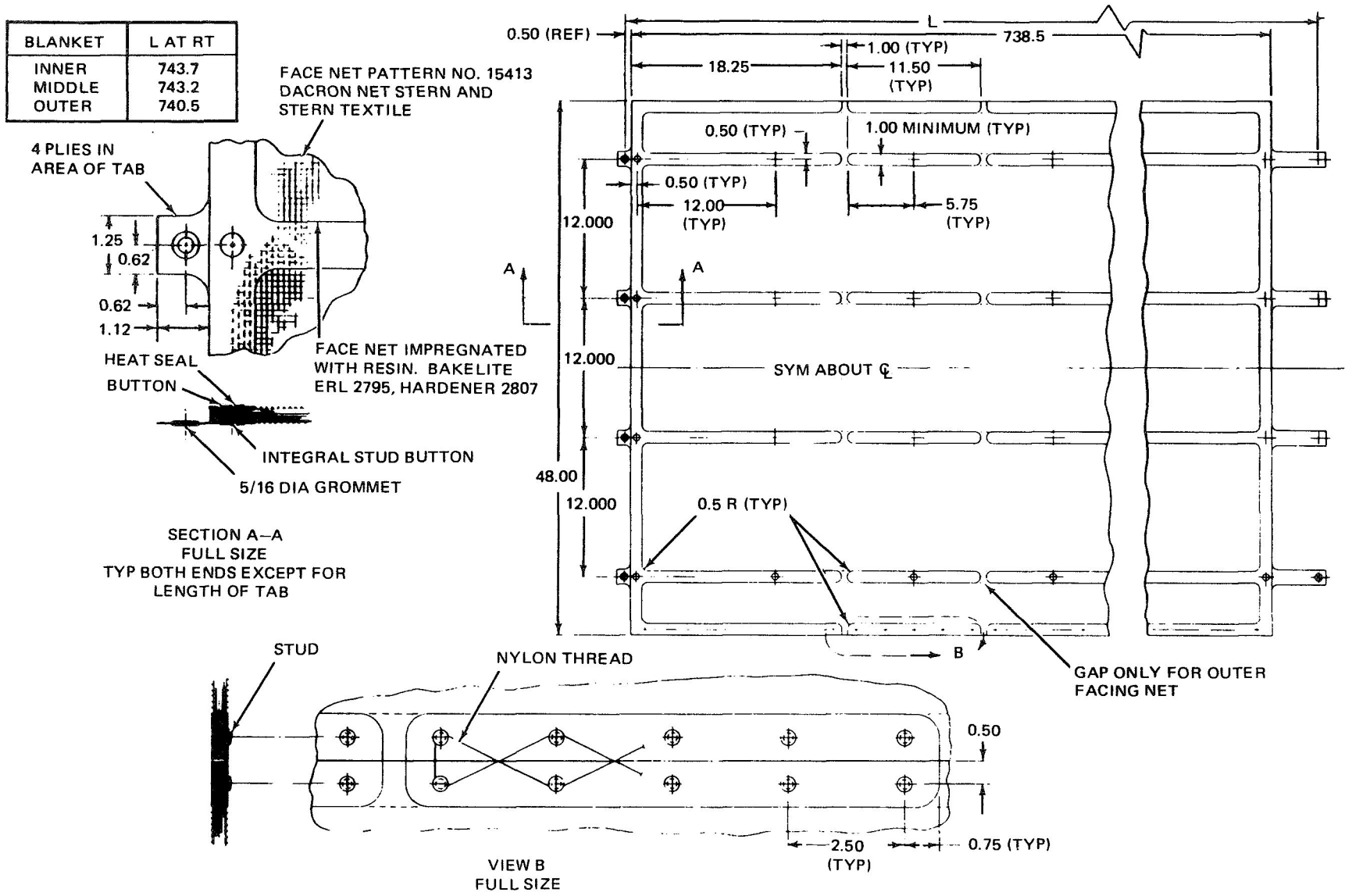

Figure 1-3. Prefabrication Panel Configuration

Table 1-1

MLI COMPONENT MATERIALS

Item	Vendor	Application	Weight
1. Mylar Double-Aluminized, 15-gage	National Metallizing Division Standard Packaging Co. Cranbury, N. J. 08512	MLI composite reflector	.0012 lbs/ft^2 per sheet
2. Mylar Perforations; Pattern 9810, 2.38 percent open area.	Perforated Specialties Co., Inc. 351 West 35th St. New York, N. Y.	Reflector perforations	
3. Net, Polyester (Dacron), Style B4A	Apex Mills, 49 West 37th St., New York, N. Y.	MLI composite separator	.0013 lbs/ft^2 per sheet
4. Net, Dacron, Style 15320 Scoured and Heat-Set Finish	Stern and Stern Textiles Hornell, N. Y.	Face sheet substrate	.81 oz/yd^2
5. Tape, Heat-Sealable, Roll, Type GT400	G. T. Schjeldahl Co., Northfield, Minn.	Face sheet reinforcement	0.055 lbs/ft^2
6. Fasteners, Swifttach, Double T	Dennison Manufacturing Co. Framinghorn, Mass. 01701	Panel assembly	
7. Cord, Tefglas, Type H-18	Holland Thread Co. Stroudsburg, Pa.	Joint closure lacing	
8. Tape, Pressure Sensitive, Polyester Film, Type 850	Minnesota Mining and Manufacturing Co.	Reflector contour dart closure	

components is presented in Appendix A. The "as installed" basic composite density was determined to be about 100 layers per in. or 3.0 lb per cubic foot.

Table 1-2 shows the insulation system's applied, evacuated thermal performance characteristics derived from the 105-in. tank test program (see Section 10). The 50 percent higher conductivity measured in Test 2 appears to be due to gas within the MLI layers. In Test 1, the MLI was extensively evacuated prior to tank LH_2 loading, whereas in Test 2 the tank was loaded with a helium purge gas within the MLI layers prior to a simulated rapid ascent evacuation. Table 1-2 also lists the prelaunch heating rate with helium within the MLI: 275 Btu/hr per square foot of tank wetted area. A significant evacuated thermal performance improvement is possible and should be readily achievable with additional development in the following areas: joint design, reduction of reflector perforations, MLI conditioning prior to tank loading to eliminate adsorbed water vapor, and face sheet weight reductions.

1.2 MLI SYSTEM DEVELOPMENT PROGRAM

Definition and development of the above MLI system was accomplished in a sequential three-phase program:

I. Flightworthy MLI system design for a Modular Nuclear Vehicle
II. Design and fabrication of a large-tank MLI system test article
III. Large-tank MLI system testing

Phase I included all studies to define and develop a flight-type insulation concept: design, manufacturing methods, component development, materials characterization and selection, and thermal and structural testing. The Phase I MNV MLI system design was adapted and applied to the existing NASA 105-in.-tank calorimeter in Phase II. A test program to simulate the thermal performance of the vehicle MLI with this tank was also defined. Phase III comprised the coordination and evaluation of the actual testing of the 105-in.-tank test article at the NASA-MSFC facility.

The program was started as a continuation of Contract NAS 8-20758, "Investigations Regarding Development of a High-Performance Insulation

Table 1-2

APPLIED MLI CHARACTERISTICS

THERMAL PERFORMANCE

	Test 1	Test 2
• Orbital Simulation		
Average Heat Transfer ($Btu/hr\text{-}ft^2$)	0.13	0.195
Effective Conductivity ($Btu/hr\text{-}ft\text{-}°R$) (thickness = 0.69 inches)	1.51×10^{-5}	2.3×10^{-5}
Conductivity-Density ($Btu\text{-}16/hr\text{-}ft^4\text{-}°R$) (density = 3.0 lb/ft^3)	4.6×10^{-5}	7.0×10^{-5}
• Ground Hold		
Average Heat Transfer ($Btu/hr\text{-}ft^2$)	-	275

SYSTEM WEIGHT

Item	Weight (lb/ft^2)
Reflector (70 layers, 15-gage double-aluminized Mylar)	0.084
Separator (68 layers, B4A Dacron Net)	0.088
Fasteners	Insignificant
Joint Closures	Insignificant
Face Sheets (4; two per panel)	0.072
Total Excluding Face Sheets (Density 3.0 lb/ft^3 @ 0.69-in. thickness)	0.172
Total Including Current Face Sheets (Density 4.2 lb/ft^3)	0.244

System." The insulation concepts, candidate materials, and recommended insulation composite resulting from that study formed the baseline for the continuing development.

This report presents a summary of the program results. Additional detail may be obtained from the seven quarterly and special reports prepared during the study (References 1 through 7). Whenever possible, the program drew upon the results of the on-going MDAC MLI Independent Research and Development (IRAD) program. Results of this work are included herein for completeness. Also, two detailed IRAD reports (References 8 and 9) covering thermal testing and purge systems design were forwarded to NASA during the course of the program. The baseline system is described in detail in Reference 10.

1.3 FLIGHTWORTHY INSULATION DESIGN STUDIES - PHASE I

1.3.1 Vehicle Installation Design Drawings

The problem of installing the individual MLI layers on a vehicle structure was solved with the definition of a modular assembly or packaging concept. In this concept, applicable to any MLI installation, the MLI system is built up from a number of these similar prefabricated insulation packages, Figure 1-3. Section 2 of the report describes the construction details.

Also included in Section 2 is a complete set of drawings for applying the insulation concept to a 250,000-lb LH_2 tank MNV. The drawings were prepared for and show a system made up of three layers of panels. However, two layers are recommended to reduce complexity and cost. Also shown on the drawings are a purge system built into the tank supports, a purge bag enclosure, and piping, support, and electrical penetration insulation. Thermal and structural design considerations and test requirements are also discussed.

1.3.2 Composite Minimum Practical Density

To achieve MLI panel thermal performance predictability, it was necessary to solve the problem of predicting the minimum practical layup density (MPD) of any given reflector and separator composite. This was one of the most significant MLI technology problem areas left unresolved by past studies. Details of the work are presented in Section 3.

Nine thickness measurements were made on each of five 2- by 4-ft stacks of the 12 candidate MLI composite materials considered in the study,

Table 1-3. Because thickness varies with the number of sheets in a panel, the measurements were repeated for each of three different numbers of sheets for each composite system. Typical results are shown in Figure 1-4.

Table 1-3
CANDIDATE MLI COMPOSITE MATERIALS

1. DAM* with nylon net spacer (baseline).
2. DAM withTissuglas spacer.
3. DAM with Dexiglas spacer.
4. DAM with foam spacer.
5. Superfloc.
6. Embossed double-aluminized Mylar (DAME) with Tissuglas spacer.
7. Embossed single-aluminized Mylar (SAME).
8. NRC-2 (25 gage).
9. NRC-2 (15 gage).
10. DAM with Dacron net, type B2A with spacer.
11. Crinkled double-aluminized Mylar (CDAM) with Tissuglas spacer.
12. CDAM with nylon net spacer.

*15-gage double-aluminized Mylar

It was found that contrary to generally accepted belief, an MLI composite does not possess any one minimum practical density value. The measured density of any group of individual material stacks is a statistical distribution. Therefore, to achieve a given minimum performance value, a corresponding design density must be selected from the distribution. Two methods for determining this design density are also defined in Section 3.

1.3.3 Thermal Performance Repeatability

If an insulation system is to be practical, any two fabricators building the system must obtain a similar or identical result. A fabrication method with required tooling to achieve this goal of repeatable and predictable thermal performance was defined and demonstrated. Details are presented in Section 3.

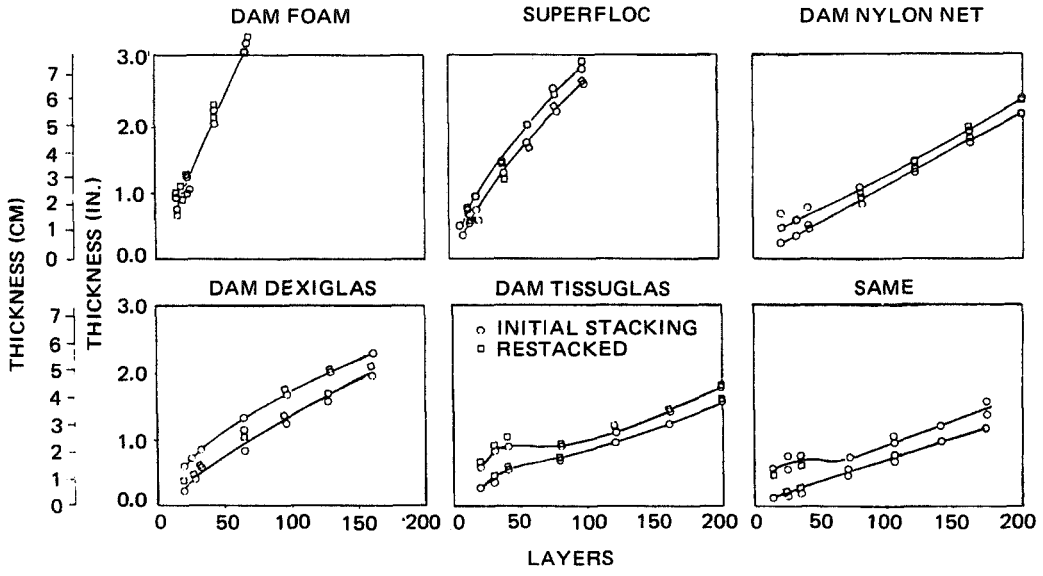

Figure 1-4. MLI Layer Density Characteristics

The method is based upon the concept of a design density which in turn yields a minimum expected repeatable thermal performance. Composite material stacks that are found to possess a greater density than the design value (poorer thermally) are discarded or randomly restacked with other material. Stacks with less density than the design value are accepted "as is" since they will yield a performance better than the design minimum.

1.3.4 Fabricability of MNV Insulation Design

The fabricability of the MNV MLI design was demonstrated through the actual construction of a full-scale dome panel, Figure 1-5, and one sidewall panel segment. Construction methods are detailed in Section 3 along with a summary of the complete manufacturing plan for the MNV insulation system. A unique, highly accurate, production-type panel thickness measurement gage, developed during the study, is also described. Some possible areas for automation of assembly operations are listed.

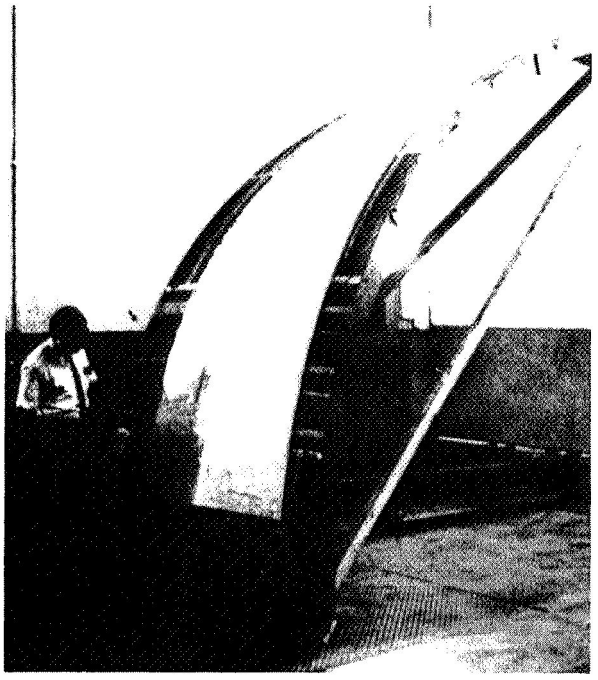

Figure 1-5. Assembled Dome Insulation Panel

1.3.5 Panel Component Development

A number of the details of panel component hardware items have been defined through test and actual panel fabrications. Results are presented in Section 4.

Of particular interest are the two types of panel outer coverings (face sheets) that were developed; epoxy-impregnated net and heat-set Mylar tape load-carrying members. Fabrication methods for both are listed. Also, three types of assembly fasteners were constructed, tested, and used: mechanical locking head, heat-set head, and commercially purchased "Swifttach" (Appendix A). Dimensions and strength test data are also included in Section 4.

Several methods for closing the panel butt joints which were tried on mockup panels are shown along with the details of the selected technique, lacing, and Velcro tabs. An important conclusion reached in the component studies was

that MLI panels should be constructed in simple geometric shapes, such as gores, cylinders, and cones, thereby reducing complexity, cost, and performance uncertainties.

1.3.6 Composite Material Properties

Results of a rather extensive effort to characterize candidate composite (MLI reflector and separator) materials are summarized in Section 5. A 15-gage (0.15 mil) double-aluminized Mylar was selected as the reflector. The nylon net separators recommended in the baseline design were found to fail to evacuate properly due to a volatile sizing (stiffening) agent. This is shown in Figure 1-6, which presents the thermal gradients within nylon net, Tissuglas, and Superfloc in MLI specimens during test on a LH_2 calorimeter. Note the abnormal high-conductivity-type gradient within the nylon net specimen. Thermal and fabricability ranking studies showed that Superfloc, a single-component composite, was highly attractive.

An alternate net material was identified to replace the above nylon material. Dacron nets (Appendix A) stiffened with a heat-set process (no volatile sizing) were defined, purchased, and evaluated. A new test method, based upon the electrical resistance analogy to the reflector-to-separator contact conductance was formulated and used as a method of rapid screening of the nets. Details of the method are presented in References 3 and 4. The resistance test data such as those shown in Figure 1-7 indicated that a Type B2A should be thermally equivalent to the baseline nylon net, and that a Type B4A showed promise of being superior to the Superfloc.

Section 6 also presents results of some pertinent material property tests: reflector emissivity, Tissuglas oxidation, and hot purge compatibility. Of particular interest are the reflector emissivities, which ranged from 0.028 to 0.033 and from 0.034 to 0.037 for 15-gage DAM and perforated DAM, respectively.

1.3.7 Component Thermal Performance Tests

Thermal performance values for full-thickness MLI panels and panel components (joints, fasteners, perforations) are needed for performance estimates of the completed MLI system. Tests that yielded these data were performed and are described in Section 6 along with the resulting design data.

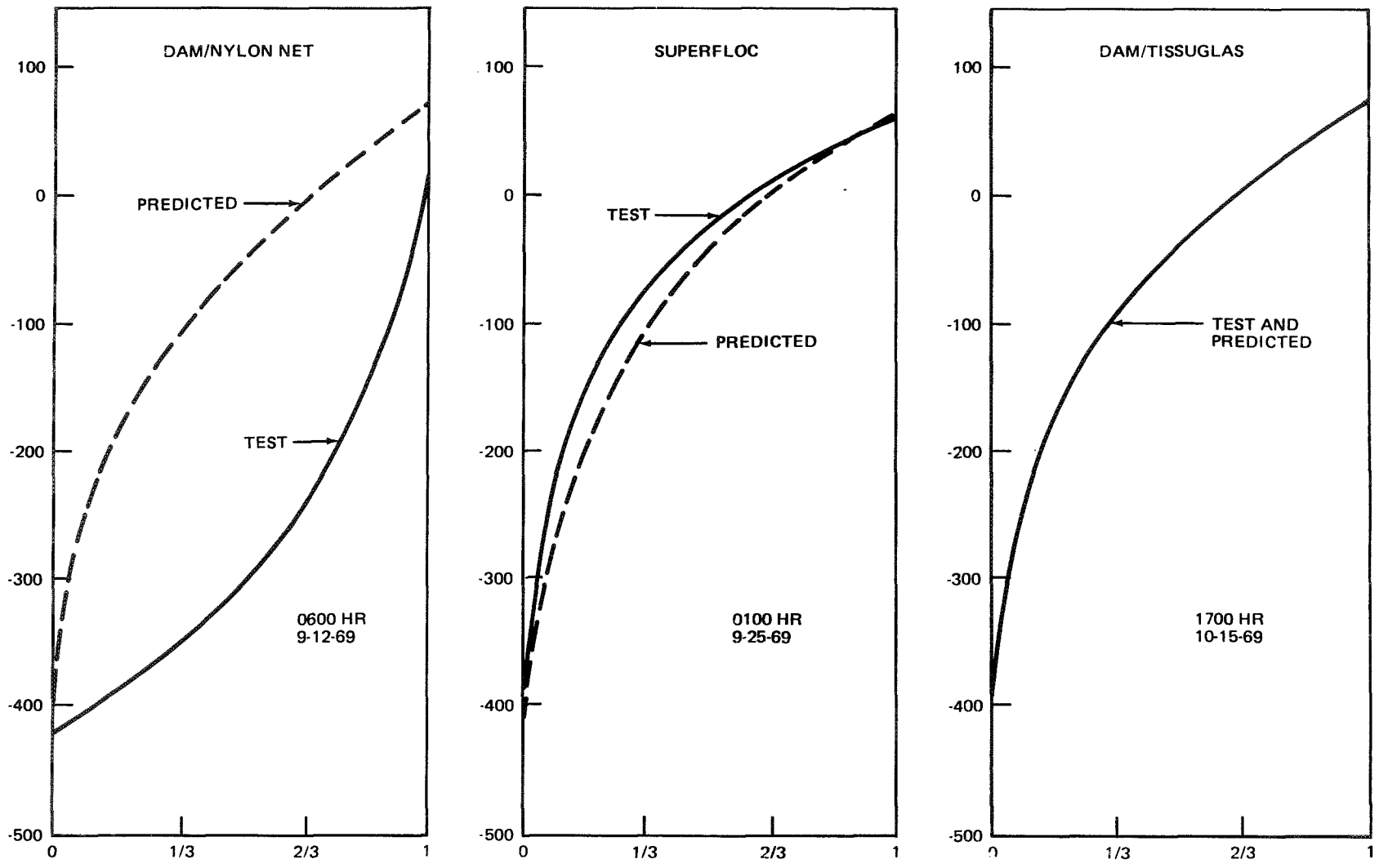

Figure 1-6. Thermal Gradients within LH_2 Calorimeter Test Insulation Panels

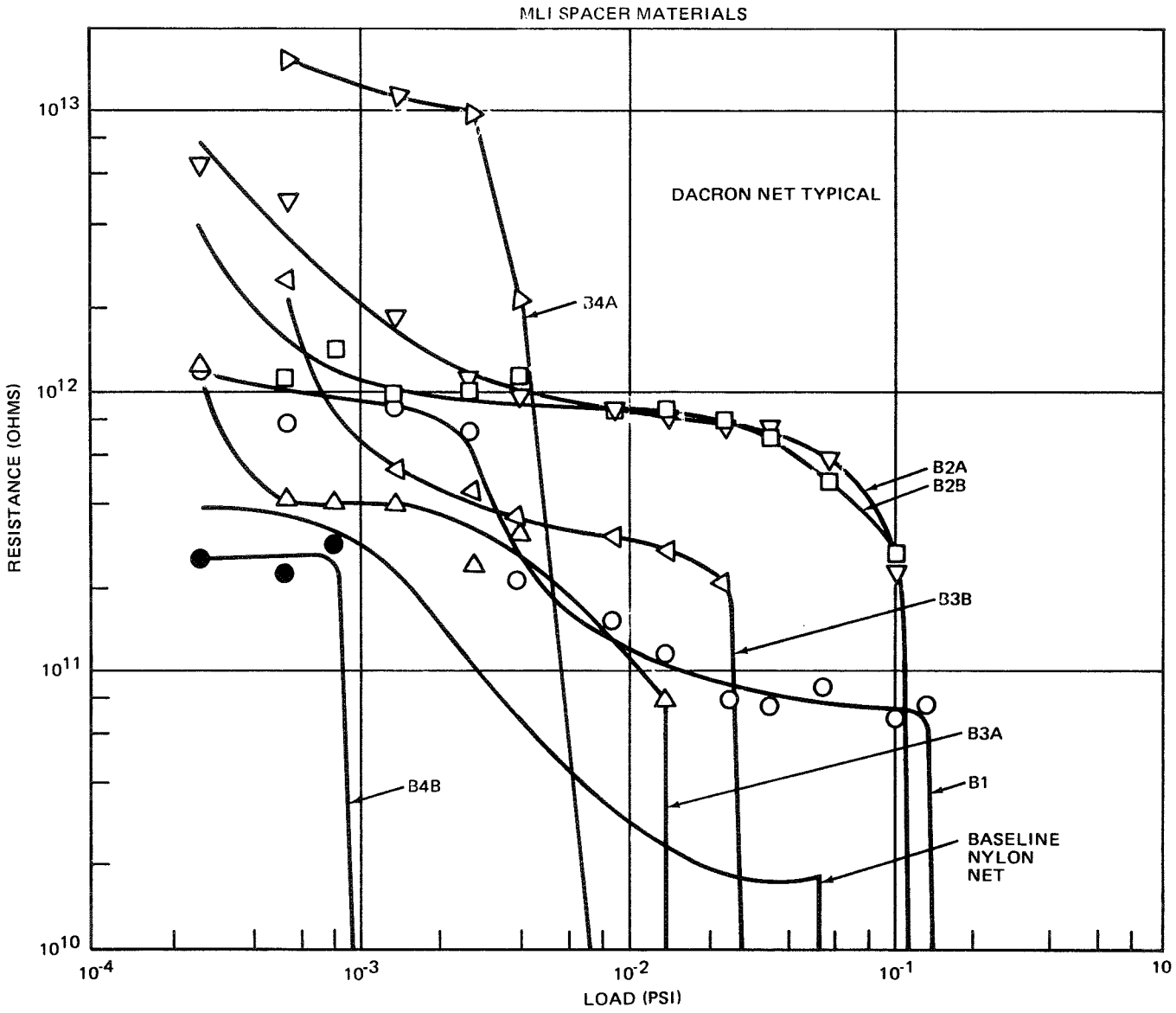

Figure 1-7. Electrical Analogy Method for Screening

Testing was accomplished with a 15-in.-diameter cylindrical LH_2 calorimeter. In addition to the above tests with the LH_2 boundary temperature, other performance data were obtained. It was observed that LN_2 cold-boundary MLI thermal data can be used to conservatively estimate the MLI performance on an LH_2 tank. Also, no performance changes were noted in MLI panels stored in a nitrogen environment.

Most importantly, the data indicate that with current design about half the heat transfer through a typical MLI system will be contributed by joints, fasteners, and perforations.

Flat-plate LN_2 calorimeter data (from NASA MSFC) for Superfloc and Dacron net Type B4A are also presented for reference in Section 6.

1.3.8 Structural Testing

The test data obtained to verify the MLI system structural design are presented in Section 7.

Component (face sheets, fasteners) strength data were obtained for design sizing. Also Mylar and face sheet expansion coefficients were experimentally measured. These show that the panel load-carrying members will remain loaded after tank-propellant-loading-induced chilling. Panel structural integrity in a Saturn acoustic environment was demonstrated down to -285°F. An unexpected result of these tests was that panels were found to fluff up. This phenomenon suggests that improved thermal performance can be expected after an MLI system has been launched.

1.4 DESIGN AND FABRICATION OF LARGE-TANK MLI SYSTEM TEST ARTICLE - PHASE II

The detailed design and test planning of the 105-in.-tank test article, Figure 1-8, is discussed in Section 8, which also includes the fabrication drawings. These drawings show a complete flight-type MLI system applied to the tank with the objective of simulating the performance characteristics of a full-scale vehicle tank.

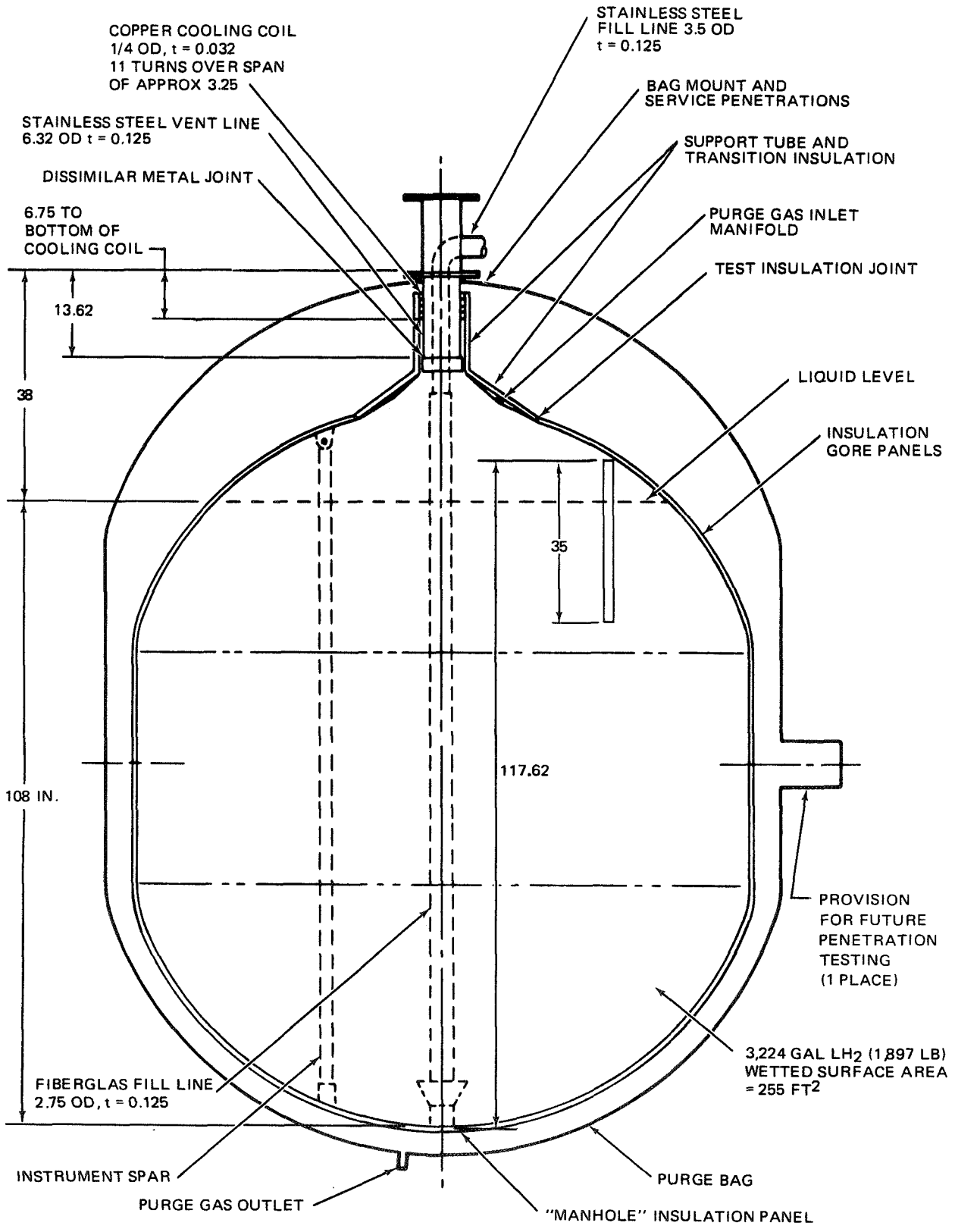

Figure 1-8. 105-In. Tank Test Article Configuration Schematic

The design criteria, which were developed from a scaling study, are indicated. It was found that the NASA 105-in.-tank will provide excellent simulation of an MNV insulation if full-thickness insulation and joints are used. Insulation on an MNV is essentially identical to that on a flat plate due to the very large vehicle diameter of 33 ft. Any insulation less than about 2-3/4 in. thick results in greater than 95 percent flat-plate simulation on the 105-in. tank, Figure 1-9.

The tank itself is uniquely suited for obtaining high-accuracy measurements of assembled insulation system thermal performance. It is a boiloff-type calorimeter in which all extraneous heat shorts have been virtually eliminated. The internal fill line is of low-conductivity material, fiberglass. The aluminum tank hangs from a sole support — a stainless steel vent tube with a bimetallic joint at the tank. Essentially all heat conducted down the support is intercepted by the cold outflow vent gas.

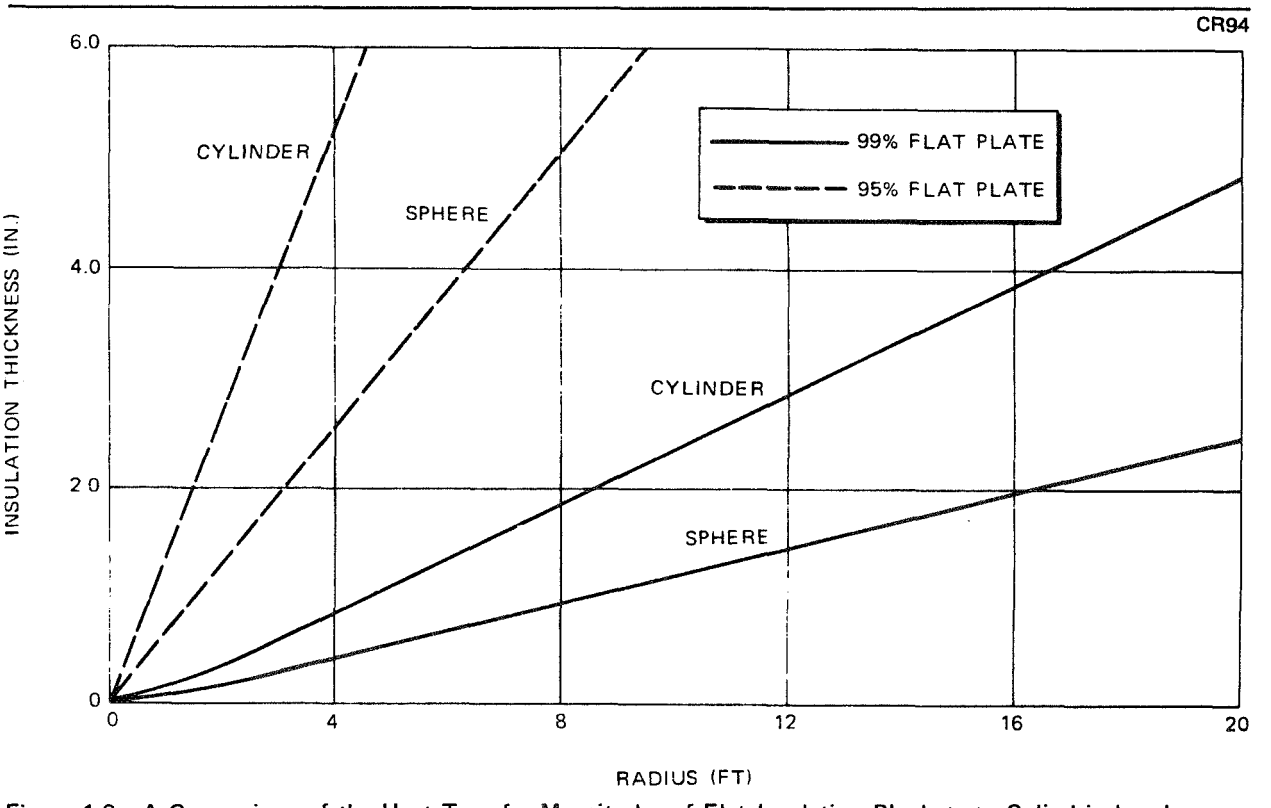

Figure 1-9. A Comparison of the Heat Transfer Magnitudes of Flat Insulation Blankets to Cylindrical and Spherical Blankets

The MLI system is identical in concept to the Phase I MNV design and includes a purge system with purge bag. The design maximum heat transfer to the tank was 50 Btu/hr, a value chosen to provide direct comparison with results of prior NASA tests with this tank. A detailed test plan for this program structured a guide to provide for future large-tank MLI test was also prepared and is also summarized in Section 8. Unique test facility requirements are noted.

Section 9 describes the tooling, materials specifications, and step-by-step procedures used to fabricate the 105-in.-tank insulation system. The methods developed in Phase I for vehicle production were used. Therefore, the tooling concepts and fabrication techniques that would be required for an MNV program were demonstrated.

1.5 LARGE-TANK MLI SYSTEM TESTING

The procedure, data, and data reduction for the 105-in.-tank test program are presented in Section 10. The test program consisted of two basic MLI performance tests: evacuated equilibrium and prelaunch to orbit simulation. Purge system tests were also planned and provided for in the test article design. However, difficulty experienced with the purge bag installation requirements and test chamber schedule limitations forced their cancellation.

As noted above, test results suggest that the insulation system developed in the program represents a technological advancement. Of particular interest is the observed discrepancy in evacuated equilibrium thermal performance between the two cases tested: evacuation before tank fill and evacuation with cold interstitial purge gas. The latter yielded about a 50 percent greater heating rate.

The MLI thermal gradient data suggest gas entrapment in the helium-purged case, either helium itself or degassing of adsorbed water vapor from within the insulation layers. The gradient in the higher heating case is flatter, similar to a gradient observed on the MDAC 15-in. calorimeter with the nylon net sample, which failed to evacuate.

The system performance data, summarized in Table 1-2, obtained in the test program may be used directly for design for installations where no further development is desired. However, as noted above, a performance better than even that shown in the non-purged case can be obtained rather readily with additional effort.

1.6 STUDY CONCLUSIONS

The study results show that sufficient technology is now available to design and apply a perforated 15-gage DAM-B4A Dacron net MLI system to spacecraft for a tank temperature as low as about -300°F. Additional structural launch dynamic load tests at LH_2 temperature are required for complete design verification of LH_2 tank installations.

Although an insulation system is now available, at this stage of development it is not optimum. Additional effort is needed in the areas of joint design, perforations, and purge preconditioning.

Due to the sparsity of component(joints, fasteners, penetrations, etc.) heat transfer data, any application of the system described will have an inherent range of performance uncertainty. This range can be greatly narrowed by performing more thermal tests of system components.

Experience obtained with the fabrication and installation of MLI panels utilizing the modular concept indicated that this is a highly attractive approach to MLI design. The shop operations are straightforward. Also, a damaged unit can be readily removed and replaced.

The NASA 105-in. tank appears to be the best calorimeter design formulated to date for testing complete MLI systems. Its use for future work is recommended.

A number of detailed recommendations specifically related to MLI system thermal testing on large-tank calorimeters are presented in Section 10. One is of particular significance: addition of heat flux gages (thermopiles) at various locations on the test article. These would provide a direct backup to the primary boiloff measurements. Also, variations in heat flux over the surface of the tank would be known.

PART I – FLIGHTWORTHY MULTILAYER INSULATION SYSTEM DESIGN

Section 2
FULL-SCALE VEHICLE INSULATION DESIGN

The objective of this task was to define the conceptual design of a full-scale insulation system for a typical MNV LH_2 propellant tank. This design was to utilize, wherever applicable, the insulation concepts recommended during prior work (Reference 10).

The study resulted in a complete insulation system design, including helium purge provisions. Design concepts are not limited to the MNV, but may be directly applied to any cryogenic propellant tankage. Throughout the design activity, an attempt was made to make the system as independent as possible of the choice of specific insulation material, thereby providing maximum flexibility for future application.

It is believed that this program has resulted in the definition of the first complete flightworthy MLI installation design. The basic design has been adapted for use on the Skylab vehicle forward dome for flight in 1973.

2.1 DESIGN CRITERIA

The MNV configuration utilized in the study consisted of an insulated tank surrounded by a load-carrying shell (Figure 2-1). Tank capacity was 250,000 lb of LH_2, sized for a 300-day Mars mission.

Also, an insulation system placed behind and separate from meteoroid shielding was chosen for the study design. Available data indicated that it was more desirable to place insulation behind the bumper configuration to minimize both particle penetration and blast cloud damage. This approach also provides maximum flexibility for future application. Where required, design computations were based upon the available Saturn environmental design criteria (the compilation published as Appendix B of Reference 10).

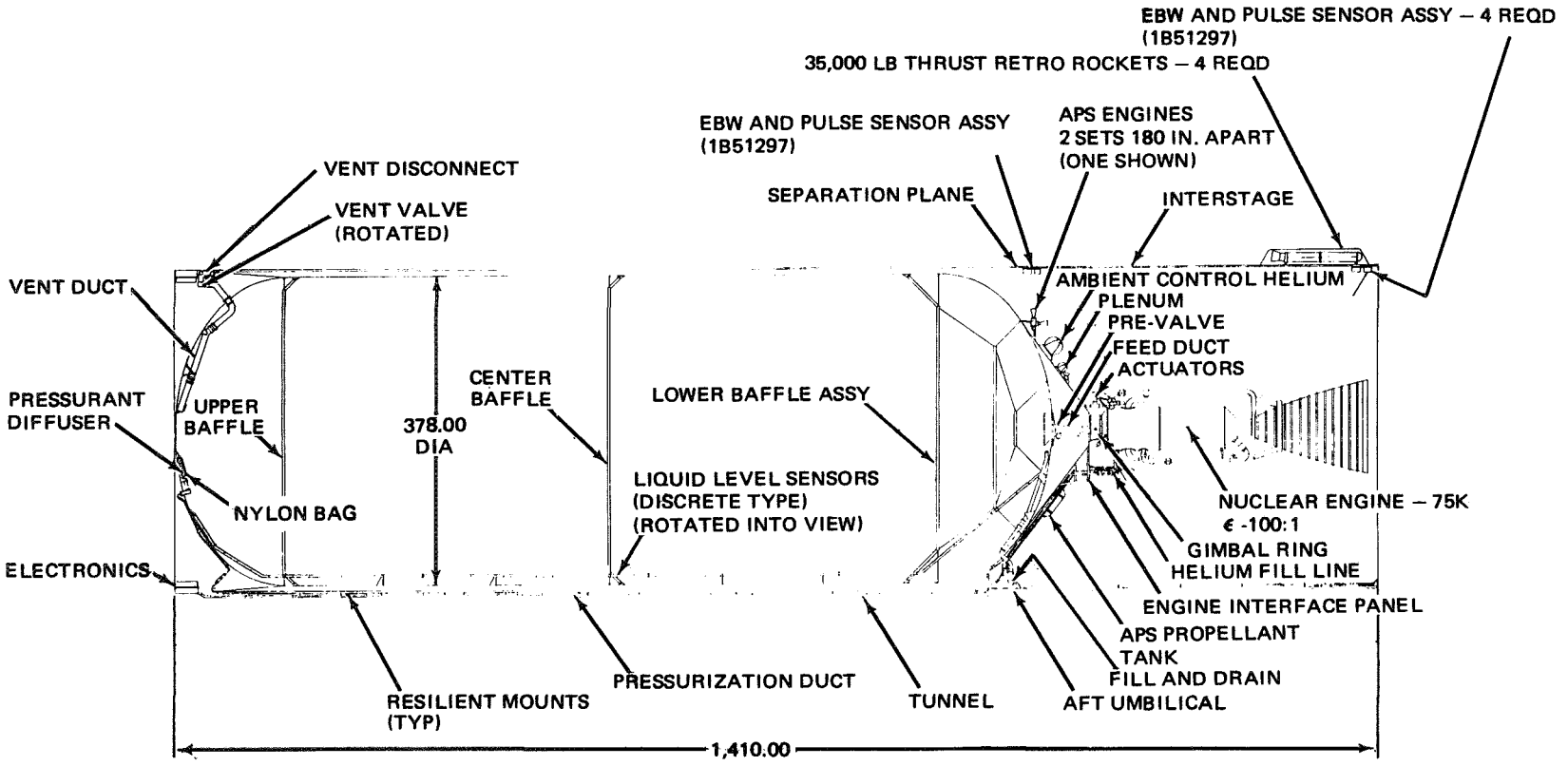

NOTE: ALL DIMENSIONS IN INCHES

SCALE – 1/20

Figure 2-1. Nuclear Stage Inboard Profile

2.2 PREFABRICATED INSULATION PANELS

The study resulted in the definition of a design concept in which the complete MLI installation is built up from a number of prefabricated individual panel packages. Thus, the characteristics of these packages (Figure 2-2) becomes the most important part of the design. All installation details depend upon this item.

In this panel, the insulation reflector-separator stack is sandwiched between load-carrying face sheets and held in place by assembly fasteners through the sandwich. Longitudinal support straps, terminating in a grommet for tank attachment, are built into the face sheets. Joint closure is effected by cross ties. During launch, load is transferred from the individual insulation sheets into the through-fastener and then into the face sheet load-carrying strap. The face sheets also provide handling protection as well as a mount for the joint cross ties.

2.2.1 Panel Assembly Fasteners

An injection-molded nylon heat-sealed head-type fastener, Figure 2-3, was selected for design, although a number of different types were evaluated (Section 4). Later work (Phase II, Section 9) showed that a one-piece molded unit, commercially available (Appendix A), was more attractive from the standpoint of ease of installation. It is recommended for future application.

A fastener spacing of 12-in. on centers was recommended in the baseline design and adopted here. Although not optimal, it is feasible and adequate. Future study may show that a wider spacing would be sufficient, cutting costs and thermal shorting.

Fastener tensile tests (Section 7) showed that the fastener is more than adequate to withstand expected postlaunch decompression loads when installed with 12-in. spacing. Decompression tests showed that the fastener (1/2-in. -diameter head) will not tear out from a 25-gage Mylar face sheet. The reinforced face sheet net used here results in an even greater degree of conservatism as the net will tend to restrain the Mylar. Heat-short characteristics were measured and are reported in Section 6.

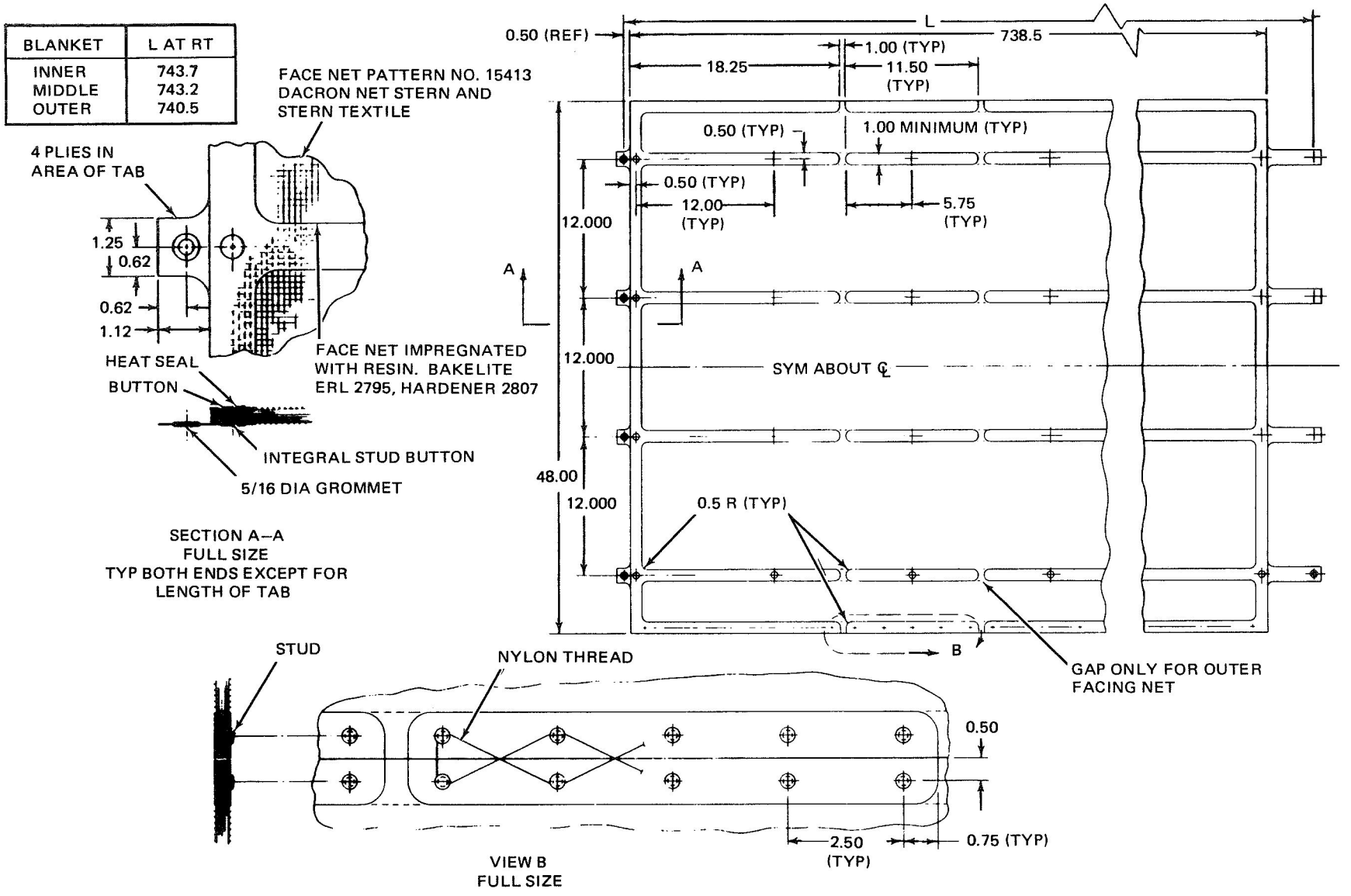

Figure 2-2. Prefabricated Panel Configuration

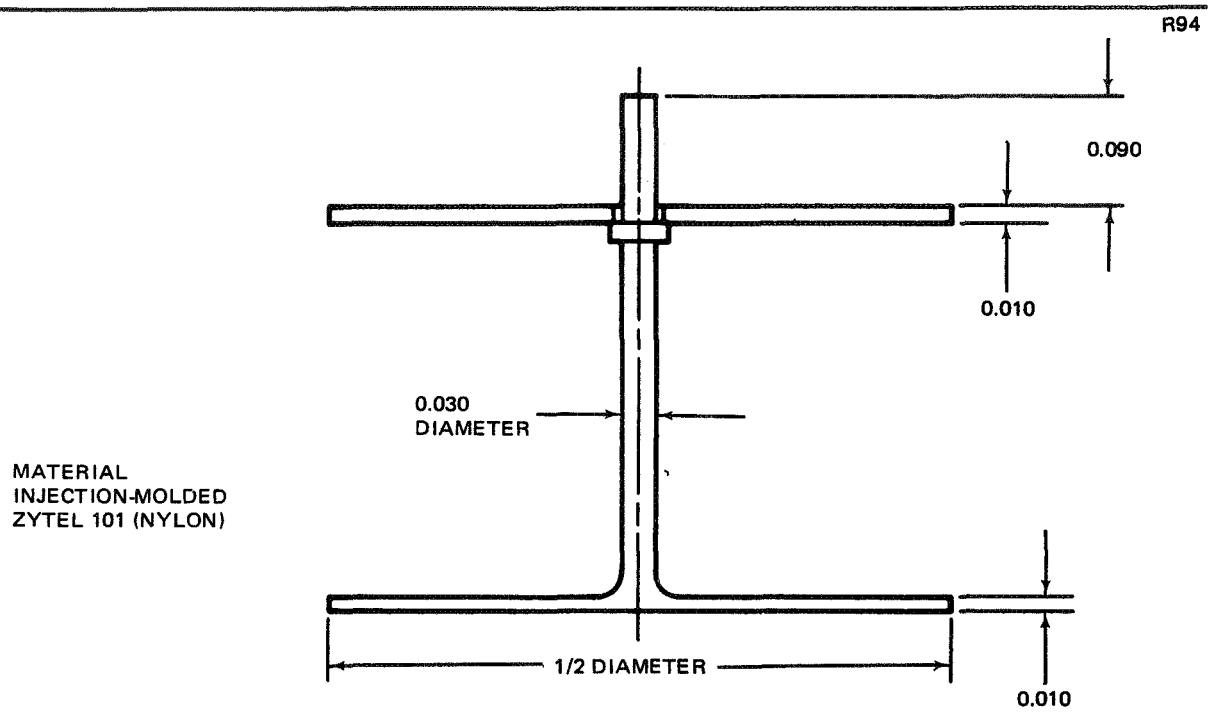

Figure 2-3. Fastener

Changing fastener spacing will not affect finished panel density. Manufacturing tests (Section 3) showed that no significant density changes occurred when panels were drilled (hollow drill) for fastener installation on 6-, 12-, or 24-in. centers.

2.2.2 Panel Width

The panel width of 48 in. shown in Figure 2-2 was used for design, although larger panels could have been applied to the large-diameter MNV with a change in fastener spacing. Insulation materials (double-aluminized Mylar and Dacron net) were available in widths up to 56 in. The selected width, however, is within the range of test data demonstrating successful post-launch evacuation (Reference 10).

More recent work pointed out the need for fasteners at about 0.5 in. from the panel edge to effect adequate joint closure. Panel width and design should be revised accordingly for future applications.

2.2.3 Face Sheets

The face sheets carry all panel loads and provide rigidity to the MLI panel package. An epoxy-impregnated Dacron net design is shown. Although this method works well, with the straps shrinking faster than the Mylar and thereby staying continuously loaded, fabrication can be tedious. Mylar tape backed with heat-setting adhesive, used in Phase II (Section 9), has similar characteristics with a much less costly fabrication. This approach is recommended (see Section 4).

Note that the load-carrying straps are continuous on one side (coldest). This provides takeup for the differential contraction between the cold and warm faces of the panel.

2.2.4 Attachments – Panel to Structure

Methodology for attaching the insulation panels to the vehicle tank and structure were not specified in the baseline design. Therefore, attachments were evaluated, and load-carrying studs attached to the structure and fastening through grommets in the insulation panel support straps were selected as a simple, reliable, positive attachment technique.

The basic stud is 0.25-in.-diameter aluminum. It is inserted into the honeycomb support structures or welded to the tank proper depending upon the point of panel attachment.

The welded stud was selected from Reference 11 which provides design data and shows the method of capacitor discharge welding. The stud is simply a cylinder with a small tip on the end which contacts the work, positioning the stud body slightly away so that an arc can be initiated. This forms the completed weld. Maximum shear loads for typical 1/4-in. aluminum studs are 415 to 830 lb. Tensile ultimate loads are 670 to 1,360 lb. These are more than adequate for full-length 60-ft MNV sidewall panels (see Section 2.7).

2.2.5 Grommet Attachment

The attachment grommet is inserted through four layers of epoxy-impregnated Dacron. The tensile strength developed by this design was

approximately 50 lb at -423°F. This strength is adequate for the maximum launch loads which are on the order of 35 lb for a full 60-ft-long sidewall panel.

The grommet has a tubular collar which is inserted into a hole in the strap. Then the retaining washer is upset, sandwiching the strap between the head of the grommet and the retaining washer. This unit yielded consistent tensile-load-test results with no fabric tearing.

2.2.6 Panel Thickness

The required number of insulation sheets has been divided up into separate panel layers installed one on top of the other. This allows simple butt joints to be used, and by offsetting each layer, no through optical path heat short results.

The criterion for panel thickness selection is the minimization of differential contraction across the panels. For the space environment, equal thickness is not optimum. The panels should increase in thickness from inner to outer. However, during the period of maximum panel load (launch) the temperature distribution through the insulation is expected to be nearly linear (thermal conduction within the interstitial purge gas). Therefore, the selected approach, equivalent thicknesses, provides an equivalent temperature differential across the panels, minimum differential contraction, and minimum potential of insulation tearing at the fasteners. The approximate temperature gradient across each panel is 58° F.

2.2.7 Panel-to-Panel Joints

Optimum joint design involves a tradeoff between joint thermal degradation and joint evacuation ability. Sufficient data to define an optimum design was unavailable, although it was known that panels with interleaved joints evacuate poorly. Butt joints appeared best.

A staggered butt joint with an overlay of 1 in., specified in the baseline design, was adopted with an increased minimum overlay of 2 in.

Thermal tests (Section 6) show that joints can be expected to contribute as much heat transfer to the tank as the basic insulation itself. Therefore,

additional joint studies are recommended. A stepped butt joint (Section 4) might yield improved performance.

2.2.8 Joint Cross Ties

Panels are laced together along their edges with Tefglas thread (less stretch than nylon). Nylon buttons 0.01-in. thick, attached to the face sheet with a small grommet, are used for lacing (Section 4). A low rounded profile results, which is needed to prevent the tearing of panels placed on top of them.

The panels are cut oversize and laced tightly so that when shrunk after tank filling no tensile load results in the joint. Shifting of the panels cannot occur if the vehicle is shipped horizontally. Oversized panels also eliminate the possibility of compression "squash" during shrinking with an attendant change in thermal performance.

Panel-to-panel attachment on the outer face only was used. However, the Phase II 105-in. tank system showed that inner face attachment is also needed. Velcro tabs across the joint are recommended.

2.3 INSULATION APPLICATION DESIGN

The MNV insulation system design and installation drawings prepared during the study are presented in Figures 2-4 through 2-14. These depict a system built up of separate prefabricated panels installed in three overlapping layers. Although the triple-layer concept was carried from the study starting point design, a two-layer system is recommended. It maintains the benefits of three layers (no through-joints or fasteners) but has the advantage of reducing installation complexity and fabrication cost. Three layers should be considered in the future only if work shows that the joint and fastener thermal degradation is great enough to warrant it. This is not expected to be the case.

Included in the drawings are the purge system details which have been combined into the MLI installation design. The system consists of enclosed purge volumes, using a flexible bag for containment where necessary, with inlet and outlet ports connected to a built-in gas distribution system.

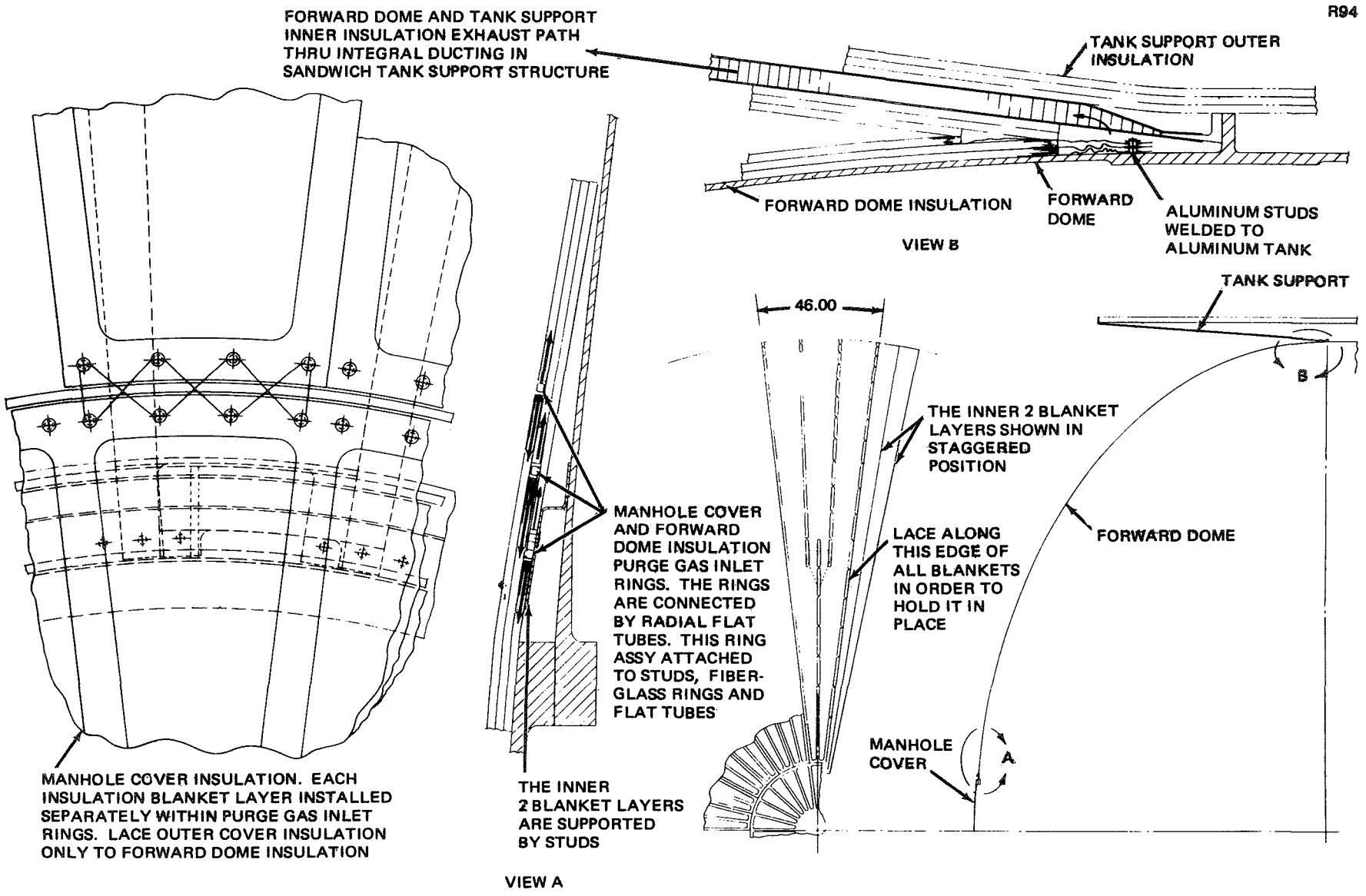

Figure 2-4. Forward Dome Gore Panels and Manhole Cover

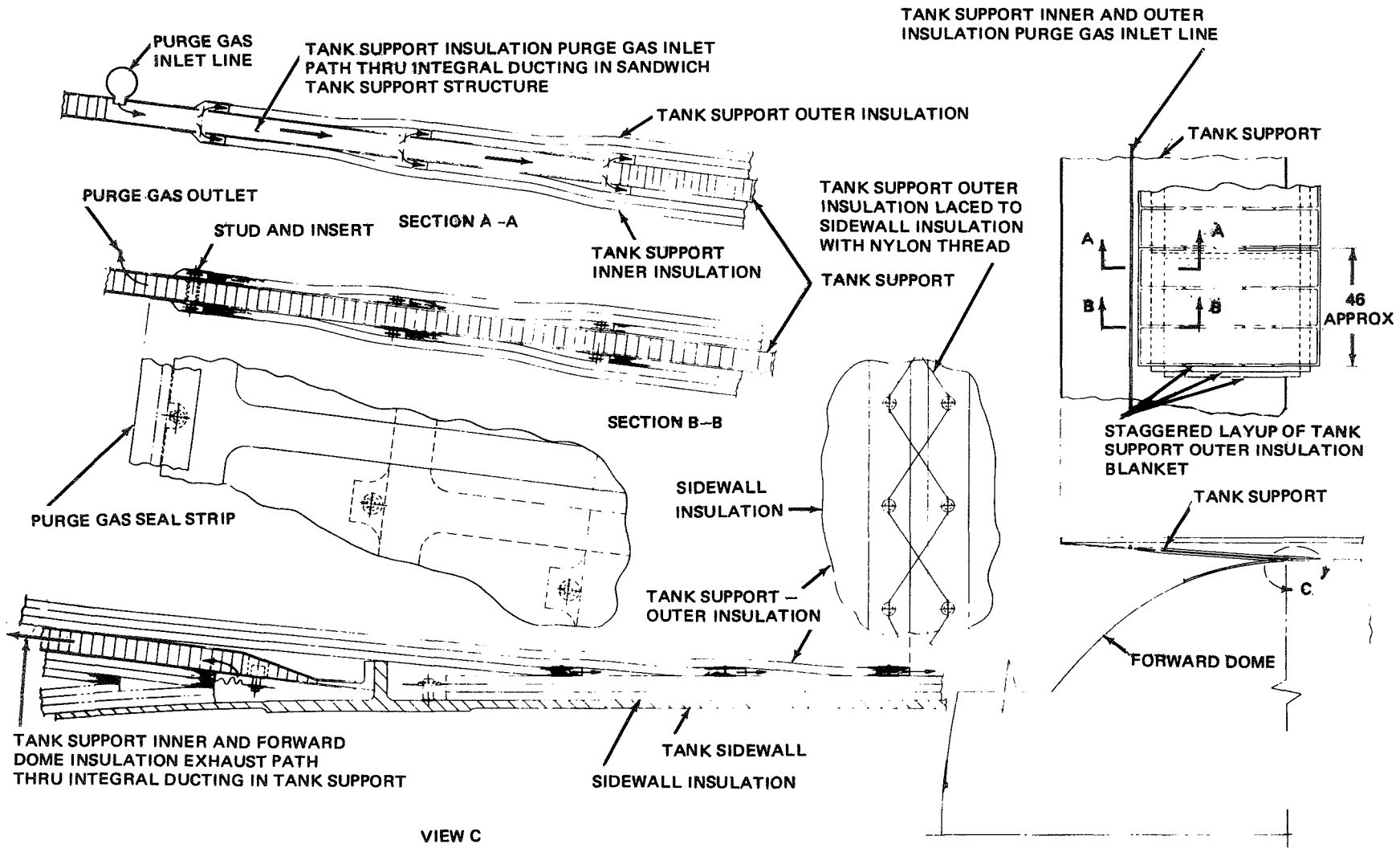

Figure 2-5. Insulated Tank Support Penetration

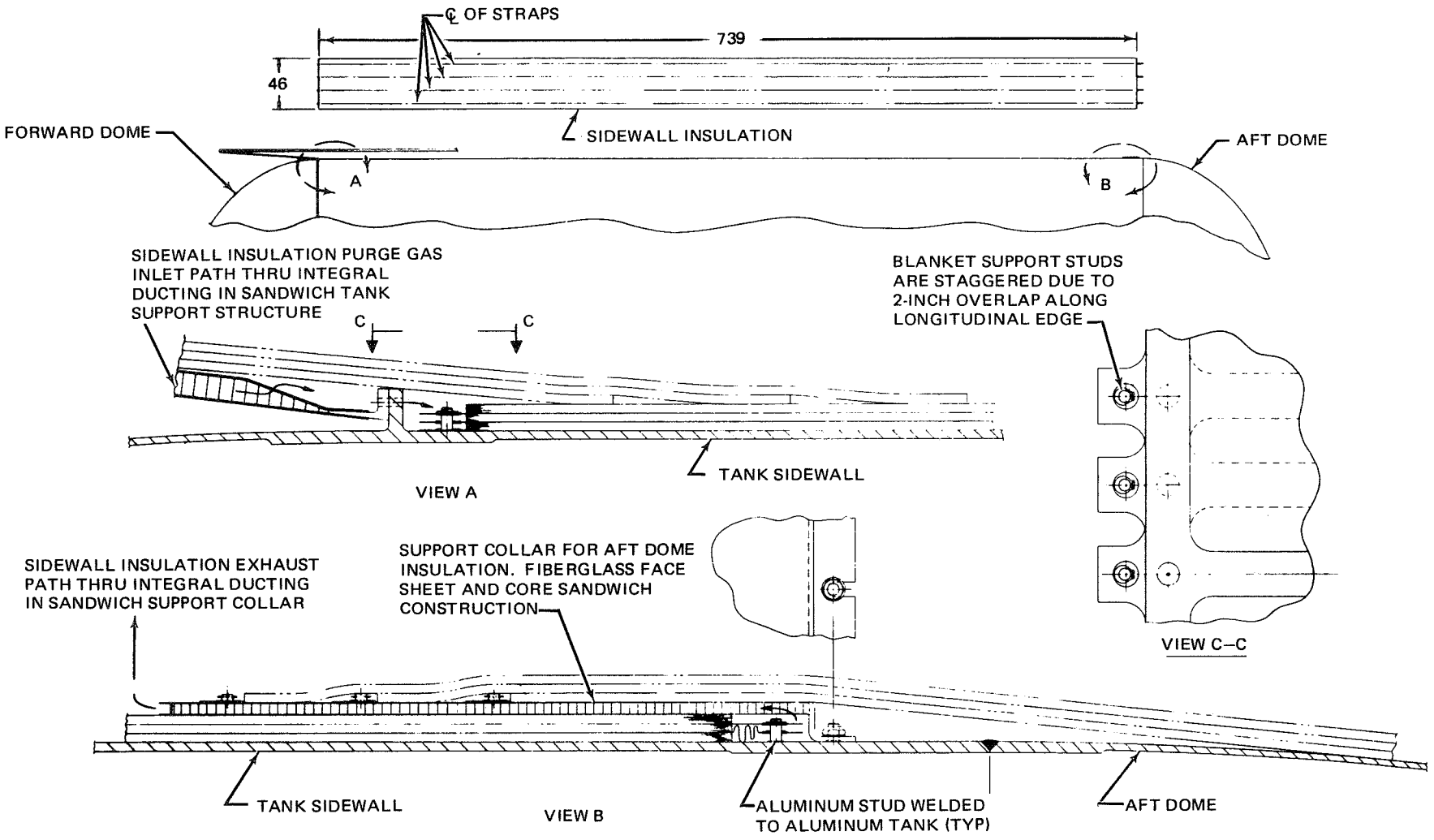

Figure 2-6. Sidewall Panel

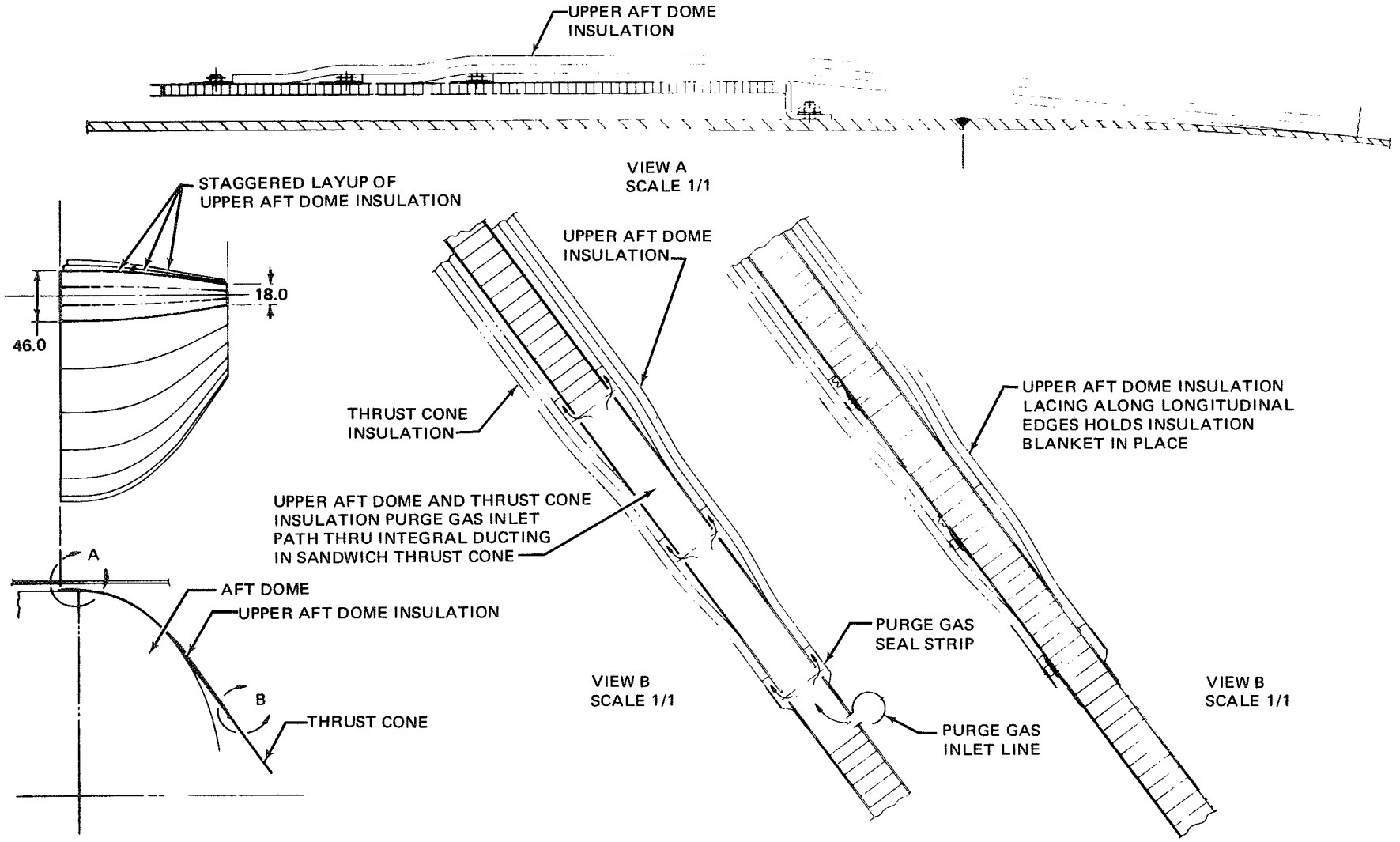

Figure 2-7. Upper Aft Dome Panels

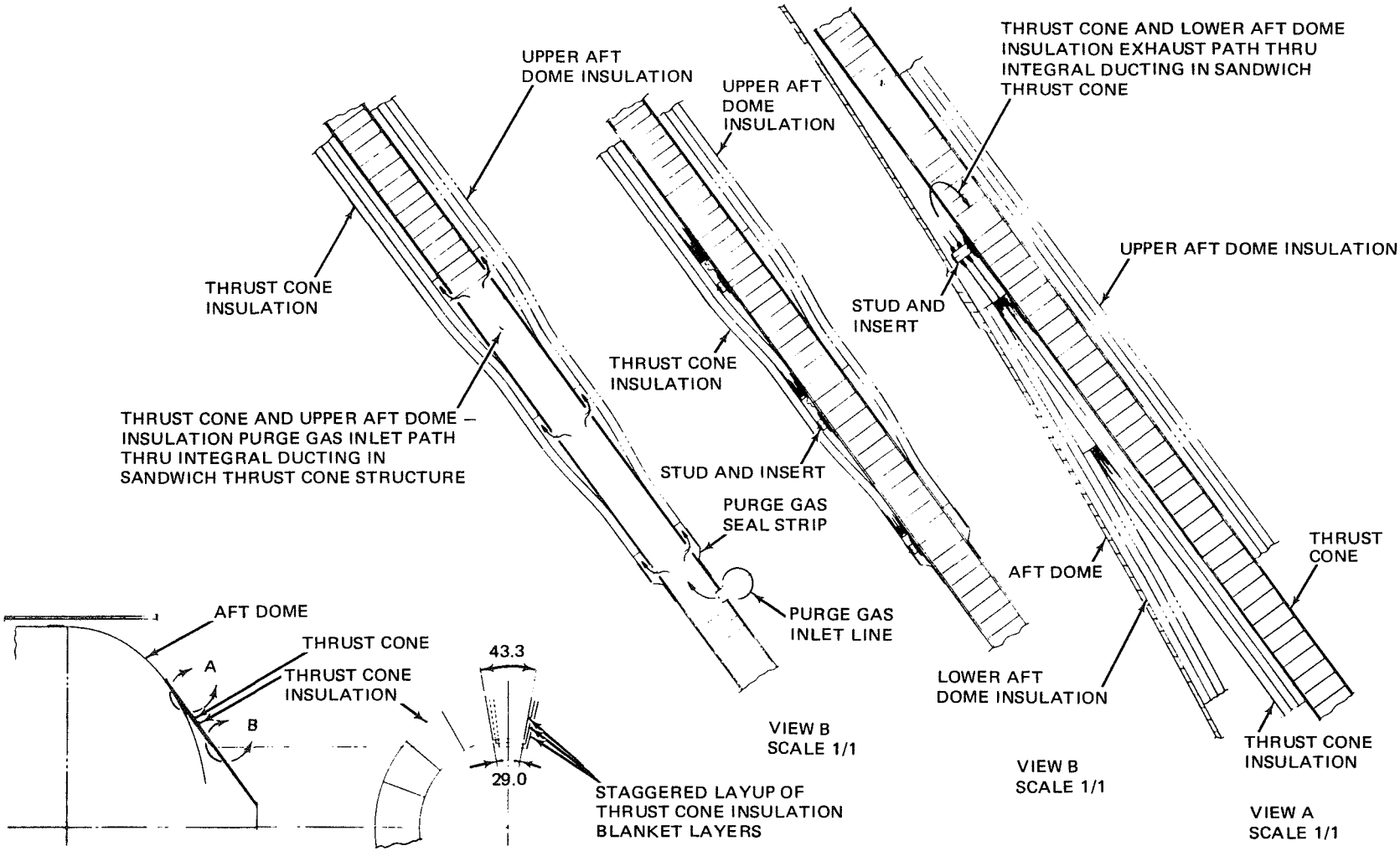

Figure 2-8. Insulated Thrust Structure Penetration

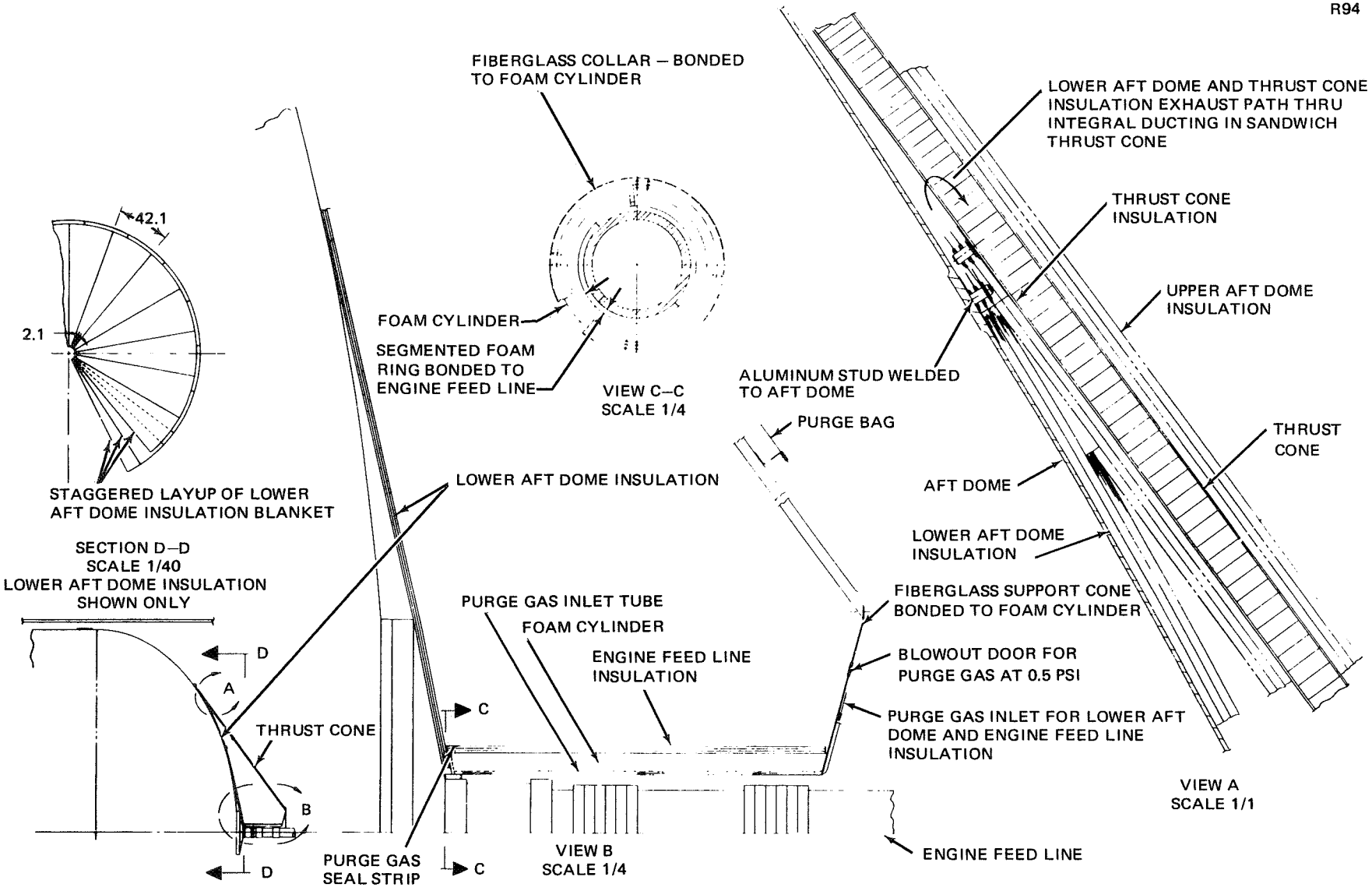

Figure 2-9. Lower Aft Dome and Engine Feed Line Insulation

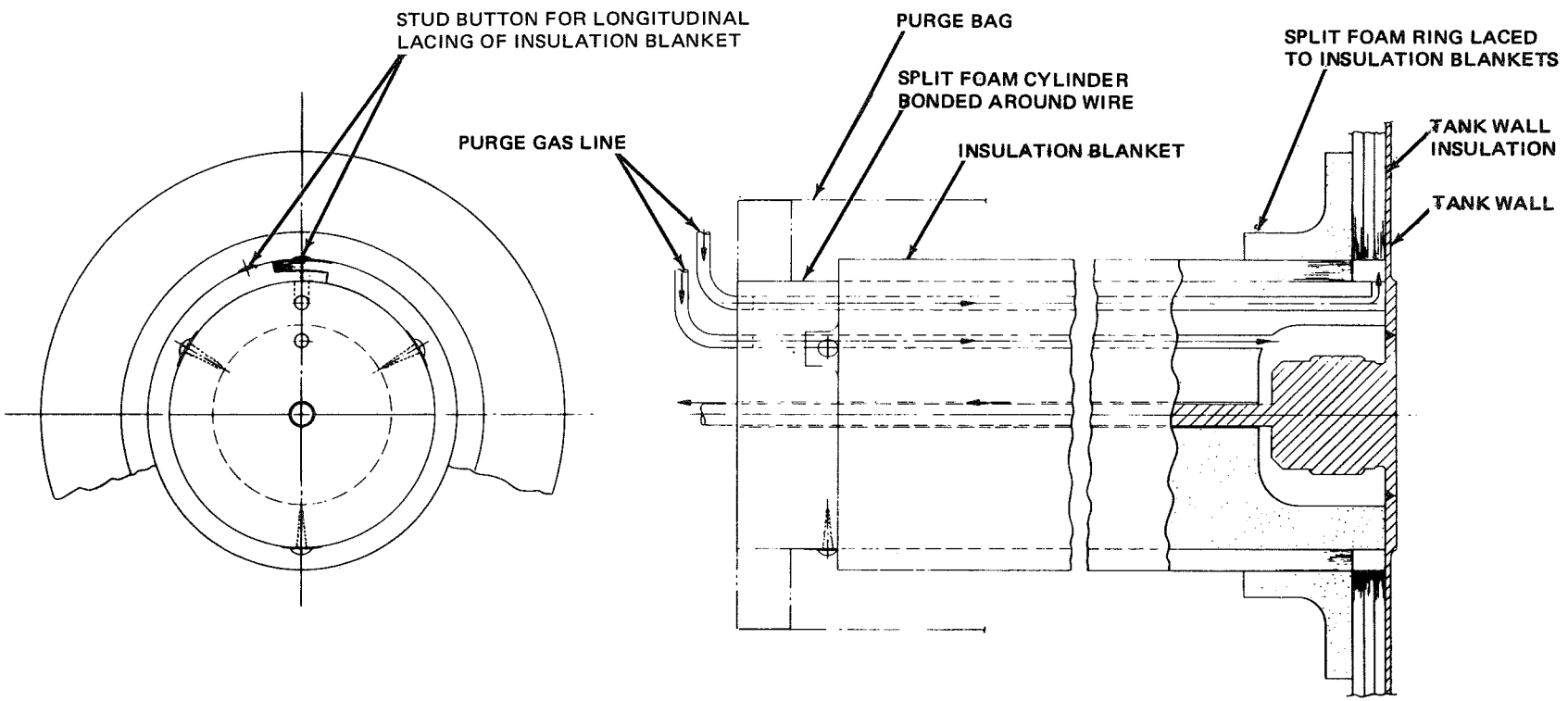

Figure 2-10. Electrical Penetration

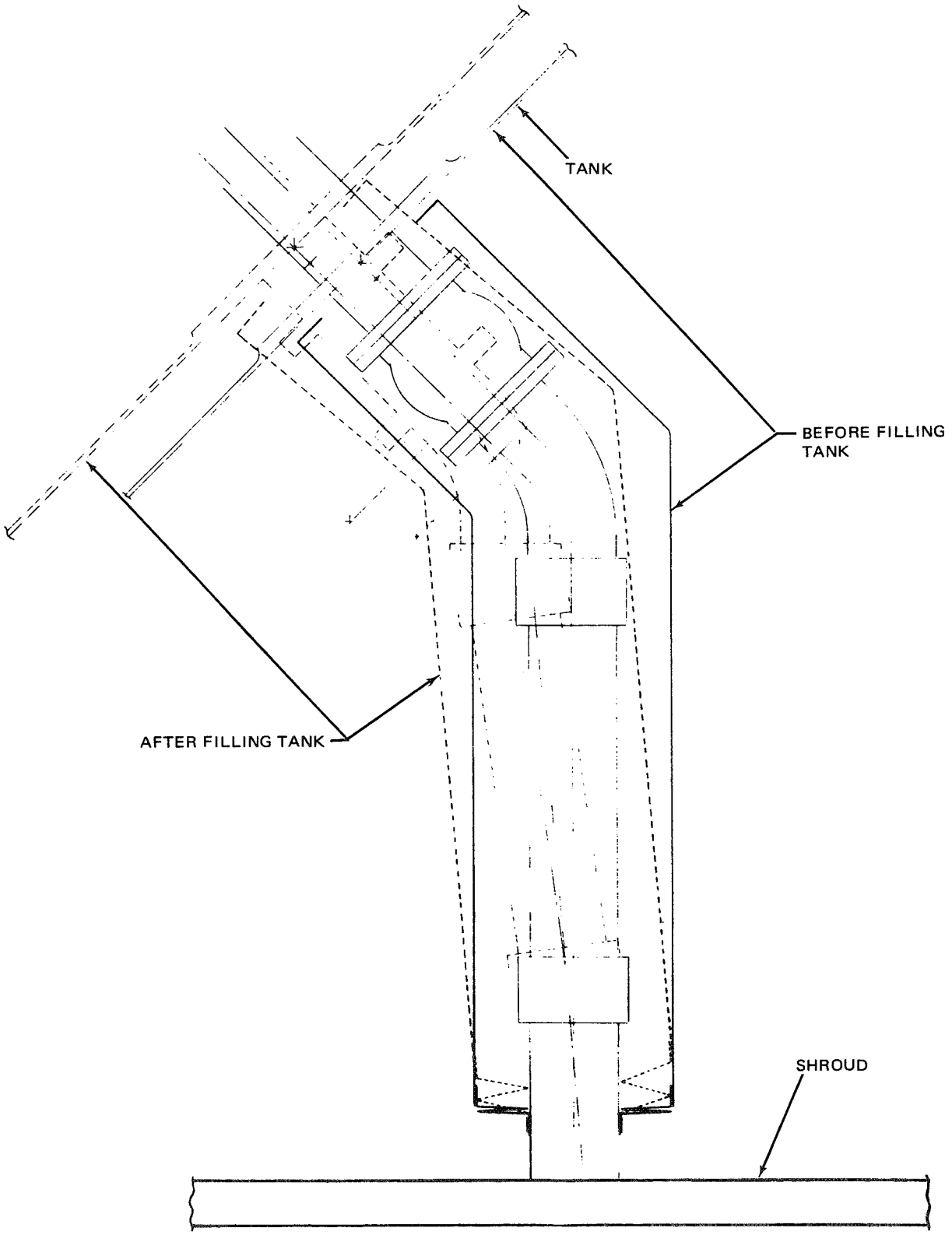

Figure 2-11. Pipe Movement Due to Tank Contraction

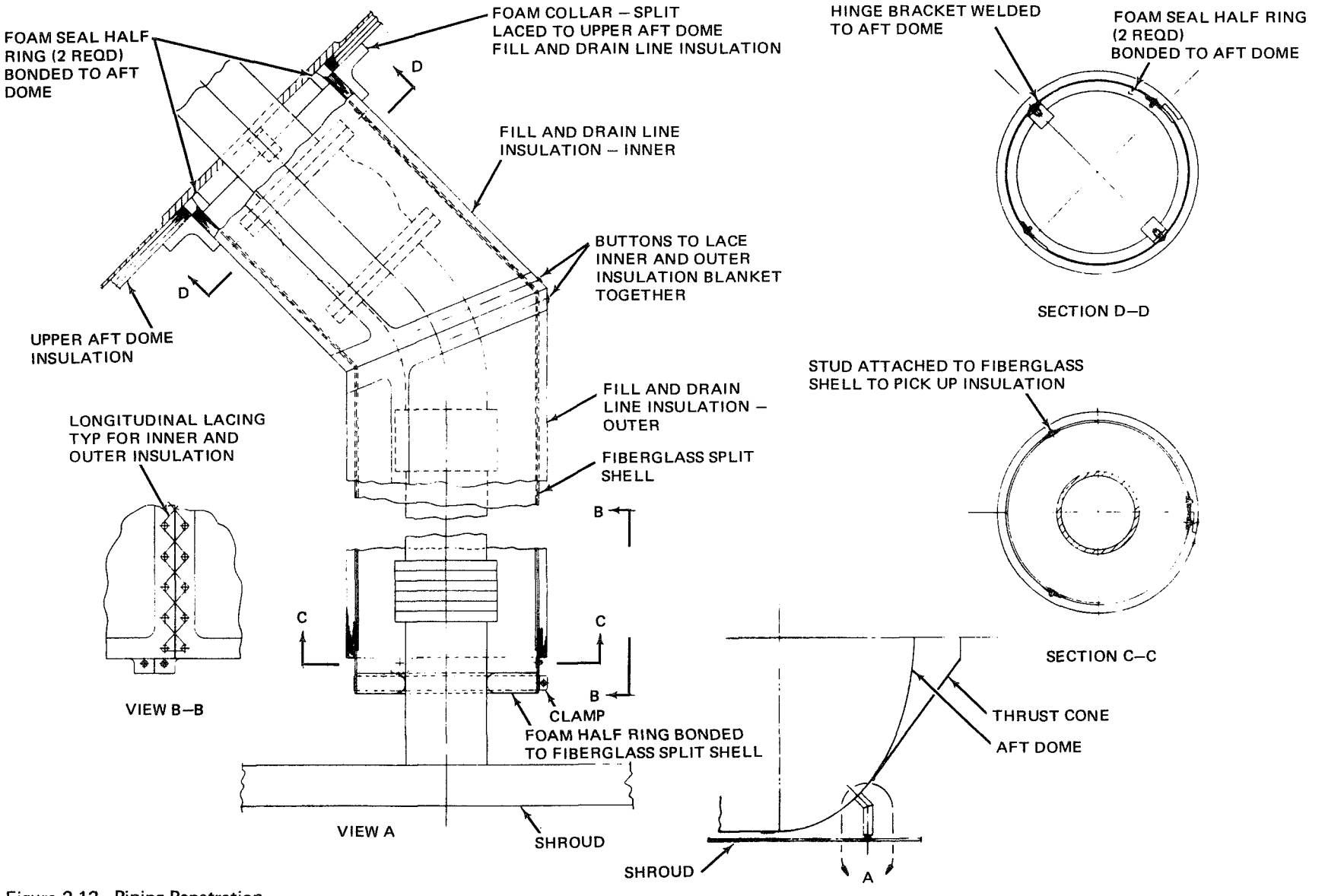

Figure 2-12. Piping Penetration

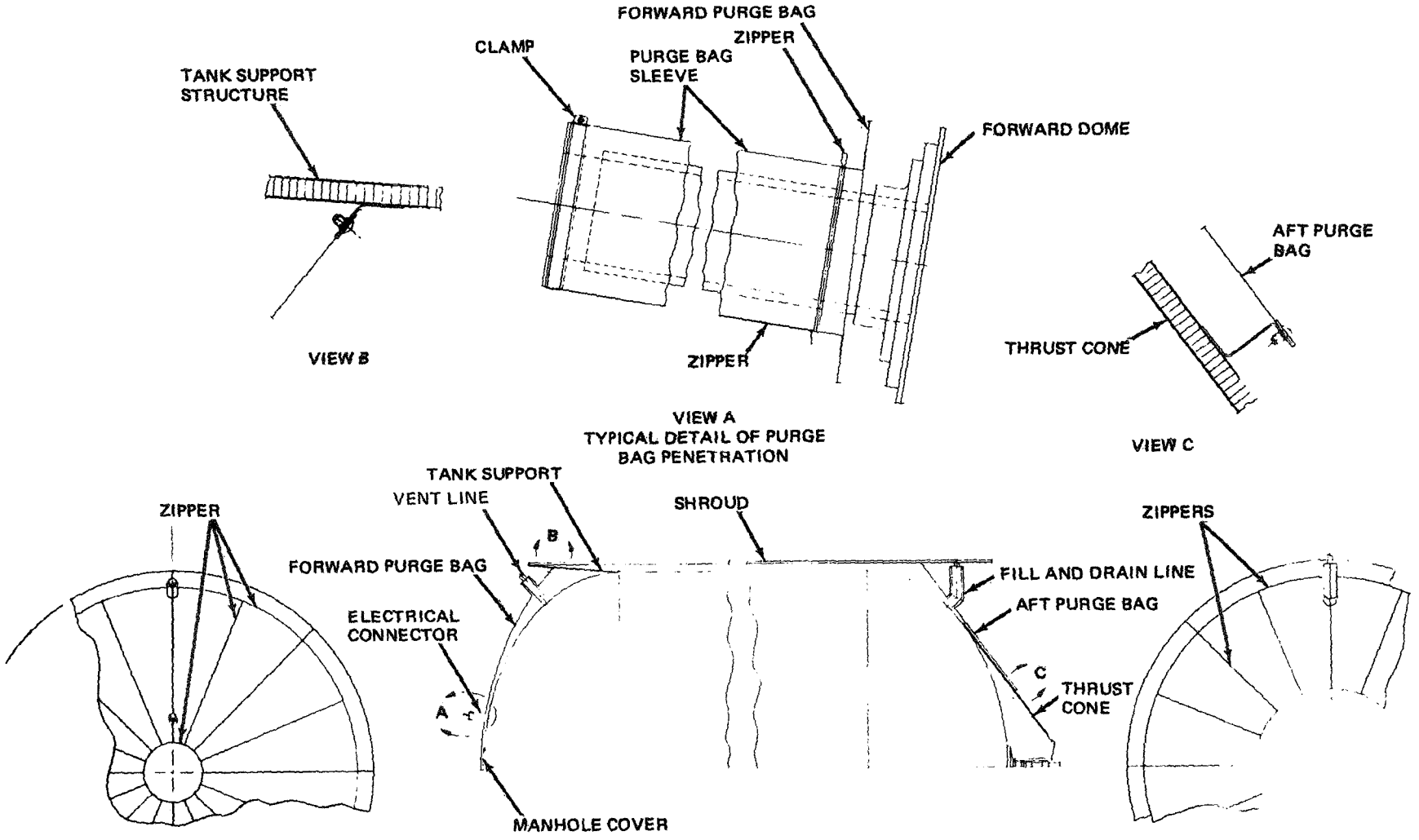

Figure 2-13. Purge Bag Concept

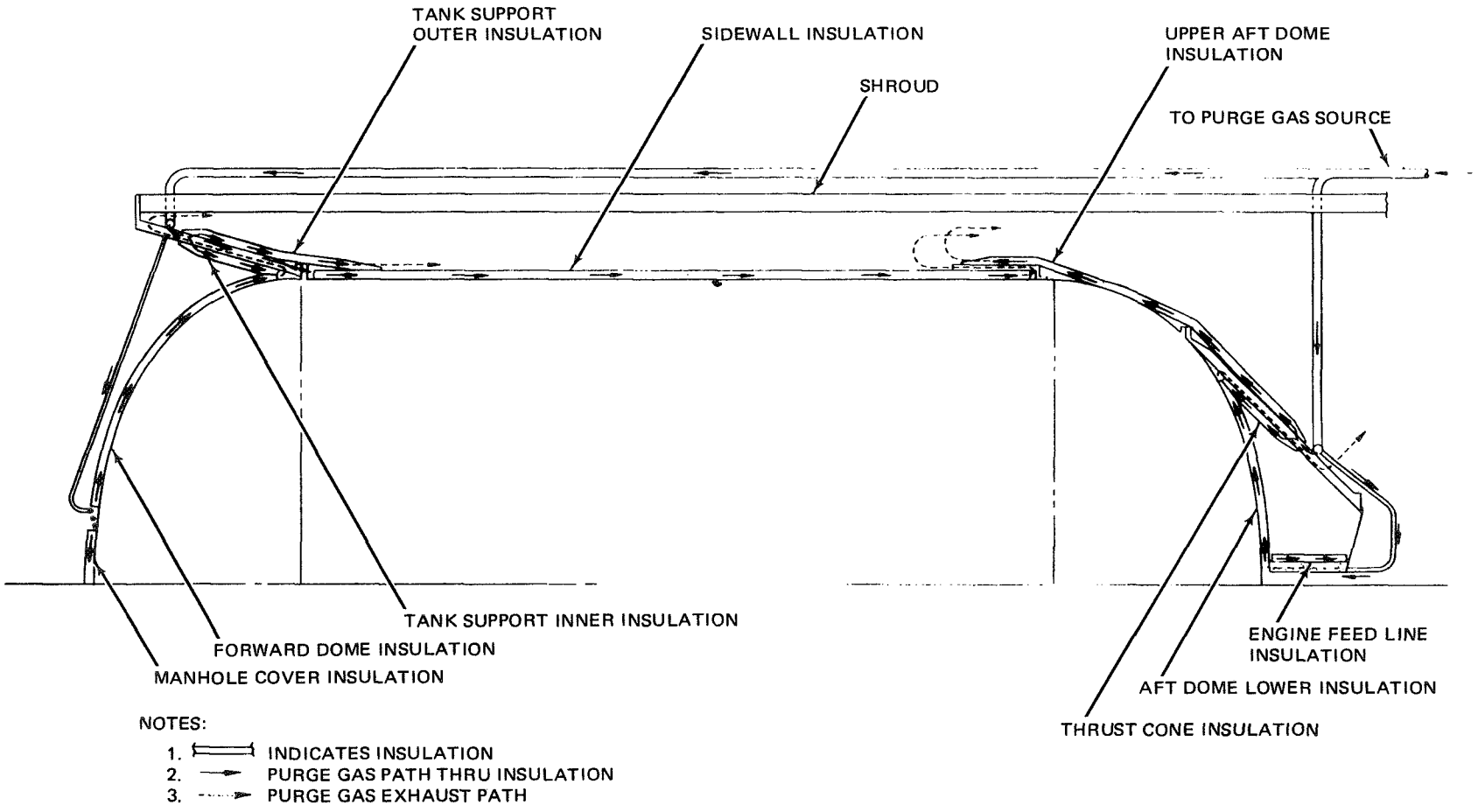

Figure 2-14. Purge System Concept

2.3.1 Forward Dome Gore and Manhole Cover Panels

The principal problems encountered here are: controlled location of panels on dome, hold-down during staging rebound loads, contraction, interface with tank support insulation, and purge system location. In addition, the manhole cover must be readily removable. The design solution is shown in Figure 2-4.

Note that a constant joint overlap, e.g., 2 in., cannot be maintained if the second layer of panels is built to dimensions identical to those of the first. The joint overlap becomes larger from the top of the dome to the sidewall interface. This larger varying overlap was accepted as panels of one standard configuration are deemed preferable. They simplify development test and manufacturing, lower tooling costs, and lend panel fabrication to the possibility of automation. Evacuation through the larger overlap may be a problem; perforated reflector sheets are recommended as the conservative design approach.

Note also that the purge lines are built into the tank support structure. This can be readily accomplished by using fiber glass channels similar to those used in DC-8 aircraft radomes. The insulated tank support must be installed after the dome gore panels as positive gore tie-downs are required in that area for rebound load conditions.

The inner two panels are supported by stud attachments in a fiber glass ring, and the outer panel is laced to the manhole cover. Note that elimination of the requirement for the third panel offers a much less complex design.

2.3.2 Tank Support Penetration

The design for the insulation on the tank support penetration is shown in Figure 2-5. Panels are attached to the structure with through fasteners. Purge channels again are fiber glass tubes. Panels on the inner side are tied down for rebound loads with a flexible strip attached to studs. On the outer side, they must be laced to the sidewall panels.

2.3.3 Sidewall Panels

The determining factors in design of these units are the loads on the straps, differential contractions between the tank and insulation, and considerations of manufacturing handling and storage of very long panels.

A full-length panel design, shown in Figure 2-6, was chosen. During installation, panels can be handled on a lightweight fixture. The full-length design is also compatible with strap loading, and complex circumferential joints are eliminated.

A "floating" panel fixed at the lower end for rebound is shown in Figure 2-6. The floating provision was included to ensure that the Mylar would not shrink more than the tank. Later test data showed that the tank will in fact shrink a greater amount than the Mylar reflector and insulation panel support straps. With such a situation, the panel lower end may be fixed directly to the tank.

The ground-hold condition is the critical contraction design condition for the insulation blankets as the temperature of the outer and center blanket is lower than at any other condition. This results in the maximum shrinkage of the tank support straps.

2.3.4 Upper Aft Dome Panels

The design and installation of these panels is shown in Figure 2-7. As was the case with the dome gore panels, a constant joint overlay cannot be maintained.

Note that a fiber glass support structure (circumferential band) is required. Sliding joints must be provided in this unit to accommodate circumferential contraction and expansion.

Note also that the purge gas enters the lower edge of these panels instead of the top as in the dome, tank support, and sidewall. Reversing the point of gas introduction would necessitate a complex manifold due to the contraction of the support. This was not deemed necessary in view of the reported

indication that diffusion of gas in the insulation governs the purge system design. The purge is then independent of the geometric point of gas introduction.

2.3.5 Insulated Thrust Structure Penetration

This unit is shown in Figure 2-8. It is similar to the upper tank support penetration, above. The insulation must be installed prior to attachment of the structure to the tank, and the joint overlap will be greater at the top than at the bottom if identical panels are used for each layer.

2.3.6 Lower Aft Dome and Engine Feedline

The lower aft dome panels, Figure 2-9, are similar to the upper panels. Note that the insulation around the feedline is held away from the line on a foam and fiber glass supporting structure to decouple the insulation from the longitudinal expansion and contraction of the pipe.

2.3.7 Typical Electrical Penetration

The major problems encountered in the design of the electrical penetration are: providing structural rigidity to the flexible components of the assembly, minimizing connector hydrogen gas leakage from penetrating the insulation, and providing ready disassembly and reassembly under field conditions.

The design is shown in Figure 2-10. A replaceable foam cylinder provides the basis for the installation. It also provides a point for purge bag attachment.

One layer of insulation with a shiplap joint (Section 4) was chosen for simplicity. This should be thermally adequate as the fasteners through the MLI are in contact with the foam insulator and not the cold tank wall; there is no direct thermal shorting. Insulation panel structural integrity is ensured by an attachment at both panel ends; it screws into the foam and is laced to a foam ring.

Even the simplest electrical penetration adds considerable complexity to the overall insulation system. Penetrations of this type should be grouped

together, if at all possible, during the early stages of vehicle design to simplify installation, enhance reliability, and reduce manufacturing and test costs.

2.3.8 Typical Piping Penetration

The same basic design problems as for the electrical penetration are encountered with pipes or lines. In addition, another was identified which has a significant bearing on the penetration insulation design: pipe movement due to tankage contraction. This is illustrated in Figure 2-11, a scaled layout from the baseline vehicle configuration. It will be noted that any insulation supports must be free to rotate.

Figure 2-12 shows the design for a pipe with a bend in it near the tank. Although it may not always be possible, it is desirable to constrain the vehicle systems piping design to straight runs in the insulated area. A difficult insulation joint in the area of the bend is thereby eliminated.

A fiber glass split shell provides the foundation for insulation attachment. To provide for practical insulation manufacture, it should consist of regular cylinders as shown. Bends should be eliminated. However, a cone could be utilized if desired. A single panel of insulation was selected as with the electrical penetration described above.

Insulation removal and replacement under field conditions is particularly important with piping penetrations as valves may require pad replacement. This is readily accomplished with the design shown. Insulation can be readily removed and the fiber glass split shell dismantled.

Although not shown, the cavity requires purging. Inlet and outlet tubes can be attached to the pipe and routed through the foam collar.

2.3.9 Purge Containment System

A system will be required to contain the helium purge gas during prelaunch ground hold. It must open at a nominal positive pressure, such as 0.5 psi, after launch.

The design approach for this system is shown in Figure 2-13. The top and bottom dome areas are enclosed with a bag similar to that demonstrated by NASA-MSFC in the past and used in the Phase II, 105-in. tank (Section 8). The vehicle shroud provides sidewall containment. It should be sealed for leaks during vehicle assembly to minimize gas losses on the ground.

Purge bag connection to a typical penetration is also shown. Design consideration must be given to bag movement as it balloons out during pressurization. The bag design shown should provide adequate flexibility. A bellows arrangement can be substituted, however, should tests in the future show that more flexibility is necessary.

A zipper is provided on the penetration to allow for quick field access. Zippers on the forward and aft dome purge bags provide for gas escape after launch. These are of the type demonstrated by MSFC to rip open at 0.5-psi differential pressure. A zipper must also be provided in the top dome for manhole cover access.

2.3.10 Inboard Profile

Figure 2-14 shows schematically the assembled insulation panels and purge gas paths. A detailed purge system design study based upon this typical configuration was accomplished as part of the on-going MDAC IRAD study. As it extended the work described here, a report (Reference 9) was forwarded to NASA.

2.4 INSULATION COMPOSITE CHARACTERISTICS

2.4.1 Insulation Thermal Gradients

As noted above, the temperature distributions expected throughout the insulation were found to be an important consideration for MLI application design. Differential contraction across an insulation panel and the total contraction of panel components must be considered. A typical environment is shown in Figure 2-15.

2.4.2 MLI Composite Material

The baseline design utilized an insulation composite consisting of 25-gage

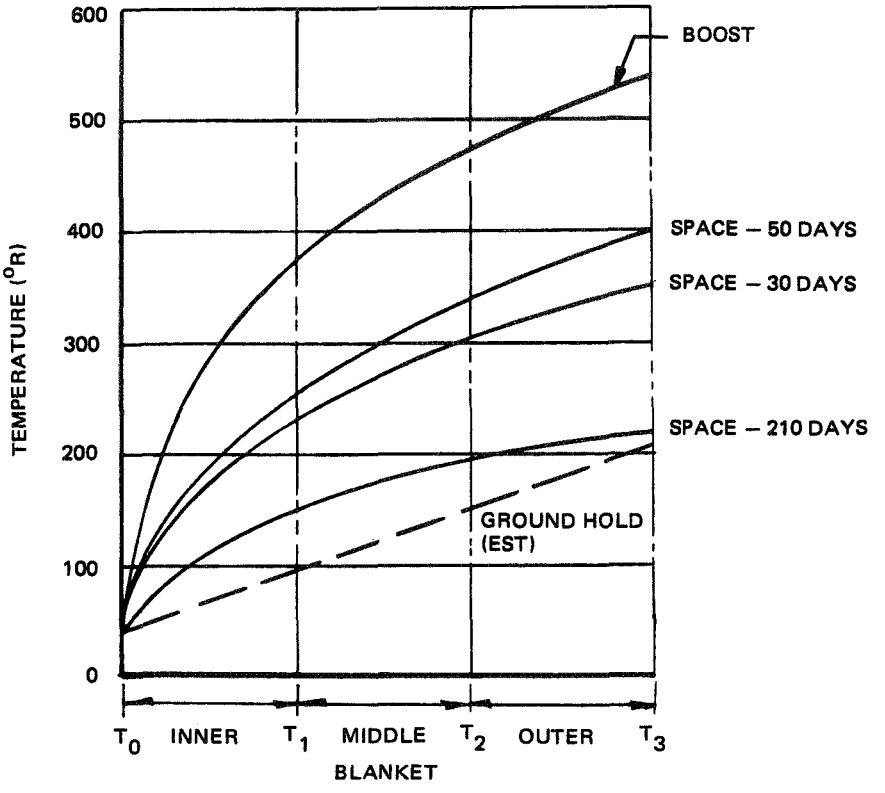

Figure 2-15. Insulation Thermal Gradients

(0.25 mil) double-aluminized Mylar reflectors with a nylon net separator. In this study, 15-gage Mylar was adopted with an attendant weight saving. The nylon net was rejected after a full-thickness panel failed to achieve evacuated equilibrium during test.

A Dacron net, type B2A, produced by Apex Mills, Inc. (49 West 37th St., New York, N.Y.) was selected from the work detailed in Section 5. As no flat-plate calorimeter data were available, thermal performance had to be estimated from the nylon data. This showed that about 70 layer pairs at a density of 96 layers per inch would be needed.

Subsequent work in conjunction with the design of the 105-in. tank insulation, Phase II, showed that a type-B4A Dacron net (same supplier) yields substantially better thermal performance. This was verified by the tank test results, Section 10. The material is recommended for future application (See Appendix A for component procurement data).

2.4.3 Reflector Perforations

A 2.38-percent open area perforation (0.055-in.-diameter holes in a square pattern, 10 holes per square inch) of the reflectors was chosen to aid in postlaunch evacuation. This problem may be more severe than expected on the basis of past joint tests with small (1 in.) overlaps, as large overlaps will be encountered in the MNV dome panels. Also, purge design studies (Reference 9) suggest that forcing helium the full length of the insulation panels is not practical — and a diffusion process (enhanced by perforations) governs the design.

The above perforation configuration is not optimal, but insufficient data were found to perform the necessary tradeoffs. However, Reference 12 shows that the largest holes which should be considered are 1/8 in. for outgassing. Also, evacuation time is reduced by reducing hole size for the same open area, and open area requirements decrease from 0.3 percent with holes smaller than 1/8 in.

Reference 13 indicates that thermal degradation due to holes increases with decreasing hole size or increase in open area. One test point was found (Reference 14), showing a 25-percent heat transfer increase with 1/8-in. holes in a 4-percent open area sample. In the absence of more substantiating data, the compromise pattern noted was specified. Future research and development is recommended.

2.5 HOT GAS PRECONDITIONING

A probable requirement was considered for preconditioning the MLI by passing hot gas through it prior to tank propellant loading. In this manner adsorbed water vapor would be driven off, leading to a much faster attainment of evacuated performance after launch.

No specific procedure was delineated here for the design due to the very limited available test data. However, Reference 12 indicates that hot helium preconditioning will be necessary. Future testing to identify requirements is needed.

The MLI composite used in the design here is compatible with the hot purge, should it be needed. A simple test (Section 5) indicated that the composite will withstand 200°F for one hour. Singly aluminized Mylar appears incompatible as this material curled at a low test temperature.

2.6 THERMAL TEST REQUIREMENTS

Most available thermal data were concentrated in the area of 10-layer samples evaluated on a flat plate calorimeter with LN_2 cold boundary temperature. However, for design, the most significant need is for full-scale component data with LH_2 cold boundary: joints, fasteners, perforations, and composites. With such data, the thermal performance of the entire system could be built up as a summation of heat transfer through the components. Such full-scale component tests applicable to the design of the Phase II test of the MNV MLI system were defined and performed as described in Section 6.

2.7 STRUCTURAL LOADS AND TEST REQUIREMENTS

Launch structural loads, both quasi-static and dynamic, were determined. Tests needed to acquire component sizing data and to demonstrate panel structural integrity were also defined and performed as reported in Section 7.

2.7.1 Quasi-Static Loading

The maximum Saturn acceleration loading, at MECO, is 4.4 g. It is transferred from the MLI layers to fasteners, then to support straps, and finally to the strap attachments anchored to the vehicle structure. The load is greatest in the MNV sidewall panels; other panels are shorter and partially supported.

The only significant loading occurs in each of the sidewall panel support straps which nominally support a 12-in.-wide panel strip, 746 in. long. This results in a load of about 31.6 lb with the design MLI, double-aluminized Mylar (DAM)/Dacron B2A net. Load on the individual insulation layers and fasteners is small. Each fastener carries only 1 sq ft of insulation, 0.51 lb. Fastener shank allowable (0.03-in.-dia nylon) is about 1 lb.

Decompression loading occurs during first-stage burn as the MLI internal pressure lags the rapidly dropping exterior pressure. At fasteners, the MLI tends to billow out and rip, pop off the fastener heads, or fail them in tension. Billowing is inhibited by the outer panels; thus, the most severe load is on the outside sheet. Also, the escaping gas tends to force the panel butt joints apart; again, this is most severe on the outside panel. The decompression loads depend mainly on joint configuration and panel width. Therefore, like acceleration, loads are greatest on sidewall panels as the others taper and thus are generally narrower.

Reference 10 suggests that decompression loads may be very low. A probe located beneath 0.5 in. of DAM/Tissuglas MLI at the center of a 57-in.-wide panel (1-in. joint overlap) yielded a differential pressure (ΔP) of 0.012 psi during a simulated Saturn launch. The same panel on a cold calorimeter (LH_2) yielded a ΔP of 0.0039 psi. Reference 15 reports a measurement of 0.004 psi ΔP on a similar panel installed on a cold (LN_2) calorimeter. Based on these data, the apparently highly conservative value of 0.01 psi ΔP was chosen as the design-test load.

It was concluded that component testing for sizing was needed in the areas of fastener tearout from face sheets, fastener tension and face sheet strength. Joint loads are expected to be very low, hence testing for initial design is unnecessary.

2.7.2 Dynamic Loading

Maximum dynamic loads on the MLI panels occur during launch: they are mechanical shock, engine ignition, and burnout; random vibration; engine and aerodynamic forces; and acoustic loading, and engine and aerodynamic noises transmitted inside the shroud.

Dynamic testing on MLI has been done previously, notably by General Dynamics and the Martin Company. The quantitative test results are not directly applicable to the study design due to different support methods and thinner Mylar used here. Test results indicate that failures, if any, will be due to Mylar tearing at discontinuities such as fasteners or tape. As vibration and acoustic loads normal to the MLI will excite the insulation, it was concluded that dynamic tests should be undertaken.

In the upper stage MNV location, primary excitation is acoustic. Therefore, the tank response to Saturn acoustics defines the mechanical vibration environment of the insulation. It was concluded that proper simulation can be provided by mounting the MLI panel on an aluminum plate, sized so that its maximum vibratory response occurs in the same frequency domain as the maximum acceleration of the MNV tank wall (see Section 7).

Brittleness, which may be a primary cause of failure in the acoustic environment, increases with decreasing temperature. Therefore, low temperature testing is necessary for conservative results. Temperatures corresponding to LN_2 were chosen for dynamic testing in this study. The high cost of testing at lower temperatures (LH_2) precludes consideration for all but final MNV design verification.

Section 3
MANUFACTURING METHODS DEVELOPMENT

The goal of this effort was to develop manufacturing methods needed for the design and fabrication of the MNV MLI system. Problems addressed were MLI stack thickness measurement methods, stack minimum practical layup density, manufacture of panels with repeatable density, effect of fastener installation on density, panel manufacturing procedures, tooling, and buckling of double-curvature panels. The work culminated in the fabrication of full-scale MNV dome and sidewall demonstration panels and a manufacturing plan for the MNV insulation system. Adaptability of fabrication to automation was also considered. This work, along with component development (Section 4), provided the technical foundation for the fabrication of the Phase II 105-in. tank insulation system (Section 9).

3.1 MLI THICKNESS MEASUREMENT GAGE

A highly accurate gage was developed for measuring the thickness of MLI stacks to determine stack (panel) density, the key thermal performance parameter. No suitable technique was previously available. This gage was used for stack density studies and measurements of assembled panel thickness. It can be readily adapted for use as a production acceptance test device.

The gage is based upon the electrical conductivity of the metallized MLI reflectors. A measuring probe and the stack top reflector sheet are connected electrically through a battery and ohmmeter. The instant of probe-sheet contact is immediately registered on the meter. This electrical approach has the advantage that a true measurement is made, and that no crushing of the stack occurs as the measurement is taken.

The device used in the program consisted of a micrometer depth gage mounted at a fixed height above a measuring surface. Lowering the micrometer probe to the surface of an insulation stack on the table yielded the measurement of stack thickness.

3.2 METHOD FOR FORMING ASSEMBLY FASTENER HOLES

Insertion of the panel assembly fasteners requires forming a hole through the entire stack of reflectors, separators, and face sheets comprising the panel. Three methods were tried for forming these holes: punching with a common punch, punching with a hypodermic needle, and drilling with a hollow tubular drill. The latter was selected.

Punching was tedious and clumsy. The hypodermic needle failed to punch a circular hole. Inspection showed that no material was removed from the Mylar reflectors; a tab remained which provided a large area heat short between the reflector and fastener. But, the drill completely removed a circular piece of the reflector. Also, it could be readily located on the panel surface with a simple jig indexed to the layup tool.

The drill used consisted of an air motor with a tubular steel bit sharpened to cutting edge. A foam block was held behind the MLI stack being drilled to provide a backup surface. Material stacks were disassembled after the hole-forming operation and examined for tearing of the reflectors. None was observed with either the drilling or punching methods.

3.3 EFFECT OF FASTENER INSTALLATION ON PANEL DENSITY

The effect on stack density of inserting assembly fasteners in the MLI stack was investigated to provide information for selecting fastener spacing. Thickness measurements of full-scale-thickness, 4- by 5-ft panels were made before and after inserting fasteners on 24, 12-, and 6-in. centers. No statistically significant change was observed. Measurements were made on panels constructed of nine different MLI composite materials (Subsection 3.6).

3.4 TECHNIQUE FOR REPEATABLE DENSITY MANUFACTURE

A technique was defined for manufacturing MLI panels to a predictable reproducible density, one of the most significant problems encountered in past MLI application. Different fabricators, using identical materials, always produced similar panels but all with a different density, hence, thermal performance.

Only one approach could be identified that always produced MLI panels with a known fixed density; i. e., slightly compress the stack of sheets to a design density value. As long as the design density is equal to the expected average natural layup density, absolute uniformity and repeatability result. Note that material stacks which for some reason are initially thinner than the design density must be discarded or restacked. A small thermal performance degradation is incurred due to the compression step, as some panel stacks will initially be less dense than the average.

The compression step is required only if a known density or thermal performance is desired. If only a known minimum performance level is required, compression can be eliminated, as this minimum corresponds to the selected design density. However, it is clear that many panels in a given production run will exhibit better performance than the minimum.

A survey of current MLI users for propellant tank application indicated that a minimum known performance was all that was required. The compression step was therefore eliminated from the study panel manufacturing requirements. However, flat and cylindrical panels of various materials were built to demonstrate the controlled density fabrication technique.

Flat or contour panels may be fabricated to a controlled density in a straightforward manner. A layup tool is used for stacking the MLI layers. A cover with edge-mounted spacers bridging the MLI stack is placed over the MLI on the layup surface. The resulting stack density under the cover is defined by the height of the spacers.

Fabrication of controlled-density cylindrical panels is more difficult. But a technique was developed, demonstrated, and used for calorimeter test samples. It is detailed in Section 6.

3. 5 MINIMUM PRACTICAL MLI LAYUP DENSITY

Two methods were defined for numerically determining the minimum practical layup density of an MLI composite material. In past efforts, the magnitude of this important parameter was based on shop experience, an

approach resulting in controversy as one shop generally disagreed with another. A different approach, measurement and statistical analysis, was used here to quantify the density which could be expected within a given stack of insulation. Although this method was successful, its application is time-consuming and requires examination of a large amount of MLI material, often not available for a new composite. Therefore, an empirical method based upon compression test data and densities obtained in prior panel fabrications was also delineated.

3.5.1 Statistical Approach

Nine thickness measurements were made on each of five 2- by 4-ft stacks of 12 candidate MLI composite materials considered in the study (Section 5). Because thickness distribution curves vary with the number of sheets in a panel, the measurements were repeated for each of three different numbers of sheets for each composite system. Details and measurement data are presented in References 4 and 5.

It was observed that data scatter was greatest with a small number (10) of sheets in a stack. However, as the number of sheets was increased, a more uniform density was achieved. Typical plots of composite layer density generated by NASA (TMX-64561, Nov. 71) from the measurement data in the previously referenced reports are shown in Figure 3-1. Curves for any of the 12 composites measured may be constructed in a similar manner, if desired.

There is no one minimum density. Stack thickness varies as a function of a statistical distribution curve. Also, expected stack thickness is a function of the number of sheets in the stack. This is why different investigators have been obtaining different density numbers for the same material. It is clear that for any selected value of density, some stacks can be expected to be more dense and others less.

If repeatable or minimum guaranteed thermal performance is to be achieved, a maximum acceptable layer density must first be selected. Then, during

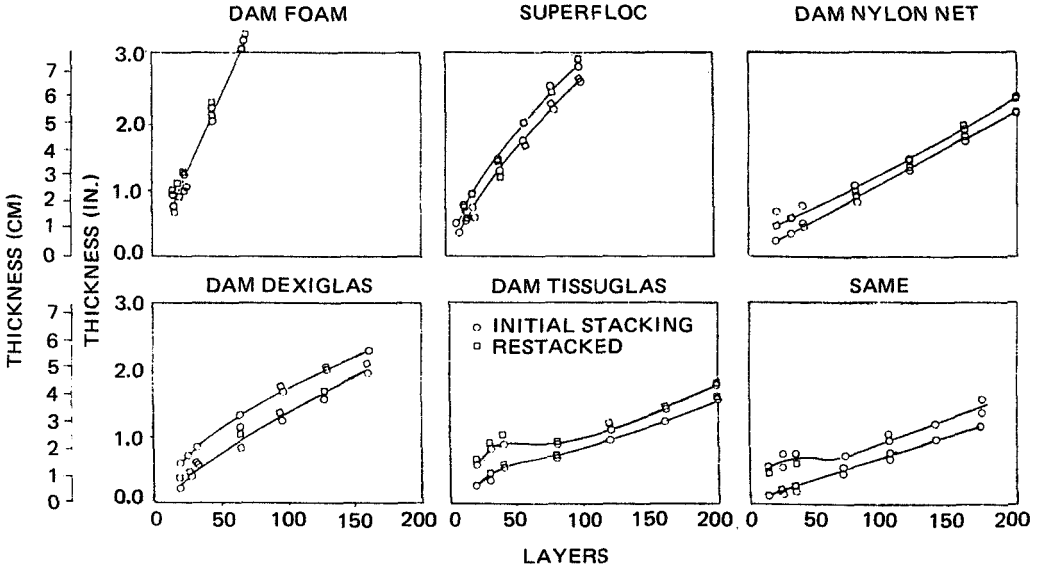

Figure 3-1. MLI Layer Density Characteristics

fabrication, all layups (stacks) that are found to be too thin (higher density) must be rejected. Measurements showed that random restacking of a rejected high-density layup will usually result in a density decrease to an acceptable value.

Selection of the maximum acceptable or design density value poses a problem. If too low, a high number of layups will be found as unacceptably dense. If too high, the thermal performance will be unduly penalized. In this study, the design or maximum acceptable density value adopted was the density at which only 25 percent of layups would be expected to be too dense or unacceptable.

3.5.2 Compression Test Approach

Application of the above method to a new, unknown, composite material requires numerous measurements to be made on panel stacks followed by a statistical analysis of the data. Frequently, insufficient material will be

available to develop the density relationship. Therefore, available data was examined to ascertain if an empirical approximate relationship could be defined.

A suitable relationship was found by correlating MLI sample compression test data (Section 5) with the postassembly thicknesses measured on the 4- by 5-ft panels constructed in the study (Section 3.6). It was found that all finished panels exhibited a density equal to or greater than that observed on a 20-layer sample under a 1.3×10^{-4} psi load. The average corresponded to a 2.5×10^{-4} psi load, a value adopted here as the minimum design density definition criterion.

A check test performed during the Phase II insulation fabrication showed this criterion to be reasonably valid. The density of a compression test sample was measured at a 2.5×10^{-4} psi load. This was found to be in good correlation with densities being measured on the completed 105-in. tank gore panels.

3.6 FABRICATION OF TYPICAL FLAT PANELS

One 4- by 5-ft panel of each of nine candidate MLI composites (Table 3-1 and Section 5), were fabricated. This effort had three objectives:

A. Quantitatively evaluate the effect of fastener insertion on panel density.
B. Demonstrate tooling and density control fabrication concepts.
C. Provide fabricability data for subsequent fabricability ranking of the composites.

Panels were assembled with nylon heat-set fasteners and the plain Dacron net face sheets suggested in the baseline design. Panel thickness surveys were made (References 4 and 5) and notes on fabrication time and the fabricability of each system were compiled.

It was observed that the plain net face sheet provided some protection for handling only. But, possessing no rigidity, it failed to provide stability to the panel package. This led to the development of the reinforced face sheet adopted for the study design. These were subsequently found to be a substantial improvement.

Table 3-1

PANEL CONFIGURATION CHARACTERISTICS

Insulation System	Density (layer/in.)	Reflector Sheets	Design Thickness (in.)	Measured Thickness (in.)	Deviation (%)
Superfloc	33	33	0.33	0.38	+15
Double-aluminized Mylar (DAM)-foam	22	72	0.81	0.86	+ 6
DAM-nylon net	90	63	0.22	0.28	+27
DAM (embossed)-Tissuglas	76	60	0.25	0.34	+36
SAME	128	216	0.42	0.37	-12
DAM-Tissuglas	81	34	0.20	0.21	+ 5
DAM Dexiglas	70	54	0.24	0.28	+17
15-gage NRC	136	268	0.49	0.38	-22
CDAM-nylon net	52	36	0.23	0.23	0

As noted in Section 3.2, no statistically significant density changes due to fastener insertion on 6, 12, or 24 in. centers was observed. Also, the density control fabrication concept was satisfactorily demonstrated. As shown in Table 3-1, only the single aluminized embossed Mylar (SAME) and the 15-gage NRC-2 panels were too dense. All others (15-gage reflectors) would have exhibited a thermal performance equal to or better than the design value.

The embossed Mylar material exhibited a change in height of the embossed pattern throughout the material used in the panel, the probable cause of the fabricated panel being too thin. Also, a tendency for the embossed layers to nest within each other was noted. No explanation was found for the NRC-2 out-of-tolerance panel. It is possible that the sheets were pulled too tight on layup (eliminating wrinkles) prior to being taped in place. Observation later indicated that this will cause high-density panels.

The tooling designed for this fabrication task turned out to be the prototype of all fabrication tooling used subsequently in the program. The primary

item was a layup surface containing through-holes at fastener installation points. Drill guides inserted in these holes located the fastener drill hole. A matching cover plate, held off from the layup surface with spacers, was also used here to control the finished panel density. Holes at fastener points in this plate provided the access required for forming the fastener heat-sealed head.

3.7 FABRICATION OF FULL-SCALE MNV INSULATION PANELS

Two full-size MLI panels, a dome gore, and a sidewall were built to evaluate the fabricability of the MNV insulation design (Section 2). The completed panels are shown in Figures 3-2 and 3-3, installed on wooden tank mockup sections which have been elevated to simulate panel mounting on the actual tank. This work indicated that the design configurations were practical from manufacturing and installation standpoints.

The mockup fixtures were constructed using a wood frame with a 1/16-in.-thick birch plywood sheet covering. As shown, the dome is a pie-shaped

CR94
N/A

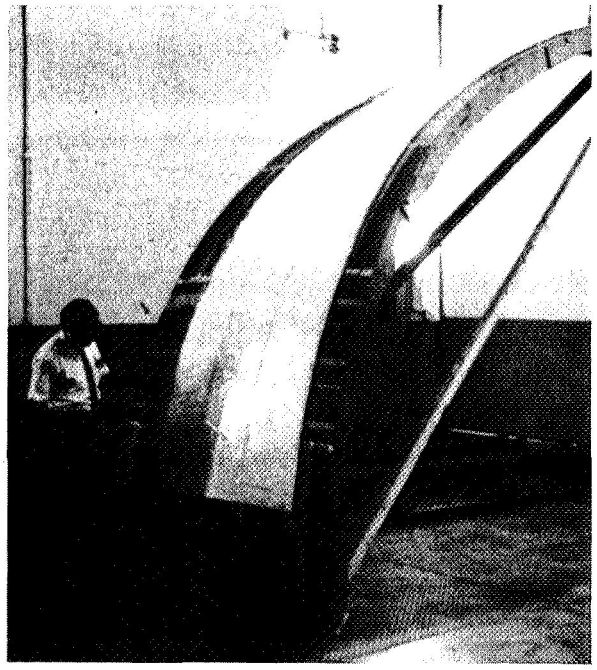

Figure 3-2. Assembled Dome Insulation Panel

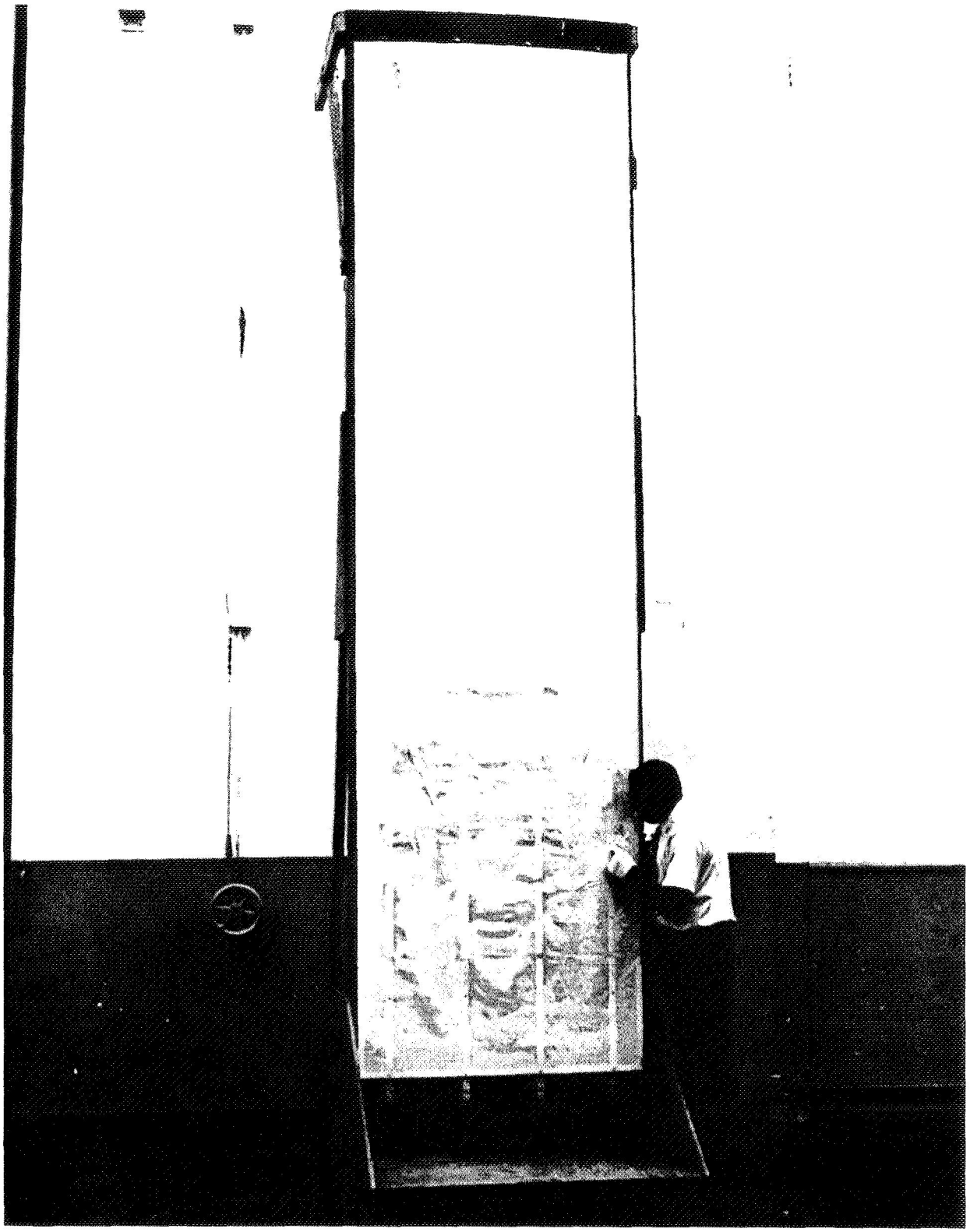

Figure 3-3. Completed Sidewall Panel

segment with the dimensions of a 33-ft-diameter, $\sqrt{2}$ ellipse. The sidewall has the same diameter curvature. These units provided the cutting and layup surface needed for insulation fabrication as well as the proper tank shape for panel attachment.

It was desirable to cut pie-shaped darts in the reflector sheets so that they would lie relatively flat without material bunching on the double-curvature dome mockup surface. Reflector fit with and without darts is shown in Figures 3-4 and 3-5, respectively. Reflector sheet cut patterns were staggered on adjacent sheets to avoid any possibility of direct optical paths through the finished insulation panel. Separator and face sheet net materials fit satisfactorily without the cuts. The need for these cutouts can be eliminated if panels are narrowed or bunching is accepted. Both alternatives affect the thermal performance magnitude and predictability.

As these panels were constructed with the goal of achieving a known finished density, fiber glass cover templates were constructed for both the sidewall and dome mockup fixtures. These were reinforced fiber glass washes laid up on the plywood mockups (Figure 3-6). They had two purposes:

A. To reduce the insulation stack to a thickness corresponding to the design density and hold it while the fasteners were installed.
B. To locate the panel fasteners and attachments.

The templates were fitted over the stack of insulation sheets and held up at the design height with edge spacers.

The insulation panels were constructed of 35 pairs of 15-gage double-aluminized Mylar with a Dacron net B2A separator at a density of 96 layer pairs per inch. The fabrication steps delineated in the MNV manufacturing plan (Section 3.7) were used. Reflector dart cutouts were closed with small overlaps, ranging from 0.03 to 0.08 in. Construction details were per the design drawings (Section 2).

The single-survature sidewall panels were fabricated on a curved layup surface. However, these panels, with their extremely large radius of curvature, can be fabricated flat and then installed on the curved tank surface.

CR94
N/A

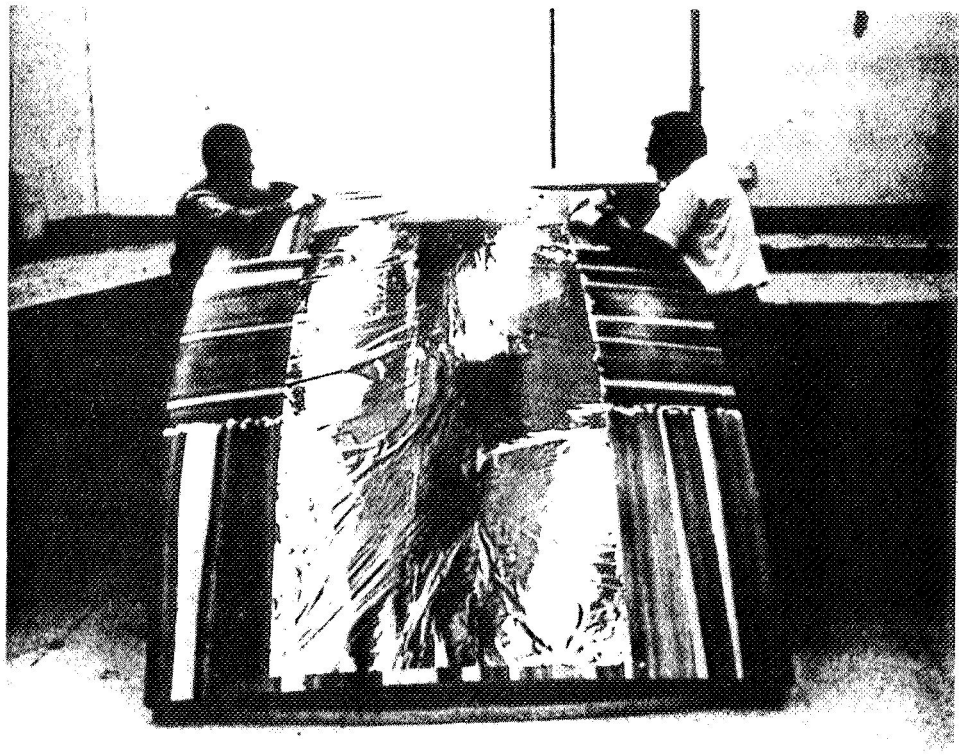

Figure 3-4. Insulation Sheet Fit at Lower Edge of Top Dome

CR94
N/A

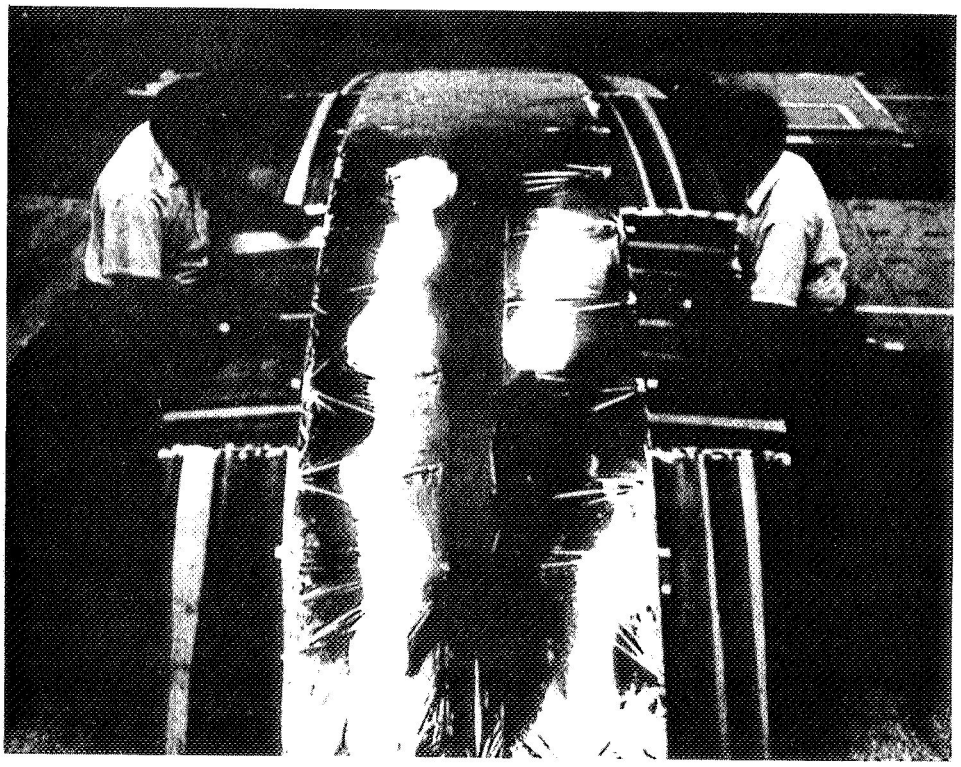

Figure 3-5. Contour Fit — Dome Insulation Sheet

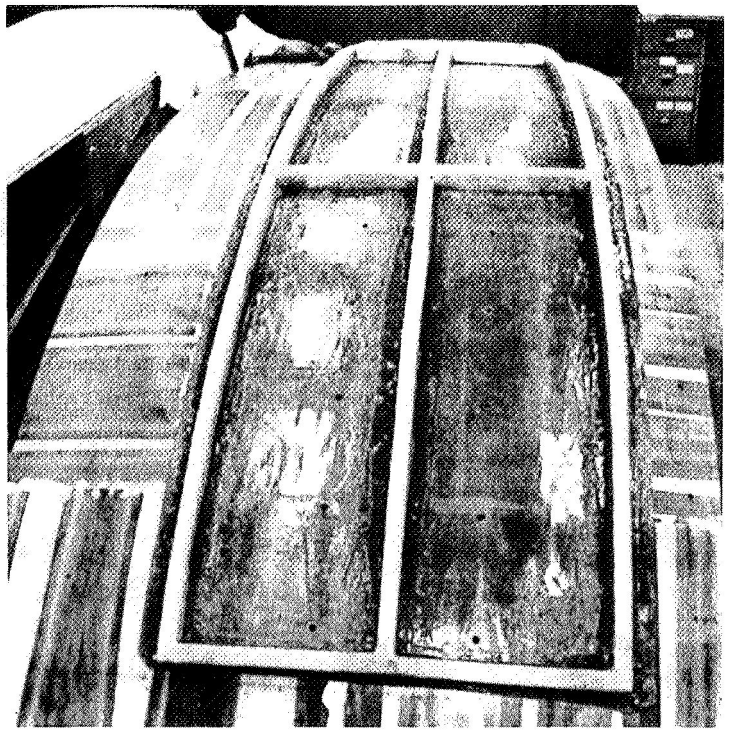

Figure 3-6. Dome Section Tooling

This was shown by a small test panel, 4 by 2 ft by 0.5 in. thick, which was built flat with fasteners on 12-in. centers. No tearing at fasteners or bunching was noted upon installation on the curved sidewall mockup.

Stacking of the insulation layers must be accomplished carefully. Each sheet must be taped down in the selvage area to prevent movement. However, there is a tendency for assembly personnel to pull out the wrinkles and tape down firmly. This compresses the stack, increasing finished density.

A metal guide for knife trimming was also found to be necessary. A tendency for blade run-out was experienced with paper and plastic guides.

3.8 MNV INSULATION SYSTEM MANUFACTURING PLAN

A conceptual manufacturing plan for implementing the MNV insulation system design was defined. As the MNV vehicle configuration itself was in a continuing process of change and evolution, a firm MLI plan was unwarranted. Therefore, the plan prepared in the study was designed to

serve as a foundation for the documentation required in the eventual vehicle hardware fabrication phase.

The plan, published in detail as Appendix B of Reference 6, is divided into four major categories - materials, panel fabrication procedures, installation procedures, and related requirements. Included are:

A. Material type, quantity, purchase requirements, and quality assurance tests.
B. Fabrication sequence and procedures for each of the 11 types of panels used in the system.
C. Installation sequence and procedure, and repair procedures.
D. Tooling, manpower, skills, and facilities requirements.

Suggested quality assurance provisions are included in each area where required. The basic plan is essentially insensitive to changes in specific MLI reflector and separator materials; therefore, it will not be invalidated should new materials be considered in future work.

Although the plan is too voluminous for inclusion here, several points should be mentioned. Table 3-2 shows the panel fabrication requirements. Note that flat, single curvature, and compound curvature panel fabrications will be encountered in a typical vehicle system. Face sheet fabrication operations are illustrated in Figure 3-7. Figure 3-8 shows a typical panel fabrication sequence. Panel installation on the vehicle tank is shown in Figure 3-9. Note here that the vehicle assembly sequence is dependent upon the MLI installation sequence. This will probably be encountered in most other vehicle installations, also.

3.9 AUTOMATION OF MLI PANEL MANUFACTURE

The fabrication procedures developed for the manufacturing plan and demonstration panel assembly were reviewed to determine the feasibility of automation. Automation would produce its usual benefits—better quality, uniformity, and potential for highly economical manufacture.

Table 3-2

MNV INSULATION PANEL FABRICATION REQUIREMENTS

Type of Insulation Panel	Fabrication Requirements								
	Face Sheets			Joints		Assembly Surface			
	Lacing	Load Tabs	Slack Straps	Butt	Ship-lap	Compound Curvature	Single Curvature	Flat	Contour Cuts
Forward Dome	X	X	X	X		X			X
Manhole Cover	X			X				X	
Tank Support–Inner	X	X	X	X				X	
Tank Support–Outer	X	X	X	X				X	
Sidewall	X	X	X	X				X	
Upper Aft Dome	X	X	X	X		X			X
Lower Aft Dome	X	X	X	X		X			
Thrust Cone	X	X	X	X			X		
Engine Feedline	X	X			X			X	
Piping Penetration	X	X			X			X	
Electrical Penetration	X	X			X			X	

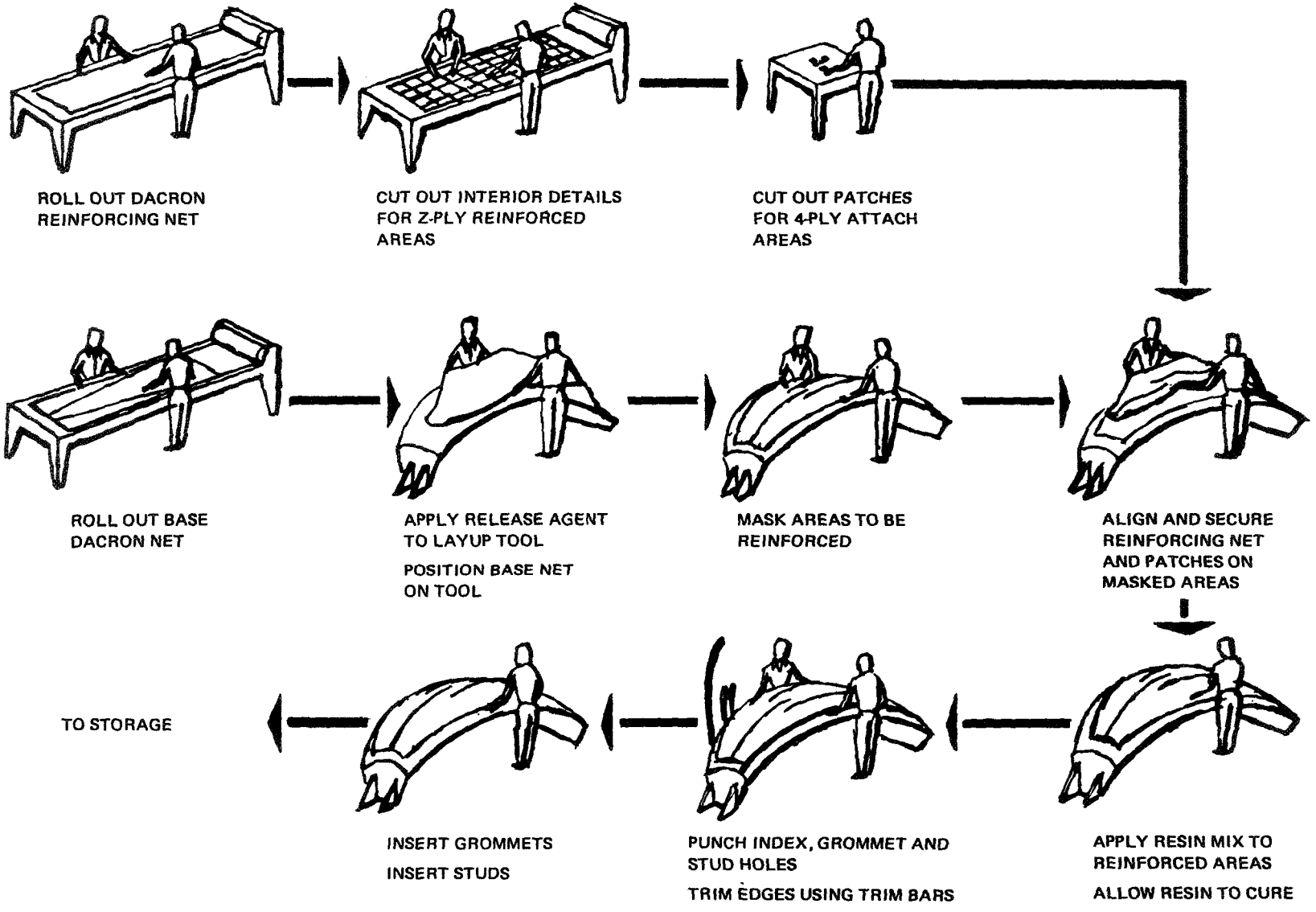

Figure 3-7. Bottom Face Sheet Fabrication – Forward Dome

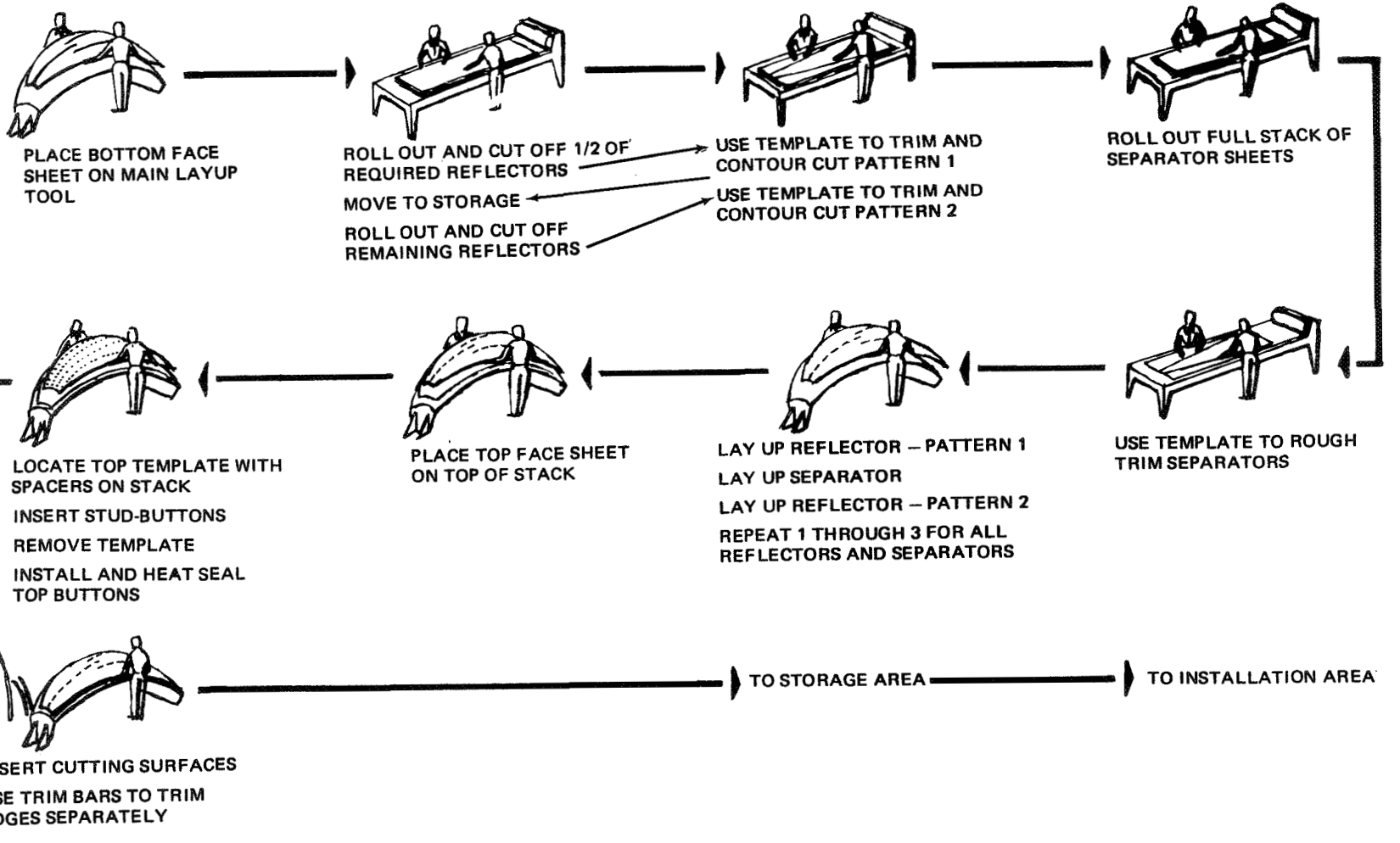

Figure 3-8. Insulation Panel Fabrication Sequence – Forward Dome

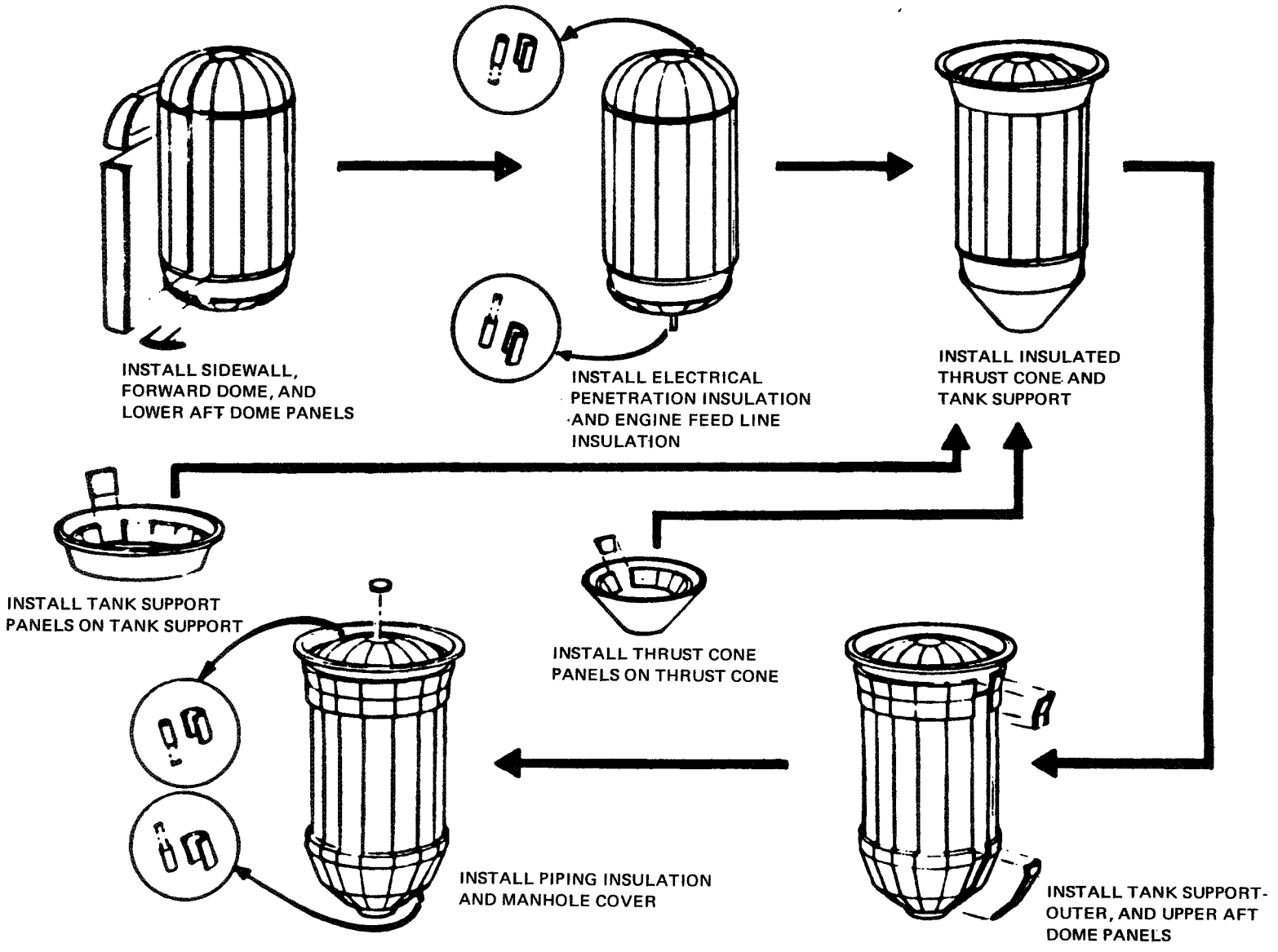

Figure 3-9. Panel Installation Sequence

The potential automation areas which were identified, along with possible methods of accomplishment are:

A. Automated material feeds from rolls mounted on tracks, either hand- or power-driven.

B. Automated rough trim of material stacks using powered cutting tools.

C. Precontoured materials for areas requiring contour cuts. Probably not feasible for reflector materials due to degradation of emittance, but possible for separator components. Involves cost tradeoffs of tooling, storage, and transport versus labor and schedule reduction.

D. Automatic, powered hole punching for fastener insertion including trunnion aids for fastener installation.

E. Automated transfer of completed panels from the fabrication area to a storage area and from storage to installation position.

F. Semiautomated tooling to speed up installation of lacing hooks and other hardware on face sheets.

Section 4

INSULATION SYSTEM COMPONENT DEVELOPMENT

An extensive effort was made during the MNV insulation design study to develop needed details of the MLI system components. These consisted of parts of the prefabricated panel packages, key element of the design. The work was directed toward defining methods for assembling and mounting the MLI composite, as these factors are the keys to achieving maximum practical MLI thermal performance. Structural integrity of the installed MLI throughout launch must first be achieved. Efficient thermal performance is a constraint which must be applied to the structural design.

The work described here included design, fabrication development, and test in the areas of: panel assembly fasteners, face sheet reinforcement materials, attachments, joints and joint closure, and, panel edge fasteners. Results were included in the design. The results of a parallel MDAC IRAD program were also used where applicable and are reported here for reference.

4.1 PANEL ASSEMBLY FASTENERS

Fasteners which penetrate the insulation stack and hold it together are the key to assembling the loose MLI sheets into a structurally sound panel package. These fasteners should be made of a low thermal conductivity material and have a minimum cross-sectional area consistent with shear and decompression tensile loads. Also, ease of installation is mandatory.

The study baseline fastener design, Figure 4-1A, was evaluated along with others. A heat-set head type (like a rivet), Figure 4-1B, was developed. To facilitate manufacture, a commercially available injection molded nylon fastener, Swifttach (Appendix A) was ultimately selected for use on the Phase II 105-in. tank insulation assembly. The baseline fastener material, Zytel 101 nylon, was adopted.

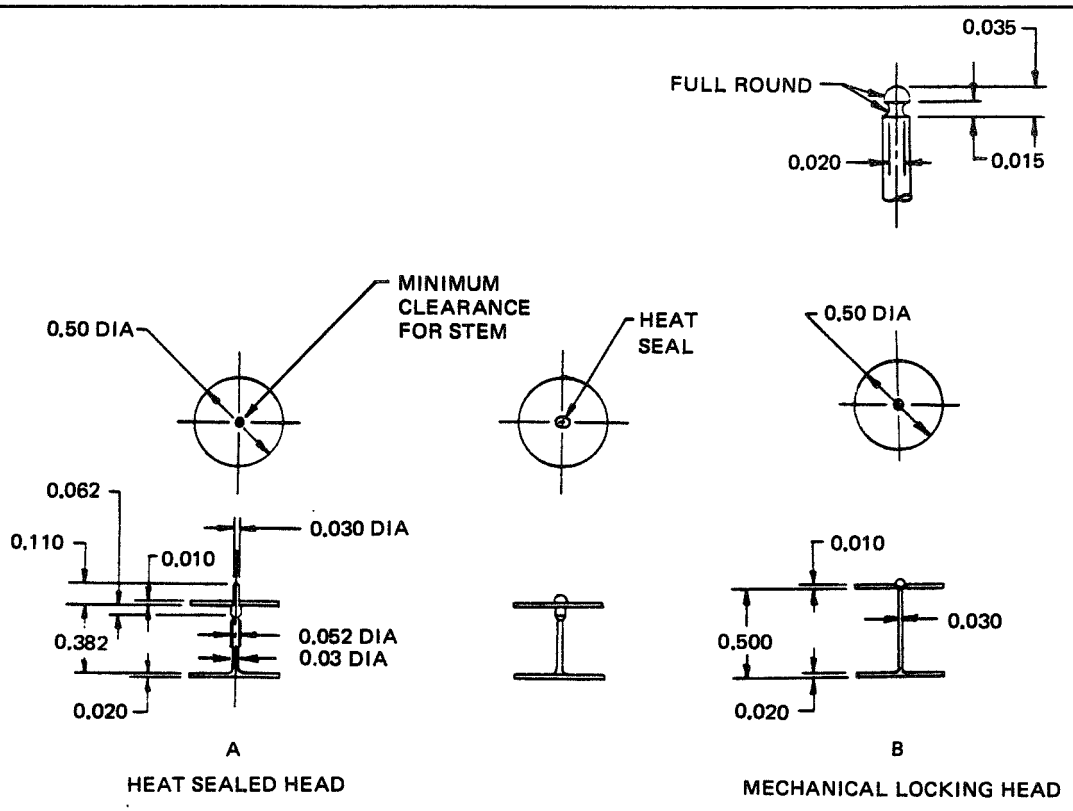

Figure 4-1. Fasteners

4.1.1 Evaluation of Fastener Configurations

The baseline mechanical-locking fastener is a two-piece unit: a stem with an integral head and a loose washer which is assembled to the other end of the stem. This fastener requires a heavy stem (or a clamping extension as in cherry rivets) to allow the end button to be snapped in place. Pressing the button in place bends the stem, tending to tear the MLI. A clamping stem, when cut off, tends to leave a sharp edge, catching and tearing the MLI panel mounted above it.

Other potential fastener configurations were postulated and qualitatively evaluated (Reference 2). This exercise was constrained to two-piece designs (methods of attaching a button head to a slender stem). Only fasteners which could be installed with a minimum perturbation to the insulation were considered.

The heat-seal head type subsequently selected for design requires melting the stem to form a bead, like an upset rivet, which holds the loose button or washer in place. This fastener concept worked out well in experimental

shop fabrications of MLI panels using the melting techniques described below. However, difficulties in achieving satisfactory quality uniformity during production assembly were encountered.

A search for a simpler, faster-assembling fastener resulted in the selection of a one-piece nylon injection-molded fastener, Swifttach. This item is shaped like the letter I and is inserted through an MLI stack with a special insertion tool supplied by the fastener manufacturer. Quality control of installed fasteners was better. However, heating was required to prevent the top and bottom pieces from cracking as they were bent for insertion through a hole in the panel. Testing showed that the load-carrying ability of these items was adequate when properly installed (Section 7). A change of material should eliminate the tendency to crack upon installation.

None of the fasteners tried was believed to be fully satisfactory. Therefore, further development effort in this area is recommended.

4.1.2 Fastener Material

Mechanical and heat-set head fasteners were injection-molded of Zytel 101 nylon as recommended in the baseline design. No reason for changing material was apparent. It was found that nylon will show some strength deterioration after exposure to the MNV radiation environment; however, loads during engine operation will be low. Maximum loading occurs during vehicle launch, prior to engine operation.

A mold furnished by NASA-MSFC (Plastic mold 5502680-48EV) was used to fabricate both fastener types. The dual-cavity mold has four inserts which produce the locking fastener with various-length shanks; any fastener shape can be made by changing inserts. Molding of the heat-sealed type required fabrication of one new insert and modifications to another.

4.1.3 Fastener Heat-Sealing Methodology

A test program (Reference 3) resulted in a method of forming an acceptable heat seal, melting the fastener shank over a 0.010-in.-thick washer, using

a modified soldering iron. In a production environment, it was found that there was a tendency for nylon to adhere to the iron, leaving insufficient material to form a seal.

A simple radiant heating tool, which never contacts the work, solved the problem. A fully developed fillet 0.05 to 0.06 in. in diameter was consistently formed.

The tool consisted of a doubled length of high-temperature heating element wire with three coils at the end to concentrate the heat, a resistor in parallel with the element, and a variable power supply. At 10 v the element became white hot and the heat seal formed readily without actual contact. The resistor limited temperatures in other wires of the circuit.

4.1.4 Washer Fabrication Method

It was determined that the thin nylon washers used on the fasteners should be formed by punching with a die. This method yielded increased strength and lent itself to quantity production with precise dimensional control.

Early in the program washers were drilled for the stem. Centering was difficult and the drilling frequently resulted in an oversize hole with a burr. Also, strength tests (Section 7) showed the punched washer to be superior. These tests also indicated that the punched washer was mandatory to achieve strength uniformity of a mechanical head fastener with its interference fit between washer and fastener stem.

A punch and die set was built. It worked well with 0.030-in.-diameter holes in 0.010-in. nylon sheet. Punching of thicker sheet requires an increase in the center hole diameter.

4.1.5 Fastener Dimensions

The heat-set fastener dimensions (Figure 4-1) were adopted, although changes in the baseline configuration's shank and stem end were needed. These changes were defined through test (Reference 3).

An 0.03-in.-diameter stem was found to be satisfactory. Tests (Section 7) showed that this size fastener mounted on an MLI panel, 0.22-in.-thick, could carry an average shear load of 11.5 lb. Design ultimate (Section 5) for the MNV panels was 0.5 lb. Minimum required stem height above the washer prior to melting was determined to be 0.09 in. The 10-mil nylon washer was adopted, as no strength difference was noted with a thicker one.

Tensile and pullout tests were performed for mechanical locking, heat-set, and Swifttach fasteners. The latter two met the design requirements as discussed in Section 7.

4.2 PANEL FACE SHEETS

A design evaluation of MLI assembly concepts indicated the desirability of building load-carrying members and some stiffness into the individual panel face sheets. This was a significant change from the plain Dacron net with separate Dacron ribbon straps suggested in the baseline design.

Separate Dacron webbing load-carrying straps were found to be inadequate. Measurement of the expansion coefficient of typical Dacron cloth indicated that it did not shrink as much as the aluminized Mylar reflectors. Therefore, upon chilling, load would be carried by the Mylar rather than by the straps.

Impregnating the plain face sheet net with plastic resin, forming reinforcement strips, appeared attractive and was subsequently developed. Many MLI panels with epoxy-resin-reinforced face sheets were built during the course of the program. A less heavy and costly method, heat-set Mylar tape reinforcing, was developed later on IRAD studies and adopted for use in the program. Both approaches work satisfactorily, but the latter is recommended.

4.2.1 Resin-Reinforced Face Sheets

The basic net substrate material was adopted from the baseline design. This was a Dacron net, with a scoured and heat-set finish (See Appendix A for specifications). In the reinforced areas, two layers were used.

Three resins were evaluated: liquid epoxy, ERL 2795; liquid polyurethane, EC 3515; and a film epoxy-nylon, FM-100. The film resin was abandoned after several unsuccessful attempts to apply it. The liquid resins, mixed with normal curing agents, were applied with a brush resulting in nonuniform distribution and voids. A rubber squeegee application was then adopted.

The EC3515 was difficult to spread at a consistency of 100 percent solids, and with 80 percent solids the layups showed many voids after cure. The ERL 2795 mixed 5 to 1 worked out well and was adopted, although it is somewhat more brittle than EC3515.

Thermal expansion coefficients of the ERL 2795-impregnated net showed that it would contract slightly faster than the Mylar reflectors for all temperatures encountered in the MNV insulation. Contraction and strength data are presented in Section 7.

Four initial demonstration face sheets were built and subsequently assembled into 4- by 5-ft insulation panels. Dacron net substrate sheets were laid out on a work surface covered with plastic film, and resin boundaries masked with tape. Resin was worked into the masked areas. A room temperature cure and tape removal completed the process.

It was not found necessary to press the layups during cure to keep them flat. However, resin migration beyond the masked edges (about 3/16 in., average) was a problem. The preventive measures tried included vacuum bagging to apply pressure to tape prior to resin application, use of Mylar tape, paper tape, and paraffin instead of tape. None was more successful than simple masking with paper tape.

4.2.2 Tape-Reinforced Face Sheet

In this concept, iron-on Mylar tape with thermosetting adhesive was substituted for the epoxy-resin-impregnated strips. The tape, Schjel-Bond GT-400 (Appendix A) was 5-mil Mylar coated on both sides with a 1.5-mil adhesive coating. Application consisted of applying a flat, Teflon-coated iron to the face sheet (Dacron net, tape, net sandwich). The iron (about 300°F) was applied briefly until the adhesive flowed.

Thermal contraction characteristics were measured (Section 7). Results show the tape approach superior; contraction is greater than Mylar yet less than the epoxy straps. The tape can also be used for above-ambient temperature applications. A significant weight saving over the epoxy straps resulted.

4.2.3 Configuration of Reinforced Areas

The reinforcement configuration adopted in the study was shown in the Section 2 design drawings. A 1-in.-wide strip around the panel edges provides stiffness and a hard point for edge fastener attachment. The load-carrying straps, 1 in. wide, are continuous on the coldest side of the panel (greatest shrinkage) to carry the panel loads. On the warm side, the straps are interrupted to allow for buckling as the panel shrinks. All through-assembly fasteners are located in reinforced areas, providing maximum resistance to pull-through under decompression loads.

4.2.4 Fastener Tearout Resistance

Decompression load tests (Section 7) were accomplished to ascertain the minimum face sheet strength to prevent tearing over the 0.5-in.-diameter assembly fastener heads. A 15-gage Mylar sheet alone was determined to be insufficient, but 25-gage Mylar was adequate. Therefore, the separate reinforced net concept adopted for acceleration load transfer and stiffness has far more strength than needed for decompression loads.

4.3 PANEL-TO-PANEL JOINT CLOSURE

Several possible methods of joint closure were suggested in the baseline design although none were recommended. These and other alternatives were evaluated, and a continuous-laced joint closure on the panel outer surface with Velcro tabs across discrete inner surface points was selected. Small, full-thickness panels were constructed to aid in selection. Further development in this area is recommended.

A number of potential concepts were defined: Teflon tabs, Dacron net sewed together, Dacron net bonded together, Velcro tabs, lacing zippers, a "bicycle chain link" between panels, and snap tabs.

Using typical 4-by-5-ft panels it was found that attachment only at discrete separate points was inadequate. Panels buckled between attachments. A continuous or semicontinuous closure was needed at least on the panel outer surface. Through fasteners near the joint edge were also needed to pull all panel sheets uniformly to the joint.

Sewing was considered impractical as it must be done with panels on the tank. Bonding poses a similar problem, in addition to providing a gas barrier directly over the joint, a point where easy gas escape is desirable. Lacing across closely spaced points was adopted.

A test joint on the 15-in. calorimeter suggested that lacing the outer surface with no cross tie on the inner would be sufficient. However, large-scale panels on the 105-in. tank showed this to be inadequate. Inner surface closure is needed but may be applied at discrete, rather widely spaced points. Velcro appears better than the other approach considered, snap tabs.

Two 18-in.-square panels were built to evaluate fastening methods. Four types of edge fasteners were installed: eyelets and lacing, hooks and lacing, snaps, and Velcro tabs. An improvement over the eyelets and hooks was subsequently adopted. This is a thin, 0.010-in.-thick, 1/2-in.-diameter nylon washer attached at its center to the face sheet with a small brass grommet (Figure 4-2). The lacing thread slips under the washer (Figure 4-3). A flat installation which will not catch any panel layer installed above it results.

Nylon thread was originally used for lacing but it was found to stretch. Teflon-coated glass, Tefglas (Section 9), circumvented the problem and was adopted.

4.4 STEPPED BUTT JOINT

The feasibility of fabricating a stepped butt or shiplap joint was evaluated for application to the insulation panels placed over fiber glass covers on the vehicle piping. Here the complexity of multiple panel layers may be avoided as through fasteners do not introduce an intolerable heat-short problem.

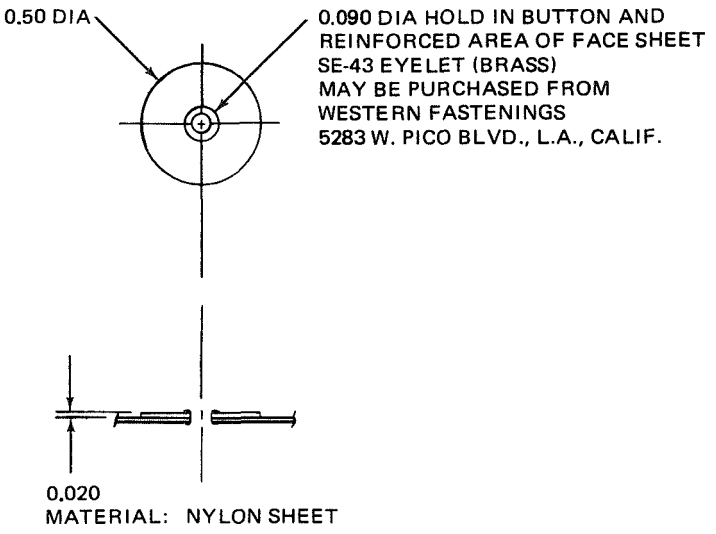

Figure 4-2. Lacing-Button Details

R94

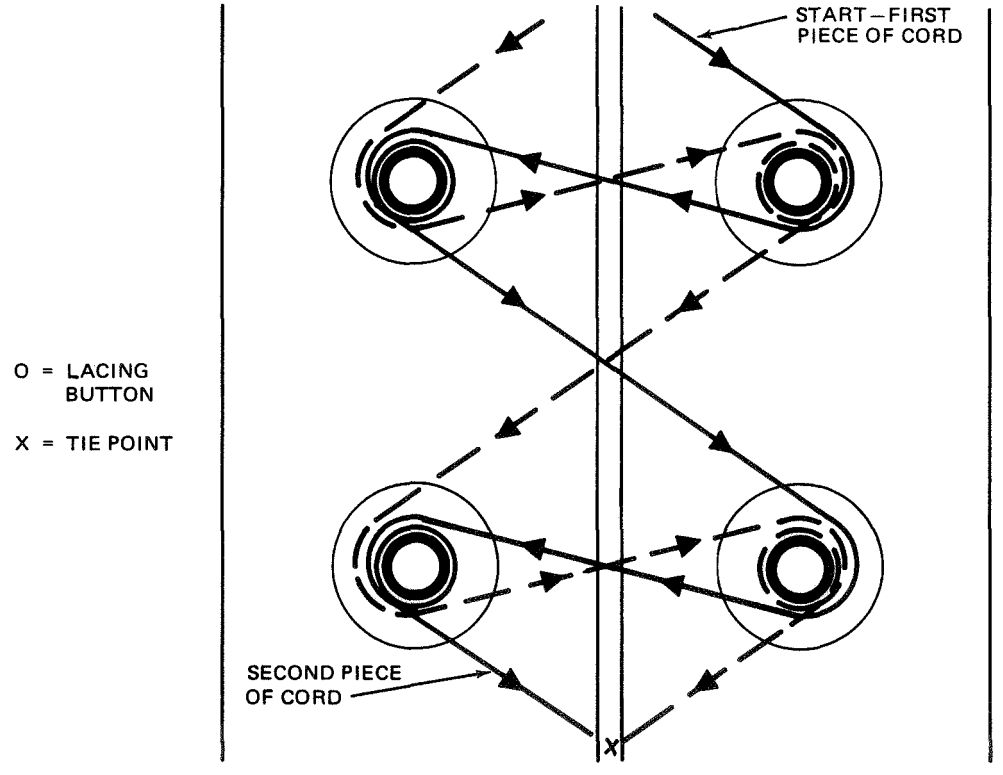

Figure 4-3. Joint Lacing Pattern

Feasibility was demonstrated with the small panel shown in Figure 4-4. No problems were encountered in this unit. A thin strip of wood was inserted in the panel, providing a knife backing to make the cut shown.

4.5 PANEL GEOMETRIC SHAPE REQUIREMENTS

The fabrication of a variety of different panel shapes was undertaken in the course of the study effort. Although no cost data was taken, it was obvious that fabrication difficulty and cost will be strong functions of the geometric configuration complexity. During design work, panel shapes should be chosen carefully. Flat or single-curvature panels yielded the greatest degree of thickness repeatability, important for thermal predictability. It was therefore concluded that a total insulation system installation must be divided into panels of the simplest practical geometric shapes: flat, cylindrical, cone, and gore, in that order.

Insulation of odd shapes such as plumbing hardware with its valves, expansion joints, and sharp bends will be encountered. Study results suggest that direct insulation of these items should be avoided. Instead, a smooth substrate which provides a uniform geometric shape should be placed over these items. The substrate should then be insulated in a manner similar to a shroud.

N/A CR94

Figure 4-4. Typical Shiplap Joint

Section 5
COMPOSITE MATERIALS CHARACTERIZATION

The objective of this work was to evaluate a number of candidate MLI composites, compare them to the study baseline nylon net separator system, and select one for application to the MNV.

Initially, a weight saving was obtained by replacing the 0.25-mil-thick Mylar reflector in the baseline composite with one 0.15 mil thick. Subsequent thermal testing showed that the baseline nylon net separator should also be rejected as the composite failed to evacuate properly when used in a full-thickness MNV panel (See Subsection 5.2).

An effort to identify a replacement net was undertaken and a number of Dacron nets with a non-outgassing, scoured, and heat-set finish were obtained (Appendix A). Screening tests identified one, a type B2A, with potentially equivalent thermal performance to an evacuated nylon net. Other, lighter Dacron nets were also identified.

Thermal and fabricability ranking of 12 candidate composites showed that Superfloc was very attractive, but sensitive to density changes induced by compressive loads. The Dacron B2A was not as sensitive to compression but exhibited a higher thermal conductivity-density. It was subsequently selected for the MNV with the recommendation for further development of the Dacron net material.

An investigation of the compression problem on a parallel MDAC IRAD program showed that MLI composites spring back after such loading, leaving only a small permanent set. This suggested that one of the other Dacron net candidates, lighter in weight, might yield improved thermal performance. An evaluation was then accomplished which identified an improved net, type B4A. This material was subsequently selected for the Phase II, 105-in.-tank insulation.

5.1 IDENTIFICATION OF PROMISING MLI COMPOSITE MATERIALS

Candidate MLI composites were selected at the beginning of the study and ranked on the basis of estimated thermal performance and fabricability. Four were then selected for further evaluation: Superfloc; 15-gage double-aluminized Mylar (DAM) with Tissuglas spacer; 15-gage DAM with a nylon net spacer; 15-gage DAM with a Dacron net spacer. This work, described in detail in References 9 and 10, is summarized below.

5.1.1 Candidate Composites

The MLI composites considered in the study were:

A. DAM with nylon net spacer (baseline).
B. DAM with Tissuglas spacer.
C. DAM with Dexiglas spacer.
D. DAM with foam spacer.
E. Superfloc.
F. Embossed double-aluminized Mylar (DAME) with Tissuglas spacer.
G. Embossed single-aluminized Mylar (SAME).
H. NRC-2 (25 gage).
I. NRC-2 (15 gage).
J. DAM with Dacron net (type B2A) with spacer.
K. Crinkled double-aluminized Mylar (CDAM) with Tissuglas spacer.
L. CDAM with nylon net spacer.

The baseline composite was that recommended in a prior MNV study (Reference 10). That effort concentrated on composites utilizing 25-gage Mylar for the reflector. In this study, a 15-gage material was found to be available from the National Metallizing Division of Standard Packaging Company, Cranbury, N. J. This material was adopted as it results in a weight saving of 40 percent per reflector or several hundred pounds in a typical MNV installation. The Dacron net material resulted from the study effort (Section 5.3).

5.1.2 Thermal Ranking Procedure

A thermal ranking was obtained by first experimentally determining the minimum practical layup density (MPD) for each composite. The statistical method developed in the study (Section 3) was used. Equations for composite heat transfer as a function of layer density and boundary temperature were then defined by modifying those formulated in the earlier study (Reference 10) for 25-gage material. As calorimeter data for both 15- and 25-gage reflectors were available for only one composite, it was necessary to use these data to ratio the equations for the other composites to yield an equation for 15-gage material. The thermal weight penalty (insulation plus LH_2 boiloff) for each composite (at MPD) applied to a 300-day Mars mission MNV was then computed.

5.1.3 Fabricability Ranking Procedure

One 4- by-5-ft panel (one-third the thickness required for MNV) of each candidate material was constructed and measured for density, and notes were taken on fabrication time and problems. A ranking was formulated on the basis of fabrication cost, predictability, and susceptability to damage. Material cost, although small in comparison with other manufacturing costs, was included as a secondary factor. To obtain a numerical ranking for each factor the leading system was assigned the value 1.0. The other composites were then ratioed upward from this base.

5.2 EVALUATION OF APPLIED THERMAL PERFORMANCE

The baseline nylon net separator material was rejected as an MNV candidate material due to the results of MDAC IRAD testing (Section 6). In that program, a full-thickness MNV insulation was tested on a cylindrical LH_2 calorimeter. The nylon material failed to evacuate properly as shown by the internal temperature profiles plotted in Figure 5-1. This phenomenon was not experienced during similar tests with the other three candidate composites. Thermal performance of the Superfloc and Tissuglas systems was about as expected. The Dacron net was somewhat higher.

At this point in the study, all work indicated that the Superfloc system was the leading candidate composite material. The baseline nylon net failed to evacuate. Tissuglas, not quite so good thermally, was found to apparently decompose with time (Section 5.4), degrading performance.

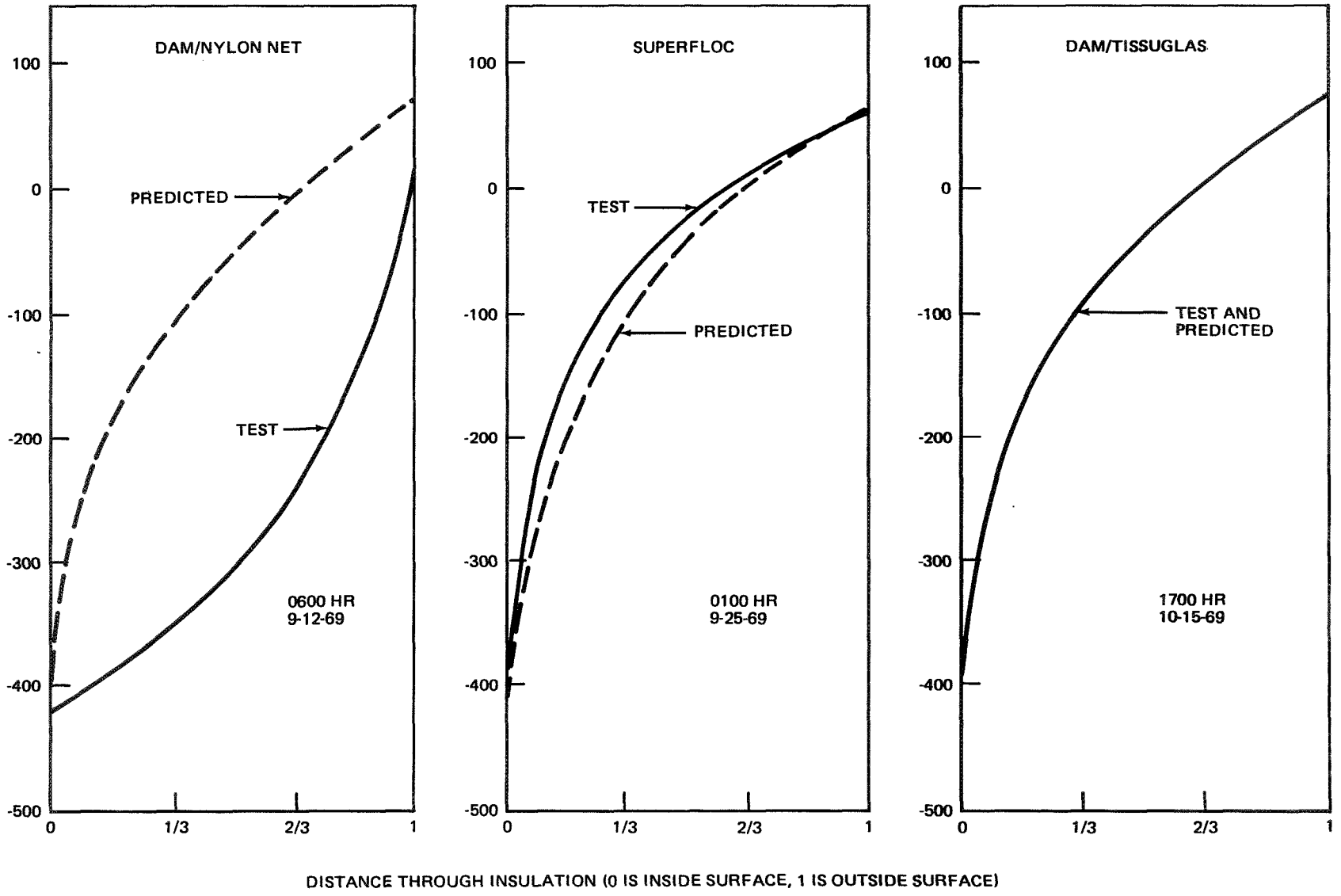

Figure 5-1. Thermal Gradients in Calorimeter Test Samples

It also was extremely fragile, necessitating great care in fabrication. The type B2A Dacron net yielded sturdy fabricated panels of exceptional uniformity and predictability, but it had significantly poorer heat transfer characteristics.

It was noted that MLI composites, when applied to an actual vehicle, would be subjected to compressive loads. These would arise through handling, purge gas contraction during tank fill, and launch acceleration. As thermal performance is strongly related to density, the effects of this compression were considered.

Composite density as a function of compressive load was measured (Reference 4). It was found that the Dacron net thermal performance was relatively insensitive to load-induced density changes. However, Superfloc was very sensitive. The degree of expected thermal degradation could not be determined as the magnitude of the expected compression loads was unknown and difficult to assess. Therefore, in the interest of a predictable conservative design, the Dacron net B2A was selected for application to the MNV with the recommendation for further development of the Dacron net materials.

It was noted that the B2A net was not necessarily the best of the available Dacron nets. Its selection was, by necessity, based upon a simple electrical resistivity screening technique (Reference 3) which showed that it should be relatively equivalent to the baseline nylon net. Some of the other sample nets were lighter but required further flat plate calorimeter testing for evaluation.

Calorimeter testing of lightweight Dacron nets was subsequently accomplished at NASA-MSFC in conjunction with an MDAC IRAD materials improvement study. A type B4A net was found to be potentially superior thermally to Superfloc and was selected for application to the Phase II 105-in. tank test (Section 8). Results of this large-scale tank test (Section 10) indicated that superior applied performance was achieved. Flat-plate calorimeter thermal data for the B4A net can be found in Section 6.

5.3 DEVELOPMENT OF DACRON NET SEPARATOR MATERIALS

This effort had the objective of identifying a net material which could be used in an MLI composite as a substitute for the baseline nylon material. Three criteria were used as constraints:

A. Outgassing reduced to a negligible value.

B. Weight equal to or less than the present nylon net.

C. Thermal performance equal to or better than the nylon composite.

Discussions with vendors indicated that nylon should be rejected as a basic material for improved nets. Elimination of all sizing resulted in a limp material, completely unacceptable for use as an MLI separator. Also outgassing will occur with any of the three standard sizing materials available for nylon or Dacron materials: melamine formaldehyde, urea formaldehyde, and polyvinyl chloride (PVC).

It was determined that stiffening with a heat-set process was possible with Dacron but not with nylon. As this solved the outgassing problem, seven different sample Dacron net materials with a scoured and heat-set finish were obtained. Net sizes ranged from 50 to 264 meshes per square inch (Reference 4). All were supplied by Apex Mills Inc., 49 West 37th St, New York, N.Y.

An electrical resistance test technique was used to provide low-cost, rapid screening. The device was designed to measure the electrical resistivity across a metallized reflector-net-reflector combination. It was assumed that the heat transfer would be proportional to the contact resistance, as it is known that conduction is dominant at low temperatures in MLI. Typical results are shown in Figure 5-2.

The type B2A net was selected as it satisfied the screening criteria:

A. A resistance at least as high as that of the current nylon net.

B. Weight equal to or less than that of the nylon.

Other nets were much lighter but did not exhibit as high a resistance. These were not evaluated further in this study. Thermal ranking would have required a determination of the conductivity-density parameter for the

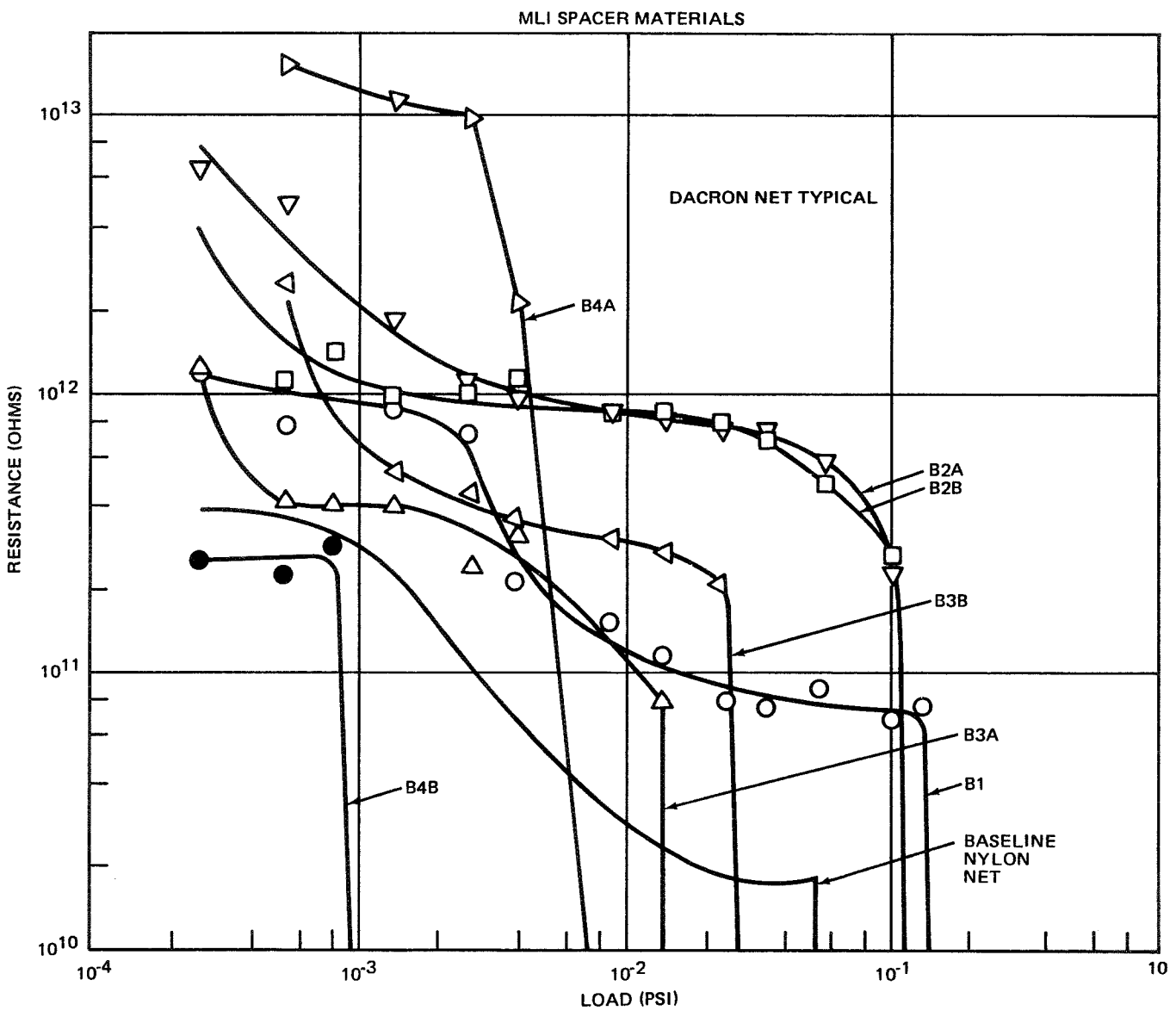

Figure 5-2. Electrical Analogy Method for Screening

candidate nets. This could not be obtained without further development of the test device or flat plate calorimeter tests and a measurement of minimum practical layup density.

5.4 MATERIAL PROPERTY TESTS

Several tests to determine specific properties and characteristics of MLI composite materials were performed. Results were utilized in the material selection studies.

5.4.1 Emissivity of Aluminized Reflectors

Reflector emissivity measurements were made with a Gier-Dunkle reflectometer on aluminized Mylar samples taken from inventory. The average emissivities obtained were: 48-in.-wide DAM, 0.028; 46-in.-wide DAM, 0.031 to 0.033; Superfloc, 0.031; and perforated DAM, 0.034 to 0.037. The narrow and wide materials had been processed by the vendor at different times.

5.4.2 Effect of Tissuglas Oxidation

The Tissuglas binder apparently oxidizes with time, resulting in an observed discoloration of the sheets. The effect of this phenomenon on adjacent aluminized Mylar reflectors was investigated.

The emissivity of reflectors taken from DAM-Tissuglas panels which had been stored over six months was measured and compared with that of new DAM. Other stacks cut from the same panels were subjected to elevated temperature, reflectors were chosen from the stack interior, and measurements were taken.

Results showed an adjacent reflector emissivity increase in all cases and it was concluded that composite thermal performance could be expected to change with time. Although emissivity changes were not sufficient to mandate rejection of Tissuglas as a separator material, they should be included in thermal computations (see Reference 4).

5.4.3 Compatibility of Materials with a Hot Purge Environment

Other studies have indicated that prelaunch preconditioning of the MLI may

be necessary to eliminate adhered gas molecules. A hot-gas purge with temperatures up to 250°F has been suggested and future work may indicate that one is mandatory. Six-in.-square samples of candidate MLI reflectors and separators were subjected to temperature environments covering the range which might be expected in any preconditioning process. The specimens were visually inspected after exposure.

Results indicated that singly aluminized Mylar was extremely sensitive to edge curling at even low temperature, 150°F. However, double-aluminized 15-gage Mylar was adequate even up to 250°F. It was concluded that for conservative design only doubly aluminized materials be used if hot purge preconditioning is contemplated. Detailed data will be found in Reference 2, Section 5.

Section 6
THERMAL TESTS OF MLI SYSTEM COMPONENTS

A test program (Reference 8) was conducted to measure the thermal performance of full-scale insulation panel configurations representative of those to be applied to an MNV. Tests were made with a 15-in.-diameter cylindrical boiloff-type calorimeter using LH_2 and LN_2 as the test cryogens. The work, performed as part of an on-going MDAC IRAD program, was directly applicable to the study and is reported here for reference.

Previous cylindrical calorimeter tests suffered from the lack of a uniform, controlled density in the MLI sample after installation on the test unit. This problem was solved. Prior to actual testing, an installation method to ensure a uniform, predictable test sample density was developed. Nine tests were then performed to evaluate: (1) thermal performance of four insulation composites; (2) the effect of storage on insulation performance; (3) effect of cold boundary temperature on the heat transfer rate; and (4) performance degradation associated with joints, fasteners, and reflector perforations.

Also reported here for reference are some preliminary flat plate calorimeter test data measured by MSFC and used in the program. These data are for 10-layer pair samples tested with an LN_2 cold boundary.

6.1 CYLINDRICAL TEST SAMPLE APPLIED DENSITY CONTROL

All known previous multilayer insulation testing, except flat-plate tests, had been accomplished with the insulation applied to a density that was not precisely controlled. That is, the density (sheets per inch of thickness) varied widely on the test surface; accurate measurements of the average insulation thickness were not possible. A considerable uncertainty is therefore inherent in the test results.

In this program, test specimen density control was achieved through control of the circumferential length of each individual insulation sheet as it was applied to the cylindrical surface. Each sheet was merely cut to the required length, as defined by the specified application density, considering the growth with increased thickness.

Two basic test insulation geometries were required for insulation evaluation tests: (1) simple multilayer configurations with no joints to allow the evaluation of basic insulation materials and (2) panels with flight-type joints.

For simple multilayer configurations, a precut sheet was applied to the cylinder, its ends were butted together, and it was taped in place. Subsequent sheets were applied similarly but with each joint staggered approximately 6 in. to a different circumferential location. Scotch 850, a 1-mil-thick tape, was used. Short lengths of tape were applied at spacings of approximately 6 to 8 in. down the length of the seam. This was sufficient to ensure true joint closure and to hold a straight seam, i.e., to prevent bowing between tape patches.

Panels with flight joint configurations were also fabricated using sheets individually precut to specified lengths. The individual sheets were stacked on a flat surface. One edge was assembled by maintaining vertical alignment of each layer of insulation. This resulted in the opposite edge being tapered. Fasteners (pins through the insulation) were then installed along the matched edge. With one edge secured, the loose (tapered) edge was realigned into a vertical stack and secured identically to the opposite edge.

This technique allows the right-angle insertion of fasteners on flat tooling. It is practical for use with both single- and dual-component insulation systems. Some difficulty may be encountered in the alignment of the tapered edge without distortion of the material, but this problem may be alleviated by using curved tooling to assist in alignment of the free edge.

To demonstrate the density control technique, two typical full-scale thickness, multilayer panels with butt joints were fabricated and installed

on a 15-in.-diameter cylindrical metal calorimeter mockup. Superfloc was used for one and 15-gage embossed Mylar with a Tissuglas separator for the other. Velcro patches were bonded to the metal mockup to provide fastener surfaces for the insulation blanket.

Results showed that the 12-sheet Superfloc panel displayed a consistent thickness and was free of wrinkles. The design density of 35 layers per inch was easily achieved. The finished Mylar-Tissuglas panel exhibited the same characteristics and controlled density as the Superfloc. A design density of 90 layer pairs per inch was achieved for the 28-layer pair panel. A typical test panel installed on a calorimeter is shown in Figure 6-1.

6.2 STANDARDIZED TEST ARTICLE DESIGNS

Standardized test article designs were developed to accommodate the configurations required for this experimental program: panel evaluation of basic insulation materials, joint effects, and fastener effects. The results are general in nature and may be used in future test programs.

CR94
N/A

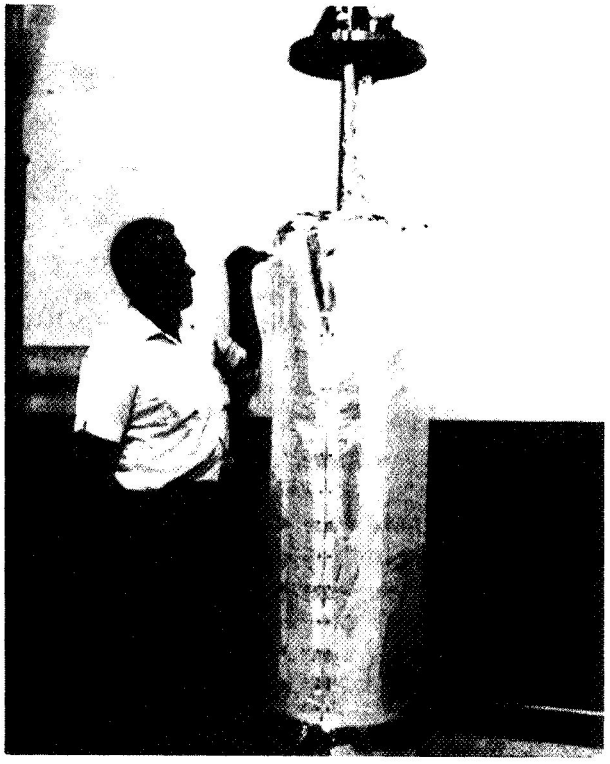

Figure 6-1. Completed Calorimeter Joint Test Assembly

Previous cylinder and tank-type tests were reviewed to search for standards pertinent to insulation design. No specific design standards had been established. However, the test results suggested several design criteria:

A. Longitudinal conduction within the insulation between the calorimeter end guards and the test section must be reduced to a negligible value.
B. Guard heat transfer must be sufficiently small to eliminate the requirement to refill during test.
C. Insulation must be installed to a known and uniform design thickness, i.e., density.
D. Test insulation must be supported in a manner that allows the calorimeter to be mounted vertically without changing the test section insulation density.
E. For simple composite materials tests, the effect of discontinuities resulting from the single-sheet butt joints must be minimized.
F. For tests with service-type joints, the design must allow for application of one or more fully assembled test panels with each panel installed as a single unit.

6.2.1 Composite Test Specimens

Figure 6-2 illustrates the design for simple composite performance test configurations. The applied insulation, wrapped to a controlled density, was not penetrated except at the supports at the top of the calorimeter, approximately 18 in. above the test section. The butt joint in each sheet was offset about 6 in. from the prior joint to minimize performance degradation due to discontinuities.

The test insulation was supported by three hollow nylon studs mounted in a stainless steel ring on the top surface of the upper guard, flush with the outside diameter of the calorimeter. The studs were held in the ring with a force fit during installation. As inner sheets were installed, the stud protrusion was maintained approximately flush with the outside insulation diameter and was then extended radially as the insulation thickness increased. The studs were then bonded to the ring in their fully extended position.

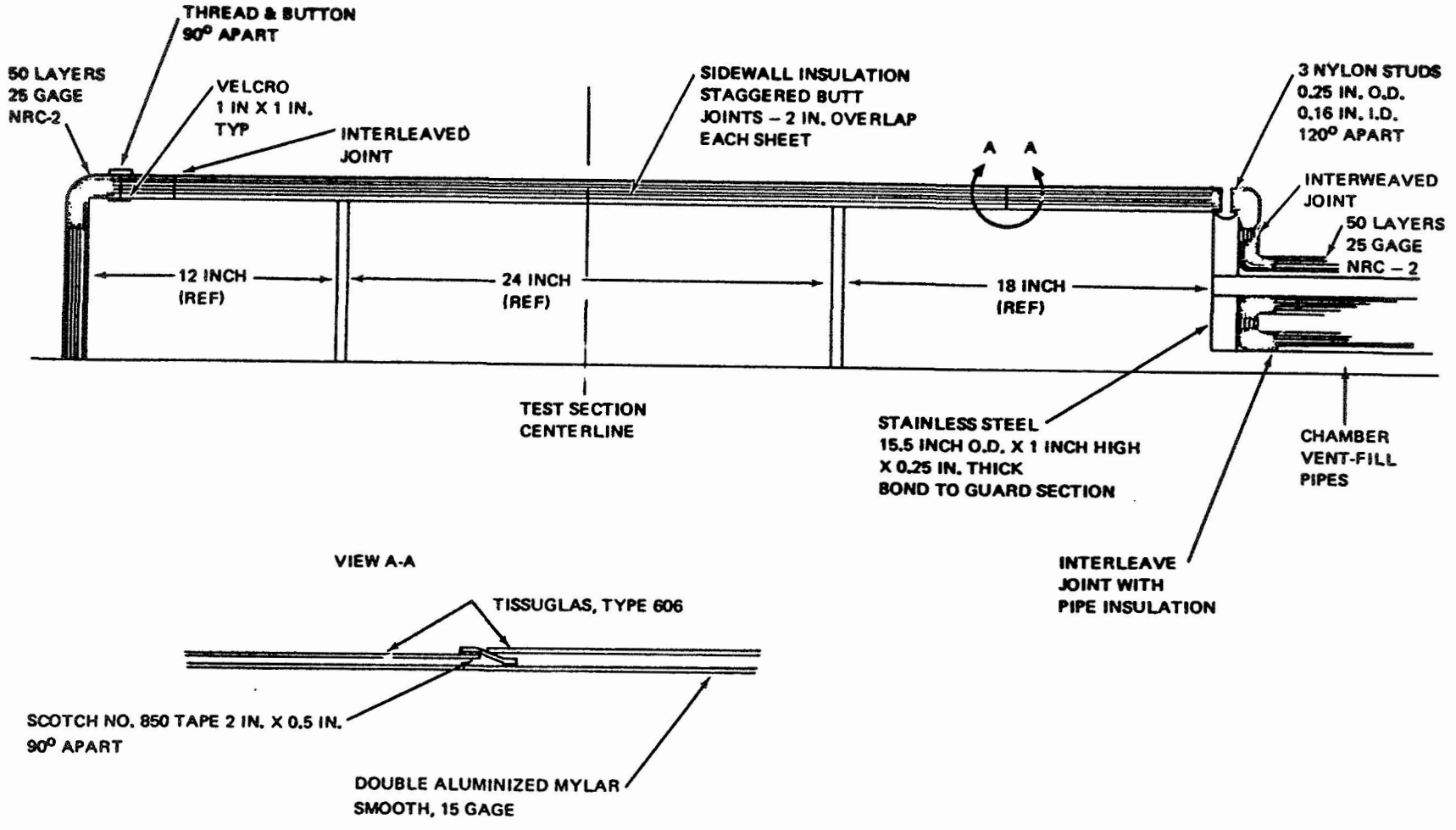

Figure 6-2. Calorimeter Insulation Design

The ends of the test insulation (at the top and bottom of the calorimeter) were interleaved fully with the cap insulation at a joint in each guard area. This was an attempt to reduce distortions in the axial thermal gradient within the insulation.

The end insulation caps and the insulation on the pipes consisted of 50 sheets of 25-gage NRC-2. The insulation surrounding each pipe was fully interleaved with the top cap insulation which, in turn, was fully interleaved with the test insulation. The lower guard insulation cap was held in place with Velcro and thread. The upper guard insulation cap required no special attachments.

6.2.2 Butt Joint Heat Transfer Test Specimens

Details of the butt joint test specimen, two overlapping panels, are shown in Figure 6-3. Each panel included two face sheets of the style 15320 Dacron net reinforced at the edges and other local areas with epoxy resin (see Section 4). Joint closure was accomplished by lacing across between buttons in the face sheet on each side of the joint. Installation on the calorimeter was similar to that described above. Section 6.1 presents test results.

6.2.3 Fastener Heat Transfer Test Specimen

The insulation panels for the fastener test were obtained by modifying the above joint test panels. The panels were removed from the calorimeter and then separately fitted over a cylindrical mandrel while additional through fasteners were installed. The fastener configuration was an 8-in. square pattern as shown in Figure 6-4.

The modified panels were then installed on the calorimeter in the same manner as described for the joint test. Note that the fasteners in the two panels were offset due to the offset of the joint locations.

6.2.4 Test Article Instrumentation

Chromel-Constantan, 30 AWG thermocouples were used exclusively to measure temperatures within the insulation. Junctions were taped to the sheet with aluminized tape. All wires were wrapped circumferentially at least 180 deg before being drawn longitudinally out along the sheet surface to exit at the upper guard area.

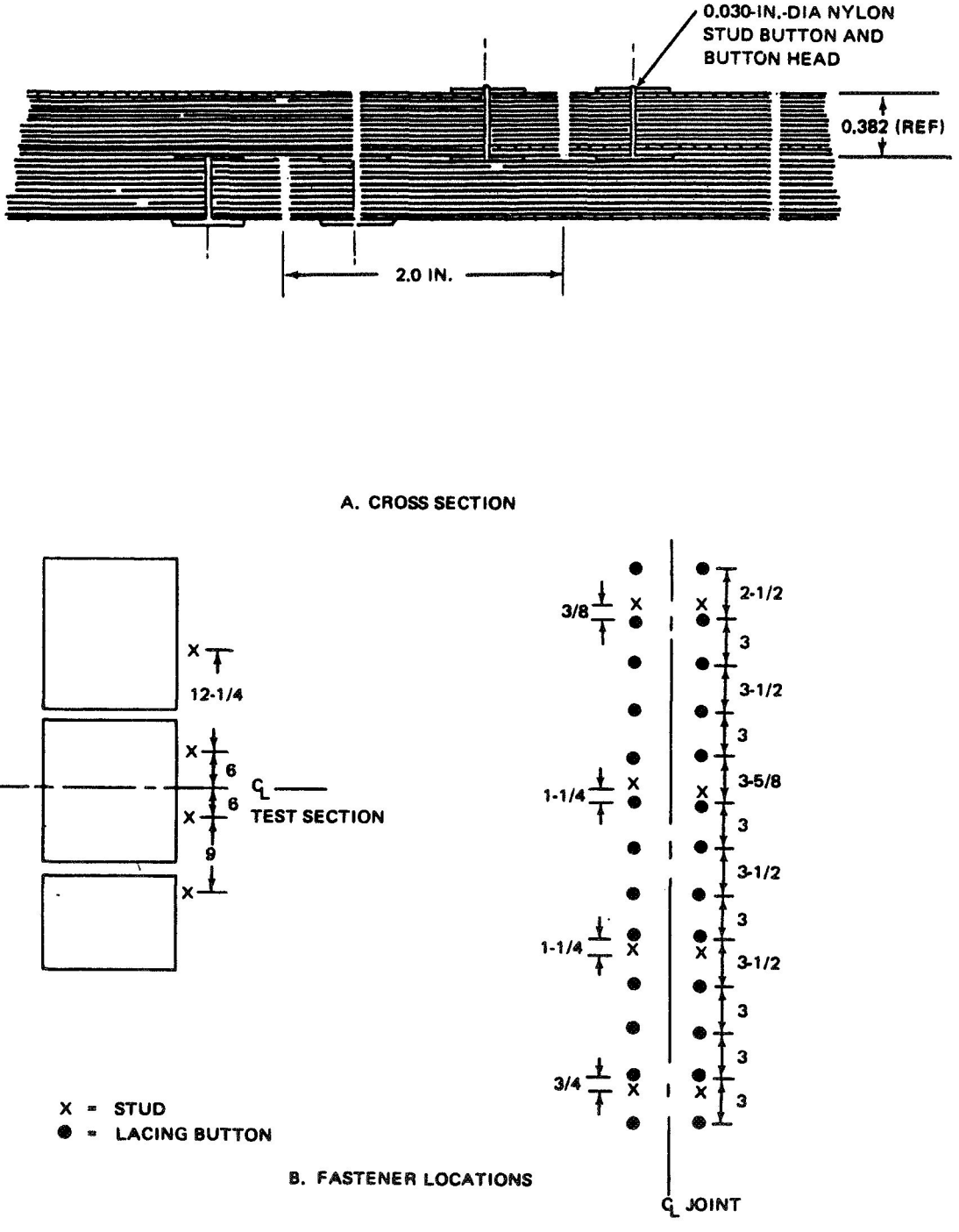

Figure 6-3. Flight-Type Joint Design

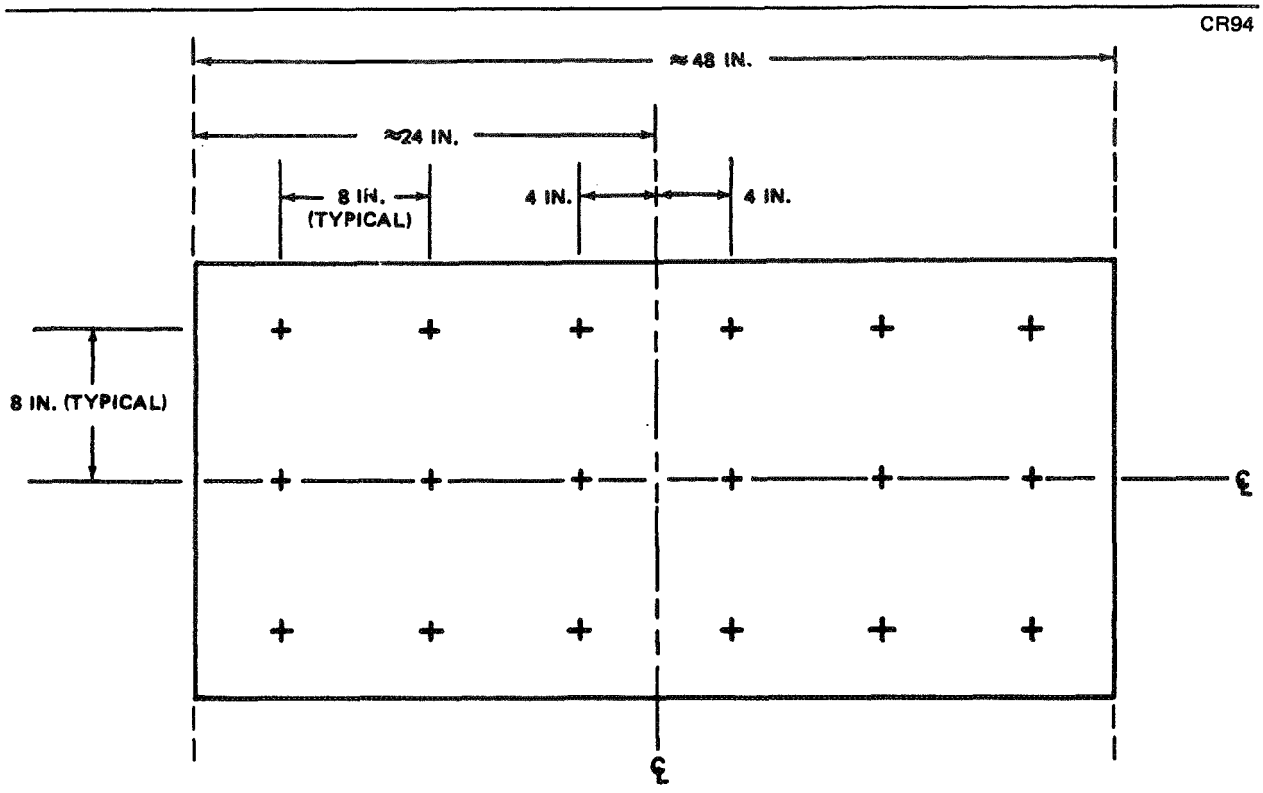

Figure 6-4. Calorimeter Test Fastener Pattern

6.3 15-INCH-CALORIMETER TEST DATA

Table 6-1 lists the insulation configurations for which thermal performance was measured. Installed test insulation specimen specifications are summarized in Table 6-2. Table 6-3 presents the test results of the experimental program, which had four primary objectives:

A. To evaluate the performance of basic multilayer insulation materials of full-scale thickness.

B. To compare insulation performance at LH_2 and LN_2 boundary temperatures to allow correlation of LH_2 full-scale test results with LN_2 flat-plate calorimeter results.

C. To evaluate the effects of flight hardware configuration requirements: reflector sheet perforations, blanket joints, and assembly fasteners.

D. To assess the effects of preflight storage on thermal performance.

Table 6-1

THERMAL TEST CONFIGURATIONS

Material System	Installed Layer Density (sheets/in.)	No. of Reflector Layers	Test Configuration			
			Simple Material Test	2.3-Percent Perforated	Butt Joint	Button Fasteners
DAM/nylon net	91	64	X			
Superfloc	29	24	X			
DAM/Tissuglas	82	34	X			
DAM/dacron net B2A	96	70	X			
DAM/dacron net B2A	96	70	X	X		
DAM/dacron net B2A	96	70		X	X	
DAM/Dacron net B2A	96	70		X	X	X

Note: All 15-gage reflectors

Table 6-2

15-IN.-CALORIMETER TEST INSULATION SPECIFICATIONS

Material System	Number of Layers	Weight (lb/ft^2-sheet)	Blanket Weight (lb/ft^2)	Corrected* Blanket Thickness (in.)	Applied Layer Density (layer pairs/in.)
DAM/nylon net spacer	64 DAM 63 net	0.0012 0.0028	0.2532	0.715	91
Superfloc	23	0.0017	0.0390	0.850	29
DAM/ Tissuglas spacer	34 DAM 33 spacer	0.0012 0.0010	0.0738	0.425	82
DAM/Dacron net, Type B2A	70 DAM 69 net	0.0012 0.0024	0.2496	0.751	96

*Corrected for thermal contraction of calorimeter: layers/applied density +0.0225 in.

As shown in Table 6-1, the basic unpenetrated composite heat transfer with an LH_2 cold boundary temperature was obtained for four different insulation materials. Each was installed on the calorimeter with a typical flight thickness. The Tissuglas specimen was retested after 6 weeks of storage in a 600-mm Hg nitrogen environment (Test 4, Table 6-3). The same specimen was retested with LN_2 as the cold boundary (Test 5). Tests 6 through 9 were evaluations of a Dacron net B2A composite: basic material; basic material with 2.3 percent open area perforations (0.055-in. holes); perforated with joint; and perforated with joint and fasteners. As the insulation layers and density were identical in these tests, the effect of each configuration could be determined separately.

Results showed that the nylon net composite failed to attain an evacuated performance value. The measured thermal gradient suggested an entrapped gaseous constituent, most probably outgassing of the organic binder on the net. The Superfloc performed as expected with the thermal gradient showing good agreement with the values predicted on the basis of flat-plate tests.

Table 6-3

SUMMARY OF 15-IN. CALORIMETER TEST RESULTS

Data	Units	Test No. 1	2	3	4	5	6	7	8	9
Reflector material	-	Dam (15-gage)	Superfloc (15-gage)	Dam (15-gage)	Dam (15-gage)	Dam (15-gage)	Dam (15-gage)	Dam (15-gage)	Dam (15-gage)	Dam (15-gage)
Separator material		Nylon net	Dacron floc	Tissuglas	Tissuglas	Tissuglas	Dacron B-2A net	Dacron B-2A net	Dacron B-2A net	Dacron B-2A net
Penetrations		None	None	None	None	None	None	Perforated reflector	Perforated reflector joint	Perforated reflector joint and button fasteners
Blanket area density	lb/ft^2	0.2532	0.0390	0.0738	0.0738	0.0738	0.2496	0.2496	0.2496	0.2496
Corrected blanket thickness*	ft	0.0596	0.0708	0.0354	0.0354	0.0354	0.0626	0.0626	0.0626	0.0626
Cryogen	-	LH_2	LH_2	LH_2	LH_2	LH_2	LH_2	LH_2	LH_2	LH_2
Data evaluation Period	hr	7	10	10	24	24	13	12	12	12
Uncorrected data period boiloff	ft^3	20.706	4.511	4.352	10.912	1.533	10.687	13.019	15.125	16.796
Integrated boiloff mass (includes meter correction and error, density error, and volumetric correction)	lb	0.1121 ±0.0015	0.02493 ±0.00033	0.02391 ±0.00032	0.05954 ±0.00076	0.141 ±0.00222	0.05948 ±0.00070	0.07069 ±0.00086	0.08116 ±0.00097	0.08956 ±0.00104
Average mass boiloff rate	lb/hr	0.01601 ±0.00021	0.002493 ±0.000033	0.002391 ±0.000032	0.002481 ±0.000032	0.005875 ±0.000093	0.004575 ±0.000054	0.005891 ±0.000072	0.006763 ±0.000081	0.007463 ±0.000087
Q (boiloff)	Btu	21.501 ±0.040	4.683 ±0.063	4.587 ±0.061	11.423 ±0.146	12.098 ±0.190	11.41030 ±0.13397	13.5613 ±0.1655	15.5698 ±0.1855	17.1821 ±0.1995
Q (corrected) (includes bubbler, lateral conduction, flat plate corrections, and errors)	Btu	19.282 +2.040 -1.918	4.577 +0.296 -0.324	4.490 +0.361 -0.352	11.697 +1.426 -1.253	12.219 +1.015 -1.166	10.565 +0.1517 -0.1197	12.163 +0.1657 -0.1777	14.7885 +0.1848 -0.1668	16.0263 +0.1981 -0.1701
$\dot{q}$ (experiment) (nominal value)	$Btu/hr\text{-}ft^2$	0.354	0.0588	0.0574	0.0626	0.0654	0.1043	0.1301	0.1582	0.1714
k_{eff} (experiment) (nominal value)	$Btu/hr\text{-}ft\text{-}°R$	4.409×10^{-5}	8.577×10^{-6}	4.15×10^{-6}	4.50×10^{-6}	6.07×10^{-6}	1.37×10^{-5}	1.69×10^{-5}	2.03×10^{-5}	2.22×10^{-5}
k_{eff} (predicted)	$Btu/hr\text{-}ft\text{-}°R$	1.15×10^{-5}	1.87×10^{-5}	1.04×10^{-5}	1.04×10^{-5}	1.37×10^{-5}	3.66×10^{-5}	-	-	-
$\frac{K(predicted)}{K(experiment)}$	-	0.26	2.2	2.5	2.3	2.3	2.7	-	-	-
ρk_{eff} (experiment) (nominal value)	$Btu\text{-}lb/hr\text{-}ft^4\text{-}°R$	1.87×10^{-4}	4.73×10^{-6}	9.02×10^{-6}	9.37×10^{-6}	1.26×10^{-5}	5.46×10^{-5}	6.74×10^{-5}	8.09×10^{-5}	8.85×10^{-5}

*See Table 3-2 for applied insulation specifications

Results with Tissuglas were similar. No effect was noted due to storage in gaseous nitrogen as differences in Test 4 and 5 agree within the probable error range. As shown, the conductivity increased (Test 5) with the decrease in cold boundary temperature from LH_2 to LN_2, consistent with flat-plate results. It was concluded that vehicle systems for LH_2 application could be conservatively designed using flat-plate LN_2 data in the absence of LH_2 data.

No flat-plate data on the Dacron net material was available for comparison. However, results were consistent with later data. The perforations were found to contribute a 23.4 percent performance degradation. Heating rates for the joint and fastener were 0.11 Btu/hr-ft and 5.72×10^{-3} Btu/hr per fastener, respectively.

6.4 FLAT-PLATE CALORIMETER DATA

During the course of this program, data from tests conducted at MSFC were utilized. These preliminary, unpublished data are reported here for completeness and as a point of reference for discussion in other areas of the report.

Figures 6-5 and 6-6 show results of 10-layer MLI samples tested on a flat-plate calorimeter with LN_2 and 75°F cold and hot boundaries, respectively. Both the Superfloc and the Dacron net specimens were tested with 15-gage DAM reflectors.

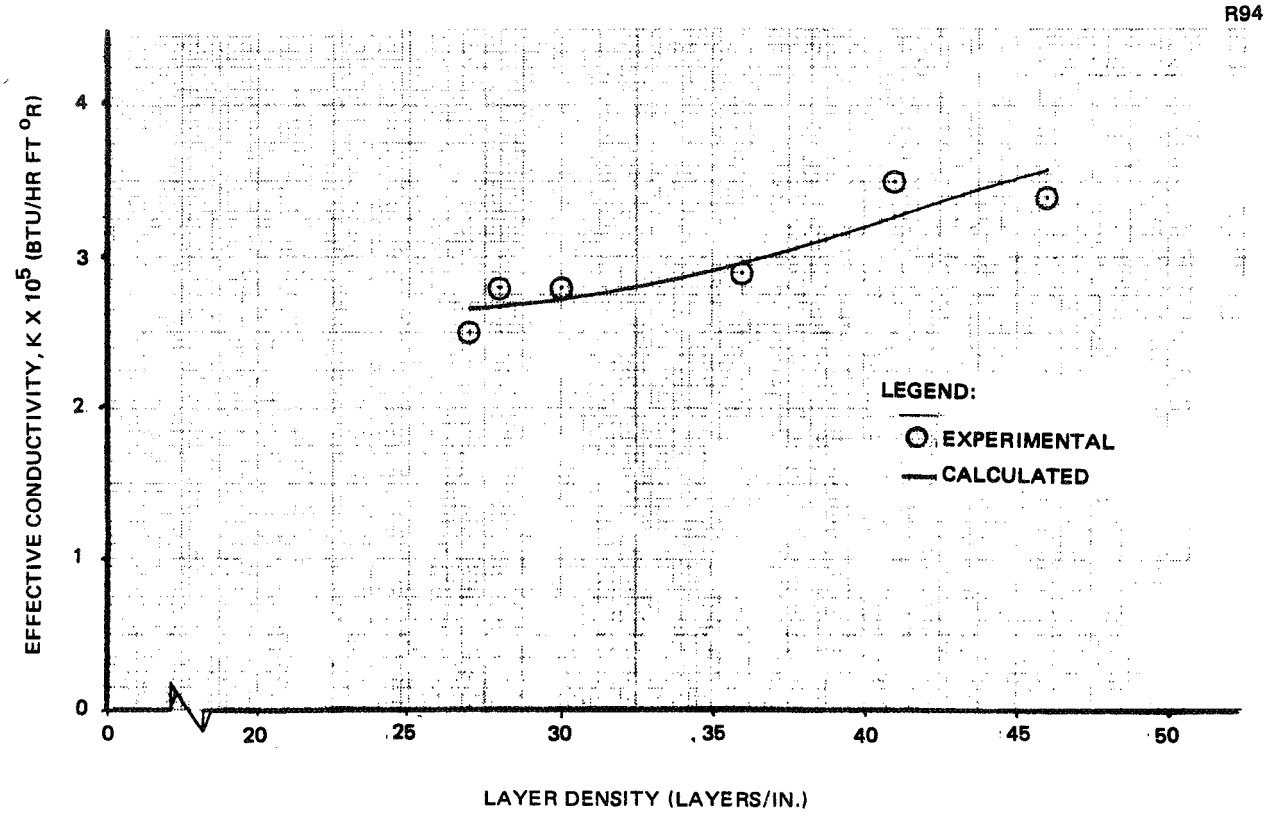

Figure 6-5. Superfloc Thermal Conductivity

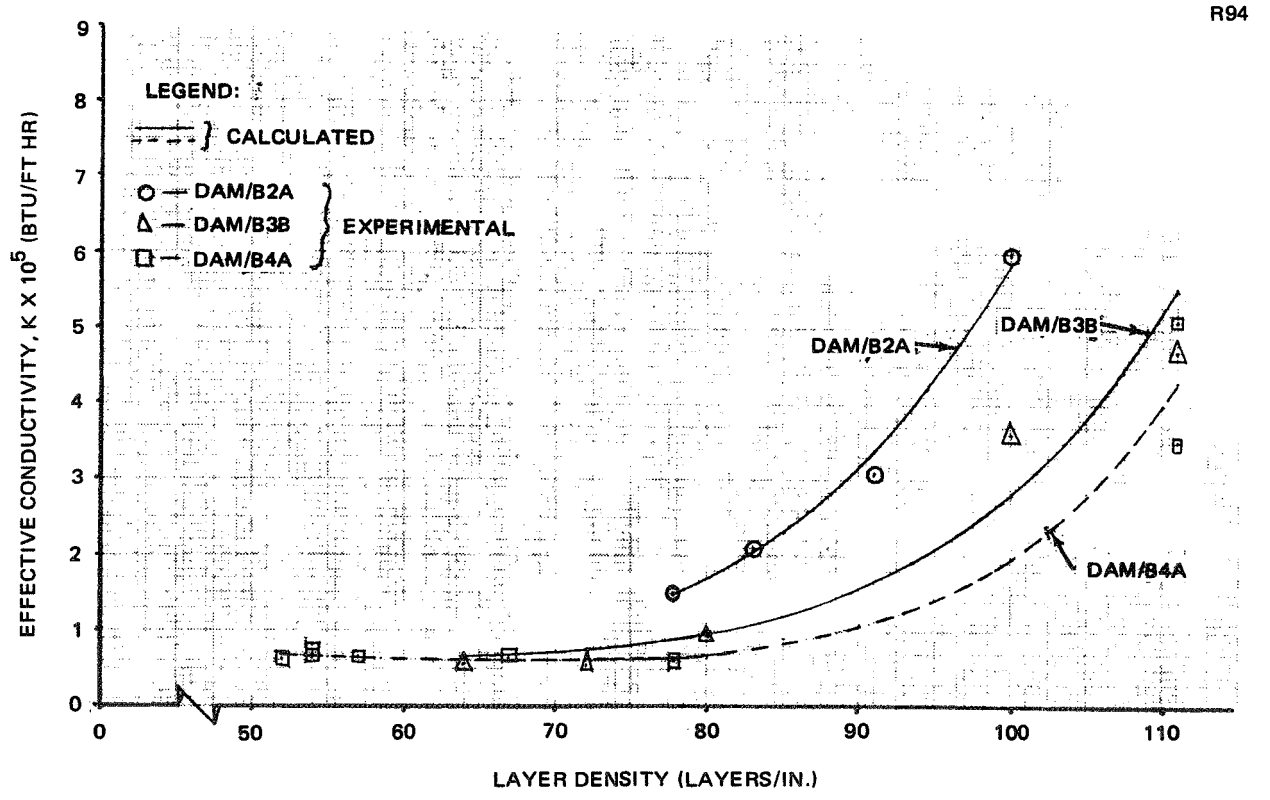

Figure 6-6. Thermal Conductivity of Dacron Net Materials

Section 7
STRUCTURAL TESTING

Structural testing was accomplished to acquire MLI panel component design data and to verify assembly structural integrity. Items tested were: decompression tearout of fasteners; tensile strength of fasteners and face sheets; and dynamically loaded panel assemblies.

7.1 TENSILE STRENGTH OF FASTENERS

The tensile load to failure was experimentally determined for three fastener configurations based on the designs shown in Figure 7-1. These were:

A. Mechanical locking head fastener, punched washer, 0.029-in. hole.
B. Mechanical locking head fastener, punched washer, 0.025-in. hole.
C. Heat-sealed head with punched washer, 0.030-in. hole.

All fasteners were injection-molded nylon Zytel 101, with a 10-mil nylon sheet stock washer. The mechanical head units were made in the mold developed earlier on Contract NAS8-20758. The mold was modified at MDAC to yield the heat-sealed fastener shown. Heads on these fasteners were formed with a radiant heater (see Section 8).

A tensile tester, Figure 7-2, was used to measure head pulloff loads. Results are summarized in Table 7-1. It was noted that the strength of the heat-set head design approached that of the basic shaft. As shown, these fasteners are more than adequate for the design load of 1.44 lb, a conservative estimate for fasteners on 12-in. centers (Section 2.7).

As expected, the tests showed that the degree of interference fit between the head and washer is extremely important with the mechanical locking fastener. Interference greater than 0.005 in. (type 2 fastener data shown) is felt necessary for the design loads expected.

R94

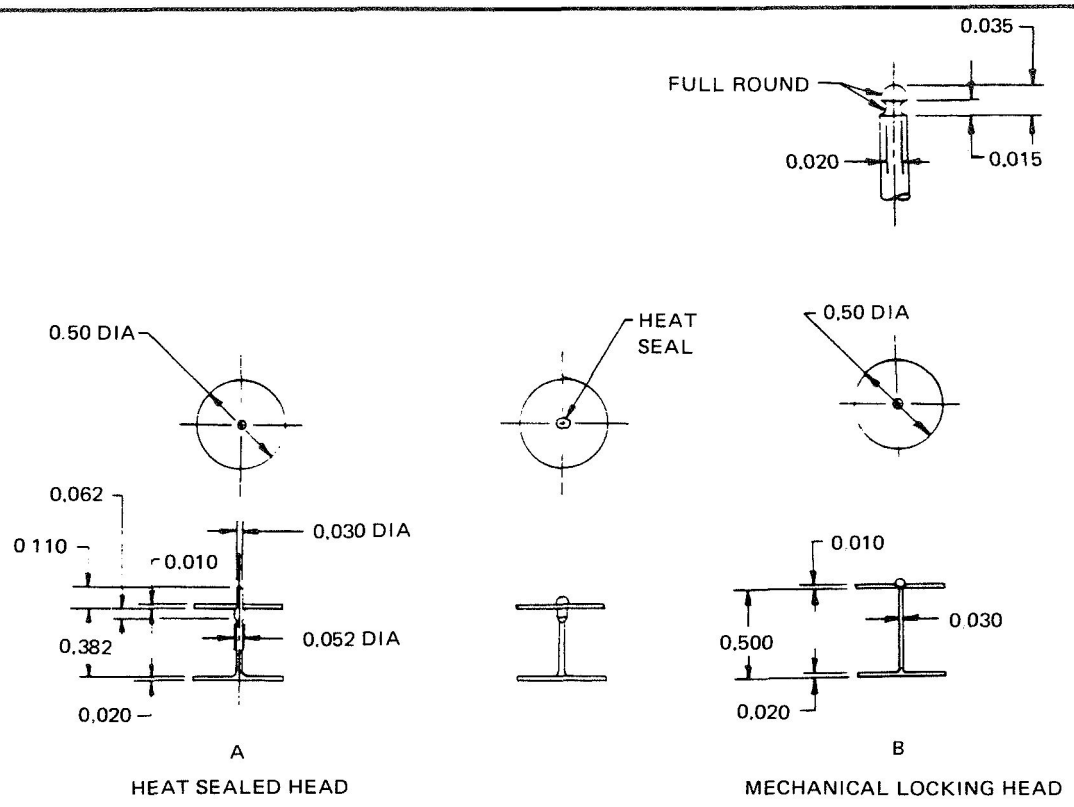

Figure 7-1. Fasteners

N/A CR94

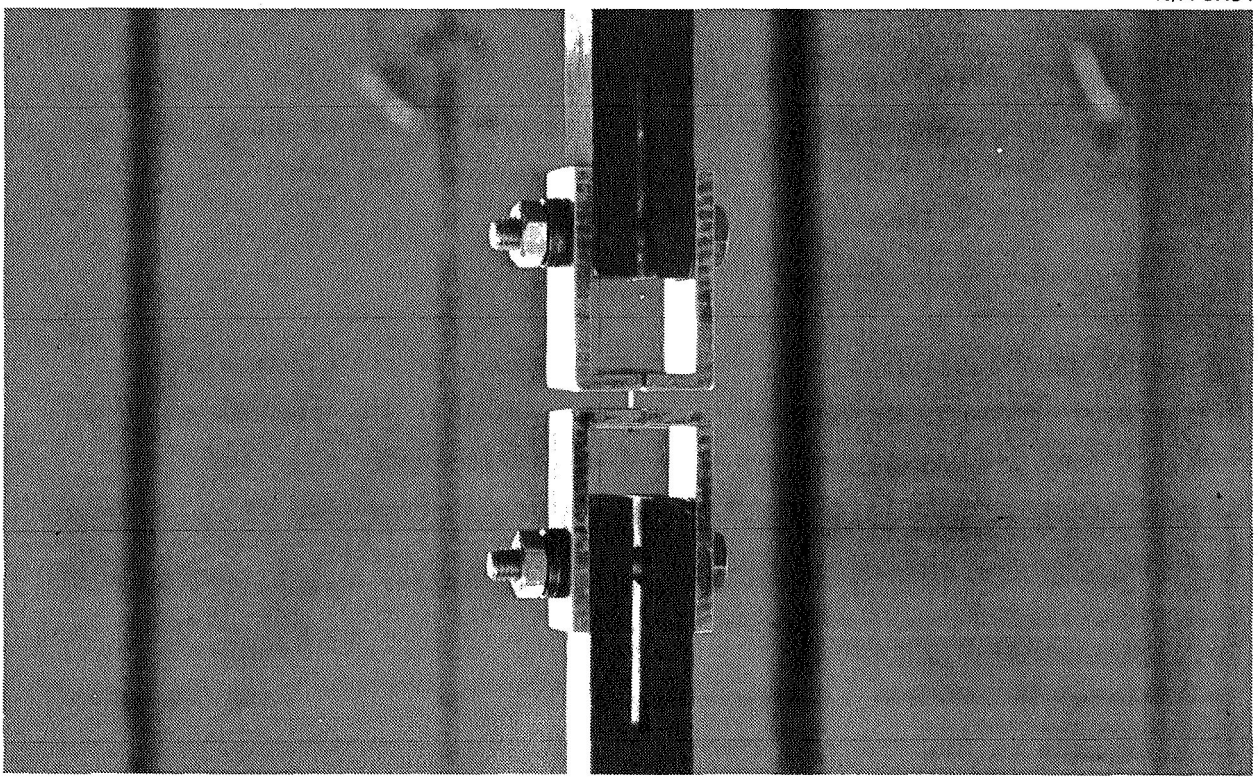

Figure 7-2. Fastener Tensile Load Test

Table 7-1

TENSILE STRENGTH OF FASTENERS

Test	Heat-Sealed Design (Figure 7-1A) Failure Load (lb)	Mechanical Lock Design (Figure 7-1B) Failure Load (lb)	
		0.029 inch hole	0.025 inch hole
1	3.38	0.32	2.34
2	4.87	0.15	2.10
3	2.64	0.37	2.05
4	3.50	0.48	1.70
5	3.05	0.28	2.05
6	4.57	--	2.43
7	3.08	--	2.78
8	2.70	--	1.94
9	4.58	--	2.34
10	4.53	--	2.30
Average	3.69	0.32	2.20
Design Load	1.44		

7.2 FASTENER TEAROUT

The objectives of this test sequence were to determine if the outer Mylar reflector would tear out over the fastener head during decompression and if the heat-sealed fastener head would withstand design loads.

The test setup, Figure 7-3, was a sheet of Mylar clamped around the top (open end) of a 24- by-24-in. box. A fastener was installed in the center of the Mylar and attached to the bottom of the box. Air pressurization of the box uniformly loaded the Mylar sheet to simulate the design ultimate decompression load of 0.01 psi (Section 2.7). A Zytel 101 nylon fastener with a 0.010-by-0.05-in.-diameter button head, heat-sealed on a 0.03-in.-diameter shank, was used.

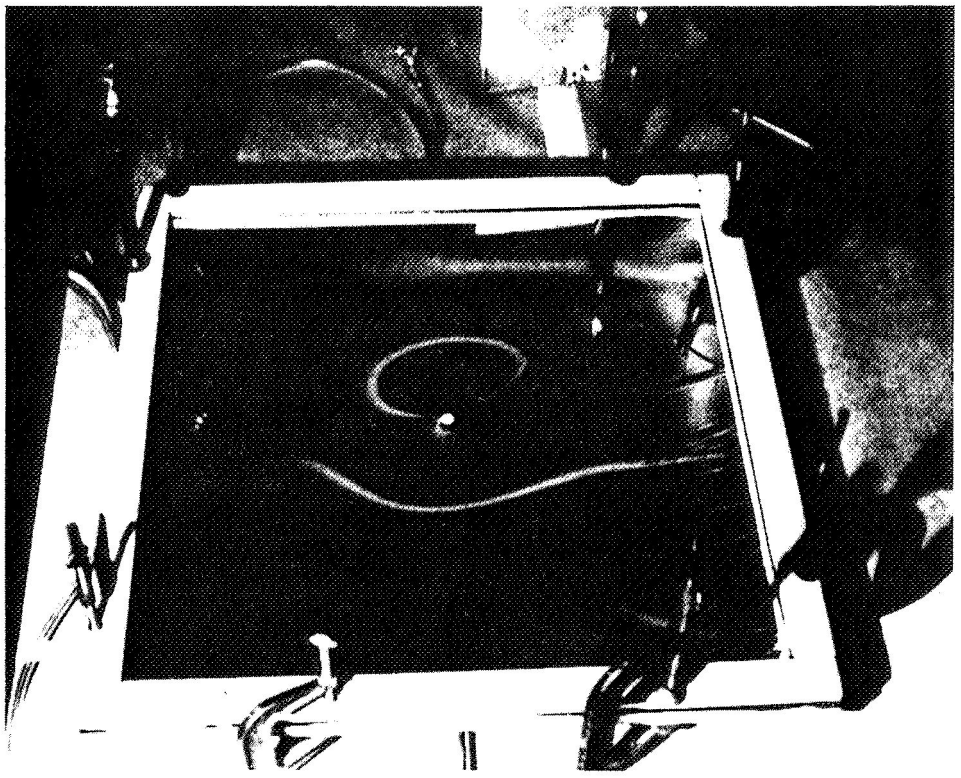

Figure 7-3. Face Sheet Tearout Test Apparatus

Results, Table 7-2, show that 0.15-mil Mylar is marginal for use as the outer layer of an MLI panel with fasteners on 12-in. centers and the 0.01-psi design load. Some strengthening, such as a face sheet, is needed to prevent tearout. However, the 0.25-mil Mylar can be used alone.

7.3 TENSILE STRENGTH OF FACE SHEET COMPONENTS

Twenty-seven tensile tests were performed to determine the load-carrying ability of the MLI panel face sheet components. The specific test objectives were:

A. Material allowables of the face sheet Dacron net substrate (Stern and Stern Textiles, No. 15320)
B. Material allowables of the support strap (two plies of net impregnated with epoxy, Bakelite ERC 2795 resin, and 2807 hardener)
C. Strap strength reduction due to fastener holes
D. Mounting grommet pullout from a four-ply strap

Table 7-2

FACE SHEET FAILURE LOAD DURING SIMULATED DECOMPRESSION

Test	Material	Failure Load (psi)	Comments
1	0.15 mil DAM	0.00975	Mylar tore out around fastener
2	0.15 mil DAM	0.0135	Mylar tore out
3	0.15 mil DAM	0.0146	Mylar tore out
4	0.25 mil DAM	0.0252	Mylar tore out
5	0.25 mil DAM	0.0202	Fastener head sheared off
6	0.25 mil DAM	0.0249	Mylar tore out

Strength measurements were made at ambient, -320°F, and -423°F. A standard tensile machine with a cryostat was used. Specimen configurations are shown in Figure 7-4.

CR94

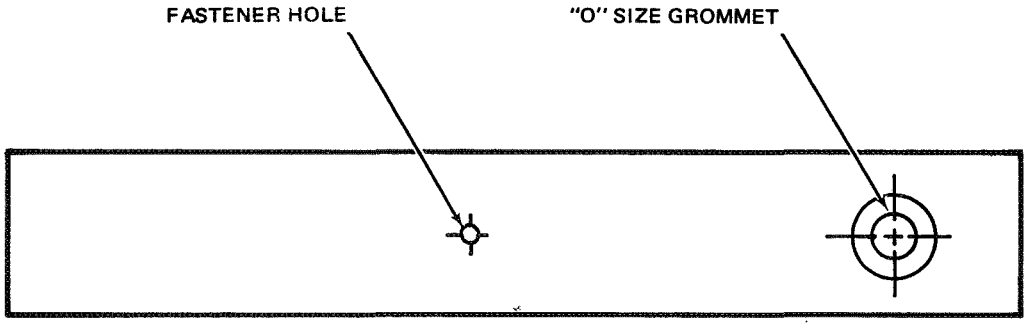

Figure 7-4. Face Sheet Tensile Specimens

Test results are summarized in Table 7-3 which lists the average strengths of the specimens tested. Data for the -423°F, except for the four-ply pullout specimens, is an extrapolation.

No distinct yield point was noted for the Dacron net specimens. The epoxy in the strap specimens cracked at yield and the specimen began to behave as a two-ply net (Figure 7-5). The presence of the fastener hole apparently had little effect, although a scatter in yield loads was observed.

Table 7-3
FACE SHEET COMPONENT TENSILE DATA

Test and Configuration	Temp (°F)	E (psi)	Yield	Ultimate
1. Dacron net (single-ply)	RT		-	52 lb/in.
	-320		-	58 lb/in.
	-423		-	58.5 lb/in.
2. Epoxy impregnated Dacron net strap (two-ply)	RT	0.34×10^6	3.5 ksi	7.7×10^3 ksi
	-320	0.55×10^6	2.8 ksi	9.2×10^3 ksi
	-423	0.61×10^6	2.6 ksi	9.6×10^3 ksi
3. Fastener hole in strap (two-ply)	RT	0.34×10^6	3.6 ksi	5.6×10^3 ksi
	-320	0.55×10^6	3.2 ksi	7.9×10^3 ksi
	-423	0.61×10^6	3.1 ksi	8.1×10^3 ksi
4. Pull-out specimen (two-ply net with epoxy)	RT	-	45 lb	46 lb
	-320	-	31 lb	33 lb
5. Pull-out specimen (four-ply net with epoxy)	-423	-	51 lb	67 lb

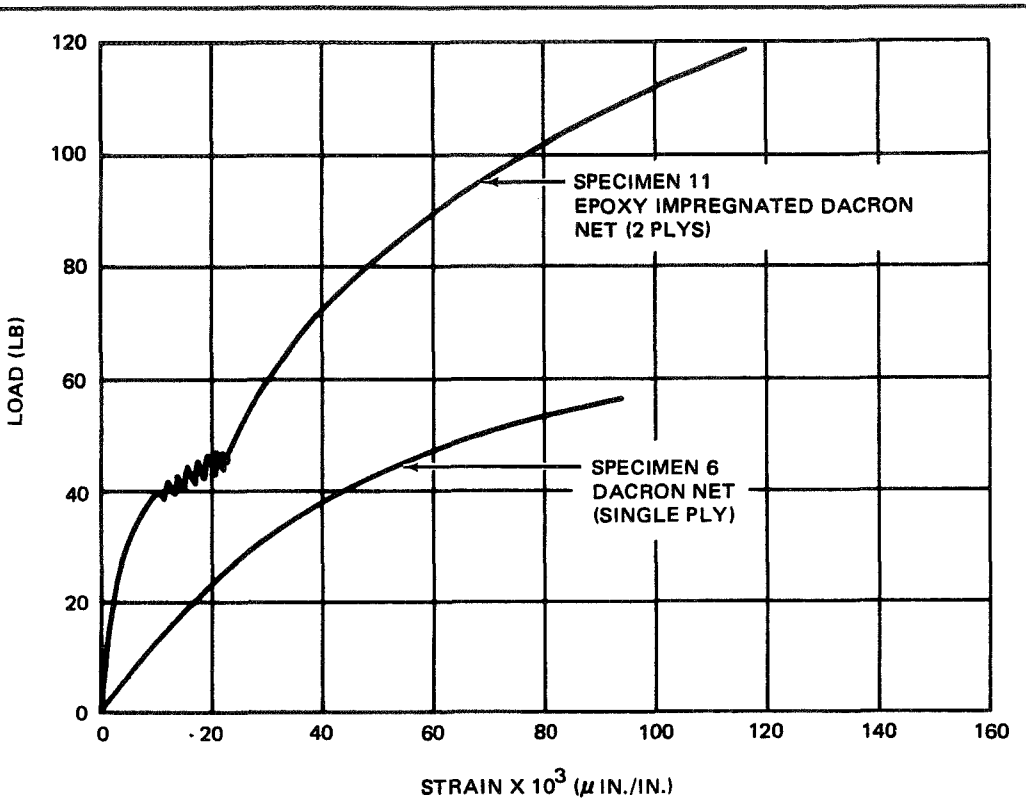

Figure 7-5. Tensile Strength of Dacron Face Sheet

7.4 TEAROUT RESISTANCE OF NYLON SWIFTTACH FASTENERS

During the study, two improvements to the MLI panel design were proposed to significantly reduce manufacturing costs: heat-set Mylar-tape-reinforced face sheet and one-piece Swifttach fasteners (Appendix A). To ensure suitability for application to the study panel design, tensile test measurements were made of the resistance of the fastener to tearout through the face sheet under decompression loads.

The face sheets used in the tests were heat-set Mylar tape sandwiched between two plies of Dacron net (Section 4). The sheets were drilled with a 0.09-in. -diameter hollow drill and fasteners inserted in the normal manner with an installation gun.

No pullthrough was experienced. The fastener head failed in tension at 3- to 4-lb load, similar to the heat-seal fasteners used earlier in MLI panel design. It was concluded that these fasteners would be adequate.

7.5 PANEL COMPONENT THERMAL EXPANSION CHARACTERISTICS

The panel design (Section 2) is such that the face sheets carry all loads, eliminating the possibility of Mylar reflectors tearing around fasteners. Therefore, face sheet materials must shrink more than the Mylar when the tank is cold. To obtain design data, thermal expansion coefficients were measured.

One specimen each of two face sheet materials (epoxy and heat-set Mylar tape reinforced Dacron) and 15-gage double-aluminized Mylar were tested in a quartz tube dilatometer apparatus. Results are presented in Figure 7-6. Note that though both face sheet materials are suitable for use with the Mylar reflector, the heat-set tape system is preferable. It is a closer match to the Mylar. Also, it can be used for elevated temperature applications.

7.6 PANEL ASSEMBLY DYNAMIC LOAD TEST

This test was designed to evaluate the structural integrity of the MLI panel design during vehicle launch. A 5-foot panel segment with vertical joint was subjected to a launch acoustic environment after cooling with LN_2. No failure attributable to dynamic loading was noted. A considerable fluffing of the MLI layers, apparently permanent, was observed. Improved thermal performance might be expected from this effect.

7.6.1 Test Environment

Test loads corresponded to a nominal Saturn boost acoustic environment, modified to reflect the response of the baseline MNV tank. This environment is more severe than the expected sine sweep and random vibration. Therefore, only the acoustic loads were imposed. A progressive wave tube was used.

The MNV sidewall MLI panel attachment straps are loaded longitudinally by acceleration (5 g) and normal to the tank by the acoustic environment. Therefore, the straps were preloaded to 5 g before exposure to the acoustic environment.

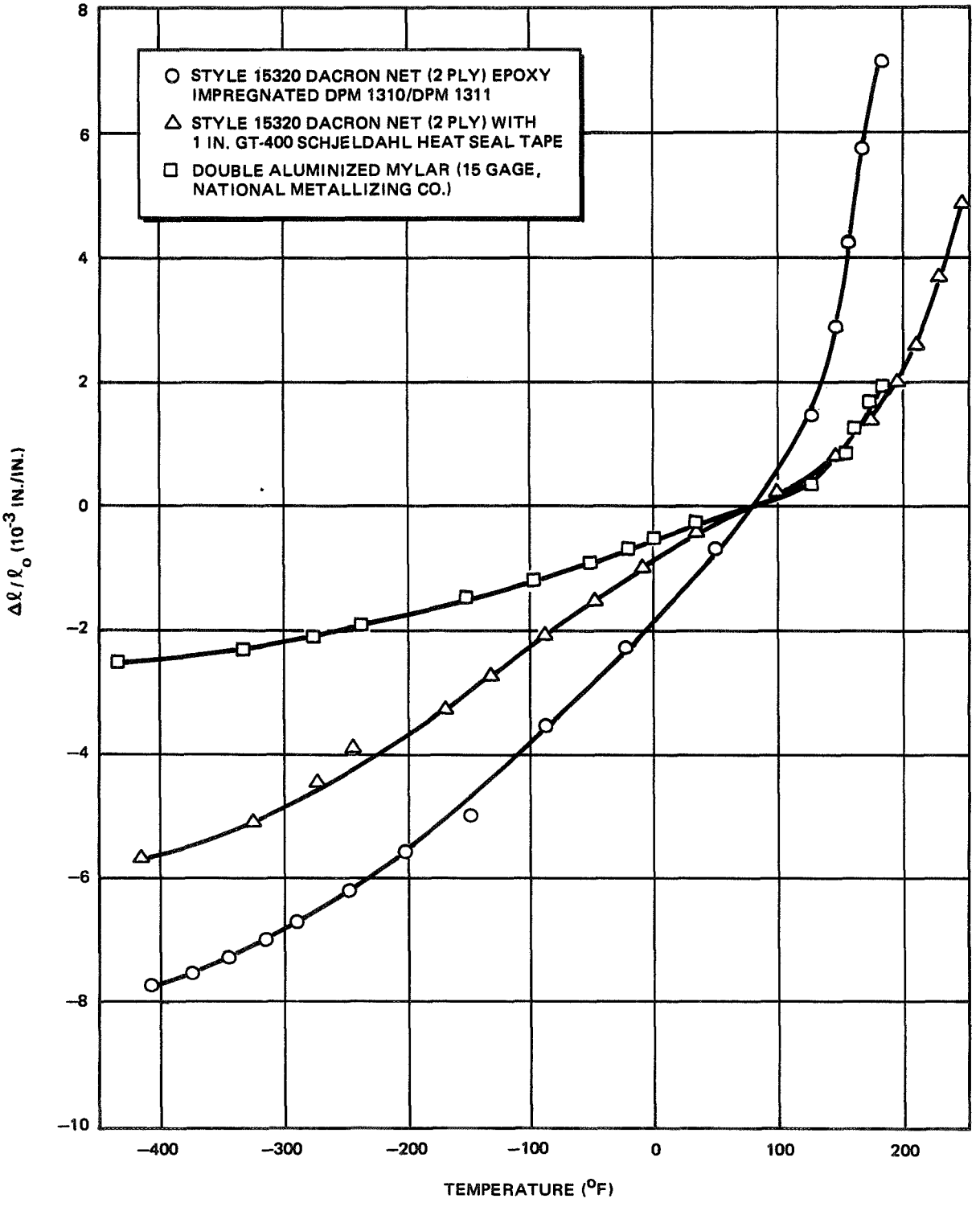

Figure 7-6. Thermal Expansion of MLI Panel Materials

7.6.2 Test Specimen

The specimen consisted of two 34-layer-pair panels of 15-gage DAM/B2A Dacron net laced together at the center with a longitudinal butt joint (Figures 7-7 and 7-8). Face sheets were the same as described earlier, two-ply Dacron net with impregnated epoxy straps. Each panel was supported by six attachment straps (composed of a four-ply impregnated tab and an O-size grommet) on the inner face sheet, with the weight being supported by continuous support straps. Outer face sheets had interrupted straps. Panel components, inner face sheet, reflector-spacer pairs, and outer face sheet were assembled with heat-sealed fasteners. Two strain gages were installed at the center of each support strap and calibrated to provide a method for measuring strap preload.

7.6.3 Test Setup

The test panels were mounted on a supporting test fixture, which simulated a plate with clamped edges, in a progressive wave tube. Specimen mounting was on the fixture outer face and the fixture acoustically loaded on its inner side (see Reference 5 for fixture details). Therefore, deflection of the central portion of the plate loaded the MLI. The specimen was attached at the fixture bottom by securing the straps to studs with a lock-nut. A tensioning device was used at the top of each strap, providing the proper strap preload.

Three accelerometers were mounted on the fixture's loaded side — one at the center of the panel opposite the longitudinal joint and one 5 in. on either side of the joint opposite the nearest support straps. Three microphones were mounted in the wave tube at either edge and at the fixture's center.

A foam box enclosure was used to introduce gaseous nitrogen to the specimen, chilling it to cryogenic temperatures. The nitrogen was metered into the box through a perforated tube and the specimen temperature monitored. A minimum equilibrium temperature of -260°F was reached.

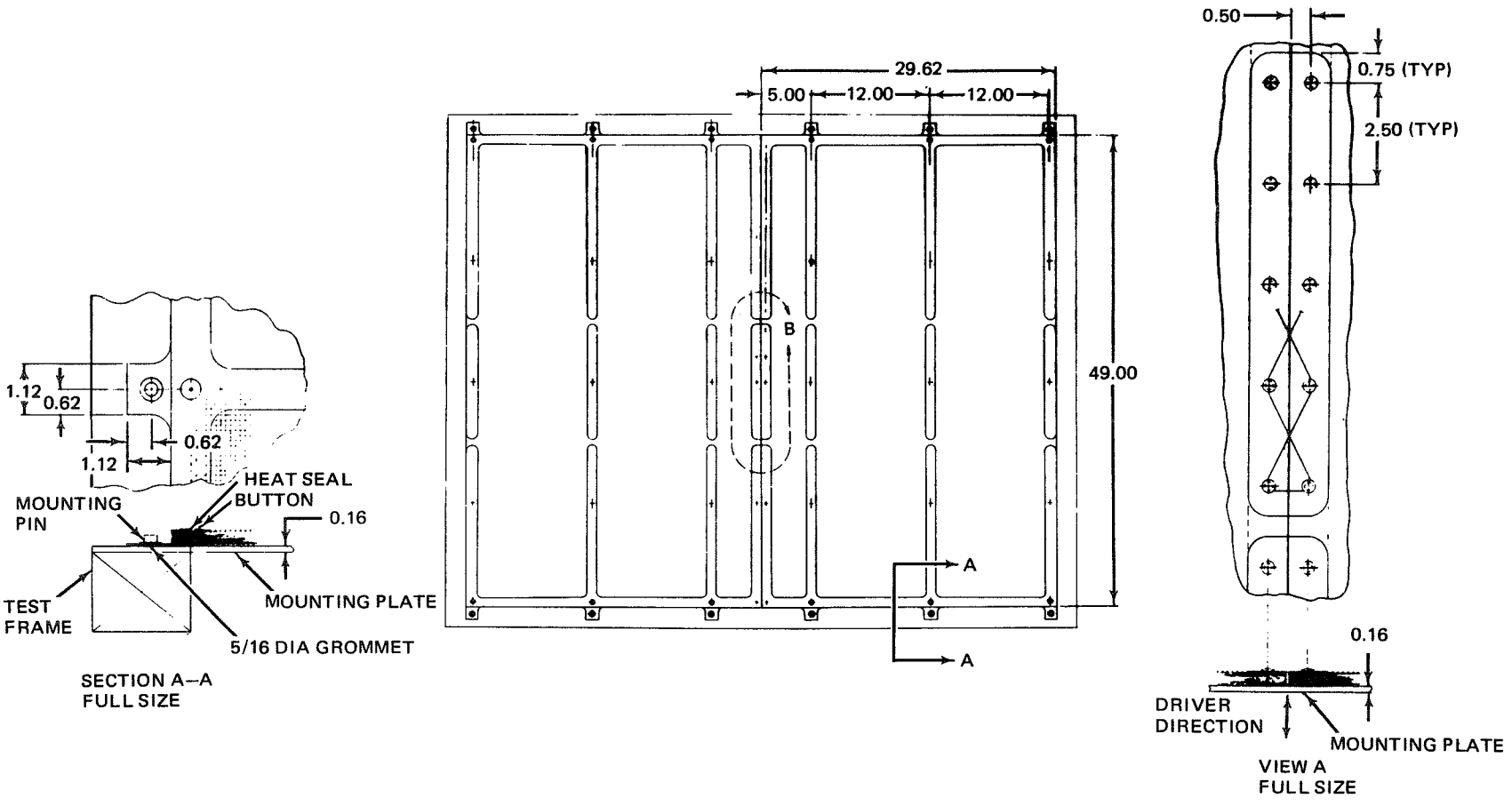

Figure 7-7. Panel Dynamic-Test Configuration

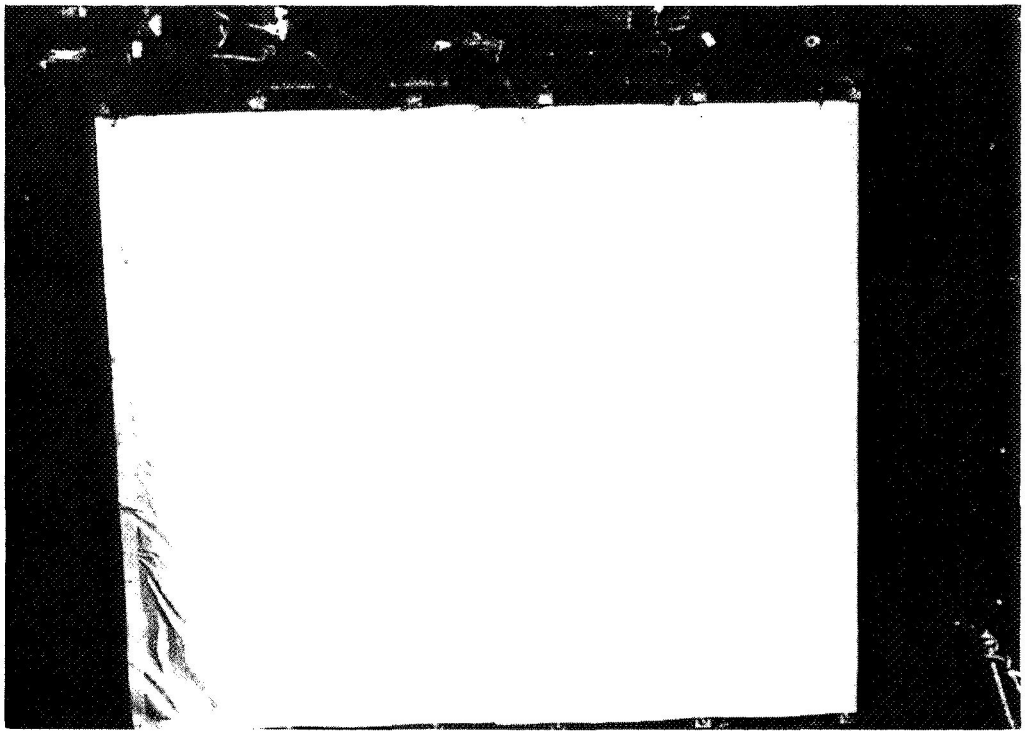

Figure 7-8. HPI Panel Specimen Installed on Test Fixture

7.7.4 Test Results

The achieved overall acoustic power spectral density is shown in Figure 7-9 (test 9-2-70). Accelerometers showed maximum levels of 55, 42, and 52 g (rms).

Damage to the face sheets, the reflector-spacer pairs, or the lacing buttons could not be observed upon a post-test inspection of the HPI panel specimen. However, four of the 30 fasteners failed at the heat seal. Three were located at the edge of the test fixture and the fourth was 12 in. from the edge. Because these locations were not loaded during test, the fastener failures are believed due to thermal shock arising from specimen precooling.

During cooling, the LN_2 was initially metered into the test enclosure as a gas, but as the flowrate increased, the LN_2 was discharged into the test enclosure before vaporizing. Any discharge onto a fastener would provide

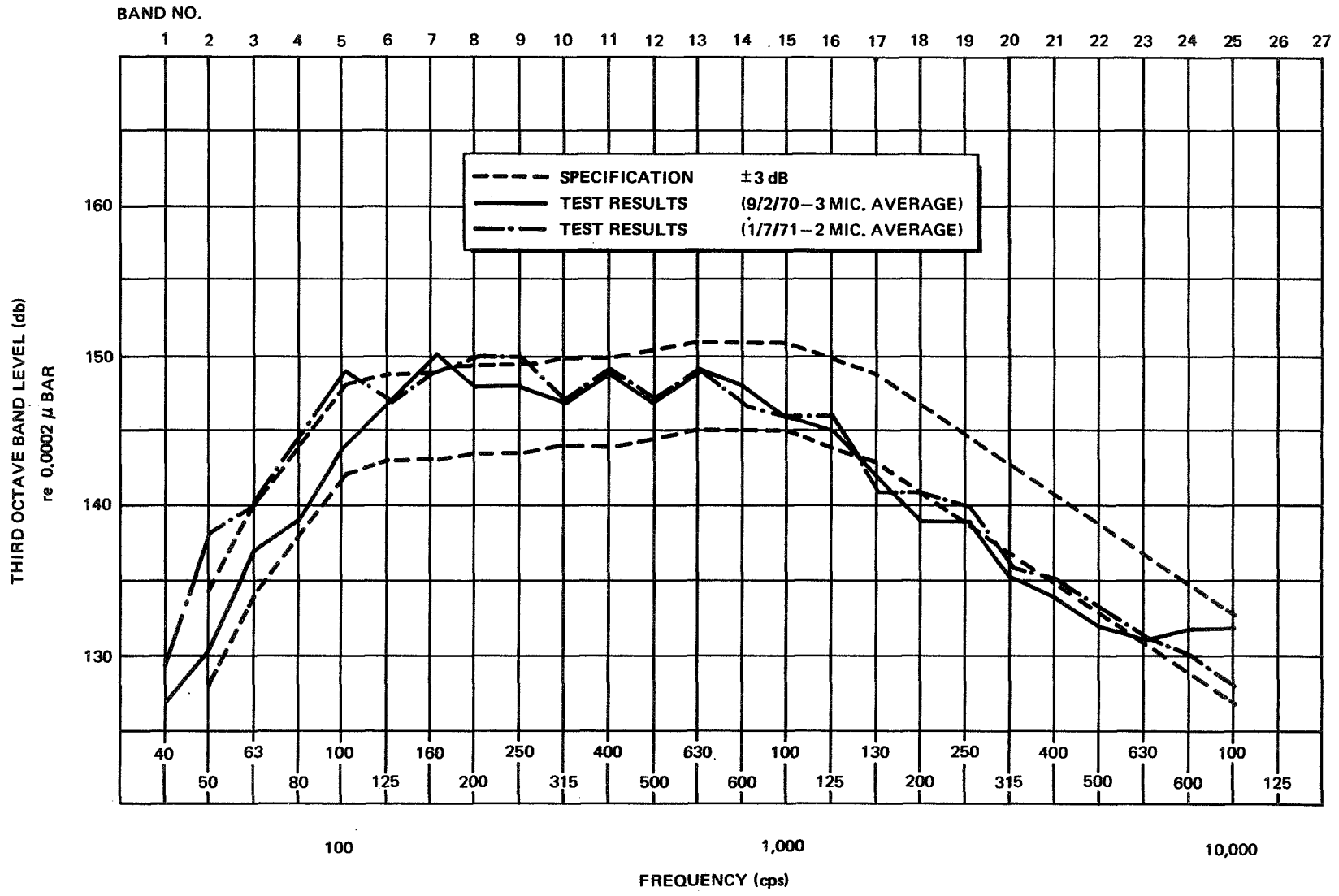

Figure 7-9. Acoustic Test Environment

enough of a thermal shock to cause the heat seal to fail. This condition would not occur in the MNV vehicle where the fasteners are cooled from the opposite side and the heat seal is cooled by conduction.

The thickness of the MLI increased by a factor of 2 or 3 after acoustic exposure; the layers fluffed. It was noted that this increase was limited at the fastener to its length.

The laced butt joint opened 0.060 in. at some locations apparently due to both the lacing procedure and design. To eliminate this problem, it is suggested that the lacing button pattern be moved in line with and closer to the fastener, and the number of lacing buttons be increased. This will allow a more efficient transfer of the lacing loads.

7.7 PANEL ATTACHMENT UNDER DYNAMIC LOAD

A second MLI specimen to evaluate panel attachments was dynamically tested in a manner identical to the above except that a smaller specimen with attachments closer to the center of the driving fixture was used. This specimen, Figure 7-10, was fabricated in the same manner as the panel specimen but differed in the overall dimensions. Test environment instrumentation and procedure were also the same. The specimen stabilized at -289°F.

The resulting power spectral density is shown in Figure 7-9 (test 1-2-70). Accelerometers registered 79, 61.5, and 83 g. These are considerably higher than in the panel test because the smaller specimen did not dampen the fixture response to the same extent.

An inspection of the specimen, particularly the attachment strap ends after testing, did not reveal any damage. There were no cracks in the epoxy-impregnated straps, nor was there any indication of damage around the grommets. Again, specimen thickness increased by a factor of 2 or 3 between fasteners; a thermal improvement.

R94

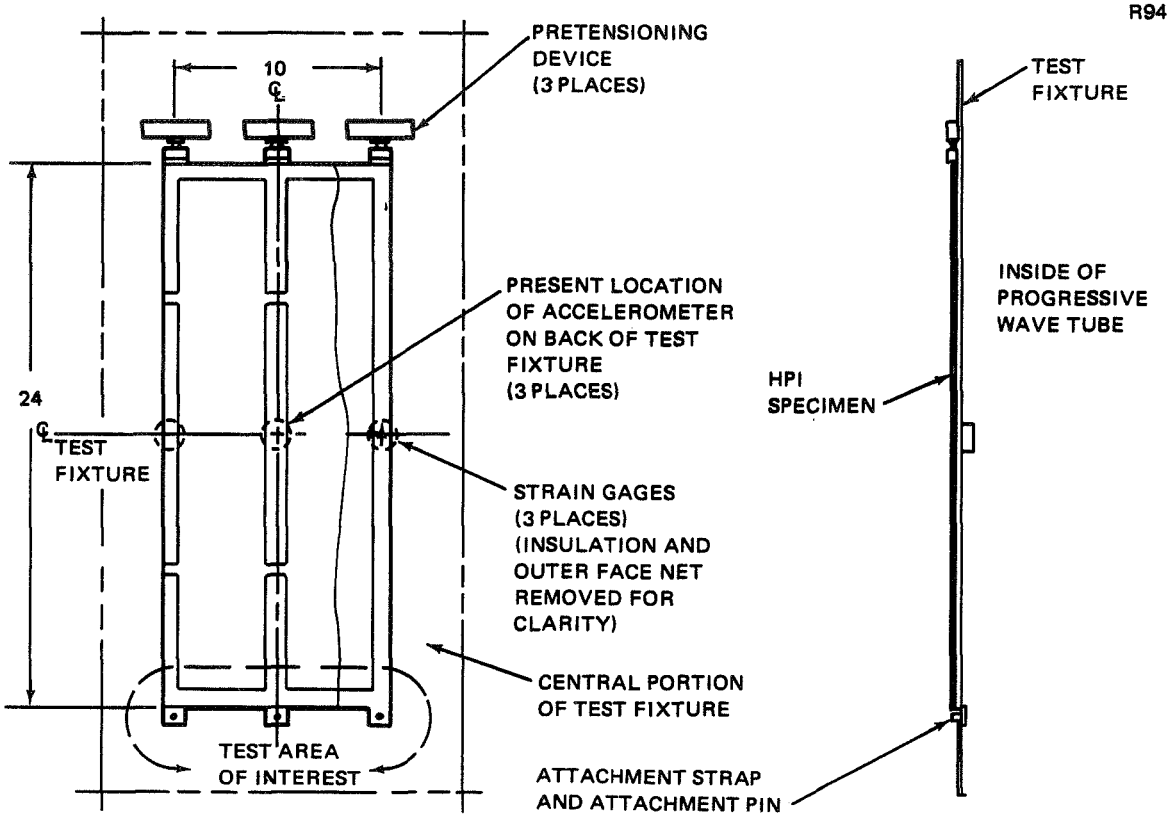

Figure 7-10. Attachment Strap Dynamic Test Specimen

PART II – DESIGN AND FABRICATION OF LARGE TANK MLI SYSTEM TEST ARTICLE

Section 8
TEST ARTICLE DESIGN AND TEST PLANNING

A complete flight-type MLI system was designed for application to the 105-in. tank with the objective of simulating, within reasonable limits, the performance characteristics of a full-scale vehicle propellant tank. A helium purge gas system, complete with a purge bag-tank enclosure, was included for preflight tank loading and launch simulation tests. Temperature instrumentation was specified for tank and MLI panel mounting to aid in interpreting the subsequent experimental thermal performance measurements.

Detailed test planning was accomplished to provide a definition of facility requirements and test procedures for the conduct of system performance tests at NASA-MSFC. Three specific tests were outlined: evacuated steady-state MLI thermal performance, purge system performance characteristics, and thermal performance throughout a simulated vehicle mission.

8.1 MLI SCALING CONSIDERATIONS AND TEST DESIGN CRITERIA

The test article definition study was started with an investigation of the scaleability of tank-type calorimeter MLI performance data to actual expected vehicle performance. The goals were to ascertain if the existing 105-in. -dia tank was large enough to directly yield full-scale vehicle data and to provide the test insulation design criteria.

The 105-in. tank was found to be sufficiently large. The key decision parameter is the tank radius of curvature which, in this tank, is sufficiently large to eliminate the need for curvature corrections in the test insulation heat transfer data. This conclusion is based upon the data in Figure 8-1.

For the study baseline vehicle, a 16-ft radius MNV, a nominal 2-in. -thick insulation would be about 99 percent flat plate both for the cylindrical side-wall and spherical ends. A thinner insulation will yield an even closer match to flat plate. Therefore, if the test tank insulation is essentially flat

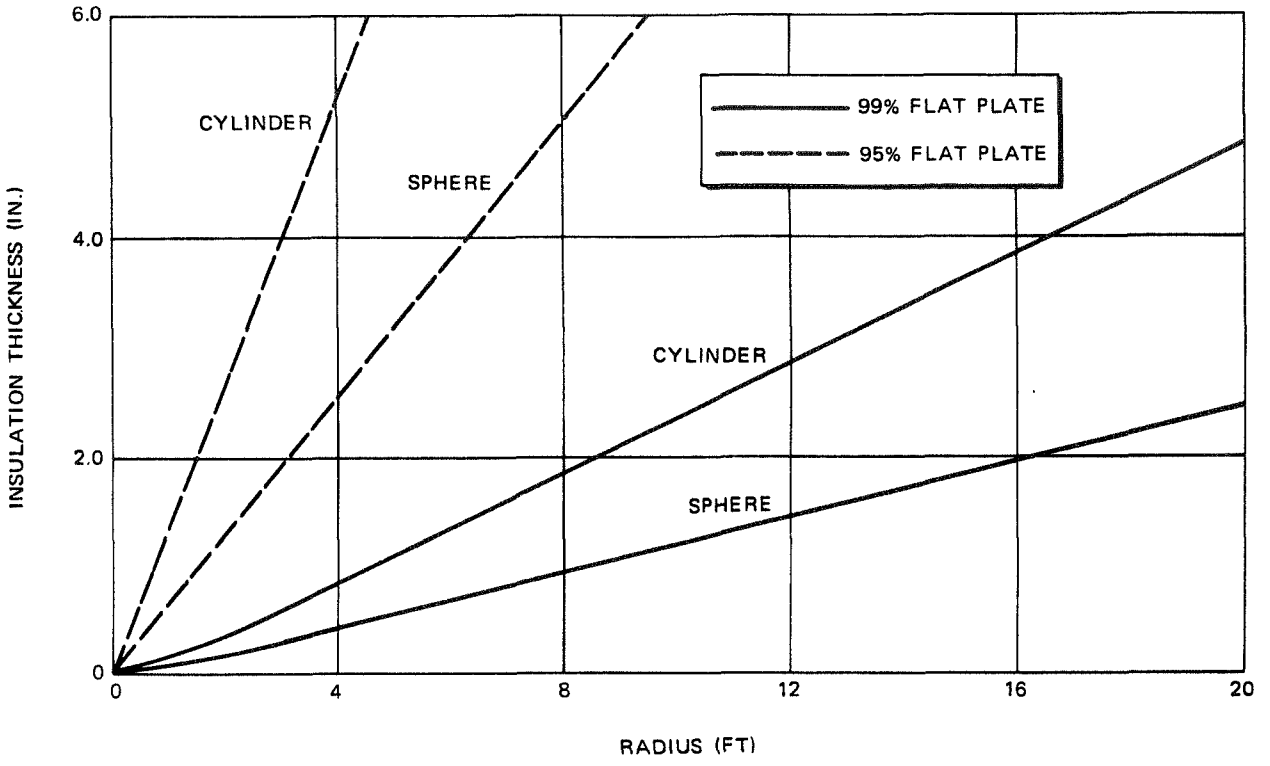

Figure 8-1. A Comparison of the Heat Transfer Magnitudes of Flat Insulation Blankets to Cylindrical and Spherical Blankets

plate and the joints well simulated, heat transfer rates can be extrapolated directly without analytical manipulations. Assuming that 95 percent flat plate (5 percent error) is sufficient simulation, Figure 8-1 shows that a test apparatus must have a minimum spherical dome radius of 3.2 ft and minimum cylindrical radius of 1.6 ft for 2 in. of MLI. With the 0.7-in. MLI selected for the test in this program, the 105-in. tank yields almost 99 percent flat plate data.

Published MLI scaling analyses were reviewed and found to yield essentially error parameters, not dimensionless scaling relationships. A dimensional analysis was then undertaken resulting in the identification of the 13 scaling rules shown in Table 8-1. The basic implication of these relationships is that exact scaling can be achieved only by testing full-thickness MLI panels. Therefore, testing a typical full-thickness vehicle insulation was adopted as a criterion for test article insulation design.

The above work led to a minimum analysis approach to test design; minimum analytical tools needed to relate test results to the actual vehicle. With this approach, heat transfer to a vehicle would be determined by adding up the

Table 8-1

MLI SCALING PARAMETERS

Variables

$T_o - T_i$ = temperature difference between the tank and outside layer of insulation.

T_o = outside insulation layer temperature.

τ = time for system to evacuate to 10^{-4} torr.

ϵ_1 = emissivity of upward-facing sides of insulation sheets.

ϵ_2 = emissivity of downward-facing sides of insulation sheets.

K_ℓ = lateral conductivity of insulation sheet.

K_n = normal conductivity of insulation sheets.

C = contact conductance between sheets.

ρ = insulation density.

C_p = insulation sheet specific heat.

R = insulation blanket radius of curvature.

t = insulation blanket thickness.

S = insulation sheet thickness.

$\mathscr{L}$ = blanket length.

W = blanket width.

N = number of sheets per inch.

ρ_g = density of the gas within the insulation.

Dimensionless Scaling Parameters*

$\pi_1 = \frac{\omega}{R}$	Relate the geometries of any two systems.
$\pi_2 = \frac{\mathscr{L}}{R}$	
$\pi_3 = \frac{S}{t}$	
$\pi_4 = \frac{t}{N}$	
$\pi_5 = \frac{t}{R}$	
$\pi_6 = \epsilon_1$	Relate the emissivity of the systems.
$\pi_7 = \epsilon_2$	
$\pi_8 = \frac{K_n \tau}{\rho C_p R^2} = \frac{\alpha\tau}{R^2}$	Time-scale relationship
$\pi_9 = \frac{K_\ell}{K_N}$	Ratio of lateral to normal heat transfer.
$\pi_{10} = \frac{tC}{K_N}$	Normal direction heat transfer indication.
$\pi_{11} = \frac{\rho_g}{\rho}$	Ratio of entrapped gas density to sheet density.
$\pi_{12} = \frac{T_i}{T_o - T_i}$	Ratio of outer surface temperature to the temperature difference.
$\pi_{13} = \frac{C_p(T_o - T_i)L^2}{K^2} \rho^2 C_p^2 = \frac{C_p(T_o - T_i)L^2}{\alpha^2}$	Ratio of stored heat to the square of the thermal diffusivity.

*From Buckingham's Pi Theorem

various heat transfer components of the MLI system. Full-scale tests of each component (joint, penetration, etc.) are required and were performed during Phase I to provide the separate component data. It was therefore concluded that the 105-in. test article should be a test of full-scale MLI assemblies installed as a group in an identical manner to the full-scale vehicle system. To assess heat transfer through penetrations and feed throughs, separate full-scale component tests should be accomplished at a later date as these are best left off a full-scale tank for its initial tests. Uncertainties in the performance of these components would cloud the primary data desired on the basic applied MLI composite.

The MLI panel outgassing characteristics should also be simulated if the test data are to be directly applicable to design. Here, a minimum analysis approach, compatible with the above for thermal effects, was adopted. Path length to the joint and the actual joint design governs the ability of the interstitial gases to escape. Therefore, test design criteria were adopted which required that the MNV joint design and panel width (4 ft) be maintained as much as possible in the scale system test article along with a panel length greater than 5 ft. With this approach, direct correlation was believed to be valid.

Due to the uncertainties associated with purge system design technology and the difference in configuration between the MNV and the test tank (supports, purge zones, etc.), purge system scaling was rejected. It appeared better to design experiments which would provide data for verification of analytical tools. Therefore, this was adopted as a test design criterion.

8.2 NASA/MSFC 105-INCH TANK-CALORIMETER

The test tank forming the basis of the insulation system test article was provided by NASA complete with internal instrumentation. Details are shown in Figure 8-2 with the insulation denoted schematically. The internal instrumentation (Section 10) consisted of liquid level sensors and fill-line-mounted thermocouples.

The tank is basically an unguarded calorimetric device which is isolated from structural heat shorts except for the support tube. This tube is the

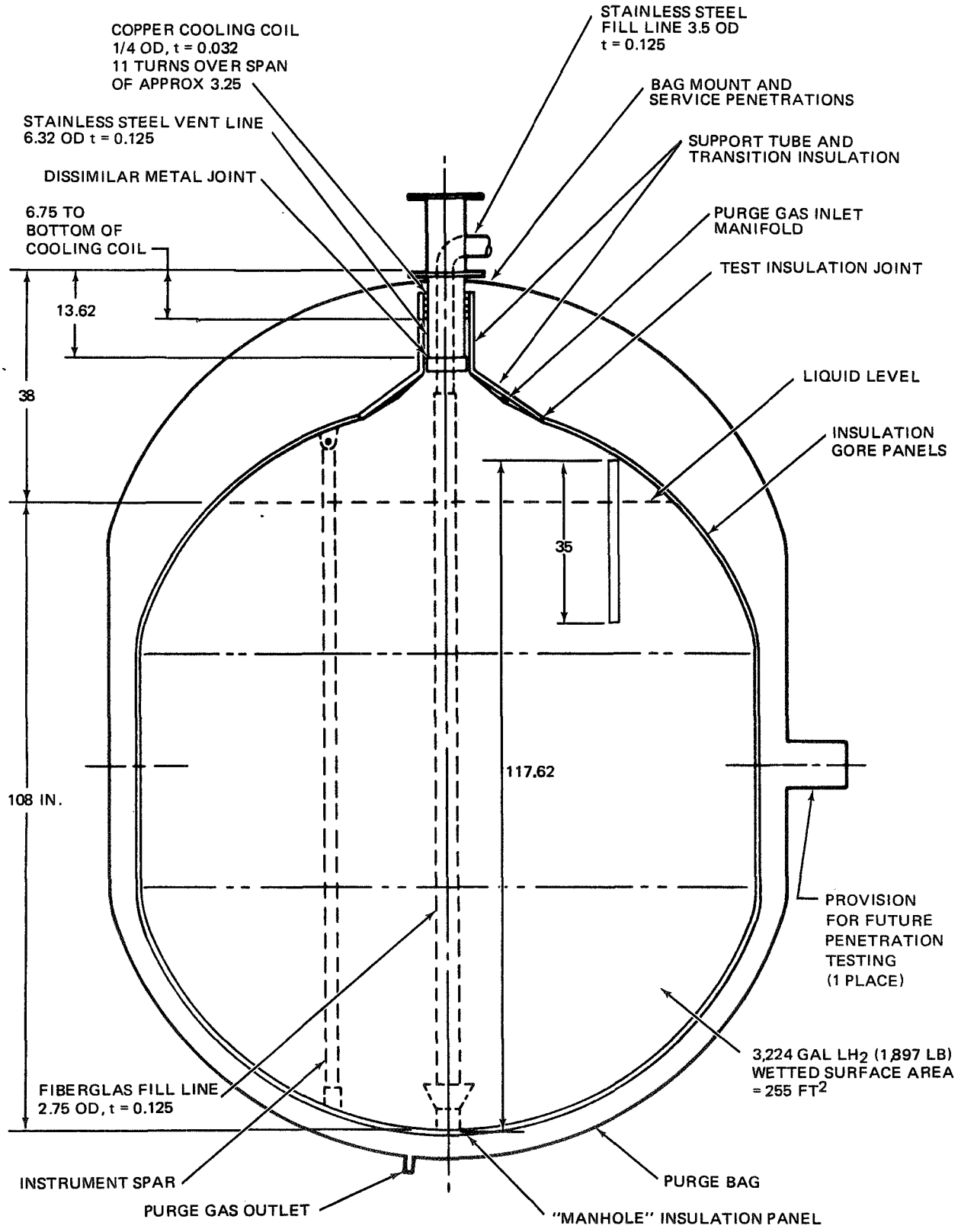

Figure 8-2. Test Article Configuration Schematic

sole structural mount. Extraneous heat leaks into the test cryogen have been minimized; the support is stainless steel and the internal fill line, fiberglass. Both are low-conductivity materials. The transition from the steel support to the aluminum tank is a bimetallic joint.

Testing and analysis performed during the program showed that this calorimeter is a highly efficient device for testing MLI systems. It is suggested that all future test tanks utilize this or a similar design. The tank achieves the ideal, complete isolation of the test insulation. Heat conducted down the fill line and support tube was found to be negligible, as it is intercepted by the vent gas.

Prior to MDAC testing, a small hole was drilled through the fill line in the tank ullage area to equalize the line internal and ullage pressure during test. This eliminates a thermal acoustic effect, noted in prior MDAC tests, where liquid tends to oscillate up and down in the line forming a heat pump. External valving connecting the closed fill line with the vent outlet could also be used. The valve is opened during test and closed for tank fill and drain operations.

The detail tank dimensions used to determine experiment requirements and instrumentation placement are shown on MSFC Drawings SK 30-4243 and SK 30-3150. Pertinent dimensions are summarized in Table 8-2, taken from a NASA computer printout for the area around the liquid level sensors which is of prime interest in experiment data reduction.

8.3 TEST TANK LIQUID LEVEL

The desired tank liquid level was selected primarily on the basis of maximization of wetted area yet minimizing the change in that area during test.

An initial propellant load of 1897 lb LH_2 was chosen. This corresponds to an ullage of approximately 4 percent. The resulting liquid level at the initiation of testing will be 22.61 in. below the bottom of the cylindrical support at the stainless steel/aluminum transition joint or 108 in. from the tank bottom. At this level, any changes in level height result in essentially

Table 8-2

TANK SURFACE AREA AND VOLUME

Height in Tank (in.)	Volume (ft^3)	LH_2 Weight (lb)	Wetted Surface Area (ft^2)
82.0000	329.8126	1451.1756	192.4441
83.0000	334.7654	1472.9679	194.7353
84.0000	339.7040	1494.6976	197.0327
85.0000	344.6177	1516.3177	199.3414
86.0000	349.4956	1537.7806	201.6665
87.0000	354.3267	1559.0376	204.0137
88.0000	359.0997	1580.0386	206.3895
88.5637	362.1827	1593.6039	207.9615
89.0000	363.7669	1600.5743	208.7989
90.0000	368.2843	1620.4507	211.2170
91.0000	372.7138	1639.9406	213.6351
92.0000	377.0518	1659.0279	216.0532
93.0000	381.2947	1677.6967	218.4713
94.0000	385.4388	1695.9308	220.8894
95.0000	389.4806	1713.7144	223.3075
96.0000	393.4163	1731.0315	225.7256
97.0000	397.2423	1747.8660	228.1437
98.0000	400.9550	1764.2019	230.5618
99.0000	404.5507	1780.0233	232.9799
100.0000	408.0259	1795.3141	235.3980
101.0000	411.3769	1810.0583	237.8161
102.0000	414.6000	1824.2400	240.2342
103.0000	417.6916	1837.8432	242.6523
104.0000	420.6481	1850.8518	245.0704
105.0000	423.4659	1863.2498	247.4885
106.0000	426.1412	1875.0213	249.9066
107.0000	428.6705	1886.1502	252.3247
108.0000	431.0501	1896.6206	254.7428
109.0000	433.2765	1906.4164	257.1609
110.0000	435.3458	1915.5217	259.5790
111.0000	437.2546	1923.9204	261.9971
112.0000	438.9992	1931.5966	264.4152
113.0000	440.5760	1938.5343	266.8333
114.0000	441.9812	1944.7174	269.2514
115.0000	443.2114	1950.1300	271.6695
116.0000	444.2627	1954.7568	274.0876
117.0000	445.1317	1958.5795	276.5057
118.0000	445.8146	1961.5844	278.9238

NOTES:
1. Capacitance level sensor lower limit, 82-5/8 in.
2. Upper limit, 117-5/8 in.
3. Initial liquid level, 108 in.

a linear change in wetted surface area. Initial liquid level will correspond to a reading of 25-3/8 in. on the capacitance level sensor.

For a nominal 50-Btu/hr experiment heat input, a total of 19 lb of LH_2 will be lost during a nominal 72-hour evacuated thermal performance test (assuming all heat goes to boiloff). The resulting liquid height change is about 1.8 in., corresponding to a change in tank wetted area of about 3.8 ft^2 or only 1.9 percent of the total wetted area.

The level change during a prelaunch and launch simulation test will be somewhat greater as the ground-hold heating rate will be much larger. For test design, a value of 110 Btu/ft^2 -hr was used, which for a nominal test period of 10 minutes results in a boiloff of 44 lb. It was assumed that this would be followed by a period of 3 minutes at the same heating rate during initial ascent, and a 72-hour period to achieve equilibrium in-space boiloff, resulting in a total liquid level change of approximately 4 in. Note that the actual measured ground hold heating rate obtained in the test (Section 10) was much higher, 275 Btu/hr-ft^2. This value should be used for future design.

8.4 MLI INSTALLATION DESIGN

The insulation system design for installation on the 105-in. tank and meeting the data scaling criteria for MNV application is described below. It simulates the performance characteristics of a full-scale vehicle tank insulated with MLI. Experimental measurements of its characteristics are directly usable, without analytical manipulation, for full-scale design.

8.4.1 Insulation Configuration

Details of the insulation system are shown in Figure 8-3. Insulation configuration is identical to that developed in Phase I for vehicle application; a total system constructed as an assembly of individual prefabricated panels. The panels are a stack of reflectors and separators sandwiched between load-carrying face sheets and assembled with nylon fasteners penetrating the sandwich assembly. Two layers of panels with butt joints are used with the outer layer offset 2 in. from the inner.

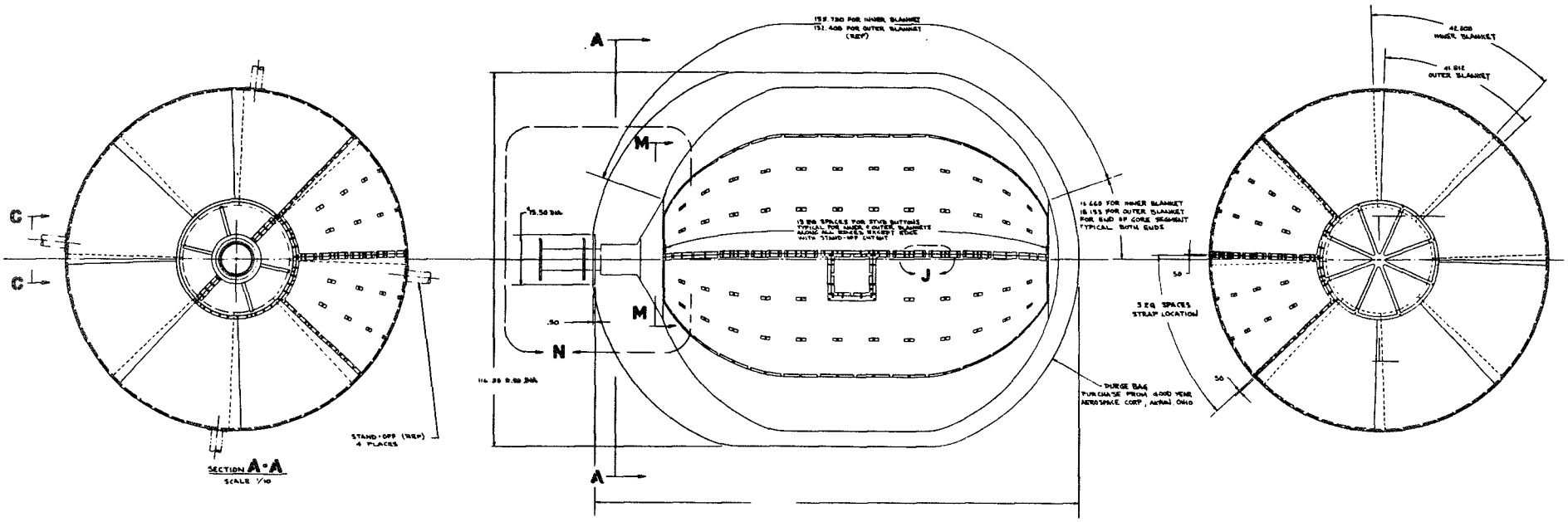

Figure 8-3. Test Article Configuration Details

FOLDOUT FRAME 1

FOLDOUT FRAME 2

CR94

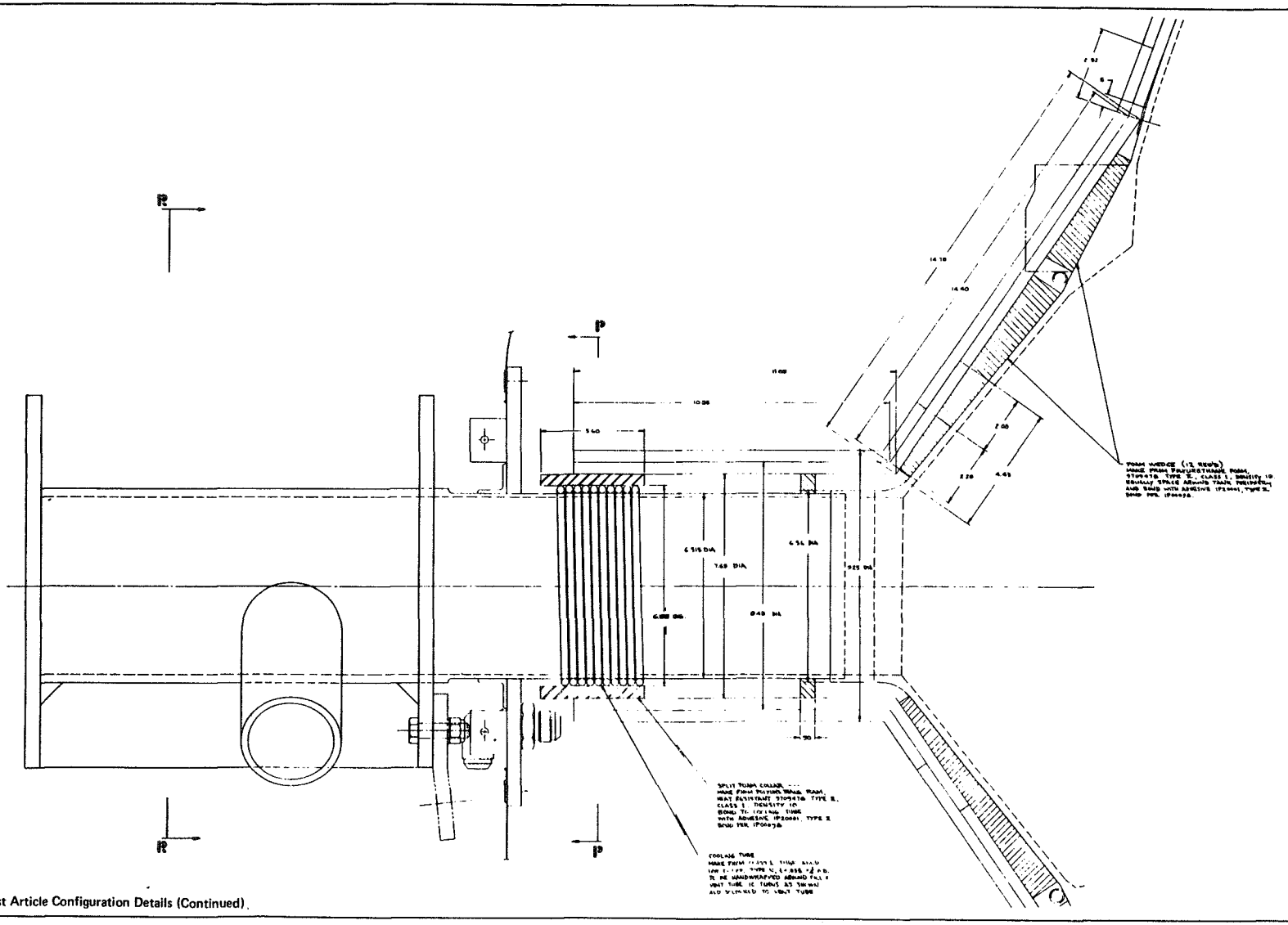

Figure 8-3. Test Article Configuration Details (Continued)

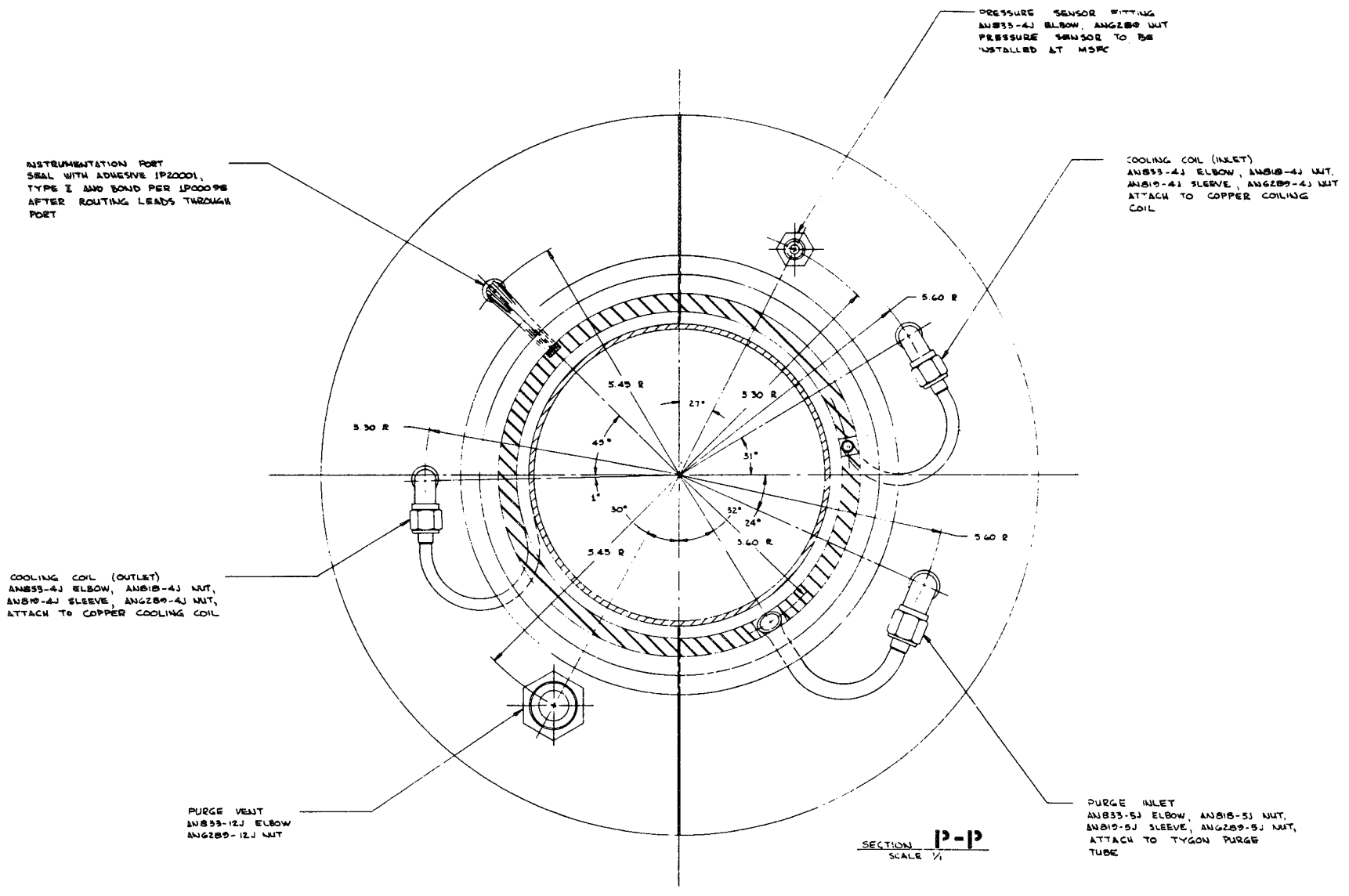

Figure 8-3. Test Article Configuration Details (Continued)

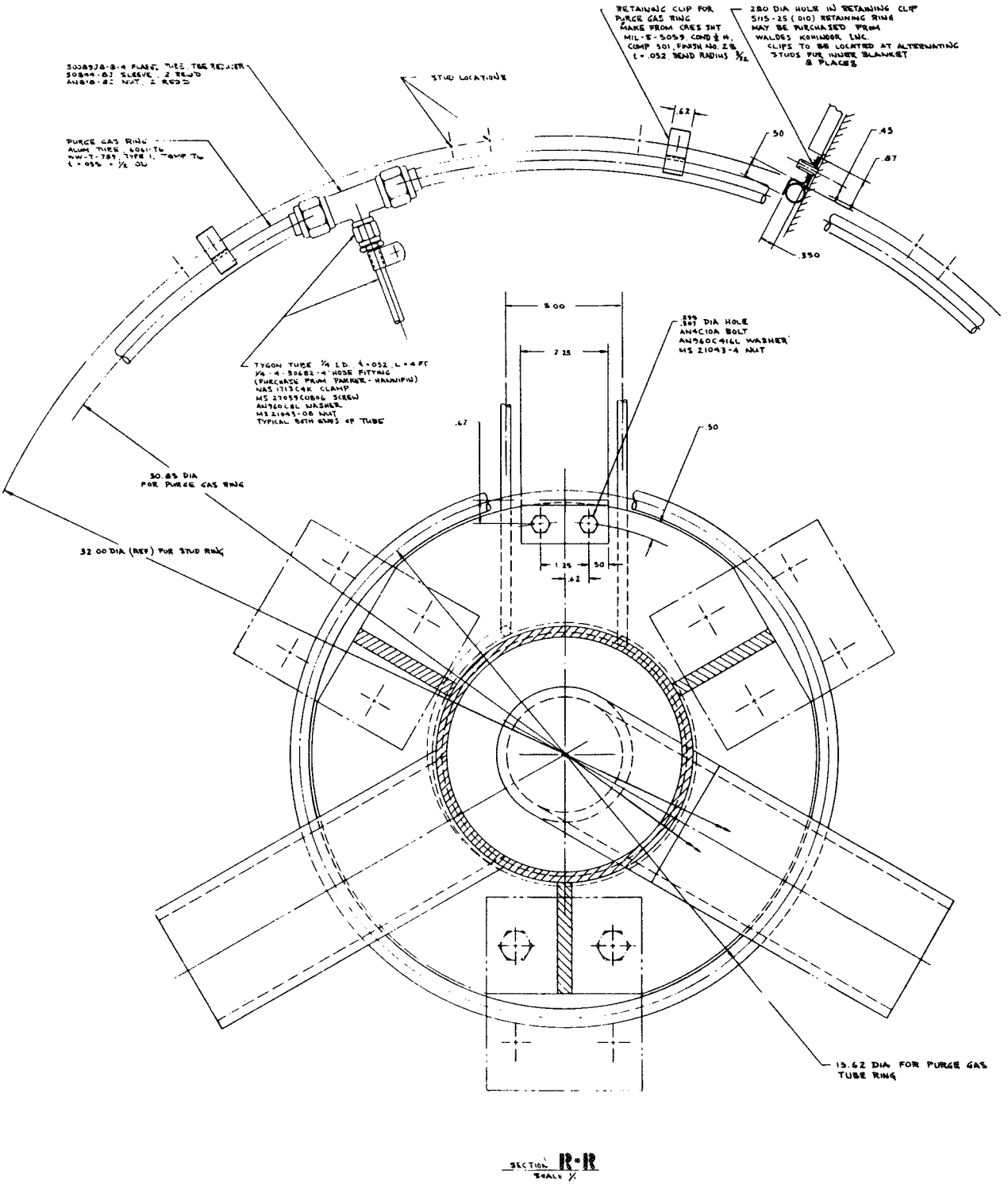

Figure 8-3. Test Article Configuration Details (Continued)

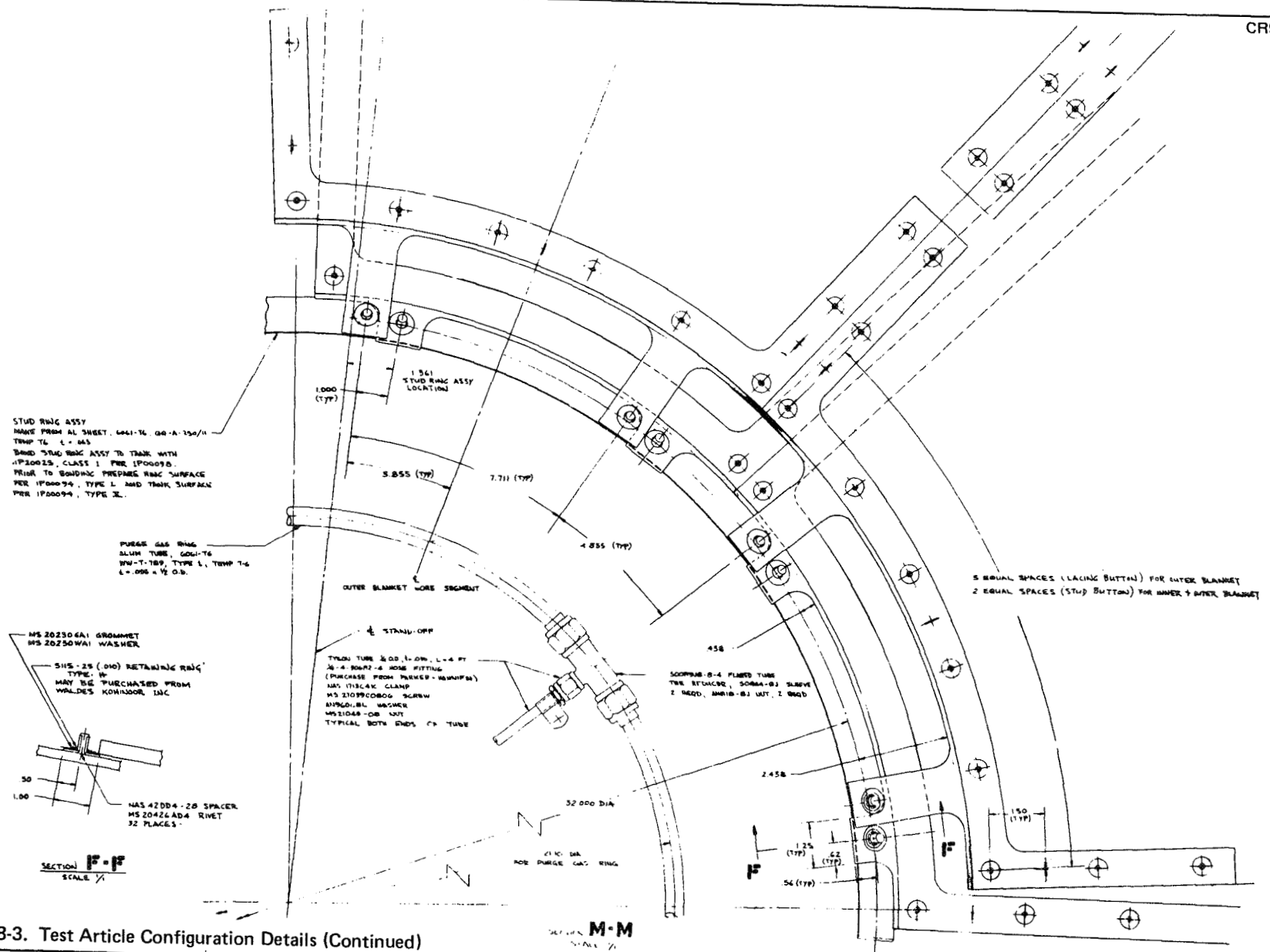

Figure 8-3. Test Article Configuration Details (Continued)

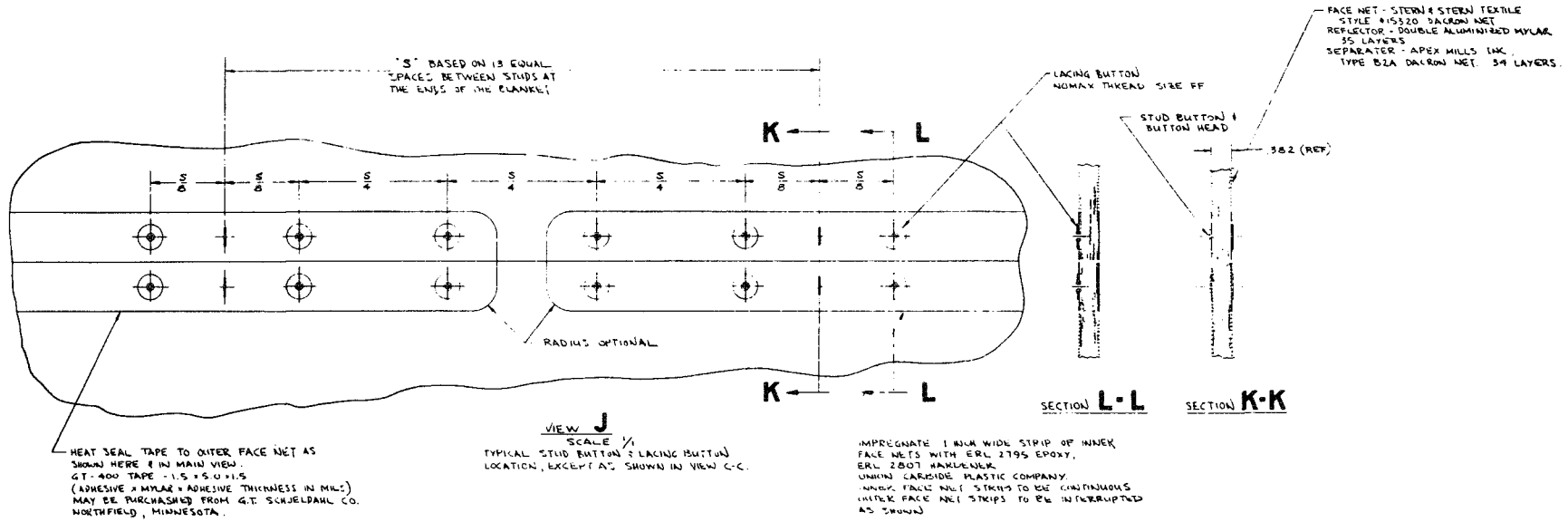

Figure 8-3. Test Article Configuration Details (Continued)

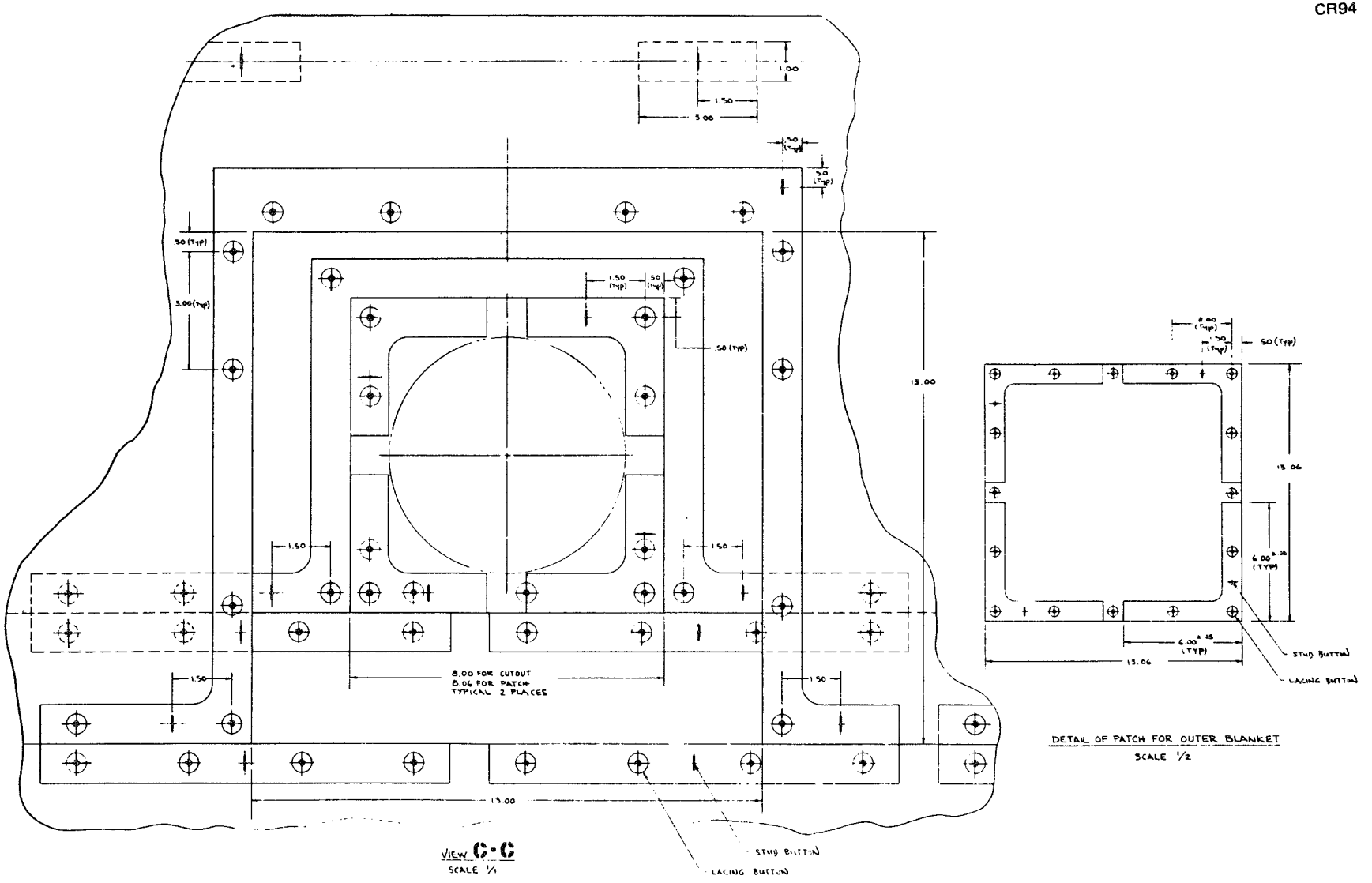

Figure 8-3. Test Article Configuration Details (Continued)

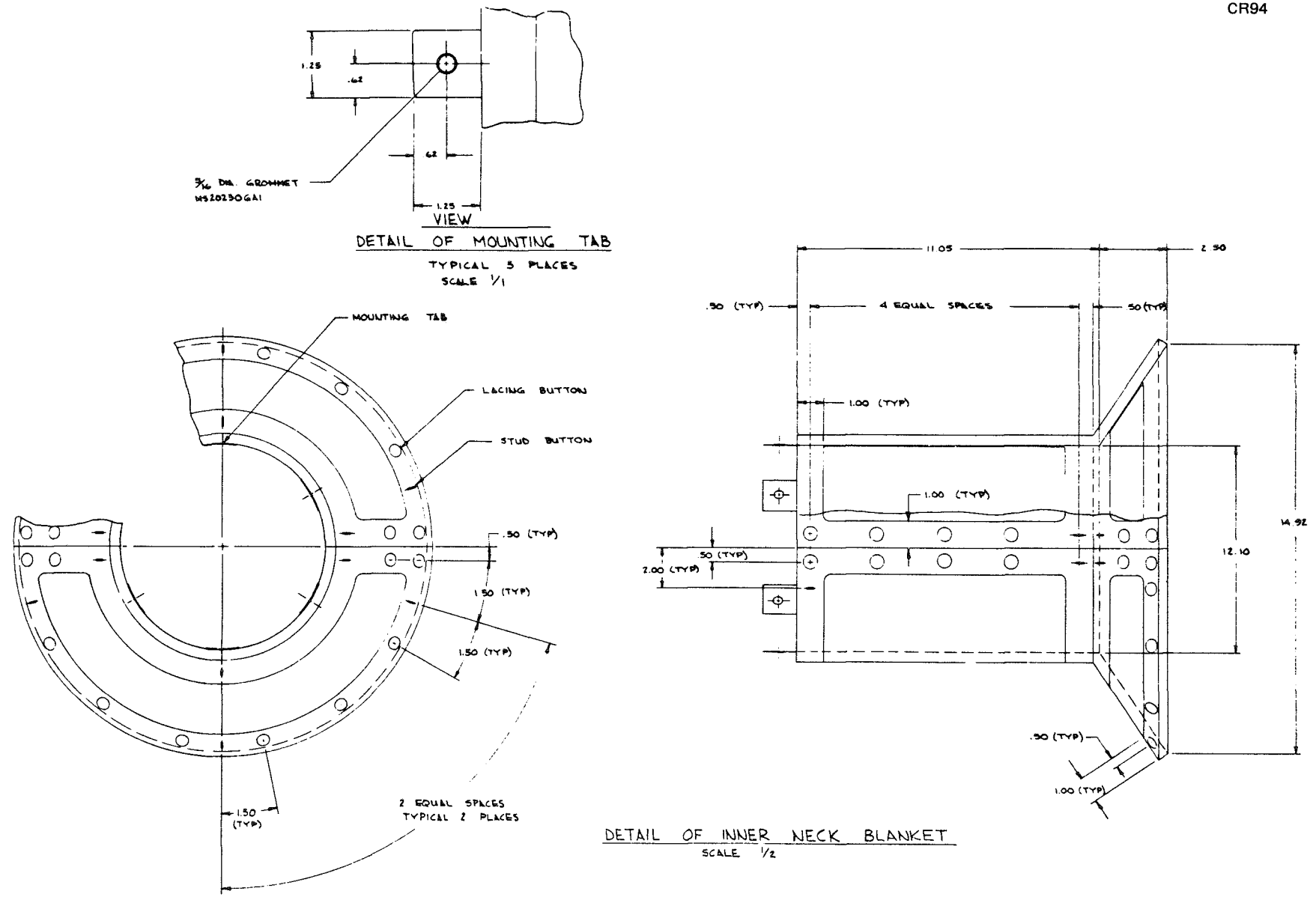

Figure 8-3. Test Article Configuration Details (Continued)

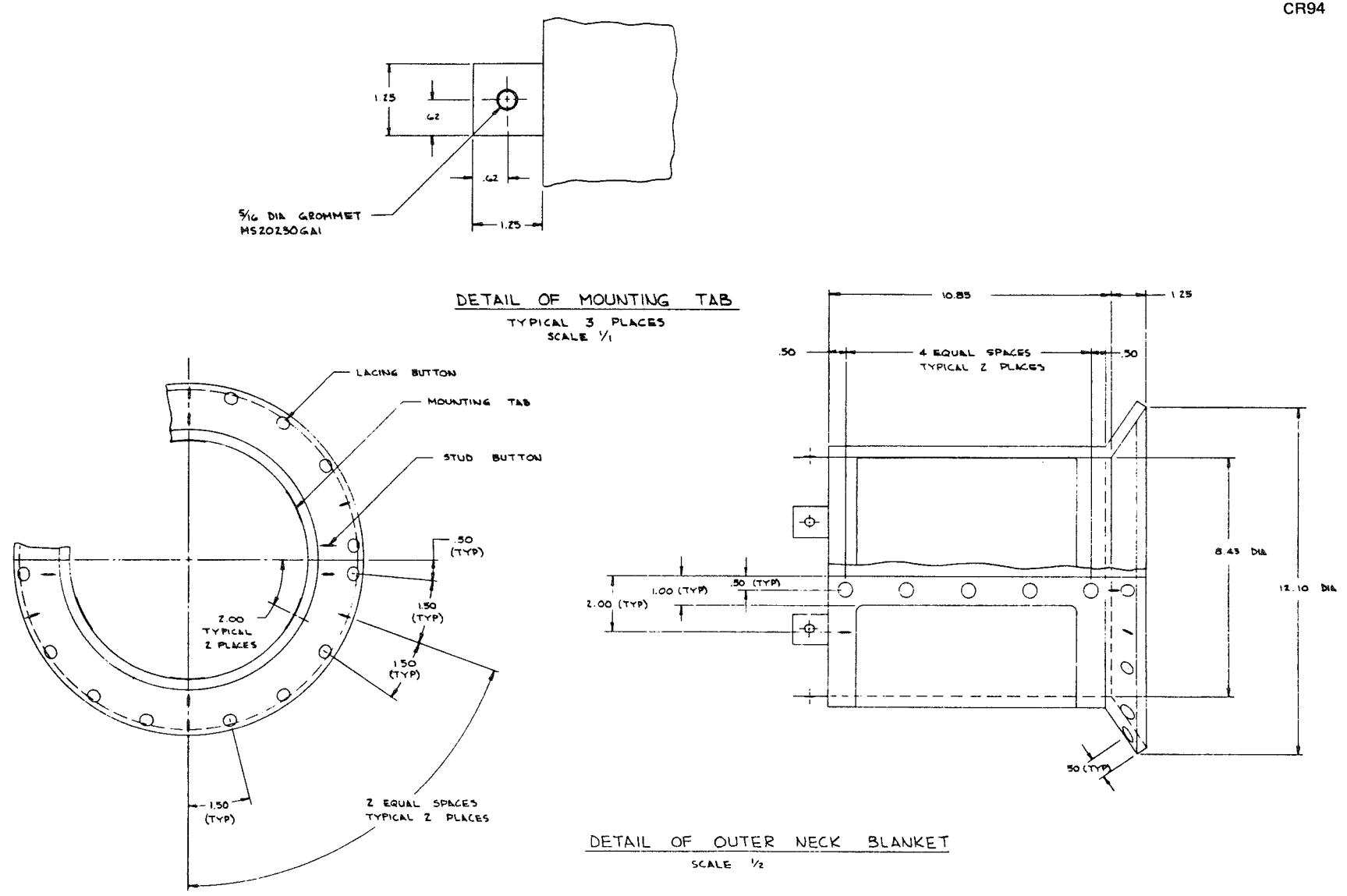

Figure 8-3. Test Article Configuration Details (Continued)

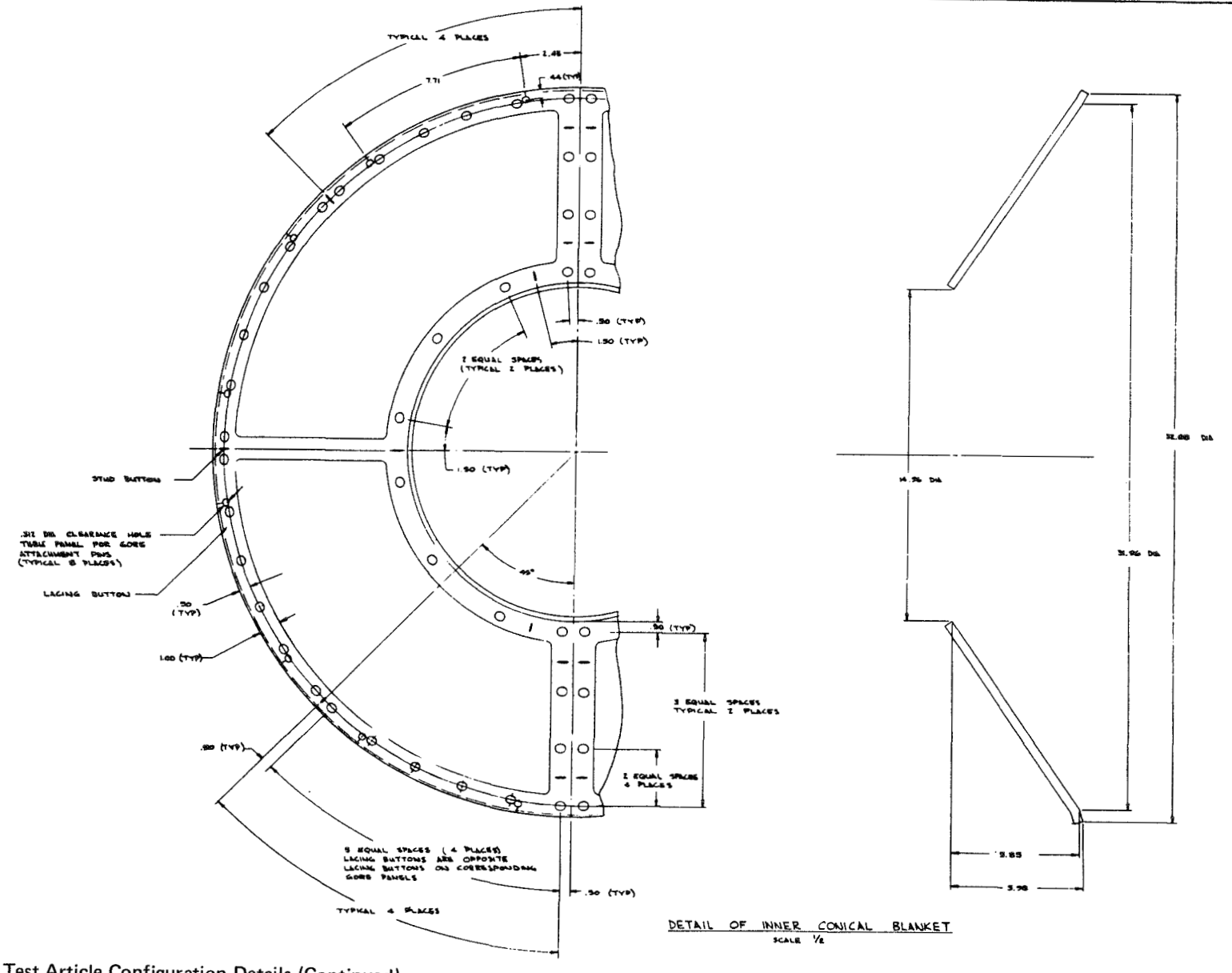

Figure 8-3. Test Article Configuration Details (Continued)

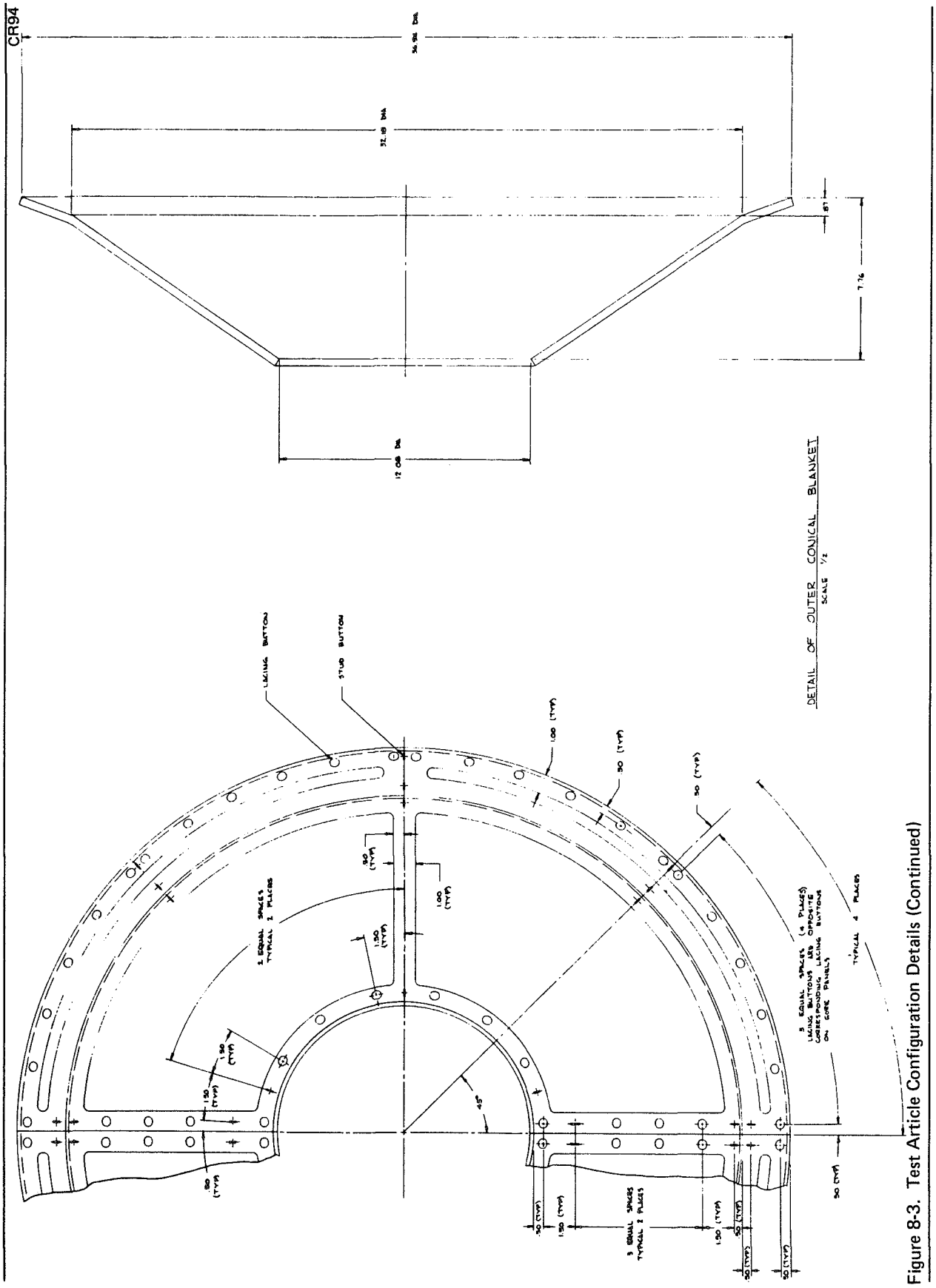

Figure 8-3. Test Article Configuration Details (Continued)

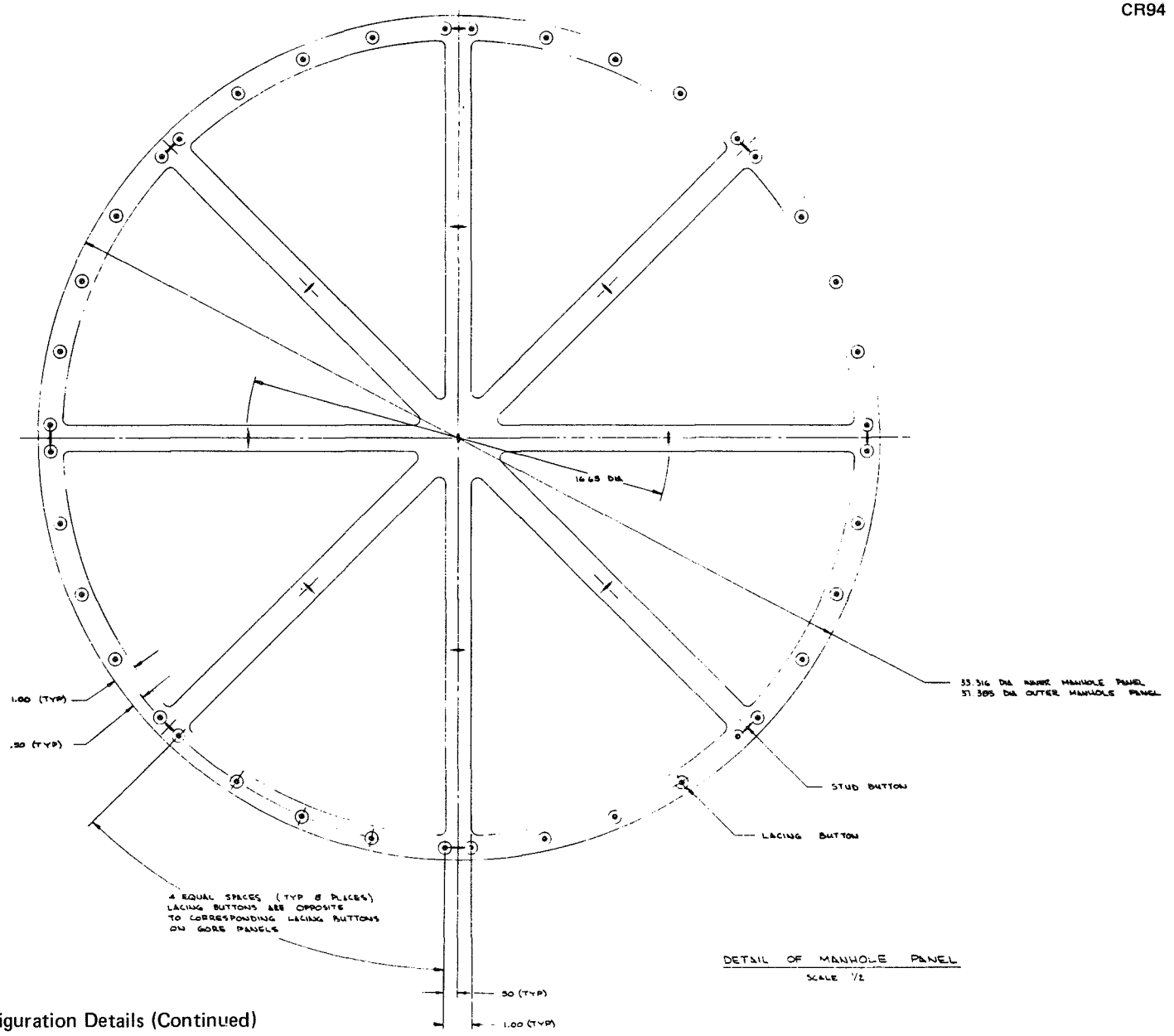

Figure 8-3. Test Article Configuration Details (Continued)

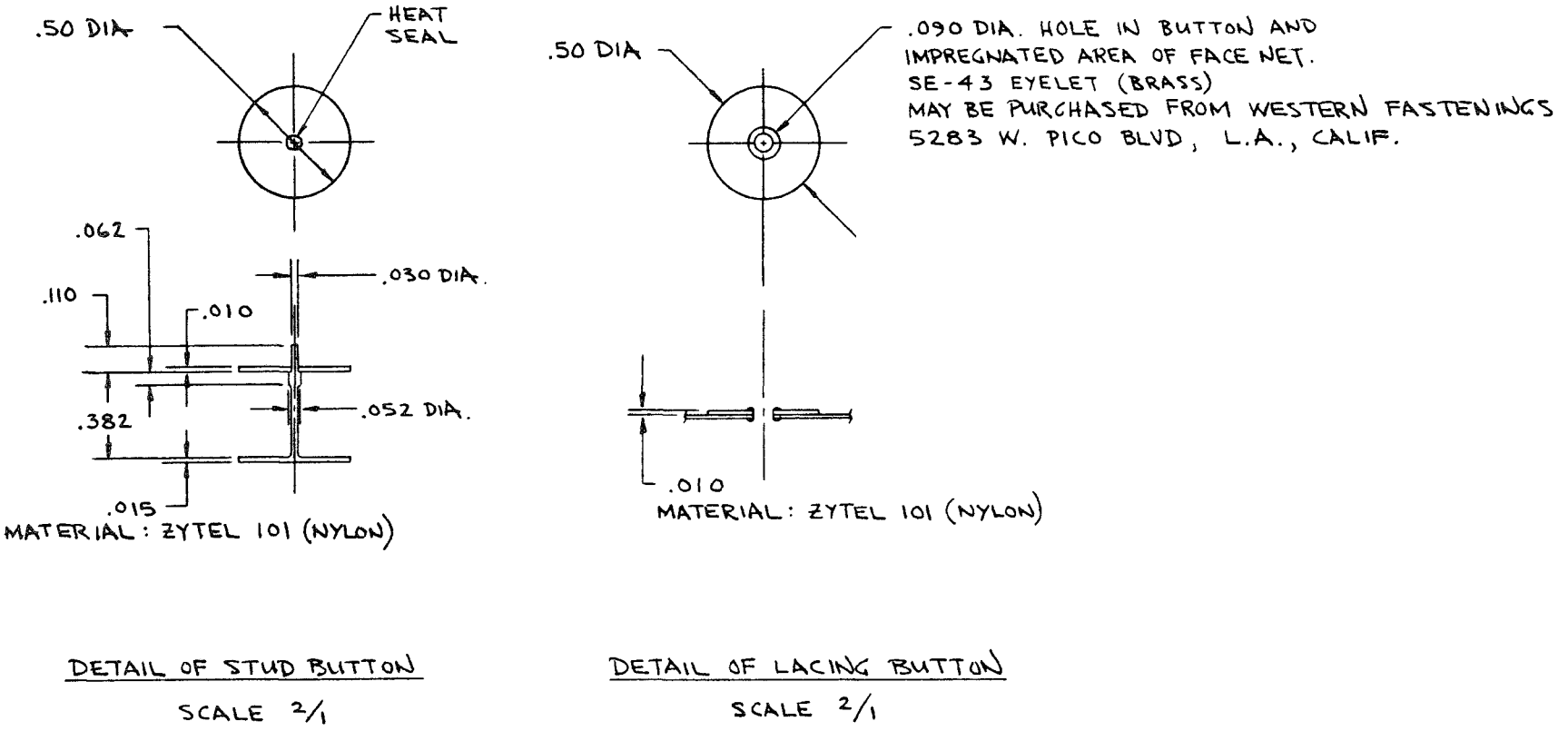

Figure 8-3. Test Article Configuration Details (Continued)

The total insulation inventory for the tank consists of 36 individual panels: 16 gore; four cone, six cylindrical support tube; two manhole; and eight patch type covering the tank shipping supports. Straps in the gore panel face sheets are attached to pins at the tank top which carry the weight of the insulation. Accessory panels (manhole, etc.) are in turn fastened to the gore panels. Joint closure is accomplished with Velcro tabs on inner surfaces and lacing on the panel outer surface.

8.4.2 MLI Composite Materials

Configuration details and procurement data for all the MLI system materials are presented in Appendix A. In summary, the test insulation composite consists of 15-gage double-aluminized Mylar (DAM) reflectors with type B4A Dacron net separators. Reflectors are perforated to a 2.38 percent open area. Each of the two panels is made up of 35 reflectors and 34 separators.

The target density for finished panels was 77 layers per inch. However, the Dacron net material supplied by the vendor for the actual fabrication was slightly different from the sample on which the design was based. The resulting layup density turned out to be considerably higher, about 100 layers per inch (see Section 9).

8.4.3 Fasteners

Injection-molded nylon pin-button fasteners with a heat-set head were developed for vehicle use during Phase I of the program. But difficulty was experienced under production conditions in achieving uniform, acceptable quality melting of the heads. A search for a new fastener design was undertaken.

The fasteners finally selected for panel assembly were special order 0.5-in.-long Swifttach units procured from the Dennison Manufacturing Co., Farmington, Mass. (see Section 9.1). Made of injection-molded Zytel 101 nylon, they are shaped like the letter I, or double T. All cross sections are circular, 0.03 in. in diameter.

Acceptance of these fasteners was based upon tensile tests of the resistance of the fastener to pull through the face sheet. No pull-through was experienced for any of the half-dozen samples tested. The fastener head failed in

tension at 3 to 4 lb load, similar to the heat-seal head fasteners used earlier in the design.

8.4.4 Face Sheets

The panel load-carrying face sheets were constructed as shown in View J of Figure 8-3. Heat-sealed tape was used for all reinforcement areas. Load carrying tabs were 4 layers of tape thick on top of the basic Dacron net substrate.

The coefficient of expansion of this tape-reinforced Mylar material was measured on the MDAC IRAD program. It was found to be compatible with the Mylar reflector, shrinking at a slightly faster rate than the reflector, a characteristic required to maintain the load in the strap.

8.4.5 Joints

Panel joints simulate those encountered on a typical vehicle installation as much as possible. It should be noted that the joint overlap dimension for offset gore panel layers will vary as a function of the gore radius of curvature on the test article, but all joints have a minimum overlap of 2-in. Gore panel joint overlap increases toward the panel center from the 2-in. minimum at the ends.

During panel installation on the tank (Section 9), the need for a positive joint closure on the inner surfaces of panels was noted. Velcro tabs across the joint were added at 12- to 18-in. intervals.

After testing, it was observed that the lacing closure shown in the drawings did maintain joint integrity throughout launch decompression loads, but a small gap at the joint butt was noted. It was concluded that further design studies of joint closure should be undertaken, although the joint used here could be applied as-is to current vehicles.

8.4.6 Insulation Support Ring

All insulation panels are located from the 16 gores which in turn are located and supported on the tank by a 0.063-in.-thick by 1.0-in.-wide support ring containing pins. As any error in locating the gore panels accurately at the support ring would be greatly magnified at the bottom of the tank, a method

was needed which would yield an installation preserving the locations of the outer and inner blankets with respect to each other and to the edges of the tank shipping support openings.

A suitable fabrication method was defined. The pins were laid out and located on a flat pattern of the support ring and riveted in place. The ring was then slipped around the tank support tube and closed with a lap joint. Final adjustment locating the ring on the tank was accomplished with a transit and the ring was bonded in place.

This procedure virtually eliminated any error in locating panels. However, the design has no provision for adjustment of panels due to inherent panel manufacturing tolerances. The need for such an adjustment became apparent during panel installation. A redesign to achieve this goal is recommended for future installations.

8.5 SUPPORT TUBE COOLING COIL

To ensure that the flow of heat into the test cryogen (LH_2) through the tank support would be small, a cooling coil was provided. The coil, shown in Figure 8-3, is made from 11 turns of 1/4-in. annealed copper tubing wrapped around and soldered to the support tube. The plan was to circulate liquid nitrogen through the coil, if necessary, to intercept conducted thermal energy. Coolant enters on the tank side of the coil and exits at the top, warm end of the support. Test results (Section 10) showed that, in actual operation, the calorimeter support tube is itself a sufficient heat block to preclude the need for the coil.

8.6 MDAC-INSTALLED INSTRUMENTATION

The location of test-article-mounted instrumentation is shown in Figure 8-4. Internal capacitance probe level sensors and fill-line-mounted Chromel-Constantan thermocouples are NASA instrumentation sealed into the tank. Not shown are two rows of three carbon resistor point level sensors, on the fill line, at 117.4 and 113.4 in. from the tank bottom, respectively.

FOLDOUT FRAME 1

FOLDOUT FRAME 2

CR94

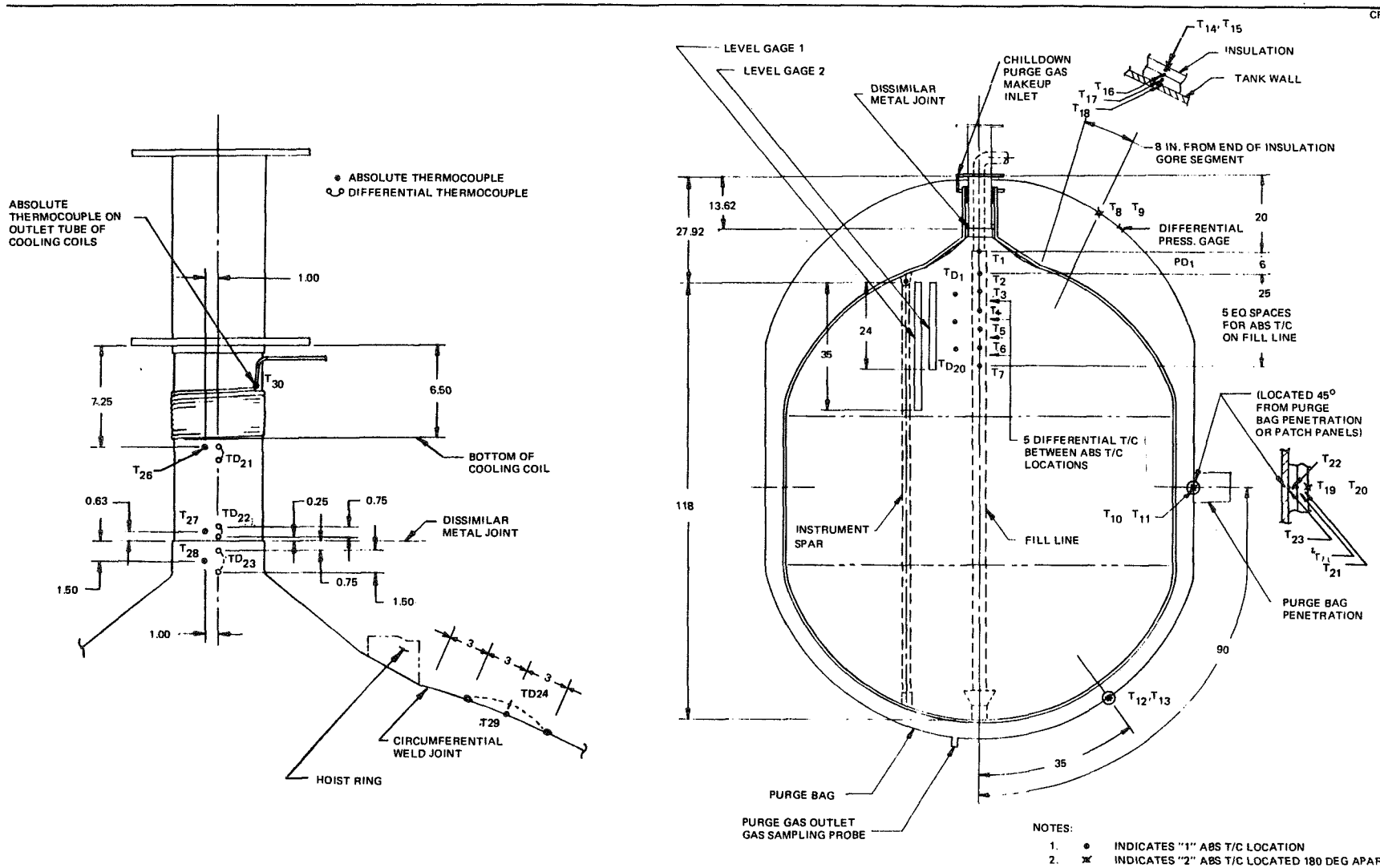

NOTES:

1. ● INDICATES "1" ABS T/C LOCATION
2. ✱ INDICATES "2" ABS T/C LOCATED 180 DEG APART

Figure 8-4. Test Article Instrumentation Schematic

External instrumentation (MDAC) consists of Chromel-Constantan thermocouples. These are wafer-type units procured from RDF Corp., Hudson, N. J., which are bonded to the tank and taped onto the insulation.

8.7 PURGE SYSTEM

A purge system consisting of two helium gas inlets, a bag for gas containment, and an outlet in the bag has been included as part of the test article. An external gas supply, control, and vent system is also required. A recommended schematic is shown in Section 8.11.

8.7.1 Gas Inlet Manifolds

One gas inlet under the insulation at the tank top introduces helium beneath the MLI where it percolates through the layers, forcing the heavier condensibles to exit at the bag bottom outlet. The high inlet tubes take advantage of the helium's tendency to rise to the bag top, displacing condensibles toward the low outlet.

The primary inlet is the 31-in.-diameter distribution ring, Figure 8-3, which distributes the gas flow through 20 No. 60 (drill) holes equally spaced around the ring. The expected flow rate for a one-hour condensible reduction period is 0.0011 lb/sec. Preinstallation testing showed that this flow could be achieved with a pressure of less than 10 psig.

Figure 8-3 also shows a second gas inlet, identified as the purge makeup inlet. It provides for additional helium flow during the tank chilldown when a pressure collapse of the helium purge gas would be expected. The additional flow serves to maintain a positive pressure within the purge bag which prevents the drawing in of condensibles due to reverse flow induced by pressure collapse. Design flow rate is 0.0098 lb/sec maximum.

8.7.2 Purge Bag and Bag Support

The purge bag, shown in Figure 8-5, constructed of polyurethane-coated Dacron fabric, is a purchased item from the Goodyear Aerospace Corp., Akron, Ohio. It is similar in material and type of construction and built from the same tooling as an earlier bag developed for MSFC by this firm. Weight is about 30 lb.

FOLDOUT FRAME

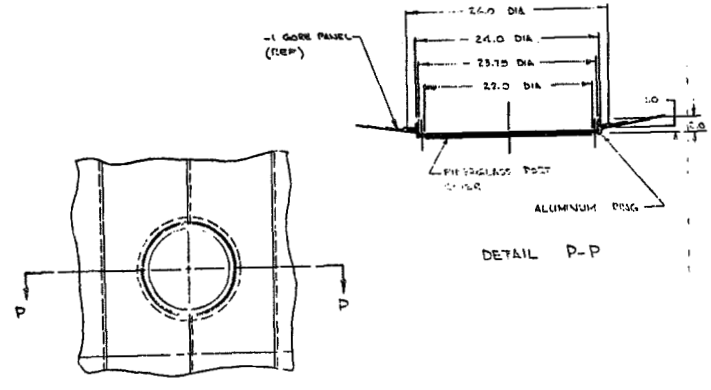

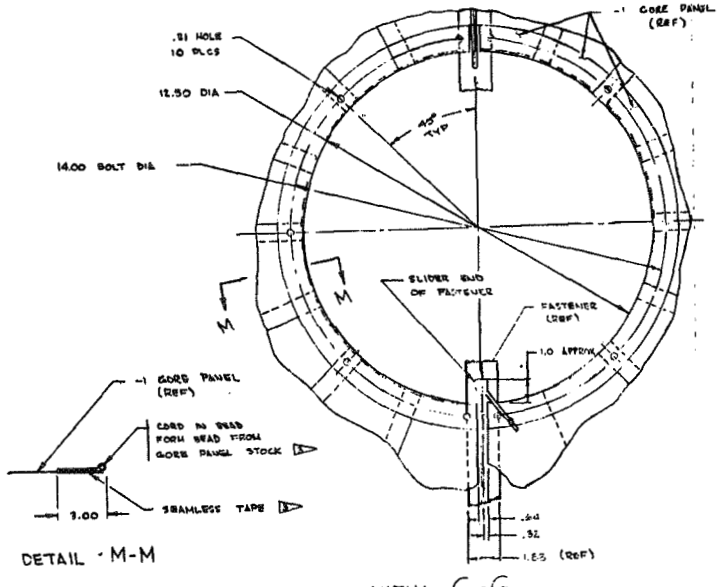

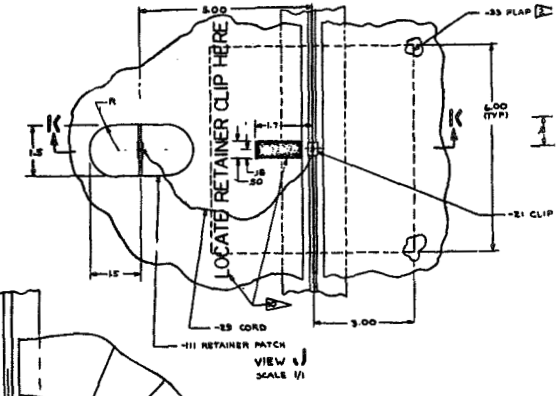

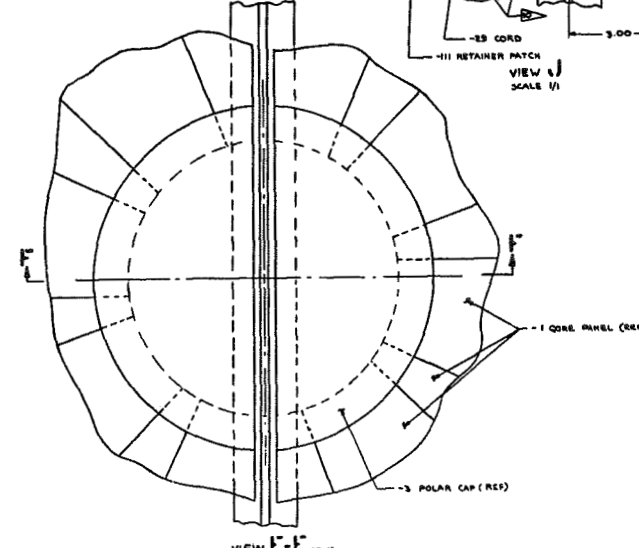

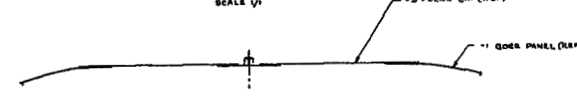

SECT. F-F
SCALE 1/1

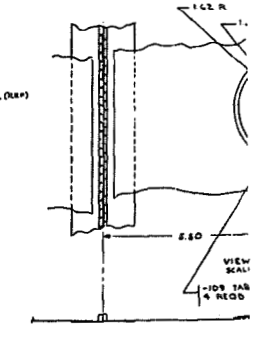

FOLDOUT FRAME

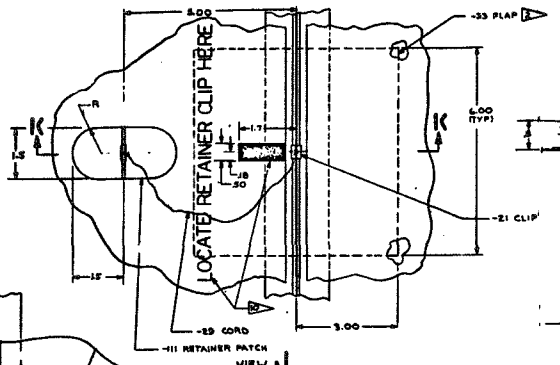

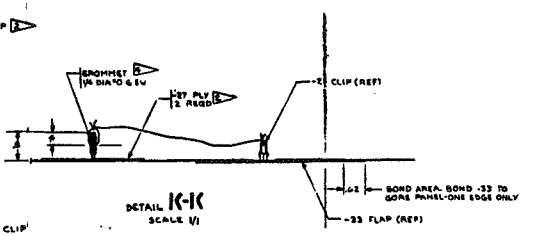

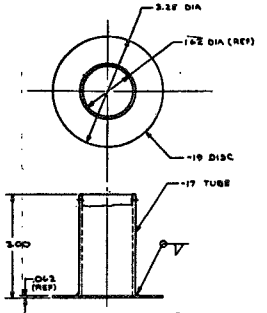

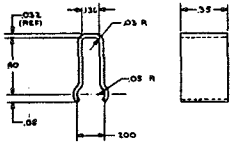

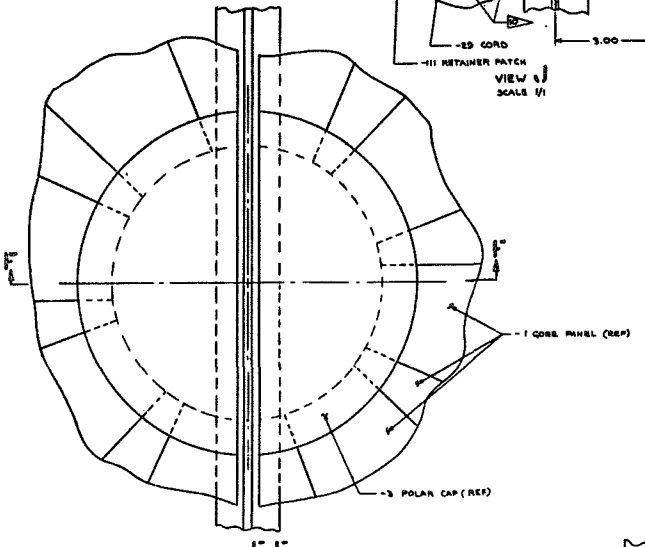

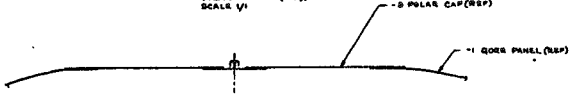

SECT F-F
SCALE 1/1

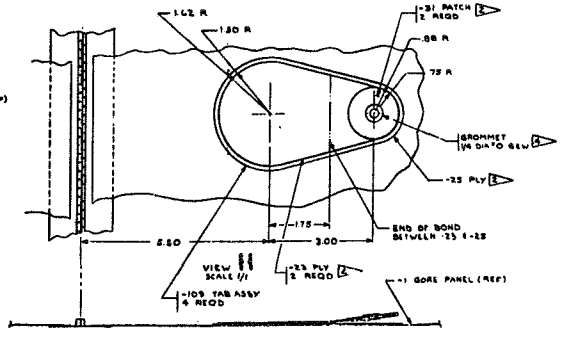

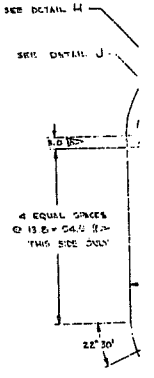

FOLDOUT FRAME

FOLDOUT FRAME

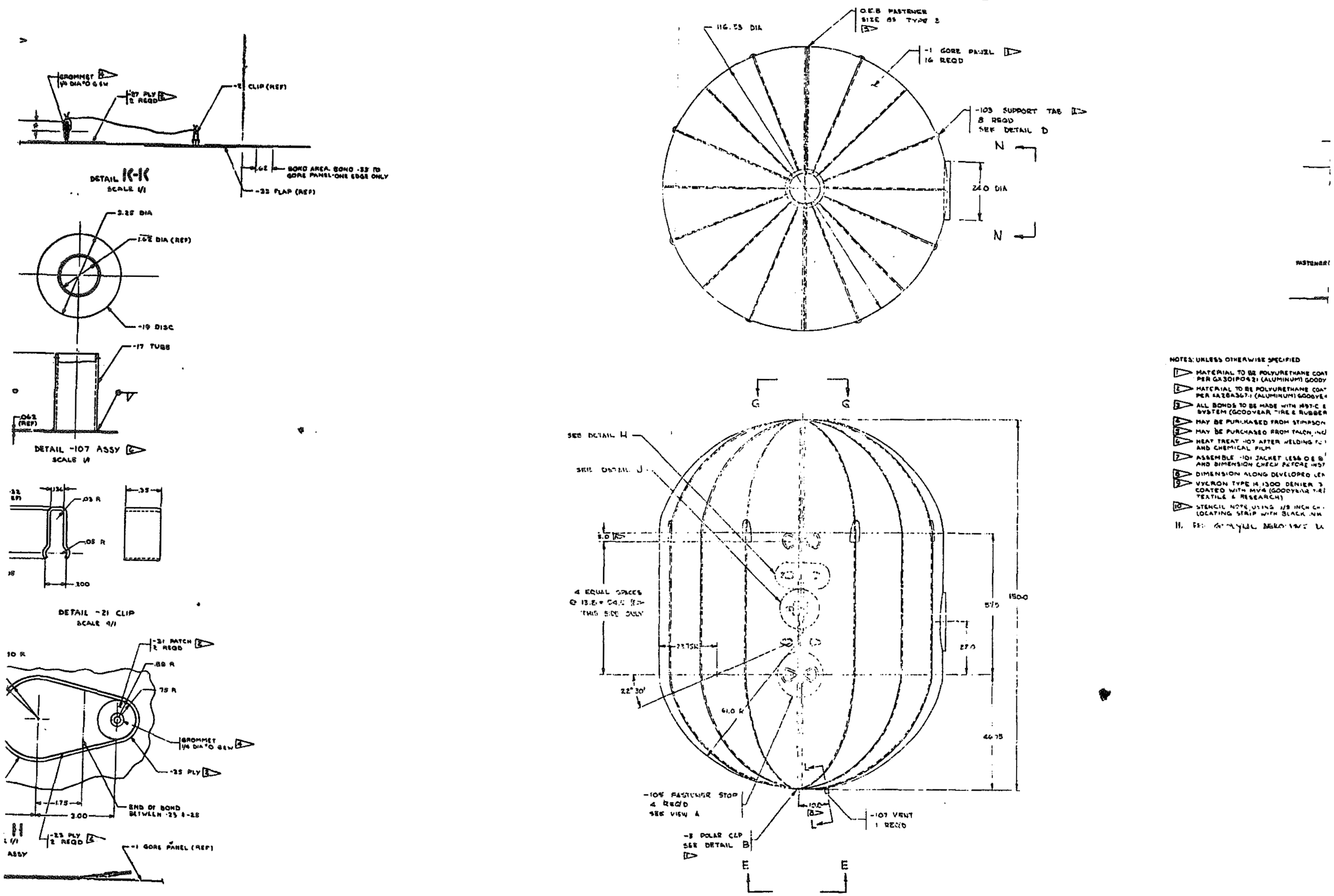

FOLDOUT FRAME

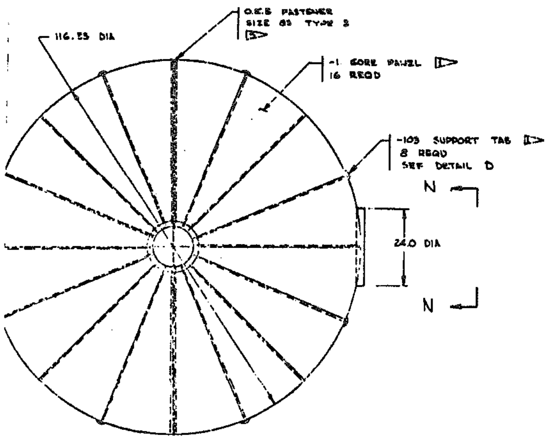

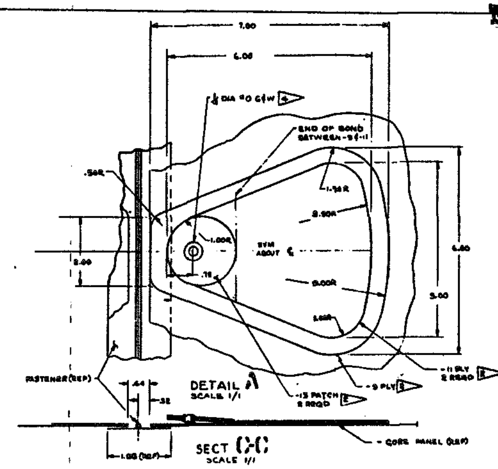

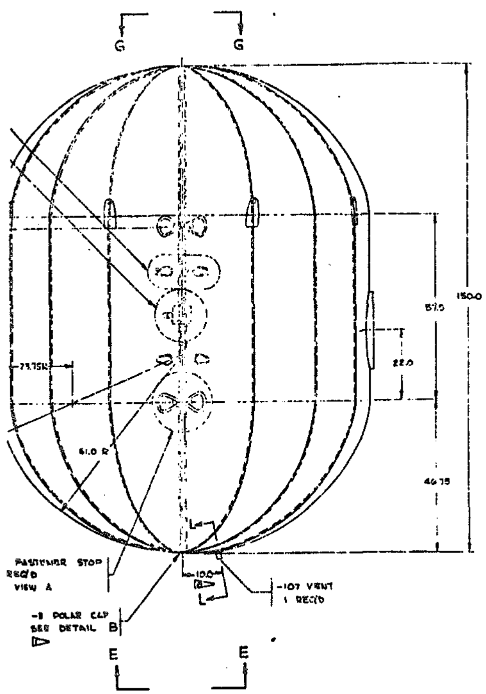

FOLDOUT FRAME

CR72

NOTES: UNLESS OTHERWISE SPECIFIED

1. MATERIAL TO BE POLYURETHANE COATED DACRON FABRIC PER GR301P0421 (ALUMINUM) GOODYEAR AEROSPACE CORP.
2. MATERIAL TO BE POLYURETHANE COATED DACRON FABRIC PER AA28A367-1 (ALUMINUM) GOODYEAR TIRE CO.
3. ALL BONDS TO BE MADE WITH 1497-C & 1473-C ADHESIVE SYSTEM (GOODYEAR TIRE & RUBBER CO
4. MAY BE PURCHASED FROM STIMPSON CO INC., BROOKLYN, N.Y
5. MAY BE PURCHASED FROM TALON, INC MEADVILLE, PA
6. HEAT TREAT -107 AFTER WELDING TO T6 CONDITION AND CHEMICAL FILM
7. ASSEMBLE -101 JACKET LESS O.E.B. FASTENER. INFLATE AND DIMENSION CHECK BEFORE INSTALLATION OF FASTENER
8. DIMENSION ALONG DEVELOPED LENGTH
9. VYCRON TYPE 14, 1300 DENIER, 3 PLY, 8/8 TWIST COATED WITH MV4 (GOODYEAR TIRE & RUBBER CO, TEXTILE & RESEARCH)
10. STENCIL NOTE, USING 3/8 INCH CHARACTERS, AND PAINT LOCATING STRIP WITH BLACK INK
11. REF GOODYEAR AEROSPACE DWG ...G 51700

-111 QTY REQD	-109 QTY REQD	-107 QTY REQD	-105 QTY REQD	-103 QTY REQD	-101 QTY REQD	CODE IDENT NO.	PART OR IDENTIFYING NO.	NOMENCLATURE OR DESCRIPTION	MATERIAL AND SIZE	ZONE	ITEM OR FIND NO.
					1		SIZE 83 TYPE 3	O.E.B. FASTENER	[5] 37'3" (448") LONG		
A/R	A/A		A/R	A/R	A/R			ADHESIVE	[3]		
1	1		1	1			1/4 DIA #0 G&W	GROMMET & WASHER	[4]		
					1		-33	FLAP	[2]		
	2						-31	PATCH	[2]		
					A/R		29	CORD	[9] 12.0 LG		
2							-27	PLY	[2]		
	1						-25	PLY	[2]		
	2						-23	PLY	[2]		
					1		-21	CLIP	2024-T4 AL AL ... [illegible]		
		1					-19	DISC	6061-T6 AL ALY SHT .062 x 3.25 OD		
		1					-17	TUBE	6061-T6 AL TUBE .62 OD x .049 WALL [illegible]		
					4		-15	PLY	[2]		
			2				-13	PATCH	[2]		
			2				-11	PLY	[2]		
			1				-9	PLY	[2]		
				2			-7	PATCH	[1]		
				1			-5	PLY	[1]		
					1		-3	POLAR CAP	[1]		
					16		-1	GORE PANEL	[1]		
X					1		-111	RETAINER PATCH			
	X				4		-109	TAB ASSY			
		X			2		-107	VENT	[6]		
			X		4		-105	FASTENER STOP			
				X	8		-103	SUPPORT TAB			
					X		-101	PURGE JACKET ASSY [7]			

PARTS LIST

CONTRACT NO.	MCDONNELL DOUGLAS ASTRONAUTICS CO. WESTERN DIVISION HUNTINGTON BEACH, CALIFORNIA — MCDONNELL DOUGLAS
ORIGINAL DATE OF DRAWING: 3 NOV 1971	105 TANK PURGE BAG
PREPARED: K. ACTO	
CHECKED	
ENGINEER	
DESIGN ACTIVITY APPROVAL	SIZE — CODE IDENT NO. 18355 — DRAWING NO. 1T42790
CUSTOMER APPROVAL	SCALE- [illegible]

1T42790

As shown, the bag is designed to part along a zippered seam into two halves at a bursting pressure of about 0.5 psid during a simulated vehicle ascent. A shock cord and tension tie release system holds the bag open. Prior to delivery, Goodyear performed and reported two tests of bag opening pressure. Opening occurred at 0.45 and 0.46 psid.

Note that a 3/4-in.-diameter vent line for exiting purge gas is provided at the bag bottom. Also, a 24-in.-diameter blocked-off penetration port was included in the bag over one of the openings in the MLI system at a tank shipping support. This was installed at MSFC request for future experimentation. When desired, the cover can be removed and replaced with a sleeve of appropriate length.

The bag is designed to hang from an existing ring on the MSFC vacuum chamber tank support spider. Tabs containing a grommet are provided around the bag circumference at the dome-sidewall interface for nylon or Dacron cord supports to go between the tabs and the ring. In this manner, the bag is at all times held up off the tank insulation. The top of the bag is clamped to a support on the tank itself.

The open top of the bag is designed to lie flat on top of the fiber glass ring, bonded to the upper extremity of the tank support. Two flat sheet metal half-rings are installed over the bag and bolted to the fiber glass, forming a fiber glass-metal sandwich with the bag in between. Rubber sealing compound poured in the joint area provides a gas-tight seal.

8.8 105-INCH TANK INSULATION THERMAL DESIGN

The insulation system thermal design objective was a total tank heating rate of 50 Btu/hr maximum. The choice of this value was made at the direction of NASA to allow direct comparison of the experimental data with that of similar, previously tested tanks.

The design approach was straightforward. Heat transfer of all system penetrations was estimated, and subtracted from the 50 Btu/hr goal to yield the allowable basic insulation heating rate. The insulation thickness

(number of layers) was then chosen to correspond to this maximum heat transfer rate. The result was a design based upon 70 layers of 15-gage double-aluminized Mylar reflector with 68 layers of type B4A Dacron net separator (35 reflectors and 34 separators in each of the two panels).

Thermal data from MDAC 15-in. LH_2 cylindrical calorimeter tests (Section 6) were used to determine the joint, fastener, and reflector perforation contributions to tank heating. NASA/MSFC supplied LN_2 flat plate calorimeter test data for the basic insulation composite. The vent line support was evaluated with an analytical computer model.

8.8.1 Limitations of Available Design Data

Component heat transfer test data upon which to base the B4A net system design were sparse. It was necessary to design with one data point each for joints, fasteners, and perforations. This was the MDAC data (noted above), the only applicable experimental heat short measurements known for the materials and configuration of interest.

However, these MDAC data were obtained with a test configuration somewhat different from that contemplated for the 105-in. tank. The reflector was identical, but the separator was a different Dacron net (Type B2A). Also, the test insulation thickness was made up of 98 layer pairs instead of the 70 reflectors - 68 separators used in the 105-in.-tank system design.

One set of flat-plate calorimeter test points was available for the selected 105-in. basic B4A insulation composite. These were taken with a 10-layer sample at an LN_2 boundary temperature. However, the use of LN_2 data is conservative for calculating composite heat transfer on an LH_2 tank.

8.8.2 Effect of Uncertainty in Component Data on Design.

The design thickness of the basic insulation (with perforations) was determined after a review of the effect that data uncertainties might have on the experiment design. The impact of the possibilities considered is shown in Table 8-3.

Table 8-3

ESTIMATED TOTAL HEATING RATE
105-IN.-TANK EXPERIMENT

Item	MLI System Fasteners and Joints as Measured		MLI System Fasteners, Joints and Perforation Heat Short Doubled	
Tank Support	2.76	2.76	2.76	2.76
Fasteners (474 @ 5.72×10^{-3} Btu/hr - Fastener)	2.71	2.71	5.42	5.42
Joints (128.7 ft @ 0.11 Btu/hr-ft)	14.15	14.15	28.30	28.30
Basic Composite (254.74 ft^2 wetted area) 68 layers @ 77 layers/in.	7.7**	10.42*	7.7**	10.42*
Degradation Due to Perforations	(0.234 Ke)	(0.234 Ke)	(0.468 Ke)	(0.468 Ke)
Perforation Heat Transfer	1.8	2.68	3.6	5.08
Total Heat Rate Btu/hr	29.12	32.72	47.78	51.98
			↑ Design Point	

*Ke = 0.62×10^5 Btu/hr-ft-°R; As measured with calorimeter LN_2 boundary temp.

**Ke = 0.45×10^5 Btu/hr-ft-°R; LN_2 data extrapolated to LH_2 boundary temp.

It will be noted that the expected heating rate uncertainty band is large. As shown, four possibilities were considered: two in which the 15-in. calorimeter data were accepted as correct, and two in which these data were doubled. The latter was believed to be a conservative upper limit. For each case, the effect of the boundary temperature uncertainty in the basic insulation conductivity was evaluated: LN_2 boundary flat plate data used directly (LN_2 Ke), and conductivity data extrapolated to an LH_2 boundary temperature (LH_2 Ke). The resulting experiment heating rates for the selected design insulation thickness (68-layer pairs) are shown.

The design point shown was chosen; heat shorts doubled with composite conductivity extrapolated to a hydrogen boundary temperature. It was believed that this case represented sufficient built-in conservatism to ensure an experiment with less than a 50 Btu/hr heating rate. Subsequent test results (Section 10) verified this conclusion. The approach used to calculate the component heating rates is discussed below.

8.8.3 Thermal Contribution of Fasteners

The nylon fasteners which penetrate the insulation panels, holding the individual reflector-separator layers together as an assembly, act as a direct heat short through the panel. By offsetting the outer panel of the two-panel 105-in. design, a direct fastener short from the warm exterior to the tank has been avoided. But a short from the exterior to the insulation center, then to the tank, exists. For a fastener offset of 2 in., the heat short per fastener pair (outer plus inner panel) was measured as 5.72×10^{-3} Btu/hr on the 15-in. LH_2 calorimeter (see Section 6 for measurement details).

Extrapolating this data to the 105-in. tank insulation yields an estimate of 2.71 Btu/hr into the LH_2 from the fasteners. The 105-in. insulation contains 474 fastener pairs below the tank support area. These are 16 shipping support closures (four per panel), 10 manhole cover fasteners, and 448 gore panel closures (56 per panel).

8.8.4 Thermal Contribution of Joints

The heat short due to a 2-in. overlapped butt joint in a two-panel system was measured at 0.11 Btu/hr per foot of joint on the 15-in. calorimeter. On the 105-in. tank there are about 128.7 ft of joint below the support area. Therefore, joint heat transfer can be expected to be about 14.5 Btu/hr during test.

Joint and fasteners thermal shorts are most significant. They alone contribute about 34 percent of the allowable total system heating rate.

8.8.5 Fill Line

The fill line in the 105-inch tank has been designed as a very highly efficient heat block. Constructed of fiber glass for a considerable distance above the liquid level, it reduces conduction down the line to such an insignificant value that it can be neglected. This was demonstrated by computations early in the program and verified through tests on a similar tank at MSFC.

8.8.6 Tank Support

A detailed computerized analysis was accomplished to estimate the heat transfer into the hydrogen test liquid by conduction down the support tube and tank in the area above the liquid level. Figure 8-6 shows the thermal model used. It models the tank, gaseous ullage, flowing vent gas, and insulation. A circumferential insulation joint (concentrated heat transfer point) was also included at nodes 105 and 112.

It was found that the support tube itself functions as a very efficient heat block. No heat enters the tank by conduction down the support. With the top of the support at LN_2 temperature, essentially all the heat entering the liquid from the support area is due to the heat transfer through the tank dome and cone insulation. This is due to the thermal resistance imposed by the long stainless steel support tube which is cooled on its interior by the venting hydrogen boiloff gas.

Heating rates at the tank wall-liquid interface were found to be essentially independent of the structural temperature at the top of the support tube, including the upper limit of 65°F. Also, doubling of the heating at the two MLI joints failed to influence the liquid interface heat transfer. Tank-to-liquid heating was always found to be less than the total heat input to the dry wall ullage area through the insulation. Assuming a liquid level 25 in. below the bimetallic joint (107.3 in. from tank bottom), heat input to the liquid was about 2.76 Btu/hr with 0.1 Btu/ft^2-hr insulation.

Although the support heat input amounts to only about 5 percent of the total design experiment heat input, an LN_2 cooling coil wrapped around the support was installed. The idea was to ensure a minimum thermal input in view of

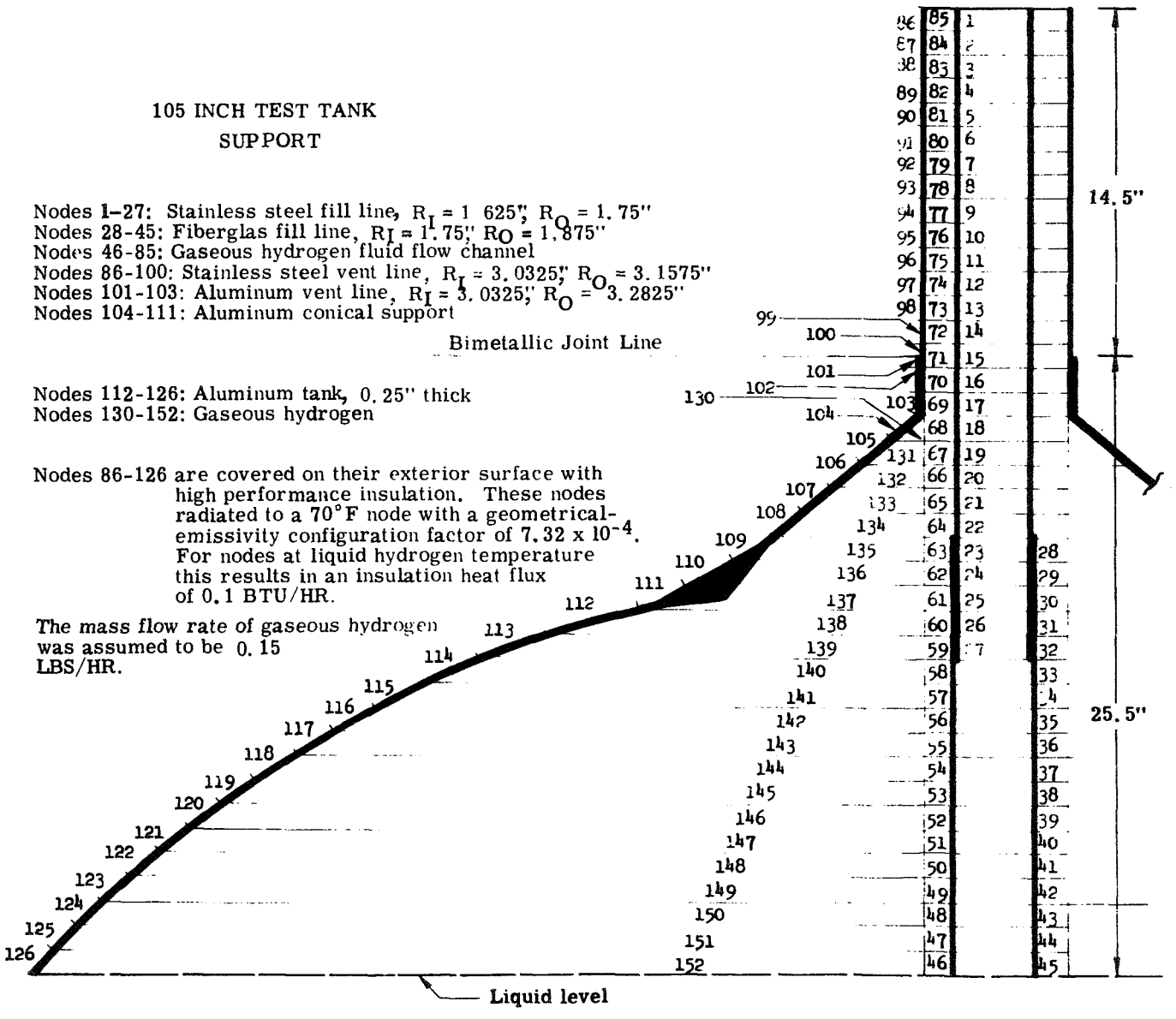

Figure 8-6. Thermal Model — 105-Inch Test Tank Support

the unknown vent rate and nonexistent past test data on temperatures of the structural members connected to the tank support top. Subsequent test results indicated that the support top can be expected to be sufficiently chilled by the vent gases; the coil can be eliminated.

The insulation joints between the cone and cylindrical pipe at the bottom of the support are not a significant contributor to tank heating. The running lengths of the two joints are relatively short, 4.21 and 7.86 ft. At the joint heat input rate of 0.11 Btu/ft measured on the MDAC calorimeter, these joints contribute at most 1.33 Btu. Even in the unlikely event that the calorimeter data was 100 percent low, the additional joint heat short would be only another 1.33 Btu at most. And, as indicated above, this heat is removed by the vent gas before it can be conducted downward through the tank wall to the test liquid.

8.8.7 Composite Perforations

It was necessary to correct the available composite (15-gage DAM-B4A Dacron net) thermal conductivity data (Section 6) for the effect of perforations in the reflectors. The data furnished by MSFL were for unperforated reflectors, whereas the 105-in.-tank insulation design called for a 2.38 percent open area perforation.

To obtain a corrected conductivity, the NASA/MSFC B4A data were increased by 23.4 percent, the percentage increase observed in the MDAC tests (Section 6) of unperforated and perforated MLI panels with similar materials and an identical perforation configuration (Appendix A).

8.8.8 Composite Heat Transfer and Design Thickness

A conductivity of 0.62×10^{-5} Btu/hr/ft° R was used for the basic unperforated MLI composite. This was the NASA/MSFC value corresponding to the expected postfabrication MLI panel density of 77 layers per inch. Including the factor for perforations, the LN_2 boundary temperature conductivity is 0.765×10^{-5} Btu/hr/ft° R ($0.62 \times 10^{-5} \times 1.234$).

Correction of the LN_2 conductivity data for the design condition of an LH_2 boundary temperature was accomplished with a least-square curve fit of the actual data shown in Figure 8-7. This procedure, generally followed in the literature, resulted in the conductivity equation:

$$K_{eff} = 3.007 \times 10^{-25} \overline{N}^{8.6} \left(\frac{T_H + T_C}{2}\right)$$

$$+ \frac{8.33 \times 10^{-2} \sigma \left(T_H^2 + T_C^2\right)(T_H + T_C) N}{(N-1)\left(\frac{2}{\epsilon} 1\right) \overline{N}}$$

where

$\overline{N}$ = density, sheets per inch

N = number of sheets

This equation yields a conductivity value of 0.45×10^{-5} Btu/hr/ft°R, unperforated composite and 0.555×10^{-5} Btu/hr/ft°R ($0.45 \times 1.234 \times 10^{-5}$) for the design perforated material.

The required insulation thickness for the tank was computed parametrically using the above. This resulted in the selection of a design thickness of 68 layer pairs with the experiment heating rates shown in Table 8-3.

8.9 PURGE SYSTEM DESIGN ANALYSES

The test tank purge system, described above, was designed with the general objective of verifying the purge system concepts recommended in Phase I for MNV vehicle application. Scaling or testing the MNV design itself was impractical. Therefore, the test tank system was designed to achieve two goals:

A. Demonstrate the applicability of the equations defining the purge requirements developed for cryogenic vehicles.

B. Add to the knowledge of purge-bag-type system operating characteristics.

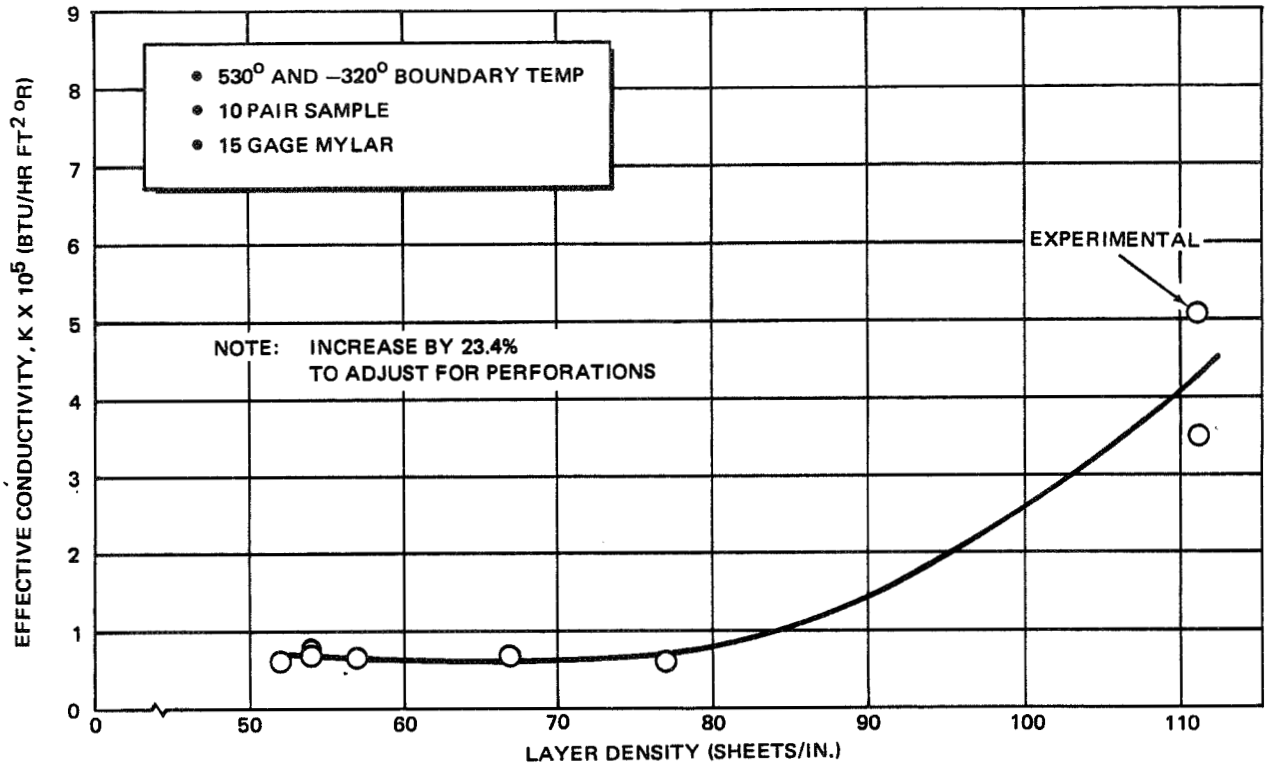

Figure 8-7. Conductivity of Double-Aluminized Mylar-Dacron B4A Net MLI Composite

By demonstrating the accuracy of the analytical methods, much more dependable predictions of purge requirements for future tankage can be made.

Purge system analyses and designs have been developed as part of an on-going MDAC IRAD program aimed at the design and test of purge systems for cryogenic vehicles (Reference 9). Results were applied to this program where applicable and are included below for reference.

8.9.1 System General Configuration

The purge system is configured to yield operation and performance tests for each of the four phases of purging: reduction of condensibles, prefill hold, chilldown and fill, and post-fill hold.

As noted, the entire insulated tank is enclosed in a single purge bag. Purge gas inlets are located at the top of the volume and an exit near the bottom. Although this yields a single purge volume rather than three separate ones

as in the MNV, the desired purging demonstration is still achieved. The single volume was sized to match each of the three MNV volumes separately.

8.9.2 Relationship of Test Purge Volume to MNV

The applicability of the test purge volume to simulate MNV conditions was evaluated on the basis of two parameters: type and thickness of insulation and ratio of insulation volume to the entire purged volume. The insulation type and thickness determines the path and the distance through which the purge gas must diffuse in order to eliminate condensibles. The volume ratio defines the amount of condensibles beneath the insulation as compared to the total condensibles to be purged. The concentrations of condensible gases at the bag outlet and beneath the insulation are thereby defined. Thus, the characteristics of the concentration reduction period for the test article and the MNV should be similar if these parameters are nearly the same.

Table 8-4 lists these parameters for a 105-in. calorimeter and the MNV. Note that the 105-in. tank and the MNV have the same insulation and insulation thickness. However, the volume ratio matches only for the MNV sidewall; it is greater for the domes. This indicates that proportionally more condensible gas is outside the insulation in the dome volume than for the test article; more trapped condensibles are free to diffuse unhindered by the insulation. But, this fulfills the assumption of a completely mixed purge volume used in the analytical derivation (Reference 9). The test results, therefore, will also provide conservative dome area design data.

Note that Table 8-4 shows that the test tank purge volume is nearly an order of magnitude smaller than the MNV. This variation is expected to have little effect on the test data applicability, since the concentration reduction period duration can be matched by adjusting the helium inflow rate and thereby cancel the volume differences. The only phenomenon that may not be accurately duplicated in the test article is the amount of helium stratification that occurs in the purge volume. That is, for the same purge concentration reduction period, the purge and condensible gases will be able to mix more readily in the test tank purge volume, since the diffusional distances are shorter. Purge gas stratification will be less in the tests, and the advantage

Table 8-4

TEST ARTICLE–MNV PARAMETER COMPARISON

Parameter	Test Article or MNV Purge Region		
	105-In.-Tank Calorimeter Test Article	Sidewall Volume (MNV)	Dome Volumes (MNV)
Insulation type	Double-aluminized Mylar and Dacron net separator	Same	Same
Purge volume	162 ft^3	3,874 ft^3	1,100 ft^3
Insulation thickness	0.75 in.	0.75 in.	0.75 in.
Surface area insulated	268 ft^2	6,150 ft^2	990 ft^2
Purge volume/insulation volume ratio	9.67	9.92	17.8

of locating the exit tubes near the bottom of the volume will not be as great as for the MNV. But, as with the volume ratio noted earlier, this discrepancy in the test article and the MNV will result in conservative MNV design data.

8.9.3 Parametric Analysis and Test Procedure

Purge requirements for the 105-in. tank with the 70-layer DAM-B4A net MLI system were parametrically defined for each purge operational phase using the design equations of Reference 9. Experimental limits for test planning were then established and working curves generated for test use. Results are summarized below (see Reference 9 for detail deviations and computations).

8.9.3.1 Reduction of Condensibles – Phase I

The required helium flowrate as a function of the condensible reduction time period for final condensible concentrations of 5, 1, and 0.5 percent is shown in Figure 8-8. Figure 8-9 presents the same data with the reduction time period and final concentration as coordinates. The latter curve is best suited for comparing the actual test concentration data with the analytical predictions. Note the rapid increase in the required flowrate as the purge period is reduced.

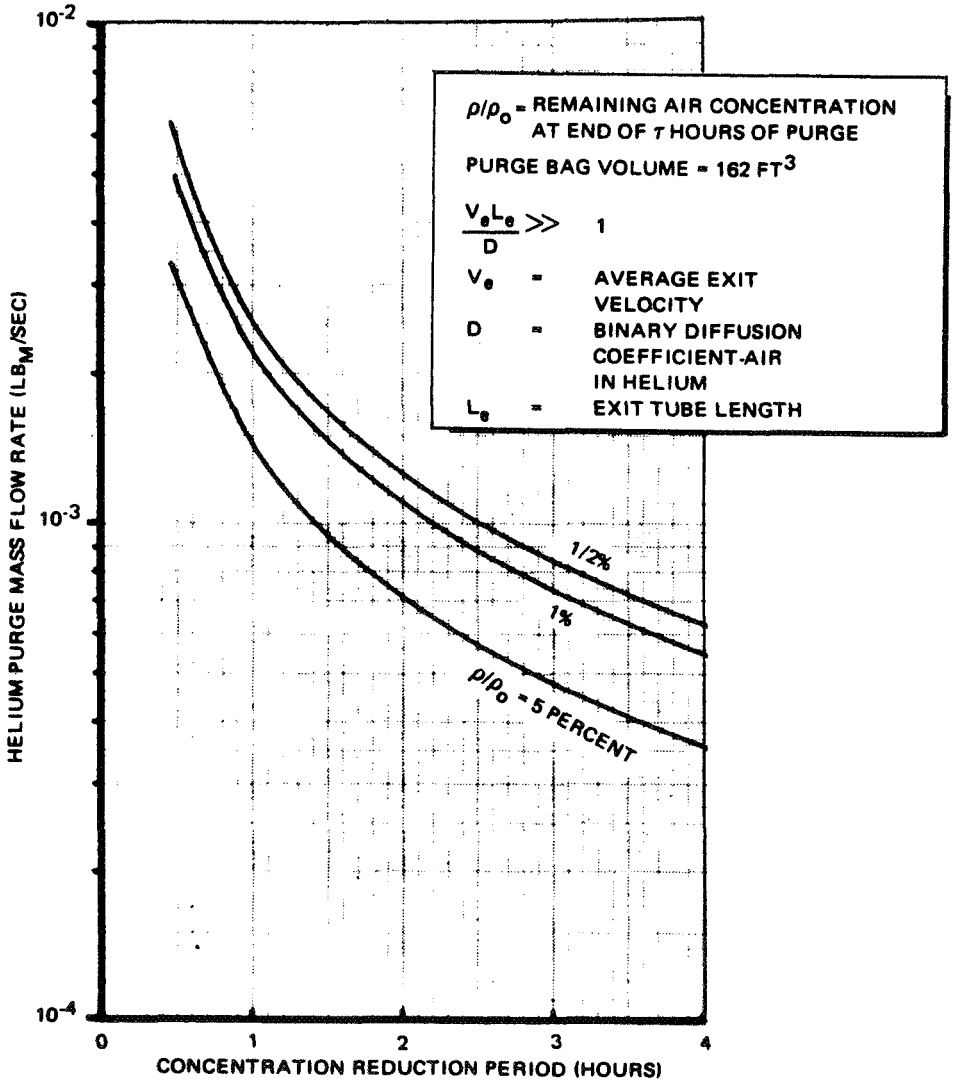

Figure 8-8. 105-In. Tank Condensible Concentration Reduction Helium Mass Flow Rate

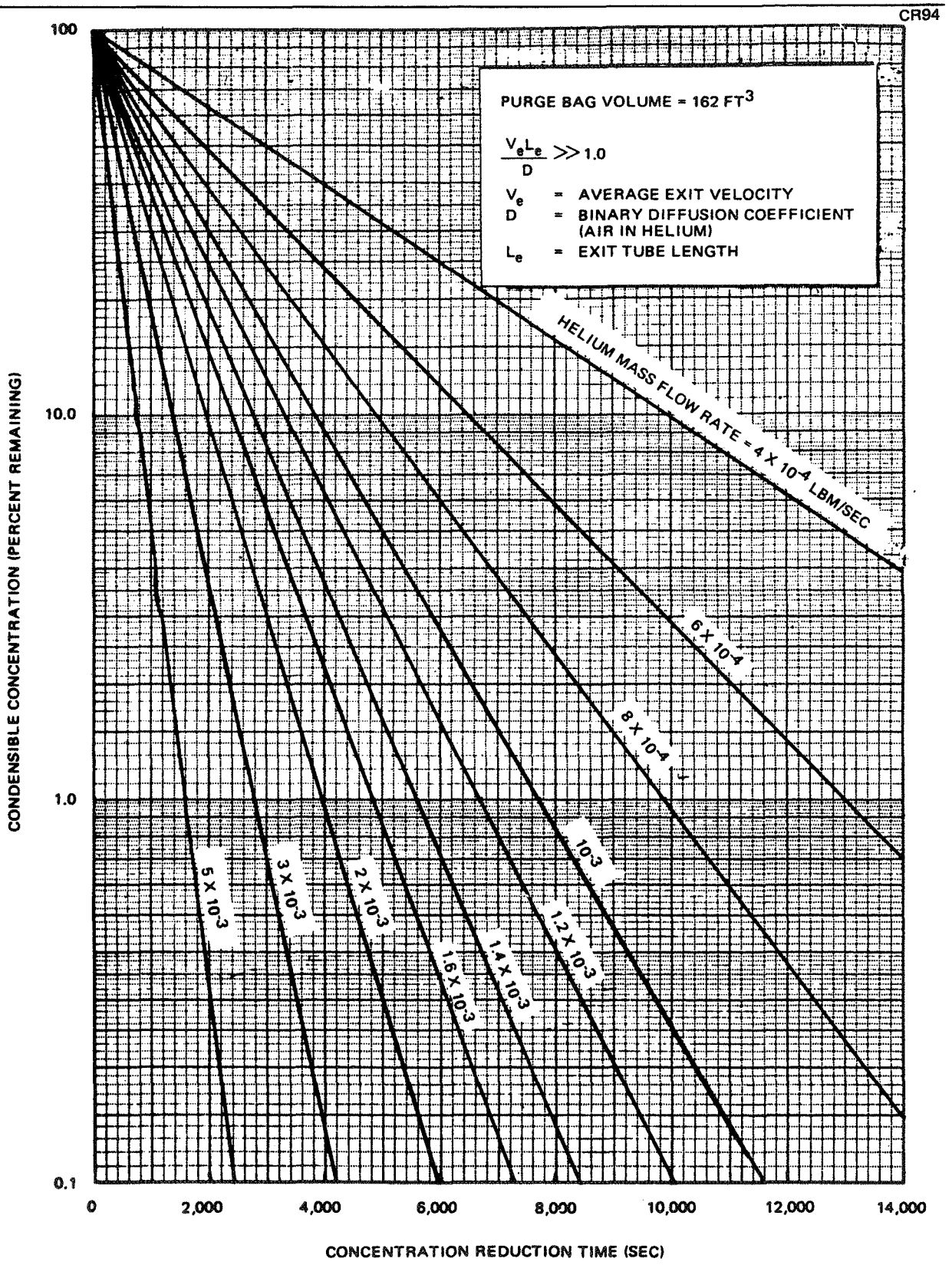

Figure 8-9. Condensible Concentration as a Function of Time and Helium Mass Flow Rate

It will be observed that the above design relationships are independent of exit flow velocity and outlet tube length. This is due to the parameter

$$\frac{V_e L_e}{D}$$

being large (>100) for a typical in-vacuum test tank installation (long outlet).

For convenience in sizing the inlet and outlet tubes, the pressure drop as a function of the helium mass flowrate was computed and is shown in Figure 8-10. A transition Reynolds number of 2,300 was used, and in the turbulent flow regime, a smooth tube was assumed.

A concentration reduction period of one hour with a final concentration of 1 percent condensibles was initially chosen as the test condition. To meet this requirement a helium flowrate of 2.2×10^{-3} lbm/sec is needed (assuming a 0.5-in.-diameter outlet tube (10 ft long) and a bag pressure of 0.25 psig). For facility compatibility, the above design flowrate was later reduced to 0.0011 lbm/sec (1.4 hr). Tube sizes were not changed.

8.9.3.2 Chilldown

The largest required helium inlet flowrate occurs during tank chilldown as propellant loading is initiated. External pressure tending to crush the bag must be reacted by adding helium as the purge gas volume cools and contracts. Thus, the design peak flow for the inlet system is defined by these requirements, shown parametrically in Figure 8-11. Here, the required helium flowrate is plotted as a function of the time for the tank to reach 40°R. The curves were calculated from the chilldown differential equation by varying the liquid hydrogen inlet flowrate. A maximum flowrate of 0.0098 lbm/sec will be required for the selected design point, a 10-minute chilldown period.

For purge system operation, it is suggested that a pressure control valve be used instead of a flow control system that follows the curves of Figure 8-11. This approach avoids the complicated task of designing a flow control system and also allows for a greater margin of error in the computation of the chilldown requirements. However, the flowrates of Figure 8-11 are

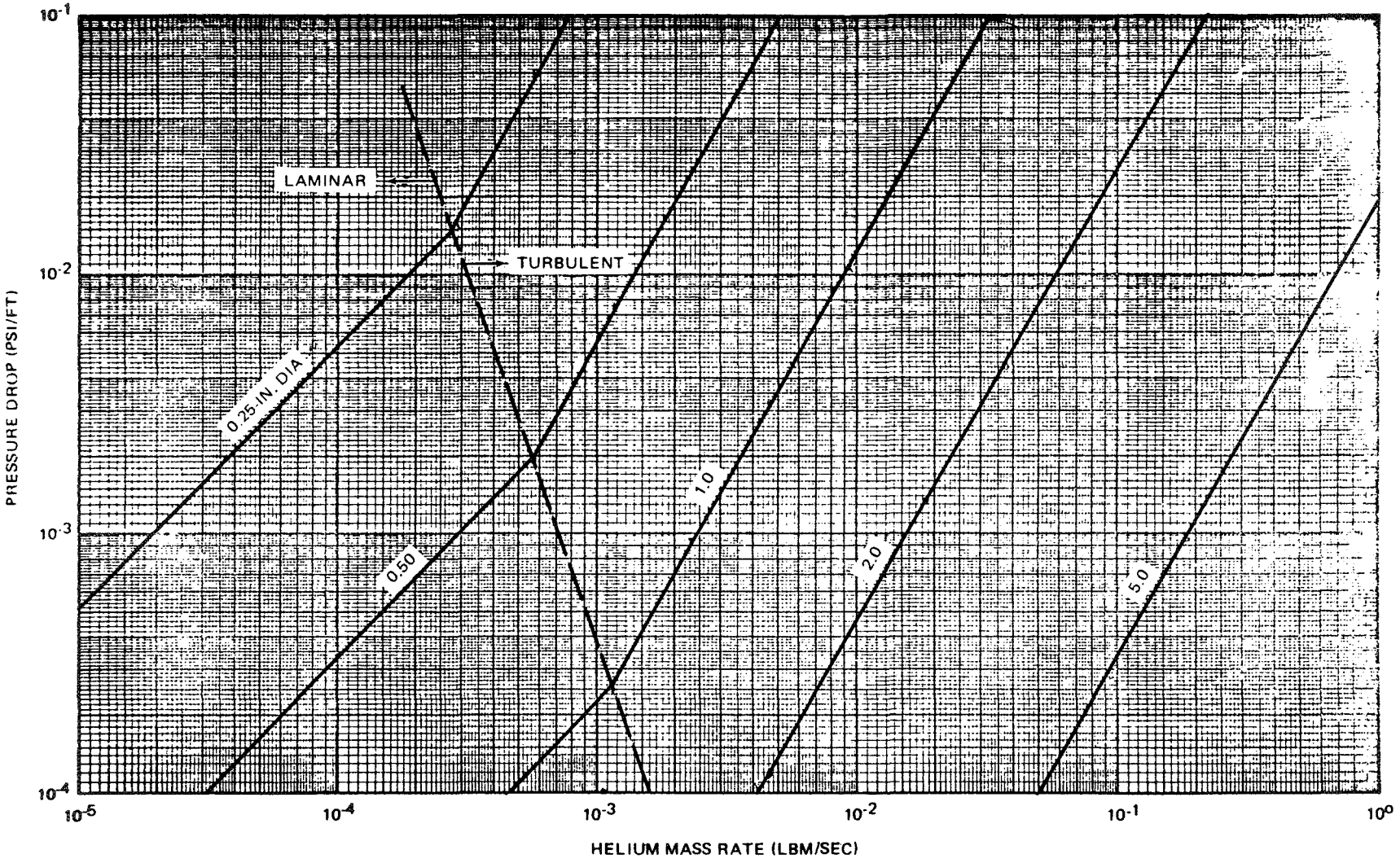

Figure 8-10. Friction Losses in Purge Gas Exit Tube

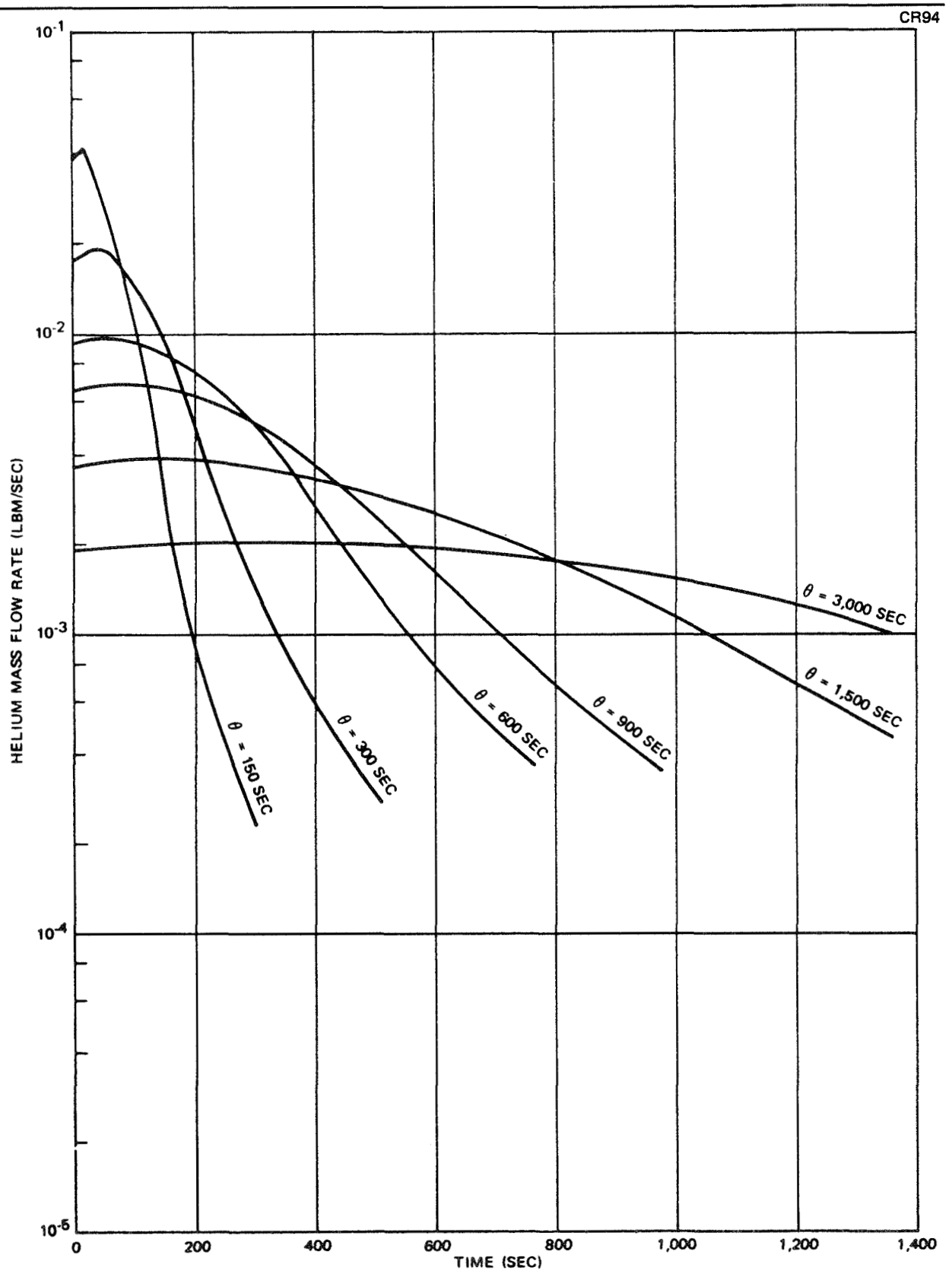

Figure 8-11. 105-In. Tank Chilldown Helium Flow Rate Requirements

required to define the maximum flowrates and the response required from the pressure control system.

8.9.3.3 Flow Requirement During Hold Periods

During any prechill and post-fill hold periods, an overpressure must be maintained in the purge bag to cause a large enough helium overflow to inhibit back diffusion of condensibles through bag leakage points. The required flowrates depend upon bag leakage, a parameter for which data are lacking. Accurate flow rates can only be established during the actual system test.

To estimate flow requirements, Figure 8-12 was prepared which shows the helium flow required to maintain condensible concentration if the exit tube valve is kept open and the bag is leak-free (a maximum condition). Note that to maintain the concentration level at 1 percent with 0.75-in.-diameter exit tube 10 ft long, the helium flowrate would be only 1.15×10^{-6} lbm/sec.

8.9.4 Purge Gas Inlet Configuration

Two helium inlet lines were specified for incorporation in the test article design: an inlet located as a port at the support collar, and a diffuser ring inlet located beneath the insulation. The inlets are located and designed so that the concentration reduction characteristics as a function of the purge inlet configuration may be defined. A comparison of concentration reduction performance data from each of the inlet configurations can be made to ultimately determine dispensing requirements for adequate purge operation. Such a comparison would also establish the validity of assuming a completely mixed purge volume in the analytical derivations.

The port inlet was also designed to provide helium gas makeup during the chilldown phase of purging. To provide the necessary chilldown flowrates, a 3/4-in.-diameter line was selected. This size is based on the assumption that the minimum anticipated chilldown time is 150 sec, one-fourth the design rate of 600 sec. The corresponding maximum helium inflow will be 4.0×10^{-2} lbm/sec (from Figure 8-12). Assuming that the control valve is placed approximately 10 ft from the chilldown inlet port and located outside the vacuum chamber, a 3/4-in. line will result in a 5.0-psi pressure drop

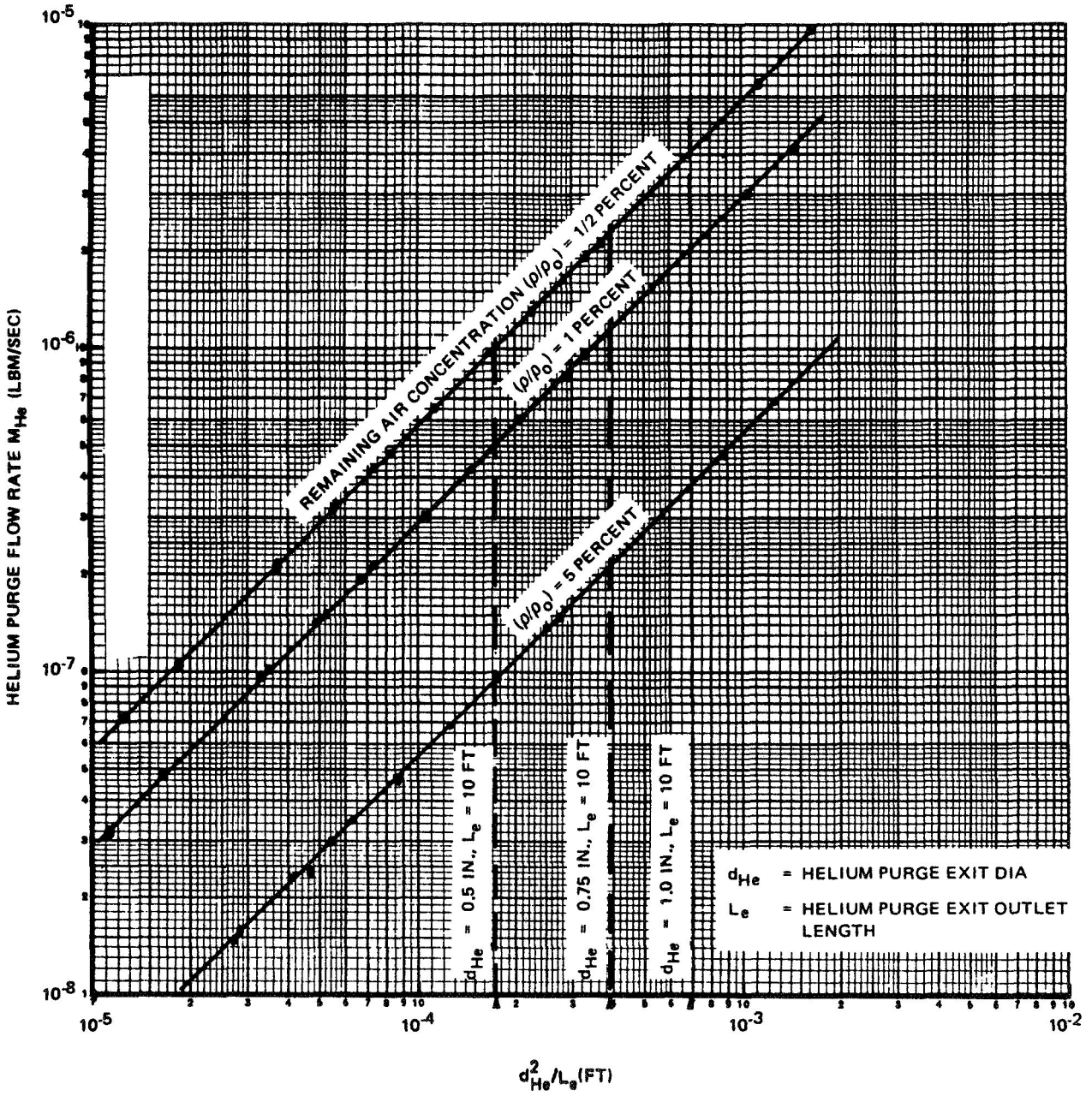

Figure 8-12. Hold Period Purge Flow Requirements for Leak-Free Bag and Open Exit Valve

from the control valve to the support collar. A 1/2-in.-diameter tube, for example, would result in a 30-psi pressure drop for the same distance. Therefore, the 3/4-in. line was selected to minimize the pressure drop from the control valve to the exit port and to provide for additional flow capacity if required.

8.9.5 Purge Supply and Vent System

A typical purge supply and vent system for use with the test article was defined during the purge design study. Shown schematically in Figure 8-13, it consists of a gas supply, vent, pressure controller, distribution lines, and instrumentation.

The system is capable of both manual and automatic operation. During the initial phase of purging (condensibles reduction), the outlet valve is opened and helium is introduced through the 1/2-in. inlet which leads beneath the insulation on the test article. Gas samples from the vent line are continuously monitored to determine the percentage of condensibles (air) remaining

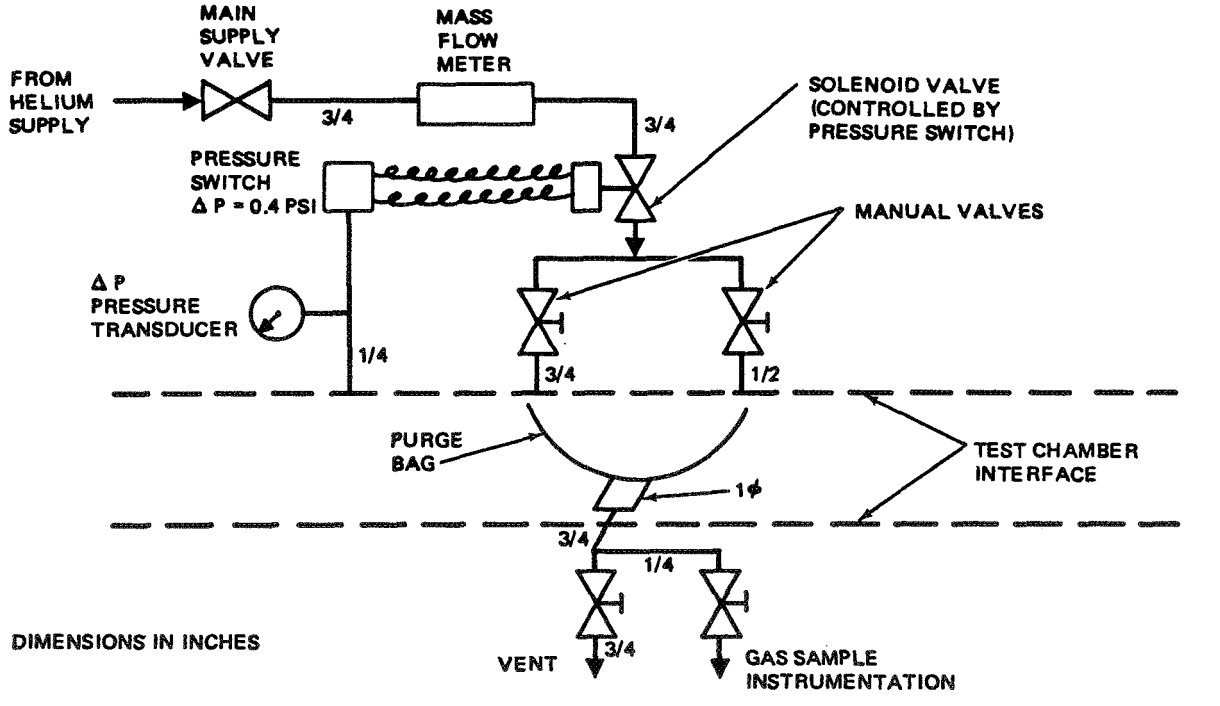

Figure 8-13. Purge Supply and Vent Schematic

in the purge volume. Upon completion of this phase, the outlet valve is closed, and the required gas to make up bag leakage is provided by manipulating the 3/4-in. inlet valve.

The most critical aspect of the purging operation is controlling the pressure difference across the purge bag which will burst open at a 0.45-psi pressure differential. Also, during chilldown, a reverse pressure differential due to gas collapse is to be avoided. Therefore, inlet flow must be carefully controlled with respect to bag pressure. This can best be accomplished automatically by a pressure controller (a pressure switch and solenoid valve) which opens and closes the main gas supply as a function of bag pressure. Should this device fail, the system can be operated manually, but in a much less satisfactory manner.

The gas supply can consist of standard helium bottles with the associated pressure reducers. A final supply pressure of about 5 to 10 psig should be sufficient. The estimated flowrate during initial purging is 0.0011 lb/sec. During chilldown, a flow of up to 0.0098 lb/sec could be required for a short period.

The flowmeter shown in the schematic consists of instrumentation which provides an output suitable for determining integrated mass flow as a function of time during the test. The vent line gas sampler mounted outside the test chamber can be an oxygen analyzer or a mass spectrometer. The only other instrumentation needed is a measurement of bag pressure difference with a readout that can be continuously monitored by the purge system operator.

8.9.6 Purge Operation

Operation of the purge system during test is as follows:

A. Condensible Concentration Reduction — Open purge volume exit valve and adjust purge gas inlet flowrate to provide desired condensible concentration reduction time period.

B. Hold Periods — Close purge volume exit valve and maintain purge bag overpressure to maintain condensible concentration at desired level.

C. Chilldown Period – Close purge volume exit valve (normally closed during hold period) and maintain overpressure in purge bag through pressure control system.

8.10 TEST PLAN

A detailed test plan was prepared (Reference 7) for the Phase III large-tank test program. The objective was to provide a document which would describe and define all testing and test requirements so that testing could be accomplished by NASA at the MSFC facility. A secondary objective was to formulate a document which could serve as a guide for future large-tank tests of this type. A series of three basic tests was included in the plan.

The first test, evacuated MLI system thermal performance, is identical to prior MLI insulated tank tests. Insulation is evacuated, allowed to degas for several days, the tank is filled with LH_2, and insulation performance (tank boiloff) is measured upon achievement of equilibrium. The resulting data are directly comparable to prior test results for other MLI systems.

The second test, purge system performance evaluation, serves as a check on the purge design analyses performed for this system. It also provides an experimental data point for use in the further development and correlation of analytical methods. This test entails loading the tank with LH_2 using the purge system to eliminate condensibles in the MLI. Condensible concentration reduction time and helium purge gas mass flow requirements during all purge operations are measured.

The final test is a measurement of MLI system performance throughout a simulated mission, including a rapid launch evacuation. The thermal performance of the MLI during prelaunch ground hold is measured. Simulation of the boost phase verifies the ability of the insulation system design to endure launch evacuation loads. Next, the time for the system to achieve steady-state evacuated performance is measured, an important parameter from a design standpoint, especially for vehicles with relatively short missions.

The test plan covers the following topics in detail: test article definition, hardware responsibility, unique test facility requirements, test description, test conditions, acceptance criteria, test instrumentation, instrumentation accuracy requirements, and output data format.

8.11 TEST FACILITY CHARACTERISTICS

Test facility requirements were defined early in the program during facility development work at MSFC. Some of the results which may be useful to others are summarized below.

The tank calorimeter main fill valve was located outside the vacuum chamber after evaluating this and three other possible alternatives: submerged at tank bottom; within the tank ullage area; and outside the tank but within the vacuum chamber. The review was motivated by a consideration of potential valve leakage, a problem encountered in some prior testing. Rated leakage was a smaller percentage of total experiment boiloff with the valve at ambient temperature.

The need to equalize pressure within the closed off fill line and the tank ullage during test was identified. A small-diameter hole was drilled in the fill line here although external valving would work as well. Without pressure equalization, liquid has a tendency to oscillate up and down in the fill line, creating a heat pump effect.

Vent systems then in use at other facilities were reviewed and a baseline system outlined for the tests here (Figure 8-14).

Mass flow transducers utilizing the hot-wire principle were evaluated and found to be suitable. These units, Thermo-Systems Inc. (St. Paul, Minn.) read mass flow directly and automatically compensate for pressure and temperature changes within a control band. A line bypassing the flowmeters handles the high-volume gas surges associated with initial tank chilldown.

The heat exchanger performs two functions. Gas temperature is maintained within that required by the transducers. Also, it keeps conditions in vent system constant and independent of fluctuating atmospheric temperatures

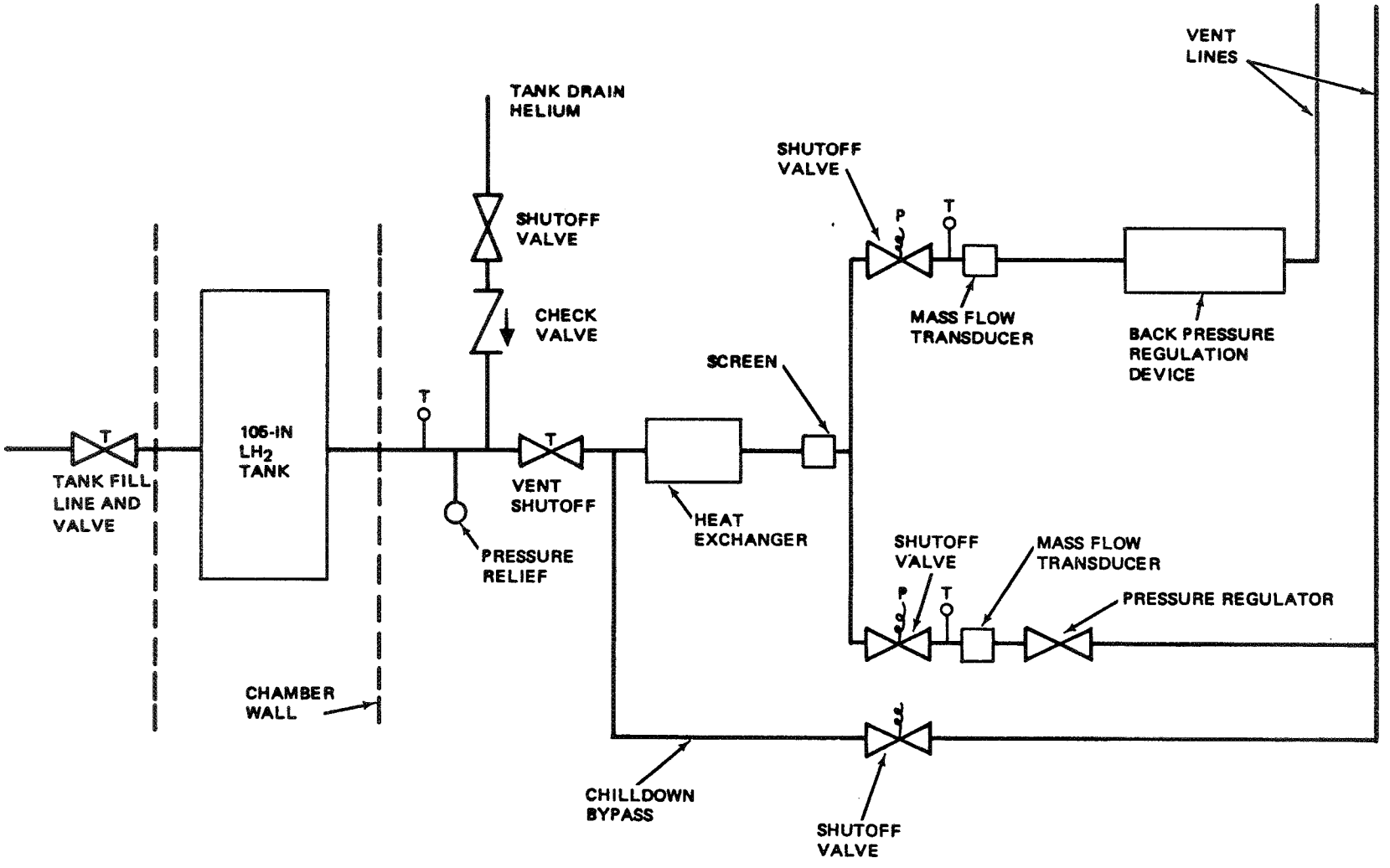

Figure 8-14. Gaseous Hydrogen Vent System Schematic

throughout the test. Temperature should be controlled at an absolute value higher than the expected atmospheric maximum during testing and within a band of ±10 °F.

A 5 to 10 micron size particulate removal screen is desirable as a precautionary measure at the inlet to the flowmeters. A thorough purge of lines prior to transducer installation is also needed.

Pressure controllers should be placed downstream of the flowmeters, thereby ensuring a narrow band of pressure fluctuations within the meter. Pressure control limits are critical from the standpoint of experiment data reduction, as error in the derived test MLI performance is directly related. The absolute value of tank pressure is unimportant, but should be just slightly above atmospheric, minimizing the pressure differential and leakage across the fill valve.

Section 9
LARGE-TANK MLI SYSTEM FABRICATION

The insulation system described in Section 8 was fabricated and installed on the NASA 105-in.-diameter tank, concluding the program Phase II effort. The tank was received from MSFC via air (Guppy) and subsequently leak checked and cleaned. Insulation assembly tooling was designed, fabricated, and checked for dimensional correctness with mockup panels fitted to the tank using the tooling configurations and MLI panel fabrication methods developed during Phase I. Panel thickness, important for subsequent thermal performance measurements, was measured prior to installation. A purge bag essentially identical to one developed earlier for MSFC was procured from Goodyear Aerospace Corporation. The insulated tank was sealed in a heat-sealable plastic bag with a Thor desiccant breather, and shipped to MSFC, via Guppy. Final installation of the MLI shipping support closeout panels and bag was accomplished at MSFC after shipment by MDAC personnel.

9.1 MATERIALS

Materials for the insulation fabrication were procured per the ordering data noted in Appendix A. Other miscellaneous items, grommets, nylon buttons, etc., were obtained from the Douglas Aircraft upholstery shop. A few items require comment.

9.1.1 Fasteners

Standard nylon "Buttoneer" fasteners were initially purchased. These were found to be made of a nylon base material which did not have the tensile strength required to carry the MLI panel design loads. A special "Swifttach" fastener in pure nylon was reordered and found to have adequate strength. However, these items were less ductile; a tendency to crack during installation was noted. This problem was overcome by heating the fastener with a hot-air gun prior to installation. The slight softening prevented cracking, with tensile strength being regained upon hardening.

9.1.2 Separator Net, Dacron Type B4A

The separator net was ordered with the same specifications (Appendix A) denoted by the vendor for sample materials supplied to the MDAC IRAD program. Although the material supplied met the above general requirements, it was found that the finished density of MLI panels using this material was higher than obtained earlier with the sample material. Density tests were made with a compression tester and predicted panel density was found to be essentially that being obtained in panel fabrication (higher than previously).

A comparison with the original sample was made under a comparator microscope. Differences in weave were confirmed. Although the pattern was similar, the weave did not seem as tight. Thread intersections did not form such a pronounced knot, but instead were several twists or knots spread over an area. It was concluded that the absence of the thick knot allowed a closer reflector spacing when stacked, yielding a denser MLI composite.

9.2 TANK PREPARATION

Prior to actual fabrication of MLI panels, all work related to the tank proper was completed. The tank was set up in the laboratory and leak checked. All tank-mounted hardware was installed and dimensional checks made with mockup MLI panels to ensure proper fit and performance of the completed MLI system. The tank was then cleaned.

9.2.1 Tank Support Jig

A Dexion tank support jig, shown with the finished test article in Figure 9-1, was constructed of steel "erector set" type structural girders to hold the tank for MLI panel installation. This was mandated by the insufficient access area around the tank when in the shipping fixture. Wood scaffolding, a platform around the tank top, was attached to the steel framing. All portions of the tank were then reachable either from a stepladder or the platform.

9.2.2 Tank Leak Check

The tank was checked for leaks which might have developed in transit from MSFC. None were observed. The tank was pressurized to 9 psig with helium

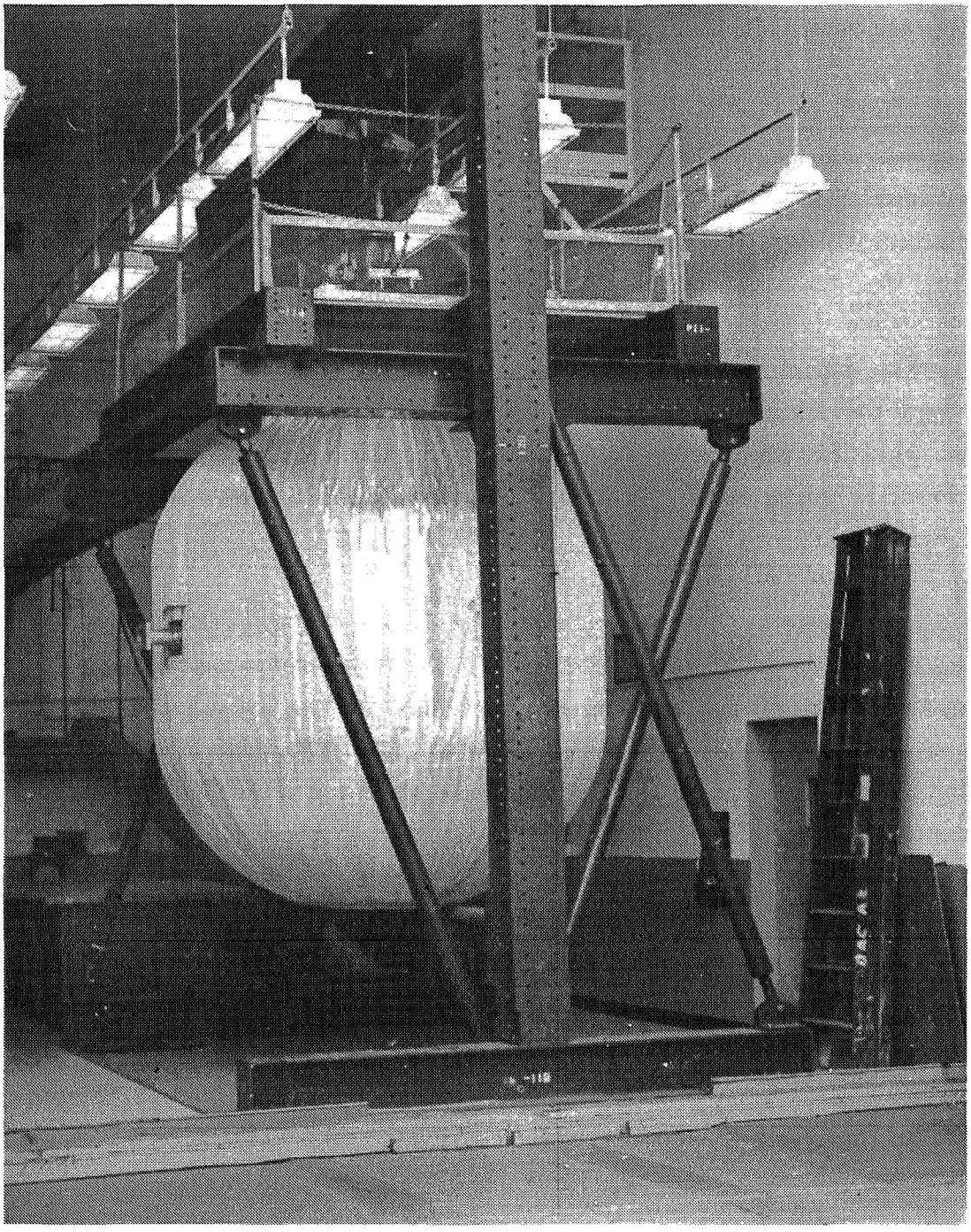

Figure 9-1. Tank Support Jig with Completed Test Article

and depressurized three times prior to a final pressurization to 21 psig for the test. All welds were then checked with a Vecco mass spectrometer type helium leak detector, Model MS-9, S/N NASA 9288, using a sniffer probe. The probing rate was about 8 to 10 in. per minute.

9.2.3 Installation of Tank-Mounted Hardware

All hardware directly attaching to the tank was installed per the drawings: cooling coil, purge bag support, foam insulation supports, gore support ring, instrumentation patches, and the purge system rings, lines, and fittings. Only the cooling coil presented a problem.

Cooling coil attachment was resolved by wrapping an annealed copper tube spirally around the stainless steel support tube and soldering in place with standard low-melting-point solder. A heat dam, placed between the coil and support bimetallic joint, was used to prevent heat soak to the joint. This procedure worked out well.

An earlier design called for potting the coil in low-melting-point alloy to increase the coil-support heat transfer. Several attempts to produce a satisfactory installation on a mockup support failed. The most attractive alloy, identified in a vendor survey, cracked when an LH_2 flow was established in the coil. No in-service failures were obtained with the soldered copper tube.

9.2.4 Dimensional Check With Mockup Gore Panels

Gore panel fit (size) and alignment after installation is very important with the selected system design; all gores are indexed from a single support ring and other panels are indexed from the gores. To ensure this fit, it was necessary to check all dimensions taken from the tank prior to cutting material. Simple measurement, the first attempt, was found wanting due to the non-uniform diameter and configuration symmetry encountered in the particular tank to be used.

A mockup gore panel was made of two layers of fiber glass cloth using the actual MLI gore layup tooling (Section 9.3). This mockup was then fitted in place at each panel location around the tank, and the fit noted. The two

layers of fiber glass were found to be limp enough to adequately simulate a gore. Minor dimensional changes were made, and the mockup panel was tried a second time. Proper gore fit was obtained.

Other panels indexing to the gores were dimensionally checked prior to fabrication with 3/8-in.-thick felt mockups. However, this was accomplished after the finished MLI gores had been mounted to the tank.

9.2.5 Tank Cleaning

Upon completion of the above tank preparation operations (prior to installing insulation), the tank external surfaces were thoroughly cleaned with Freon PCA (precision cleaning agent). The purpose was to remove any volatile matter which might be drawn off into the MLI while in the hard-vacuum test environment.

9.3 TOOLING DESIGN AND FABRICATION

It was necessary to design and construct tooling for each of the four MLI panel fabrication steps: raw material pre-cut; face sheet fabrication; panel assembly; and panel installation. An installation tool was needed only for the large gore panels; however, each panel configuration or type required specific tooling items for use in the other three manufacturing steps. Tooling of the same concept and type defined in the Phase I manufacturing study was used here. Specific tools used are illustrated in subsequent sections which show details of actual panel construction.

9.3.1 Layup Fixtures

Tool design was based upon the concept of interchangeable prefabricated MLI panel units. The primary tool used was a panel layup and assembly surface; gore and cone units are shown in Figure 9-2. This layup tool, which has a surface of the same contour as the desired finished MLI panel, was used for stacking up the individual composite layers. As these sheets must be oversize, scribe marks were provided for positioning. As shown in the photo, index holes for positioning panel assembly fasteners were drilled in the surface. Mounting brackets were also built into the tool for the attachment of metal final trim templates. In this manner, tolerance control was "built in" and uniform finished panels resulted. It should be noted that the layup tool was also scribed for the position of face sheet components, thereby providing a layup surface for making these subassemblies.

CR94
SM 541087

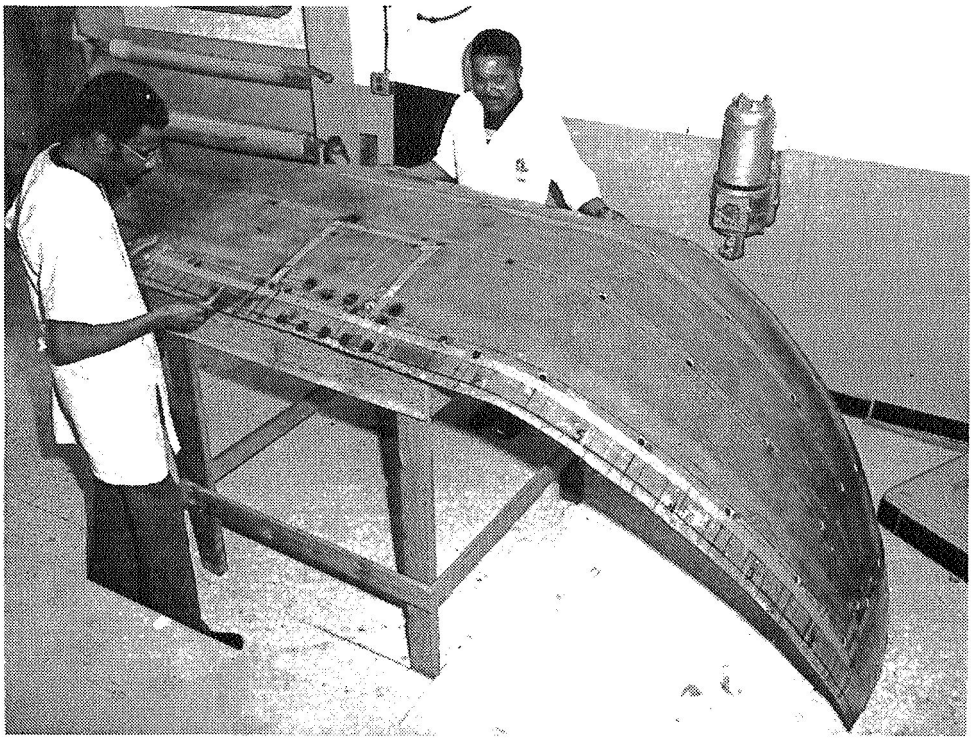

a) GORE

SM 540879

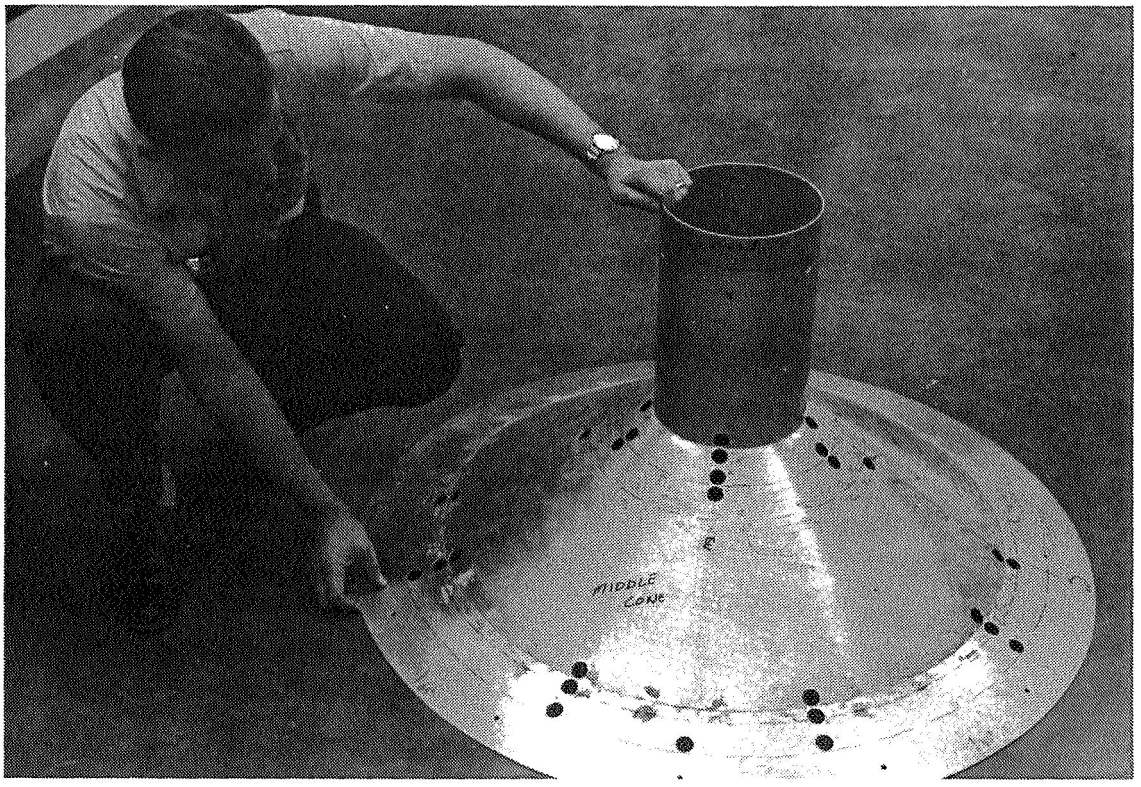

b) CONE

Figure 9-2. Typical Panel Layup Tools

Separate inner and outer panel layup tools were used for each panel configuration (gore, cone, etc.) due to the difference in effective curvature radius between the two (panel thickness). This was found to be adequate for building a one-item system with relatively thin (0.35 in.) panels such as the test article constructed in the program.

For production, three layup tools for a two-panel system would be much better: one each for the inner surface, outer panel inner surface, and outer panel exterior. This was tried for the relatively complicated cone panels used on the tank. The third or outer surface tool is used for constructing the outer panel face sheet. On thick panels or those with sharp curvature, the panel outer face sheet must be laid up on a tool with the corresponding curvature. If built from a tool possessing the curvature occurring at the panel inner surface, it will not fit properly.

Layup tools used in the program were constructed of fiber glass, gores; plywood, manhole and shipping support closeouts; and metal, cone and cylindrical tank support.

A fiber glass mold was made of a section of the tank proper. A second fiber glass mold which became the inner gore layup tool was made in the tank mold. Two-inch-square foam strips covered with glass cloth were used as structural reinforcement of the mold's back face which resulted in a rigid, lightweight structure (Figure 9-2). The simple wood bench seen in the photo was constructed to hold the tool at bench height and to provide access underneath for installation of the MLI panel assembly fasteners. An extra fiber glass wash, made in a similar manner, served as a storage rack for completed panels awaiting installation.

The metal and wood layup tools were constructed from theoretical dimensions instead of the mold procedure, above. However, final trim lines were located only after a 3/8-in. felt mockup panel had been made on the tooling and fitted to the tank. This provided a highly important dimensional check.

9.3.2 Material Precutting Templates

All insulation materials were precut slightly oversize leaving enough material for postassembly trim. This necessitated the use of cutting templates. Typical examples are shown in Figure 9-3 for gore, cone, and cylindrical tank support panels. Thin sheet aluminum was chosen for templates used on cuts through stacks of material. Plastic sheet templates were made for cutting thin face sheet tape and net components.

9.3.3 Final Trim Templates

Final trim of finished panels to size was accomplished with an X-acto knife using metal trim templates as a guide. As noted, these were bolted to index blocks attached to the layup tools. This provided the proper finished dimension and clamped the panel layers firmly in the selvage area, minimizing any tendency to tear during the cut.

Gore and cone final trim templates, typical for all panels, are shown in Figure 9-4. The method of attachment to the basic layup tooling is also shown. The rather complex knife holder, also illustrated, was initially used for trimming but found to be cumbersome and unnecessary. A simple straight-edge guide was all that was needed if the technician was careful to hold the knife perpendicular to the guide.

9.3.4 Special Hand Tools

The injection-molded pure nylon, double T, Swifttach fasteners and installation tooling are shown in Figure 9-5. Tooling items (counterclockwise) are a standard air-powered drill motor; drill guides which fit into layup fixture index holes, centering the drill; hollow drills; installation tool; and hot-air blower used to soften the fastener prior to insertion through the needle of the installation tool.

Other hand tools were also used for face sheet fabrication, such as an iron, punch, and metal grommet installation items. These are illustrated in subsequent sections showing manufacturing techniques.

9.3.5 Panel Installation Handling Fixture

All panels, except gores, were found to be rigid enough to be simply picked up by hand and fitted into place on the tank. However, the long curved gores

SM 541811 CR94

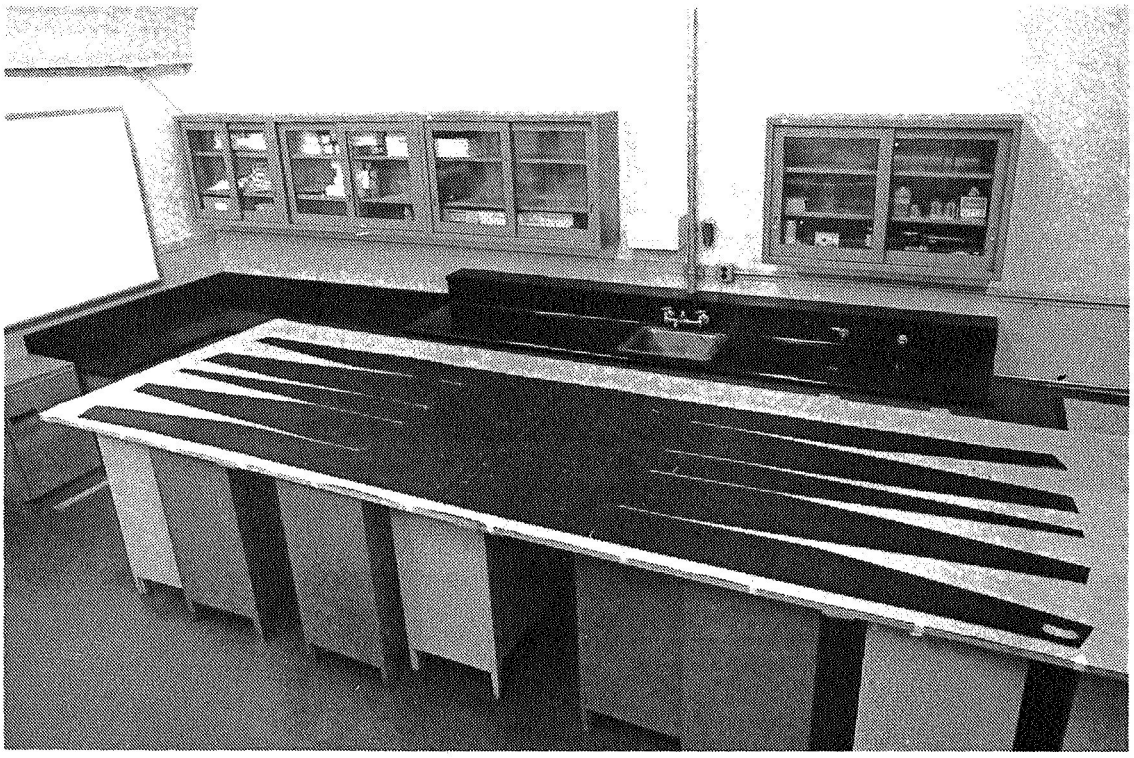

a) GORE

SM 541516

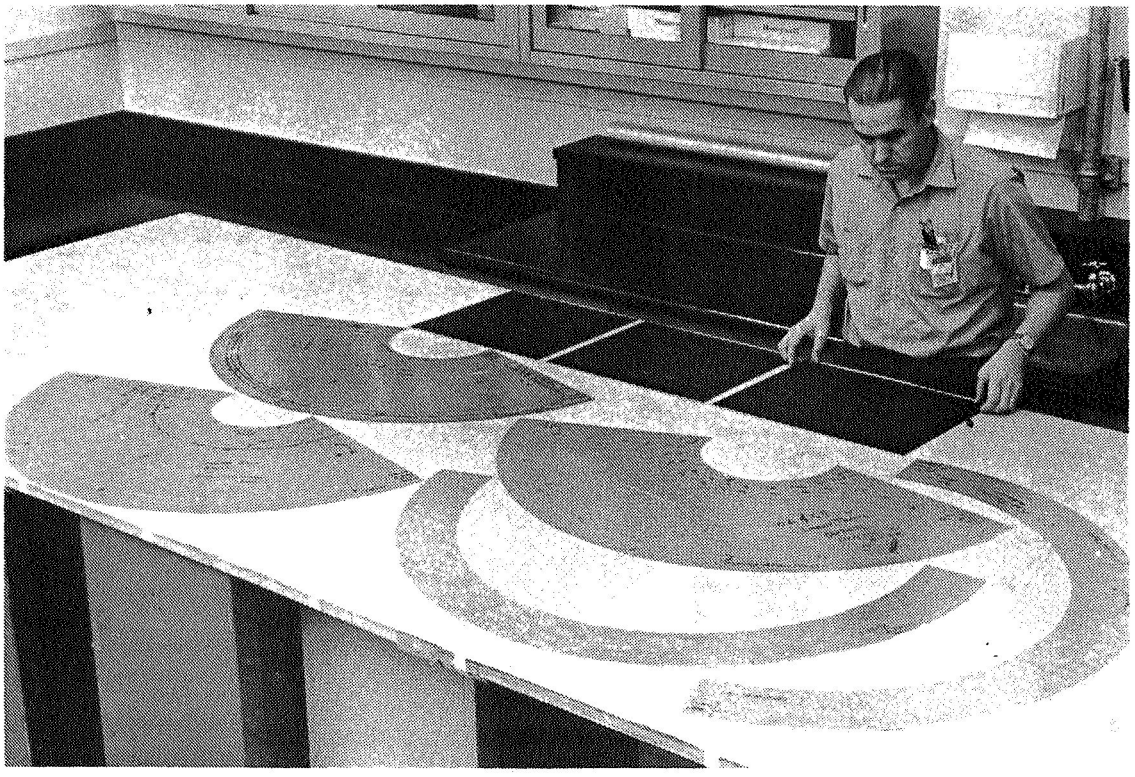

b) CONE AND CYLINDER

Figure 9-3. Material Precut Templates

SM 541806

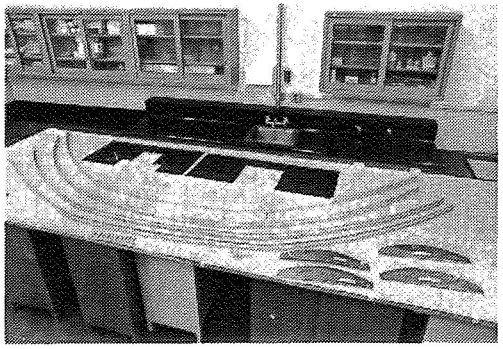

GORE TRIM COMPONENTS

SM 540433

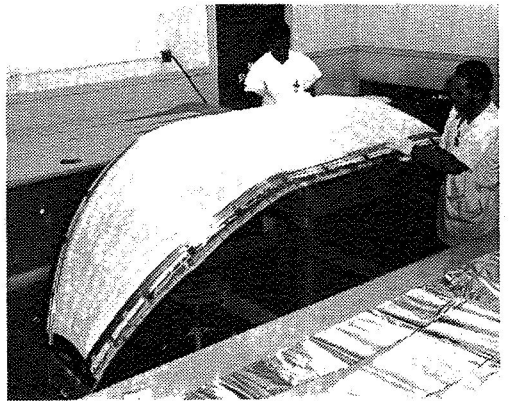

MOUNTED GORE TRIM TEMPLATES

CR94
SM 540438

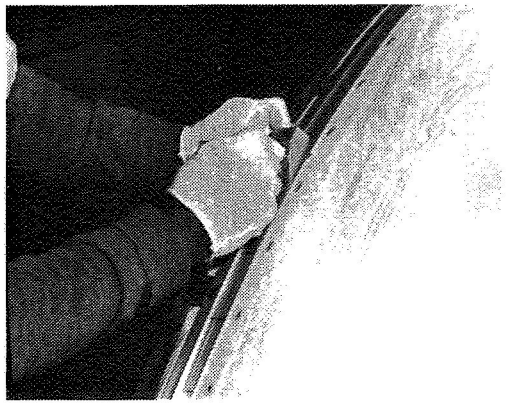

KNIFE HOLDER

SM 541525

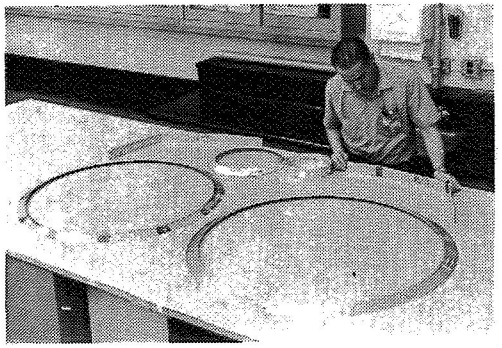

CONE TRIM COMPONENTS

SM 541073

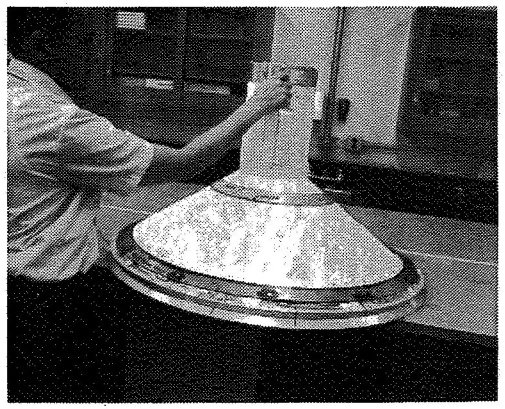

MOUNTED CONE TRIM RINGS

SM 541045

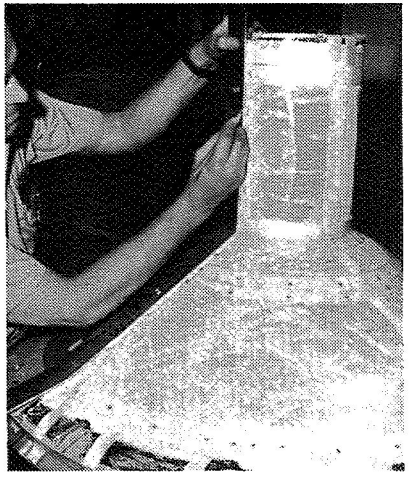

MOUNTED CONE VERTICAL TRIM TEMPLATE

Figure 9-4. Final Trim Templates

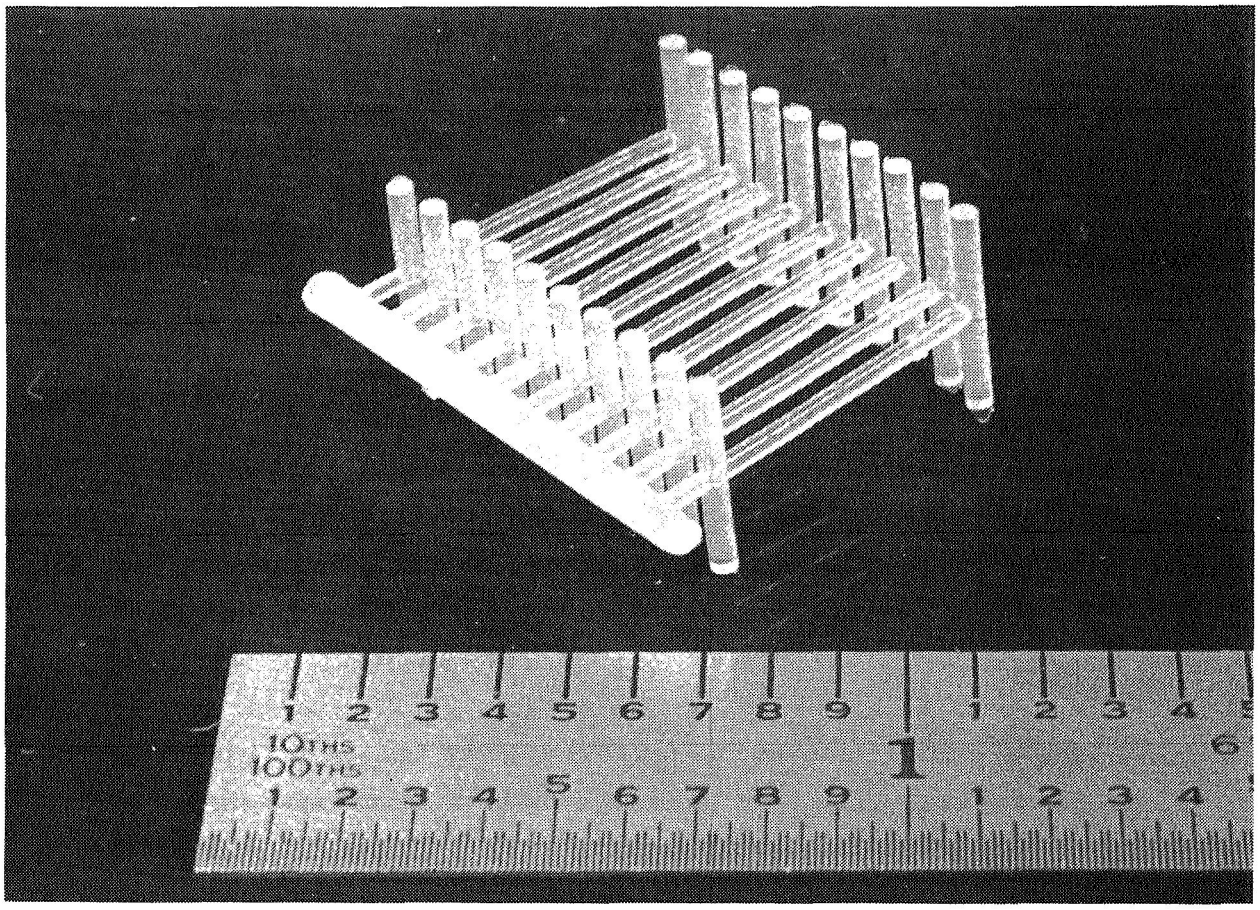

a) FASTENER

SM 541805

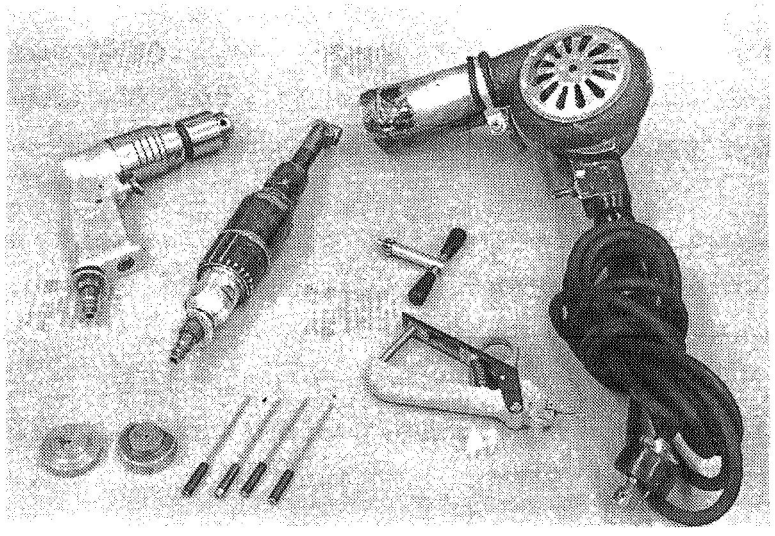

b) REQUIRED INSTALLATION TOOLS

Figure 9-5. Panel Assembly Fasteners with Tooling

had a tendency to straighten, introducing tearing stresses into the MLI reflector layers. A handling fixture was built of fiber glass (like the layup tools) and used with success (see Section 9.6 for details).

9.4 FACE SHEET FABRICATION SEQUENCE

The sequence of operations involved in gore panel face sheet fabrication is shown in Figure 9-6. These steps were essentially the same for all panel configurations (gore, cone, etc.). All face sheets required for a given type of panel were made as a batch as the first step in panel assembly.

Materials were initially precut to shape, Figure 9-6(a). The Dacron net substrate sheet, reinforcing net strips, and the heat-sealable Mylar tape were cut separately. Note that the substrate sheet was cut in a manner which allows the sheet to conform to the proper double-curvature contour without buckling.

Closure of the contour cuts is shown in Figure 9-6(b) as the substrate net is draped on the layup fixture. The tape (adhesive on both sides) was fixed in position to form the load-carrying straps, panel edges, and cut closures, and a strip of reinforcing net applied over the tape. Marking the substrate net for the future location of attachments and lacing buttons was also done at this point.

Bonding of the tape-net sandwich was done through heat application; an iron was used as shown in Figure 9-6(c). After this operation, the face sheet was removed from the layup tool for assembly of the remaining components.

Metal grommets specified in the design for attachments are shown in Figure 9-6(d). Installation was done with a simple forming tool to assemble the two grommet halves.

Lacing buttons consist of a nylon washer on the outer side of the face sheet, held together with a metal grommet, Figure 9-6(e). A standard punch was used to form the hole in the face sheet, and the components were assembled by crimping the grommet with forming pliers, Figure 9-6(f). Following this operation, the face sheet was complete and ready for assembly into a panel, Figure 9-6(g).

(a) PRECUT COMPONENTS

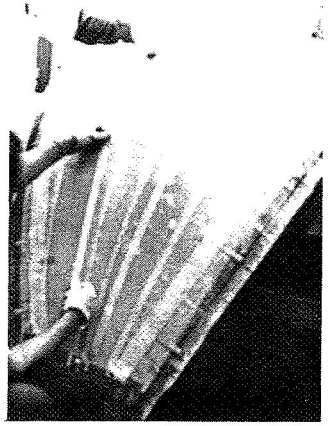

(b) LAYUP AND LOCATE COMPONENTS

(c) BOND STRAPS

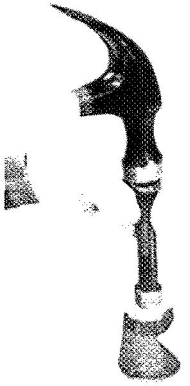

(d) INSTALL ATTACHMENT GROMMETS

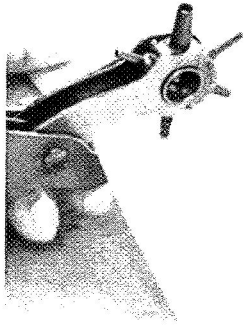

(e) PUNCH FOR LACING BUTTONS

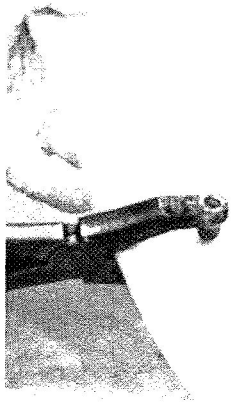

(f) ASSEMBLE BUTTONS

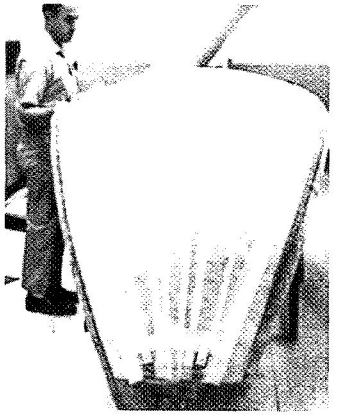

(g) COMPLETED FACE SHEET

Figure 9-6. Typical Face Sheet Assembly Sequence

Many of the operations depicted lend themselves to the use of automated tooling for production.

9.5 MATERIAL PREPARATION

Individual panel assembly was started by stacking the required number of reflector and separator pairs on a table and precutting them to size with a X-acto knife and template, as illustrated in Figure 9-7. Individual stacks were made for each gore panel. All cone cylinder and manhole panels were cut from one common stack.

Pulling reflectors-separators from rolls (Figure 9-7) to create a composite stack can be a time-consuming operation. The 15-gage reflectors and lightweight separators require care in handling to prevent tearing and distortion. A better approach appears to be mounting the roll on a movable carriage and pulling the carriage across the table, feeding out material.

Figure 9-7 shows that dart cutouts were made to allow the material to lie relatively flat on the sharply curved tank contour. Dart positions were determined by trial; a flat sheet was placed on the layup tool and as few as possible evenly spaced dart cuts made to eliminate material bunching. The dart pattern was offset to one side of the panel centerline. This allowed an entire stack to be cut at one time without the resulting cuts lining up one above the other when stacked on the layup tool. One sheet was positioned on the tool and the next turned upside down before stacking. Offset dart cuts resulted.

It was found that dart cuts, if brought to a sharp point in the Mylar reflector material, would cause a tear to readily originate in the material at the point. This difficulty was eliminated by first drilling through the stack with the hollow fastener drill at the dart point. Cuts for the dart were then terminated within this hole. This technique is recommended as tearing was completely eliminated.

9.6 PANEL ASSEMBLY SEQUENCE

All the MLI panels, although consisting of several different geometrical shapes, were constructed in a similar fashion with procedures common to all.

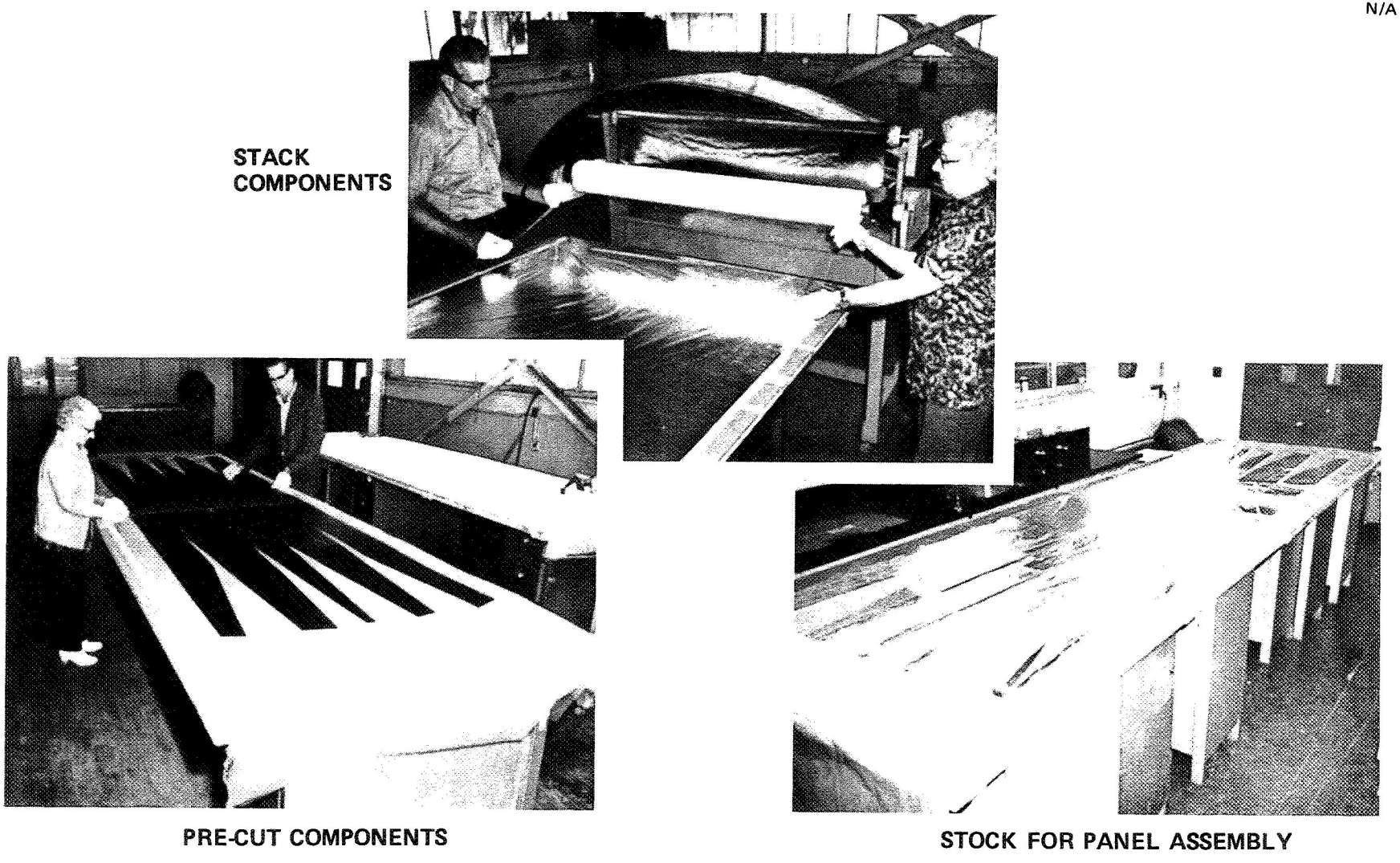

Figure 9-7. MLI Gore Panel Material Preparation

9.6.1 Gore Panels

The gore panel assembly steps are illustrated in Figure 9-8. It will be noted that the assembly area, Figure 9-8(a), was set up in a semiproduction manner. A complete stack of material, ready for layup, was positioned on a table directly alongside the layup tool. The provision for storing two additional furnished panels can be seen on the storage and installation fixture (background).

Prior to starting layup, 1/16-inch plywood strips were taped to the layup tool over the trim lines to serve as knifepoint backing during final trim. Layup consisted of alternating layers repetitively. The panel inner face sheet was positioned (per locating marks) on the layup form, and the reflectors and separators individually stacked on top. Each layer was lightly taped down in the selvage area to prevent movement. Figure 9-8(b) shows how the contour cuts in the reflectors were closed with bits of tape during this operation. The top face sheet was then positioned on top of the completed stack.

Clamping the stack in place for the subsequent assembly and trim operations was done with trim guides which position the cutter for final trim to size. The trim guides, metal strips shown in Figure 9-8(c), were installed along the panel edges. As noted earlier, their position was controlled by locating blocks built into the layup tool.

The molded nylon, "Swifttach" type fasteners were inserted with a special gun. Holes were first drilled through the panel with a hollow drill (a cut-off, sharpened hypodermic needle, Figure 9-8(d). As noted earlier, their location was controlled by the indexing holes in the layup tool. Note that a piece of foam was used as a backup plate for the drilling. Actual fastener insertion, Figure 9-6(e), was done after the nylon fastener was slightly softened with hot air from a portable hand blower.

Trimming to final size was the last step in the assembly sequence, Figure 9-8(f). In this particular case, a knife with a new blade was used for each cut. The cutting dimension was controlled by being built into the tooling. Velcro strips were added to the joint inner faces of completed panels prior to installation.

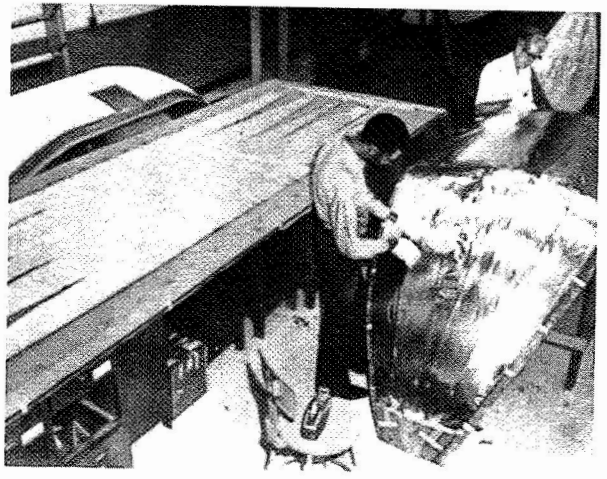

(a) ASSEMBLY AREA WITH PRECUT COMPOSITE STACK

(b) INDIVIDUAL COMPONENT LAYUP

(c) CLAMP LAYUP WITH TRIM GUIDES

(d) DRILL FASTENER HOLES

(e) INSTALL FASTENERS

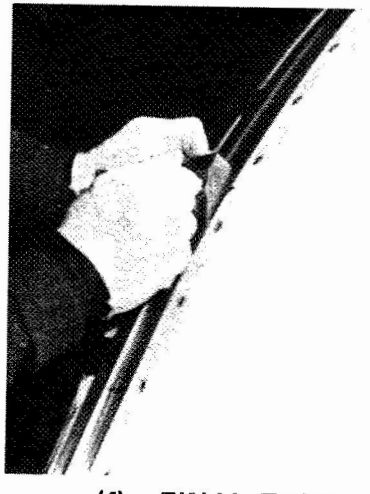

(f) FINAL TRIM

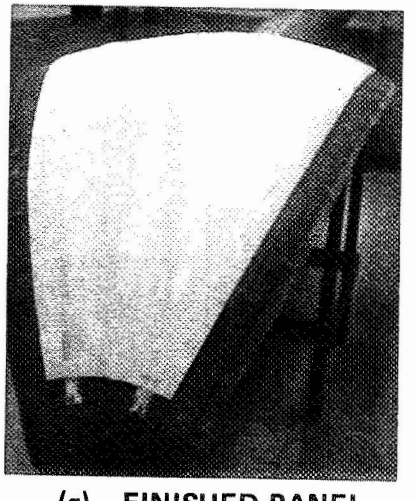

(g) FINISHED PANEL

Figure 9-8. Typical Panel Assembly Sequence

Figure 9-8(g) shows a finished panel, ready for installation, with some of the panel details described earlier. The attachment tabs, face-sheet straps, and joint closure lacing buttons can be seen.

9.6.2 Tank Support Cone and Cylinder

Panels to cover the tank support cone and cylinder penetration were made as one-piece 180-deg units and cut apart into a conical panel and a cylindrical panel containing the cylinder cone transition. Assembly procedures are shown in Figure 9-9.

All steps were identical to the gore panel work described above except at the cylinder-cone transition. Here reflector layers were interleaved to avoid a through optical path.

9.6.3 Manhole Cover

A prefit check with a 3/8-inch-thick felt mockup panel showed that the manhole cover panels could be fabricated flat and installed without any resulting significant buckling. The completed flat panel (outer), both before and after installation, is shown in Figure 9-10.

The simple plywood manhole panel layup tool with the metal final trim template attached is also shown in Figure 9-10. Index holes for fastener positioning can be seen. Also note the scribing for positioning face sheet reinforcement tape, allowing the same tool to be used for face sheet fabrication. A separate layup tool was used for the inner and outer panels.

9.6.4 Shipping Support Closures

Cutouts in the gore panels provided an opening for attachment of the shipping support. Upon removal of the supports for test, MLI panels were inserted in the openings. These panels were made integrally with the gore panel and were simply the material available after making the gore cutout. Figure 9-10 shows the cutout being made with a template, along with the completed panels.

9.7 PANEL INSTALLATION PROCEDURE

Installation was similar for all panels except that a special handling fixture was needed for the large gores, which were subject to tearing stresses if simply picked up and moved.

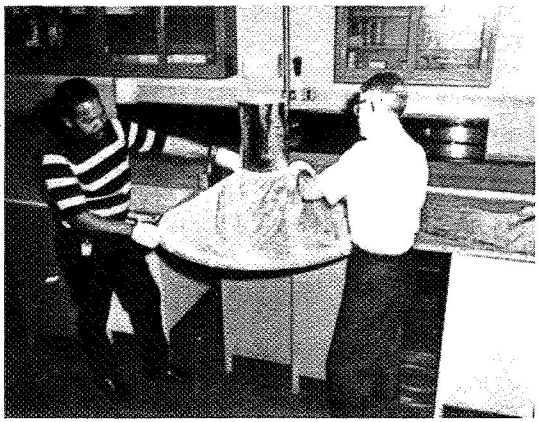

LAYUP COMPONENTS

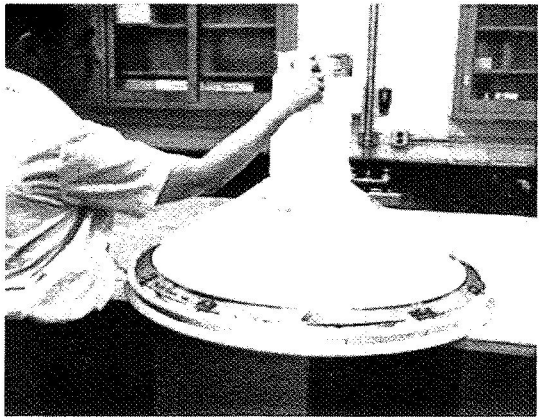

ATTACH TRIM GUIDES

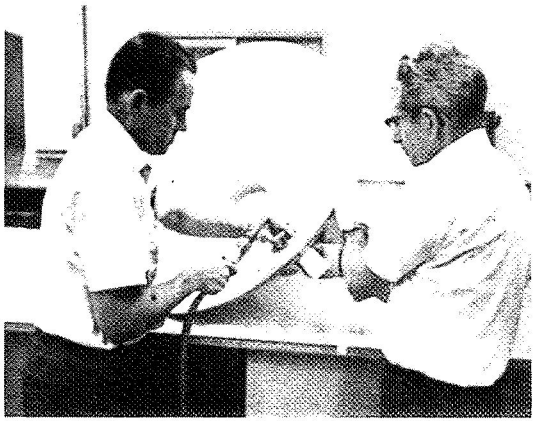

DRILL FASTENER HOLES

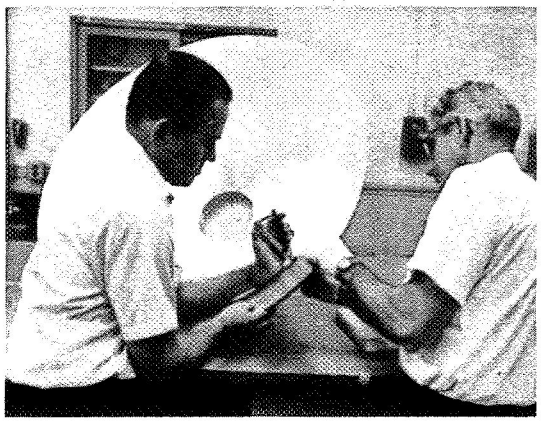

INSTALL FASTENERS

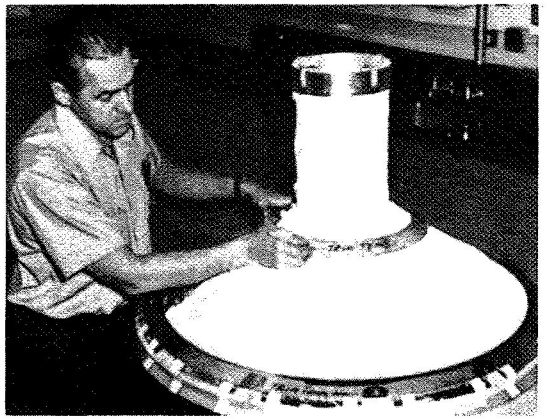

FINAL TRIM

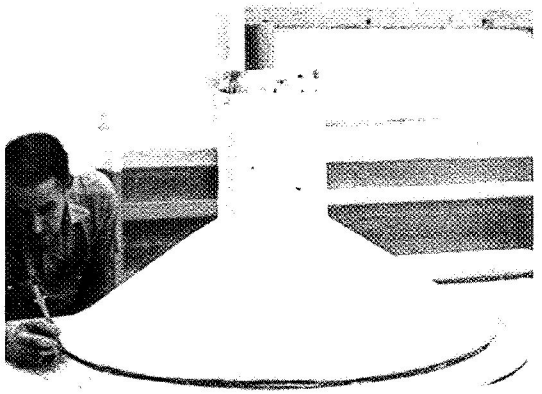

FINISHED PANEL

Figure 9-9. Assembly Sequence–Tank Support Panels

SM 541730

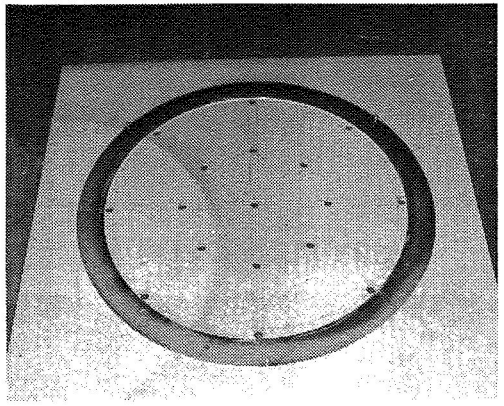

PANEL LAYUP TOOL

SM 541741

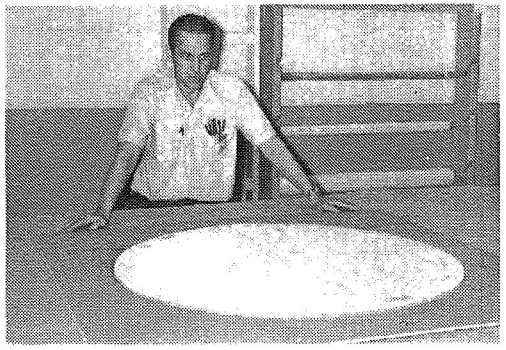

FINISHED CIRCULAR PANEL

SM 541809

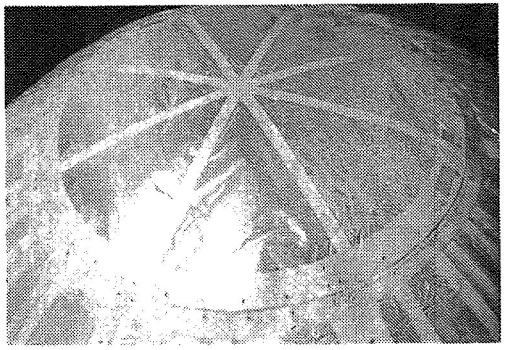

INSTALLED MANHOLE PANEL

SM 540439

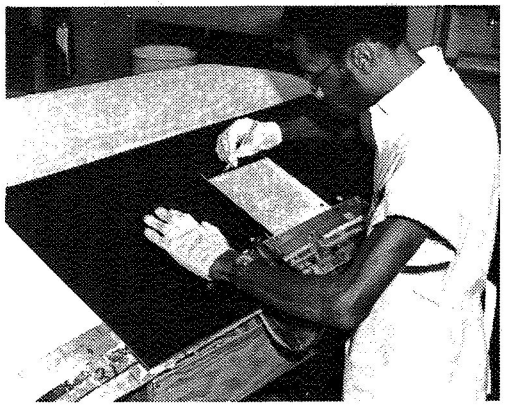

CUTTING OUT TYPICAL CLOSURE PANEL

SM 541747

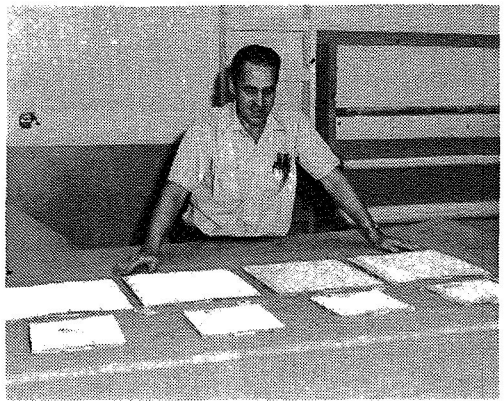

FINISHED CLOSURE PANELS

Figure 9-10. Manhole and Shipping Support Closure Panels

The gore handling fixture which was found to work best is shown in Figure 9-11(a). It was constructed of fiber glass, foam strip reinforced, in a manner similar to the layup tools, Section 9.3. Plastic strips, cut from thin sheet stock, were clamped to the fixture holding a panel in place so that it could be raised vertically for installation, Figure 9-11(b). The reinforcing strips may be seen in this photo. After attaching the panel in place on the support ring at the top of the panel, the strips were slid out and the fixture backed away. Placing the panel into the fixture was simple. The plastic strips were used to clamp the panel to the convex layup tool. This tool was lifted, inverted, and lowered into the concave installation fixture. As the strips were slid out, the panel dropped into place on the fixture as shown.

An attempt was made to hold the panel in the fixture by covering it with thin plastic sheet and pulling a vacuum on the panel backface. Panel crushing resulted due to the coarse vacuum control equipment available. Also, being more cumbersome than the previously described approach, the vacuum idea was abandoned.

The gore panel support ring with studs for panel attachment is shown in Figure 9-11(c). The two layers of gores are shown in place.

The tank support closure panels are conical and cylindrical. Figure 9-11(d) shows the inner layer in place prior to joint closure. Note how the support strap of the outer layer of gore panels was fixed in place over the inner cones. This technique reduces disturbance of the inner panel layers at the joint.

It was found that on large panels, the joints have a tendency to buckle, and positive closures along the entire length of joint appear necessary. As noted earlier, the joints here were a butt type held together on both inner and outer faces. Outer face lacing of a shipping support closure panel with Tefglas thread is illustrated in Figure 9-11(e). On the inner faces, Velcro tabs were fastened to both panels across the joint. Figure 9-11(f) shows the completed, installed manhole cover with joints.

(a) INSTALLATION FIXTURE

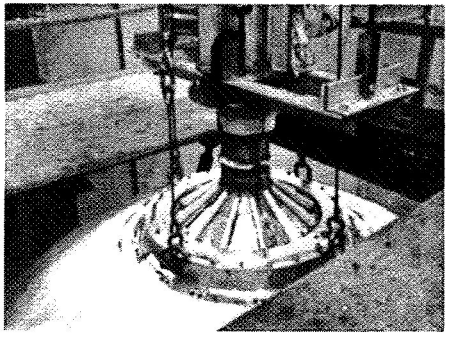

(c) PANEL SUPPORT ATTACHMENTS

(b) INSTALLATION

(d) SUPPORT COVER IN PLACE

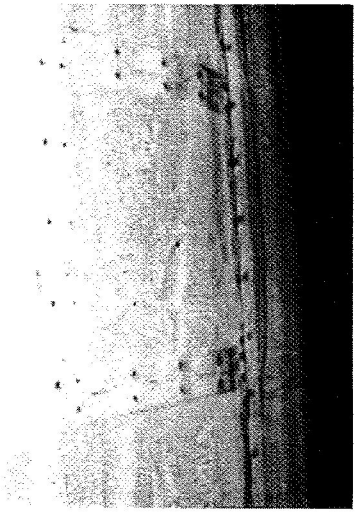

(e) JOINT CLOSURE LACING

(f) COMPLETED MANHOLE COVER

Figure 9-11. Panel Installation

9.8 AVERAGE FABRICATION COST

Some measure of MLI system fabrication cost is desirable for use in future planning when application of an MLI system to a new vehicle is contemplated. Any general number is difficult to derive, as costs will be a function of the geometric complexity, number of layer pairs, degree of shop personnel experience, etc., involved in the proposed application. However, for planning, a cost of seven hours per sq. ft (2 panels of 35 layer pairs) is suggested for estimating MLI assembly and installation costs. This figure, based on an overall average of all the program 105-in.-tank panel fabrications, should obviously be used with care but will provide a quantitative yardstick. Cost data for each detailed fabrication operation were not obtained during the program, as such detail was not believed to be meaningful at this stage of fabrication development.

9.9 STATIC ELECTRICITY DURING MLI PANEL ASSEMBLY

The buildup of a significant static electrical charge within the MLI layers was observed as the MLI reflectors and separators were pulled off the "as received" rolls and stacked on a table for pre-cutting (Figure 9-7). This resulted in a tendency for the sheets to stick together making the restacking of the sheets on the layup surface (Figure 9-8) a difficult and time consuming process.

Although the amount of charge was not measured, it was obvious that it was strongly related to the room relative humidity. The effect was sharply reduced as relative humidity was increased from 20 percent to 50 percent but sheet sticking was not entirely eliminated.

Elimination of static was accomplished by passing a "Static Eliminator Bar (Model 210)" over the MLI stack prior to removing a sheet for restacking on the layup tool. This device, obtained from the 3M Company, produces an Alpha particle cloud from an internally contained radioactive isotope source.

9.10 105-INCH TANK INSULATION THICKNESS

An extensive number of insulation panel thickness measurements were made to determine an average insulation thickness for use in the post-test MLI system thermal performance computations. An average value of 0.69 in. was obtained.

The edge thickness of each insulation panel was measured immediately after fabrication on the layup tool prior to tank installation. Although the thickness after installation might be more representative of actual performance, this measurement is impractical to obtain. Also, a layup tool measurement yields a repeatable or baseline standardized value. Several hundred individual measurement were made in all; typically, 24 on each gore panel. All were subsequently arithmetically averaged.

9.11 PURGE BAG

Purge bag fabrication by the vendor, Goodyear Aerospace Corporation, was reported to have been essentially identical to the earlier fabrication for MSFC. The wooden layup tooling built during that program was used. Fabric strips (Section 8) were laid up and bonded. A special zipper was built to order by the Talon Corporation.

Two tests of the bag opening pressure (zipper failure) were accomplished at Goodyear. Burst differential pressures of 0.45 and 0.46 psi were obtained.

Difficulty was encountered in attaching the purge bag to the fiberglas ring support at the top of the tank support tube (Figures 8-3 and 8-5). As shown, the bag has a lip which goes over the top of the flat horizontal ring and is clamped in place. This necessitated bending of the zipper around the support edge, which produced a gap between the support and bag. A sealing problem resulted which was not satisfactorily resolved.

Redesign is suggested for future applications of purge bags. It is believed that the bag-to-structure joint would be much better if the bag at the joint were cylindrical in cross section and fitted over a cylindrical support. Bending of the zipper is eliminated in such an installation. A simple continuous band clamp could also be used with this joint configuration.

9.12 PACKAGING AND SHIPPING

Delivery of the insulated tank was accomplished in a manner similar to prior programs. The tank was completely encapsulated within the shipping container with a leak-free bag constructed of heat-sealable plastic film conforming to MIL-P-131. The bag was cylindrical, made in two halves of

strips of material. A hose from each of two Thor-Delta tank breather desiccant units was inserted into the bag. Thus, external pressure changes could be accommodated and incoming water vapor eliminated. Upon uncrating at MSFC, no apparent shipping damage was observed.

9.13 FINAL ASSEMBLY AT MSFC

The tank was shipped with insulation panels missing to accommodate the shipping supports: a ring in the top cone-dome area and four standoffs at the tank equator. Closeout MLI panels were shipped separately on their layup forms (eliminating distortions) and installed at MSFC after the tank was uncrated. The purge bag was attached to the tank bag support at this time.

No problems were encountered with the MLI installation. Panels were simply dropped in place and joint closure accomplished. It appeared that any panel, such as a damaged one, could be just as readily replaced. Therefore, it was concluded that the design would be very attractive for extension to reusable systems, where such a requirement is certainly to be encountered.

PART III – LARGE TANK MLI SYSTEM TESTING

Section 10
105-INCH-TANK MLI SYSTEM TEST RESULTS

Phase III of the program consisted of performance tests of the full-scale insulation system, constructed and installed on the NASA 105-in. tank calorimeter during Phase II. All tests were conducted at the NASA-MSFC facility, using LH_2 as the test cryogen. Data defining MLI performance throughout a complete mission environment was obtained which is directly applicable to future vehicle design.

10.1 TEST PROGRAM SUMMARY

The test program was composed of two basic MLI performance tests: evacuated equilibrium, and a launch-to-orbit simulation. Purge system tests were also planned. However, difficulty experienced with the purge bag installation requirements and test chamber schedule limitations forced their cancellation. Prior to testing, a detailed test plan, including a description of the test article and test procedures, was prepared (Reference 7). This plan resulted in an ordered and effective program and is suggested as a model for future test programs of this type.

10.1.1 Test Objectives

The objective of the first test was to establish the thermal performance of an evacuated flightworthy insulation system as installed on an LH_2 filled tank. The plan was to test the system first in the same manner as that used in other MLI programs to provide a direct comparison of the results with those from the various MLI systems tested in the past.

The second test had the goal of establishing the MLI performance throughout a typical mission, including prelaunch loading to evacuated space equilibrium. A comparison of results with Test 1 was expected to yield information on the effect of launch on structural integrity, performance changes due to decompression fluffing of the MLI layers, and the time from launch to orbital steady state.

10.1.2 Test Setup and Procedure

In Test 1, the test article was installed in the MSFC vacuum chamber with the MLI surface openly exposed to a temperature-controlled shroud covering all vacuum chamber walls. The chamber was pumped down to between 10^{-4} and 10^{-5} torr and held for over 48 hours to allow time for any MLI degassing to occur. The tank was then filled with LH_2 and allowed to reach thermal equilibrium with the chamber shroud (about 68°F). Boiloff was continuously measured as well as ullage pressure and insulation and tank and shroud temperatures.

The same setup was used for Test 2. The chamber was pumped down to 1 psia, immediately backfilled with helium, and again evacuated. This was repeated two more times. The tank was then loaded with LH_2 and allowed to stabilize; ground hold thermal data was taken. A rapid pumpdown using a steam ejector was imposed upon the chamber to simulate a Saturn launch. The MLI was then allowed to achieve an evacuated thermal equilibrium condition. As in Test 1, this required several days.

10.1.3 Results and Conclusions

Results showed that the applied thermal performance of the insulation system represents a state-of-the-art advancement. This is illustrated by Figure 10-1 where test results are superimposed upon a NASA technology summary curve. It should be noted also that the system built and tested here was a flightworthy unit. Some or all of the others indicated on the curve were not. Therefore, to yield a valid comparison, the weight of insulation panel face sheets and fasteners was not included in the $k\rho$ computation here. Applied $k\rho$ for Test 1 was determined to be 4.59×10^{-5} Btu-lb/hr-Ft^4-°R.

Test 1 showed that the total heating into the tank was significantly less than the upper limit expected. Design was for a 49.8 Btu/hr experiment maximum, whereas 37 was experienced. The minimum expectation was 30.83 Btu/hr.

This design maximum was determined by doubling the MLI component contributions attributed to joint, fastener, and perforations as determined in 15-in. calorimeter tests (Section 8). The test results suggest that this approach is overconservative and a lower uncertainty factor should be used.

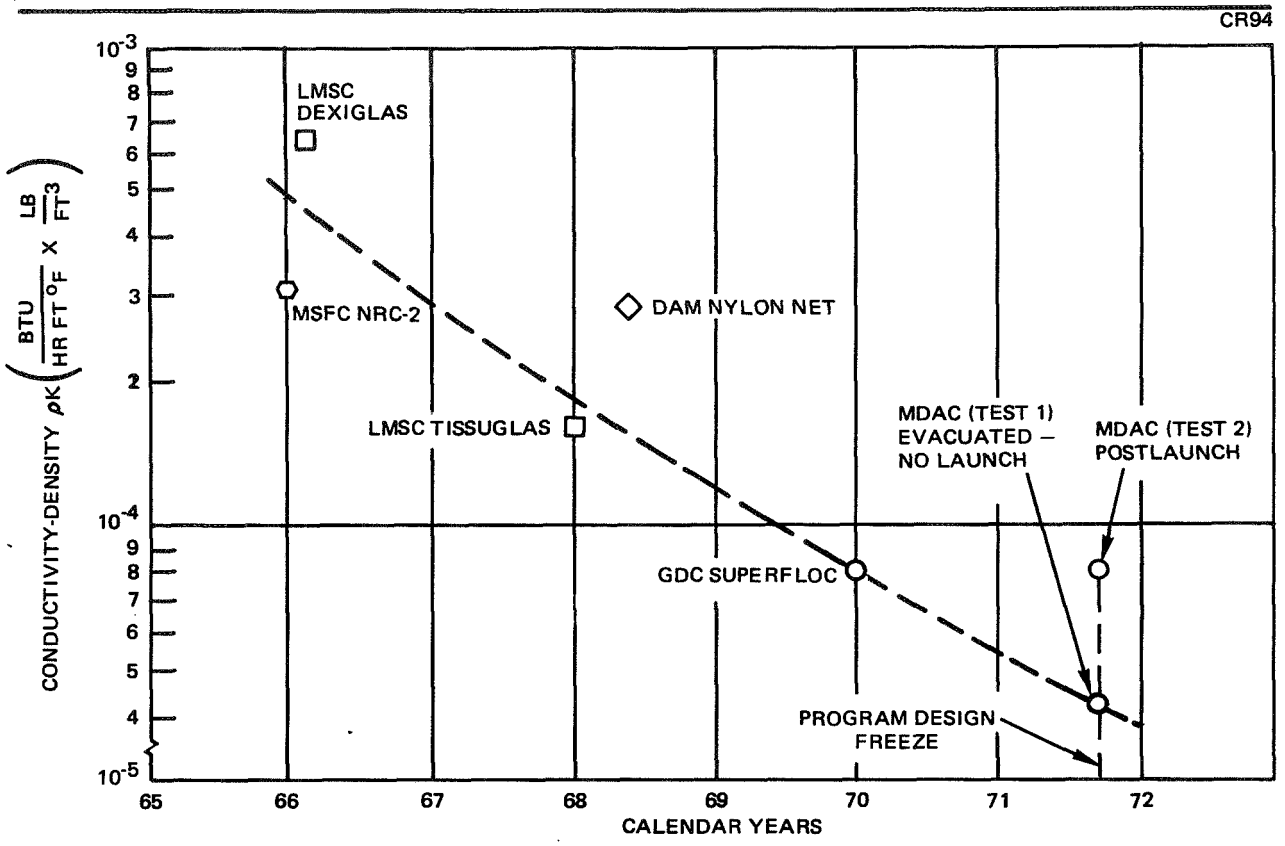

Figure 10-1. Large-Tank MLI System Performance Evolution

Although the MLI test system performance was excellent, it should be noted that significant improvements are possible. The reflector perforations can probably be decreased in size from the 2.3 percent open area used here to about 1 percent. Optimization of the joint configuration should yield significant benefits; nearly half the measured heat input can be attributed to the joints.

Test 2 (MSFC Test 4) yielded much design data. The prelaunch ground hold heating rate of 275 Btu/hr-ft^2 on the wetted portion of the tank was substantiated by an analysis which attributed all heat transfer to the interstitial helium conductivity.

Structural integrity of the MLI panels during launch was demonstrated. The rate of chamber evacuation exceeded that of a typical Saturn launch in the region above 10 torr, the area where highest pressure gradients in the MLI will occur.

Postevacuation data showed that, as expected, the heating rate to the tank dropped rapidly, reaching a low point, then slowly rose to achieve evacuated equilibrium at 14.5 and 50 hours after launch, respectively. The total tank heating rate was found to be about 50 Btu/hr, a higher value than the 37 Btu/hr measured in Test 1. This is believed to be at least partially due to the presence of degassing water vapor within the MLI sheets. It is also possible that the joints opened slightly during rapid evacuation; however, no significant changes were observed upon post-test visual inspection. Pertinent MLI evacuated thermal performance characteristics for Test 1 and Test 2 are compared in Table 10-1.

Several conclusions regarding testing techniques also are pertinent. The NASA calorimeter design used here can be used as a standard for MLI system test measurements. The test MLI is essentially completely isolated from the external environment. It was found that the heat input through the fiber glass fill line and stainless steel vent-support was negligible. Cold vent gas chilled the top of the support to the point where essentially all heat entering this area was carried out the vent.

Every effort should be made to start each test with a nearly full tank; the ratio of dry to wetted area and wetted area change should be minimized. The band of uncertainty in the calculated MLI performance varies greatly as this ratio is decreased for the type of calorimeter used here.

Heat flux gages (thermopiles) should be included on the tank or in the insulation of future mission simulation tests. These units, with their smooth readout characteristics, would provide a very useful check and secondary source of heat transfer data, particularly if anomalies and excursions occur in the flowmeter readouts. They should also be used to measure the differences in heat transfer over the tank surface such as in the tank dome versus the sidewall or bottom and at joints. Thermonetics Corp. of San Diego, Calif, is a typical supplier. At present gages are limited to a theoretical calibration at LH_2 temperatures.

Table 10-1

APPLIED MLI CHARACTERISTICS

THERMAL PERFORMANCE

	Test 1	Test 2
• Orbital Simulation Average Heat Transfer ($Btu/hr-ft^2$)	0.13	0.195
Effective Conductivity ($Btu/hr-ft-°R$) (thickness = 0.69 inches)	1.51×10^{-5}	2.3×10^{-5}
Conductivity - Density ($Btu-lb/hr-ft^4-°R$) (density = 3.0 lb/ft^3)	4.6×10^{-5}	7.0×10^{-5}
• Ground Hold Average Heat Transfer ($Btu/hr-ft^2$)	-	275

SYSTEM WEIGHT

Item	Weight (lb/ft^2)
Reflector (70 layers, 15-gage double-aluminized Mylar)	0.084
Separator (68 layers, B4A Dacron Net)	0.088
Fasteners	Insignificant
Joint Closures	Insignificant
Face Sheets (4; two per panel)	0.072
Total Excluding Face Sheets (Density 3.0 lb/ft^3 @ 0.69 in. thickness)	0.172
Total Including Current Face Sheets (Density 4.2 lb/ft^3)	0.244

Ullage or vent outlet temperature instrumentation would also be useful, particularly for ground hold testing to determine the amount of ullage heating and verify the analyses of support tube heat transfer.

Provisions for longer level sensors should be made to ensure liquid level readout throughout test. The capacitance sensors used in this program were found to be a good backup to the vent flow measurement during periods when level data were available.

To permit detailed evaluation of MLI performance, techniques should be perfected for surveying the thickness of the MLI after tank installation and after test.

10.2 TEST 1 — MLI SYSTEM BASELINE EVACUATED PERFORMANCE

This test yielded the steady-state evacuated performance of the MLI system for direct comparison with systems built and tested during other MLI technology programs. Results are tabulated in Table 10-1.

The criteria used for determining steady-state conditions were based on the rate of change in output of 10 thermocouples within the MLI and the vent flowrate stability. These criteria required as prerequisites that uniform pressure be maintained in the ullage, fill valve leakage be negligible, and that steady-state cold wall temperature exist.

It will be shown that the temperature stability criterion was achieved but that anomalies disrupted a potentially stable vent flowrate. It was also found that the barostat (vent system back pressure controller) did not perform as expected with the result that ullage pressure underwent wide excursions. Because of these difficulties, it was necessary to be sufficiently conservative when reducing the data so that the resulting computed MLI performance represents an upper bound on the uncertainty in the actual performance.

10.2.1 Test Procedure

The test tank was installed in the vacuum chamber, instrumentation checked out, and evacuation accomplished with roughing, then diffusion pumps. After exposing the MLI to a chamber pressure of less than 10^{-4} torr for several days, the tank was filled with LH_2 and allowed to reach thermal equilibrium. At apparent steady state, the test was terminated. The significant post-fill events are noted in Table 10-2.

Table 10-2

TEST 1 – SEQUENCE OF EVENTS

Time (Minutes)	Remarks
0 (8:37:45 PM, 9/25/72)	Data system on
38.6	Completion of initial fill
82.25	Completion of LH_2 replenishment
202	Ullage pressure stabilized and barostat controlling
2893.25	Terminate test, detanking
4972.25	Data system off

10.2.2 Test Article Environment

Successful measurement of insulation performance requires that the tank environment be controlled. These parameters, cold wall temperatures, chamber pressure and fill valve leakage, were all maintained at acceptable values during this test.

10.2.2.1 Cold Wall Temperature

The chamber cold wall shroud provided a stable external thermal environment for the MLI. All 15 thermocouples on the shroud indicated temperatures within a band of 68° ±10° F throughout the test. In general, all measurements showed a gradual, uniform downtrend of approximately 10° F over the 4,800 minute test.

10.2.2.2 Fill Valve Leakage

Fill valve leakage, an often overlooked crucial parameter affecting the boiloff measurement, was essentially zero.

10.2.2.3 Chamber Pressure

The vacuum chamber pressure, monitored continuously during test, was in the 10^{-5} torr range throughout the test. This met the acceptance criteria of a 10^{-4} torr minimum.

10.2.3 Steady-State Insulation Temperatures

A total of ten Chromel-Constantan thermocouples, within the MLI panels, were monitored to determine the achievement of steady-state conditions and to record temperature profiles within the MLI. Four (T19, T21, T22, T23) were located one above the other at the midpoint of the test tank sidewall (see Figure 10-2) on sheets 5, 17, 35, and 70 (counting out from the tank itself). Number T20 was on the outermost sheet on the opposite side of the tank. A second set (T14, T16, T17, T18) was similarly located on the upper dome: sheets 5, 17, 35, and 70. Number T15 was 180 deg away on the outermost sheet. Thermocouple T22 was found defective at the pretest checkout.

The thermocouple response in the two profile positions is shown in Figure 10-3. The average rate of change in thermocouple readings over the last 300 minutes in the test program is listed in Table 10-3. Note that temperatures were very near a steady-state condition and all are within a target steady-state criterion of 0.5°F/hr, maximum change. Actually, it is believed that any period after 4,000 minutes (see Figure 10-3) is sufficiently close to steady state for insulation performance computations.

Figure 10-4 shows the two steady-state temperature profiles. Notice that the dome profile has a flatter characteristic and exhibits lower temperatures than the sidewall. This suggests that sheet-to-sheet conduction is more significant in the dome area, which would appear to be logical. The probable causes are the weight of the MLI panels compressing the dome layers more than the sidewall, closer joint spacing in the dome, and the dome's double curvature which precludes ideal MLI sheet spacing.

10.2.4 Ullage Pressure

A barostat was used in the vent line just in front of the atmospheric outlet to maintain constant vent and tank ullage pressure. It failed to achieve the results expected because the resulting tank pressure was erratic.

Five independent ullage pressure measurements were made, but consistent similarities among them could not be found. Figure 10-5 shows the output of the primary sensor (D616A) and a backup sensor with the most similar trend.

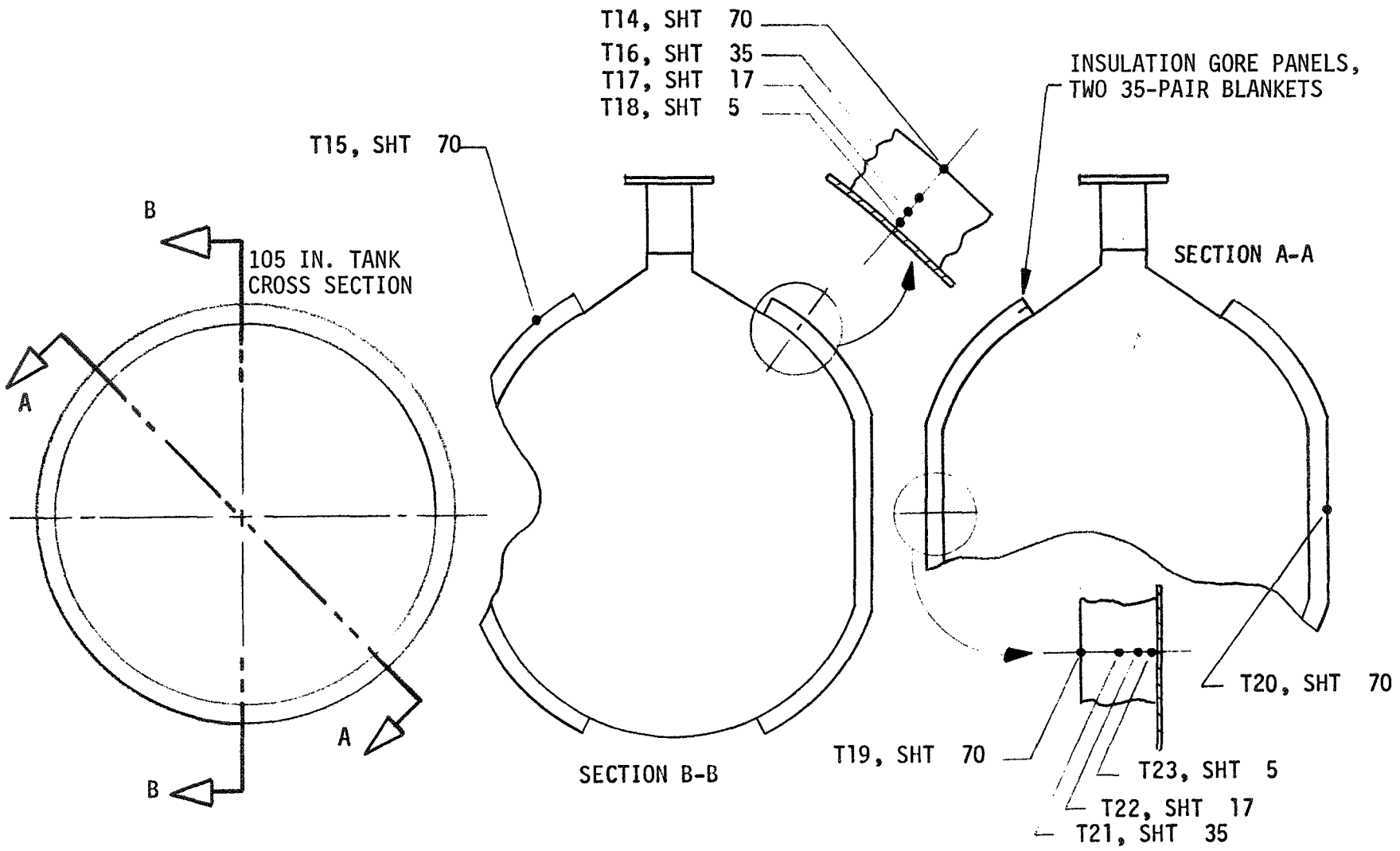

Figure 10-2. Insulation Thermocouple Locations

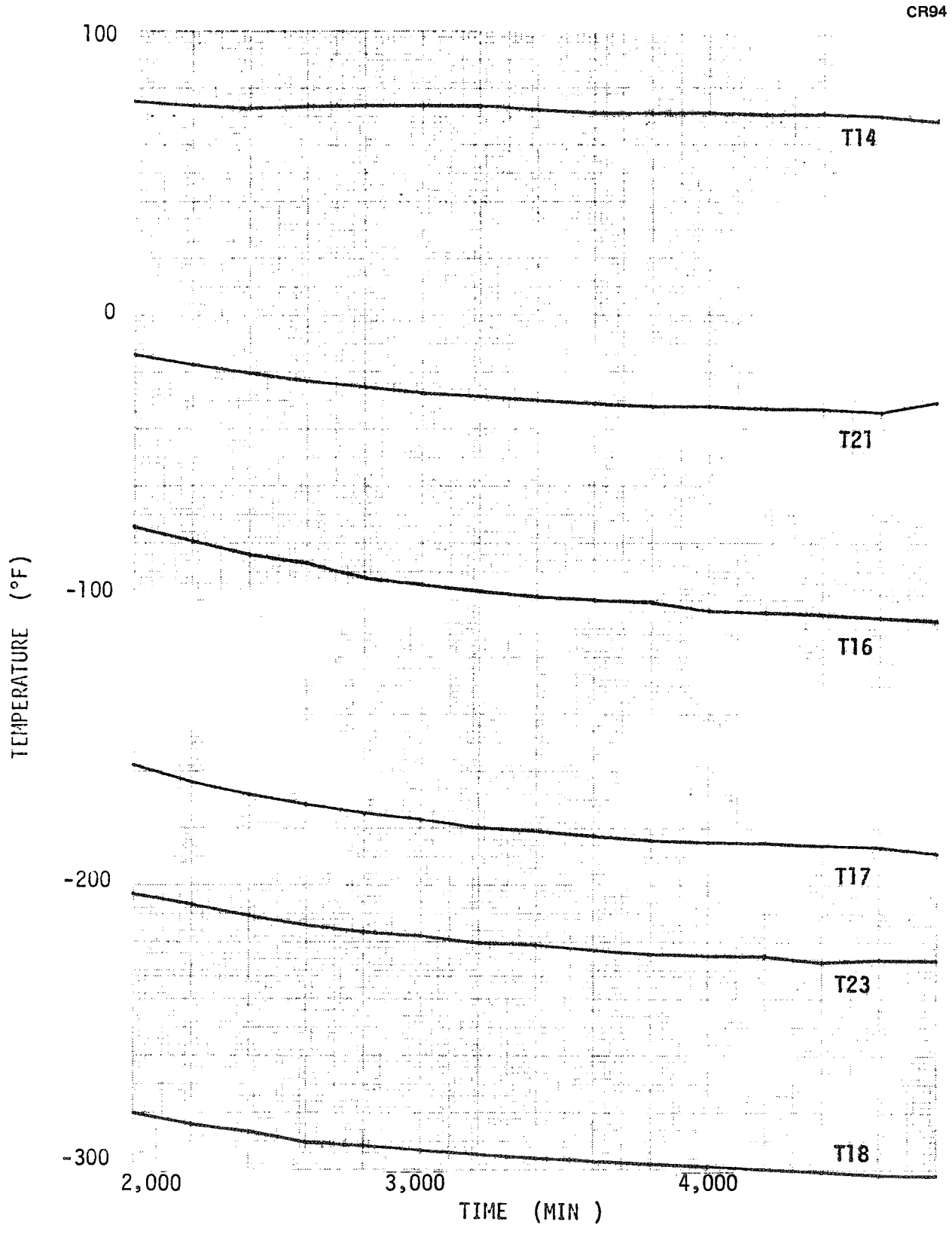

Figure 10-3. MLI Temperature Profiles

Table 10-3

TEST 1 – RATE OF MLI TEMPERATURE CHANGE
(Between 4,600 and 4,900 minutes)

Thermocouple	Temperature Change
T14	-0.2°F/hr
15	-0.15
16	-0.3
17	-0.4
18	-0.25
19	No consistent trend
20	No consistent trend
21	No consistent trend
23	-0.35

A negative calibration shift was applied to D624 and D619 in the Figure 10-5 data as shown. It appears that D616A was drifting downward and the correction required varied in some unknown fashion throughout the test. Maximum excursions were about 0.1 psi and appear to be related to the changes in ambient air temperature and pressure (Figure 10-6).

It is of interest to note the variation in heat storage associated with the pressure excursions measured in this test. The saturation temperature of LH_2 changes 0.04°R in going from 16.3 to 16.4 psia. There was approximately 1,950 lbm of LH_2 present (C_p = 2.4 Btu/lbm-°R) and approximately 1,670 lbm of aluminum present (C_p = 0.0025 Btu/lbm-°R). Using these values, the net change in heat capacity is 190 Btu or 19 Btu/hr in a 10-hour period, a value half the average heat flux through the insulation.

The period from 3,100 to 3,600 minutes was selected as most closely approximating steady state. Here, three pressure transducers, D617, D618, and D624 plus D619, were in agreement that the net change in ullage pressure was negative or zero. Therefore, with a reduction in the saturation temperature, the boiloff measurement in that interval should be conservative if it is all attributed to heat flux through the insulation and down the support tubes and no stored energy correction must be made.

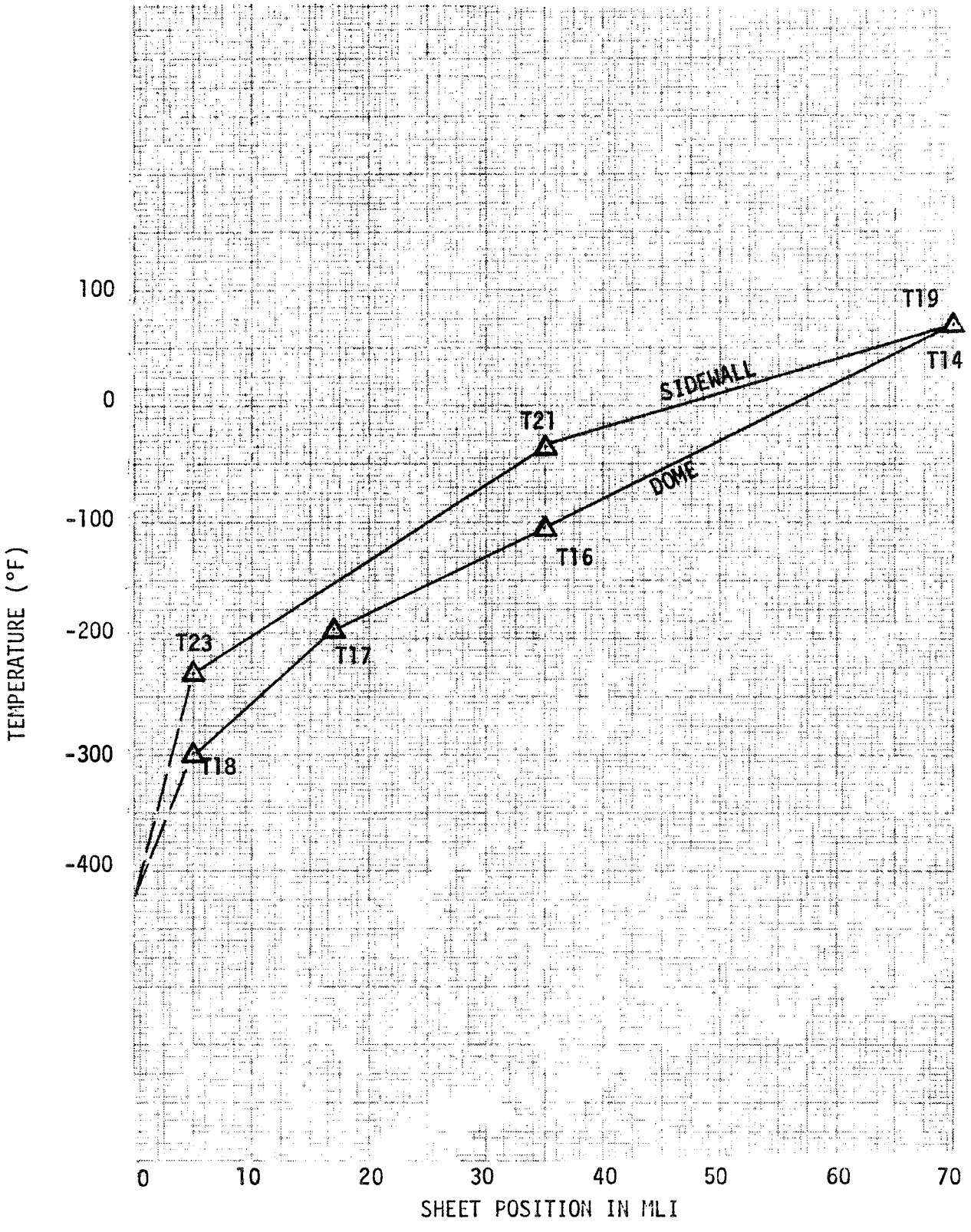

Figure 10-4. Steady-State MLI Temperature Profiles

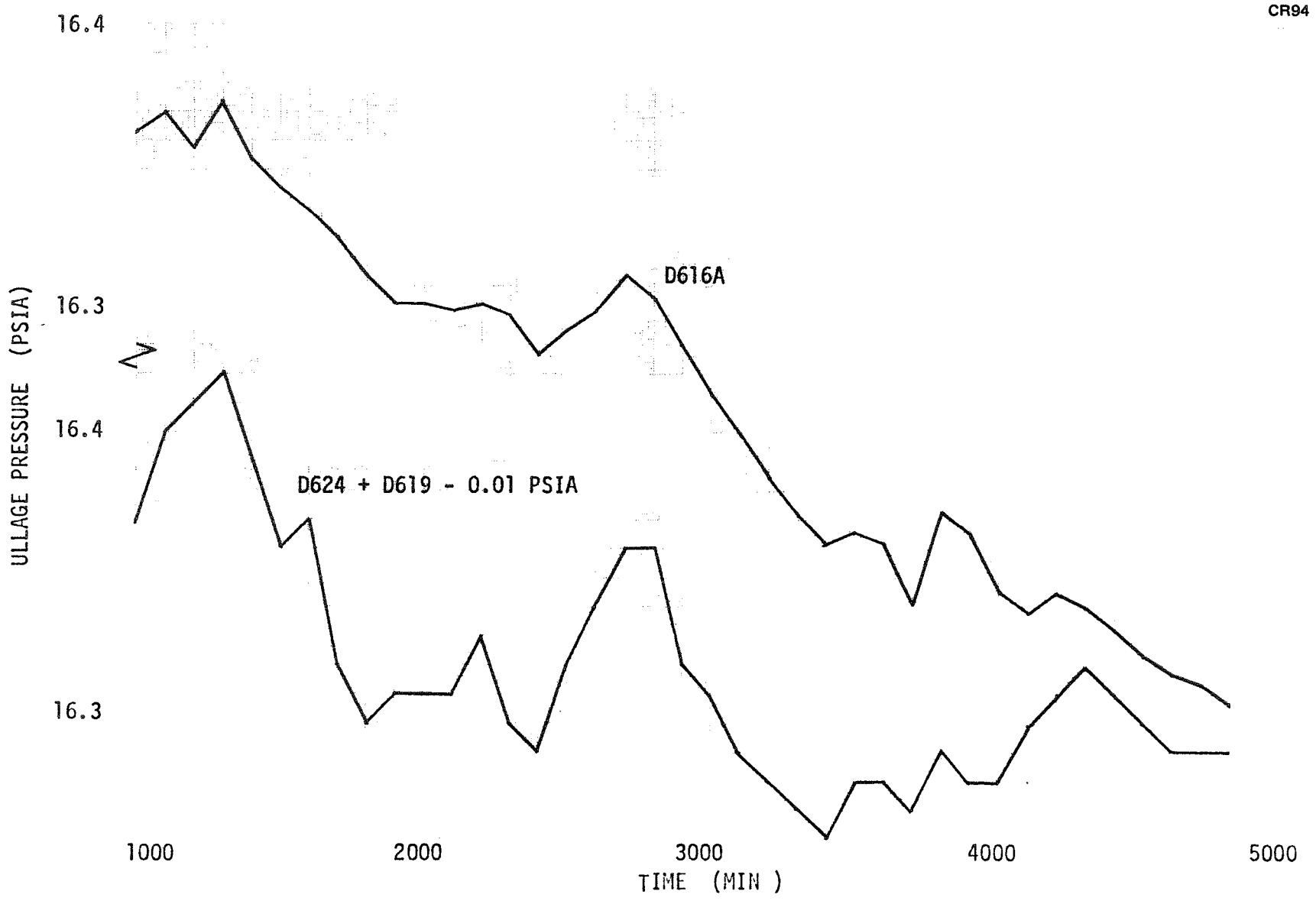

Figure 10-5. Ullage Pressure Measurements

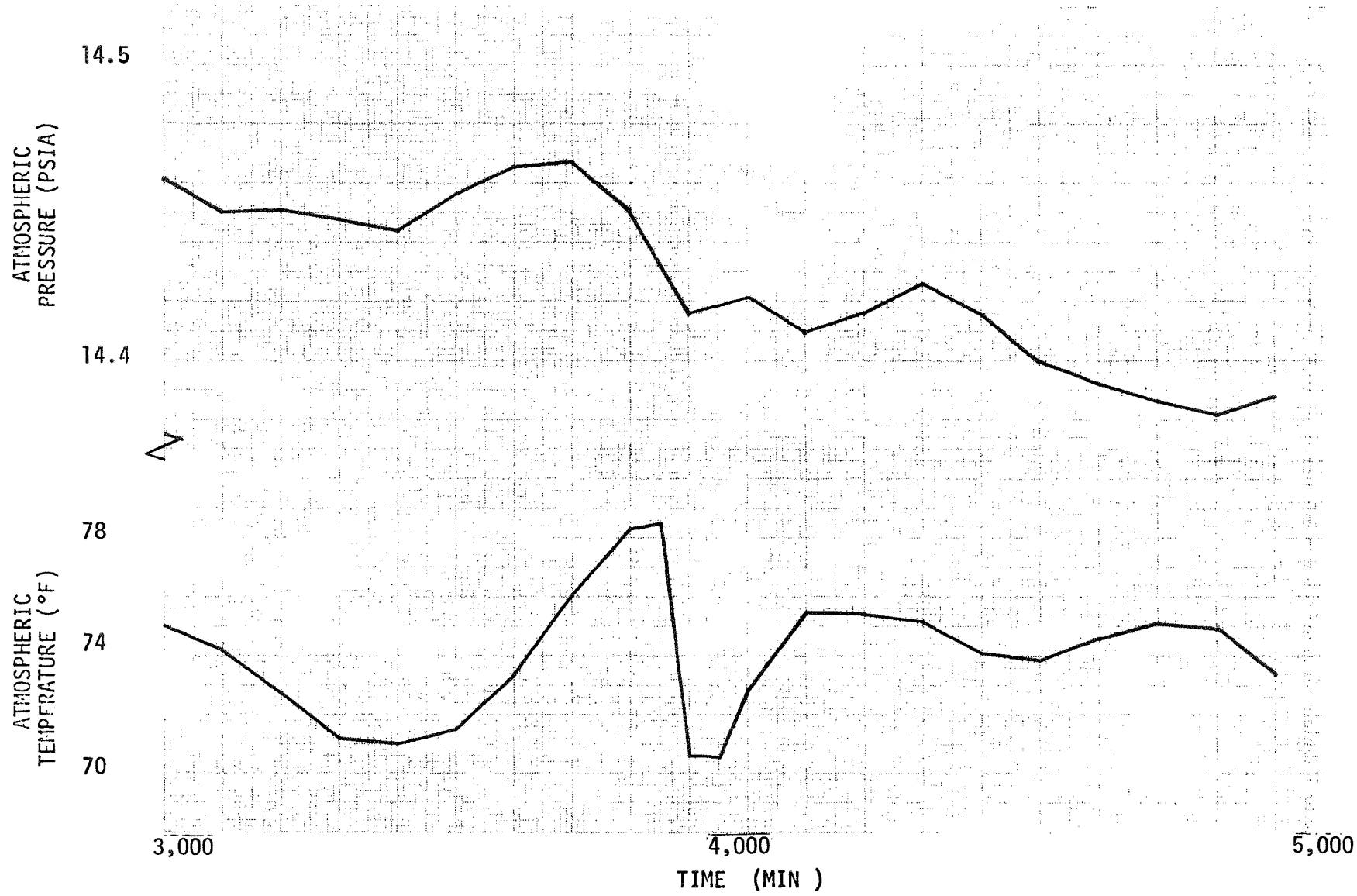

Figure 10-6. Atmospheric Conditions

Note that this period does not correspond to the post-4,000-minute steady-state period defined by the insulation temperature measurements. But it does correspond to a period of highest measured boiloff and greatest amount of boiloff data stability (see Section 10.2.5). The flowmeter reading in the post-4,000-minute period was recovering from a severe anomaly and appeared to be leveling off at a value somewhat below that recorded during the chosen steady-state period. Consequently, it is believed that the 3,100-to- 3,600-minute period yields the best representative conservative value for the true steady-state MLI heat transfer.

10.2.5 Total Tank Heating Rate

The corrected steady-state boiloff mass flow for the test was 0.66 sfcm which corresponds to a total tank heat input of 37 Btu/hr at an ullage pressure of 16.35 psig.

In the test setup, vent gases were routed from the tank ullage through a temperature-conditioning heat exchanger, two series-mounted Thermo-Systems anemometer GH_2 flowmeters (F088 and F089), and a barostat which acted to maintain a uniform pressure in the vent system and tank, and were finally disposed of at a propane burner unit. In addition to the two flowmeters, the vent-line instrumentation included pressure and temperature sensors.

The output of the primary vent gas flowmeters (F089) is shown in Figure 10-7 for the last 2,000-minute portion of the test. Before this period, both units exhibited large variations in flowrate, F088 being especially erratic. Meter F089 was specified as the primary measurement by MSFC.

The impressive features of Figure 10-7 are the two precipitous drops in the vent flowrate at 3,600 and 4,000 minutes. The flowrate recovers quickly from the first and much more slowly from the second. Clearly, steady-state conditions were disrupted to a large degree. A satisfactory explanation has not been found.

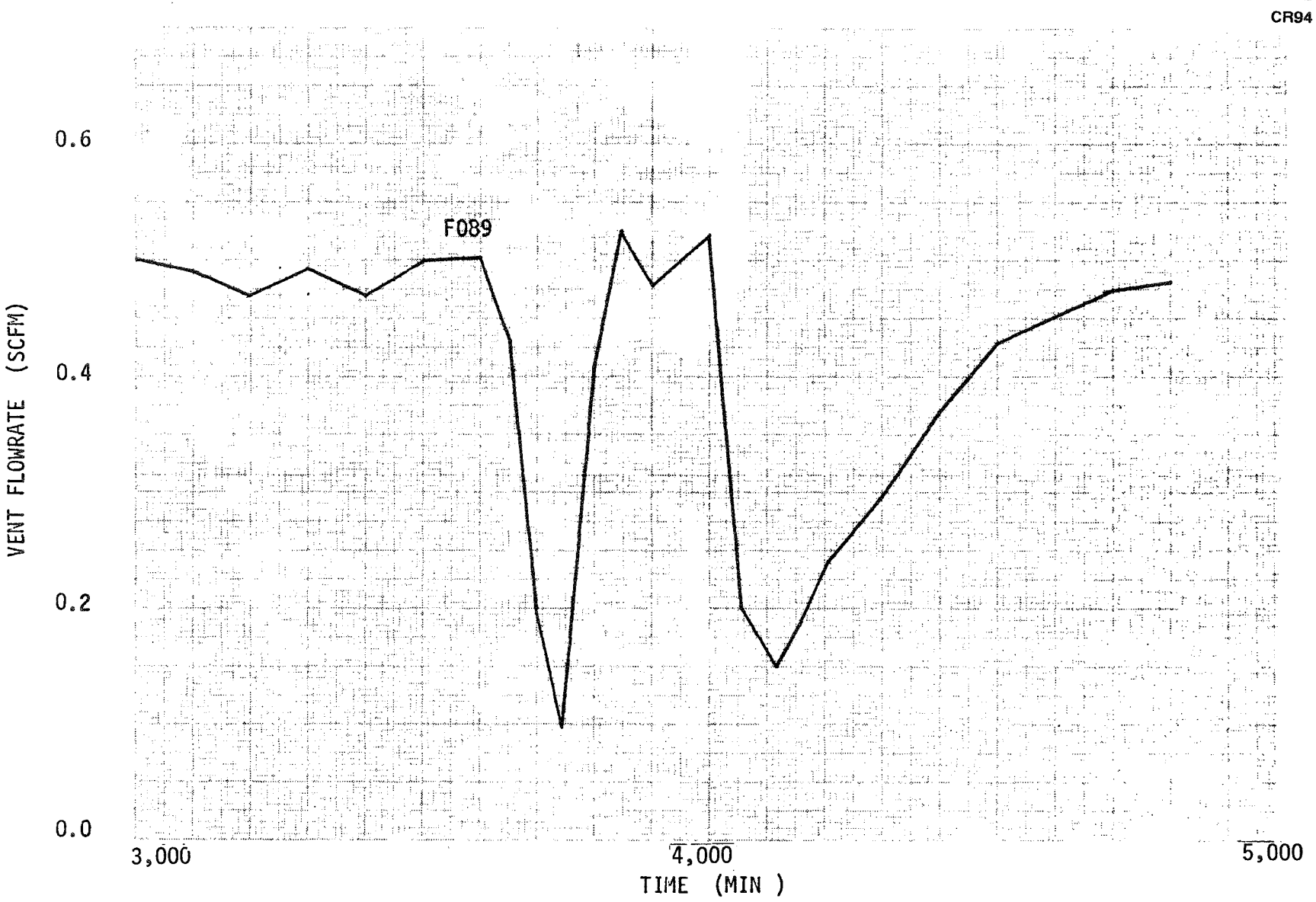

Figure 10-7. Primary Vent Flow Measurement

At a time corresponding to the rapid decay in flowrate, the thermocouples on the tank support (T29, T30) and the top of the fill line (T1, T2, T3, T4) show rapid temperature drops. These thermocouples quickly return to a preceding quasi-steady-state value following the drop in flowrate at 3,600 minutes. However, after the drop at 4,000 minutes, these same thermocouples tend exponentially toward a new and significantly lower temperature than the previous quasi-steady-state values. This behavior indicates the possibility of liquid moving back up the fill line, which chills the neck support region. The corresponding increase in ullage volume might account for the drop in vent flowrate. However, this explanation is not supported by any facts that explain why liquid would be moving up the fill line. There is no change in fill valve leakage nor does the test log note any sequencing of the fill valve.

The vent gas temperature and pressure histories are shown in Figure 10-8. Variations in the ambient temperature and pressure are plotted in Figure 10-6. It is apparent that the heat exchanger was not successful in isolating the vent gas from atmospheric variations in temperature. However, the magnitude of the excursions in gas temperature and pressure do not require corrections to the vent flowrates.

As noted in the discussion of ullage pressure, the time between 3,100 and 3,600 minutes was selected as the steady-state period. Here, both flowmeters appeared to be functioning properly and the temperatures in the support tube area were steady. Also, the vent rate is conservative when compared to the value exhibited at the end of the test (489 minutes). Table 10-4 shows the average flowrate during this period. The correction applied to each flowmeter was that reading each instrument indicated when the vent flow terminated following the test. No reason for the zero shift could be found. The 0.66 scfm flowrate shown corresponds to a tank heat input of 37 Btu/hr at the 16.35 psig steady-state-period ullage pressure.

10.2.6 Liquid Level and Tank Wetted Area

The liquid level during the steady-state period can only be estimated, as the two capacitance probe level sensors in the tank did not function. However, the two rows of three carbon resistor point level sensors did perform as

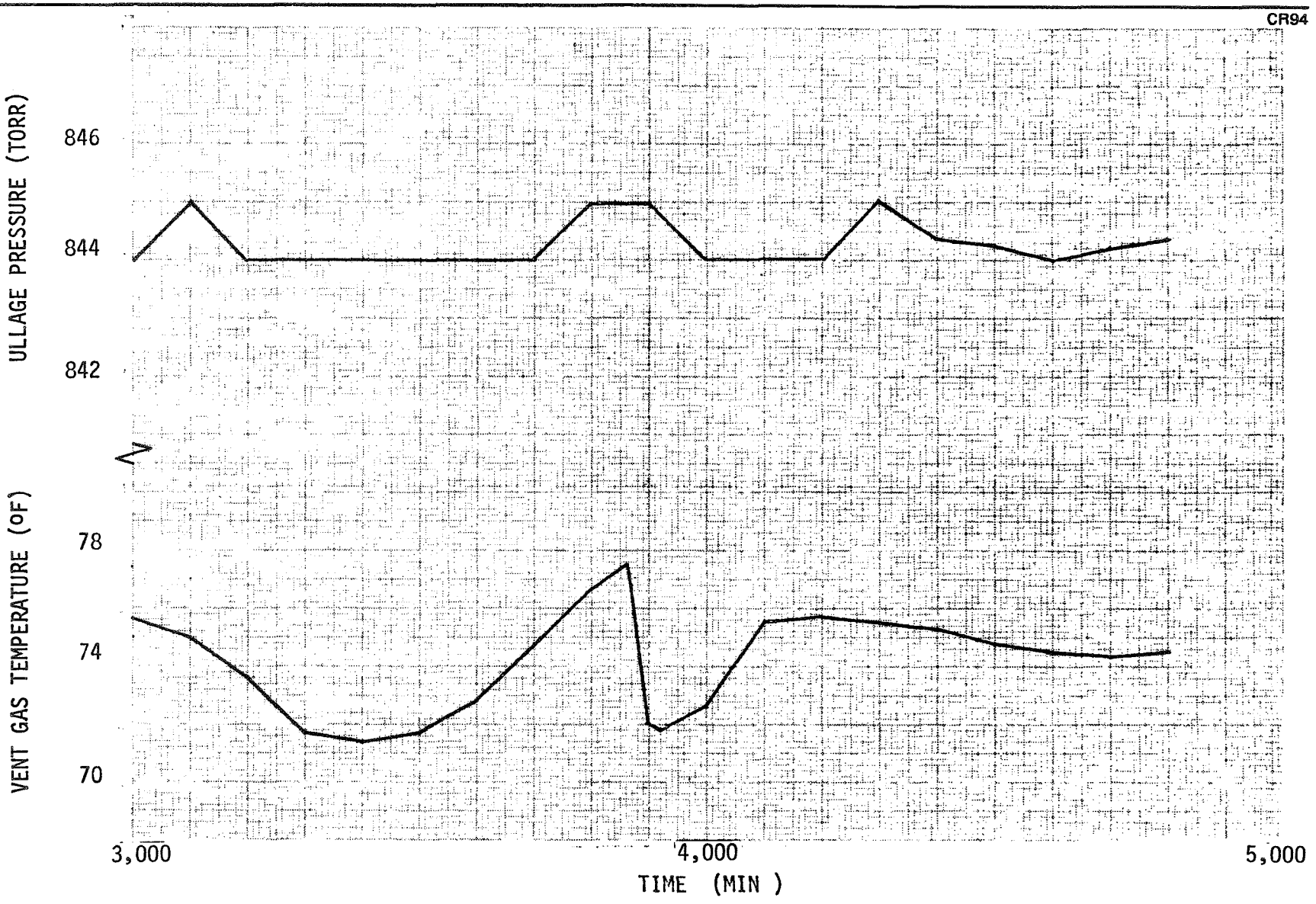

Figure 10-8. GH_2 Vent Conditions at Flowmeter

Table 10-4

TEST 1 – STEADY STATE VENT FLOWRATE

Instrument	Observed Average Flow	Zero Correction	Corrected Average Flow
F088	0.62 scfm	+ 0.03 scfm	0.65 scfm
F089	0.48	+ 0.18	0.66

expected. All six were submerged during the pretest tank replenishment operation and then uncovered as boiloff removed liquid over the period of 67 to 69 minutes. It was not possible to determine the moment of sensor uncovering as it occurred between data sampling points. Linear extrapolation cannot be used as the tank volume change is not linear with height in the area of interest. The liquid volume change must be first computed and then liquid height determined from the volume-depth relationships for the 105-in. tank given in Reference 7.

Point level sensor rows were located 117.6 and 114.6 in. above the tank bottom. The volume of liquid required to fill the tank to the lower row of point sensors is 442.7 ft^3. An average heat flux to the liquid of 40 Btu/hr for the duration of the test (80 hr) would result in a loss of 3.9 ft^3 of liquid, dropping the level approximately 2.7 in. if it is assumed to initially be at the lower row (114.6 inch depth). The nominal liquid depth will therefore be assumed to be 113.4 in. (depth corresponding to a volume of 442.7-0.5 x 3.9). The corresponding liquid volume and tank wetted area are then 441.2 ft^3 and 267.6 ft^2, respectively.

10.2.7 Insulation Thermal Performance

Data reduction to obtain the insulation thermal conductivity was accomplished by subtracting extraneous heat shorts from the total heat input and evaluating a corrected boiloff. No fill valve leakage occurred and results showed that heat conducted down the fill line was negligible. Also no heat was conducted down the tank support into the test liquid as heat is completely intercepted by the gas venting through this support structure. The resulting "as applied"

heat transfer, density, conductivity, and conductivity-density of the MLI system were 0.13 Btu/hr ft^2, 3.0 lb/ft^3, 1.53 x 10^{-5} Btu/hr ft°R, and 4.59 x 10^{-5} Btu/lb/ft^4°R, respectively.

10.2.7.1 Fill Line Heat Input

Twenty differential and seven absolute Chromel-Constantan thermocouples were located on the fiber glass fill line located on the test tank centerline as shown in Figure 10-9. Sensor DTI indicated the largest differential temperature (ΔT) as 2.6°R; about 1°R for all others. The absolute temperature at DTI was about -392°F, ranging down to an indicated -415°F for the lowest absolute sensor. However, some of these sensors should have read -423°F as they were assuredly covered with LH_2 as indicated by the liquid level computed above.

The estimated heat conduction down the fill line is about 0.02 Btu/hr, a negligible value. This results from using the largest ΔT (in the ullage) and the fiber glass conductivity at -415°F, 0.06 Btu/ft-hr-°R. Sensors were mounted 1 in. apart.

10.2.7.2 Tank Support Heat Input

The thermal input to the LH_2 through the tank support was evaluated with the computer code discussed in Section 8.8. The total heat input was found to be about 2.31 Btu/hr at the test liquid level, 113.4 in. from the tank bottom.

Absolute and differential thermocouples were positioned on the support as shown in Figure 10-9. Only T30 yielded a reading within a believable range, -385°F. However, this does not present a significant problem. Even if the support is totally neglected and all heat charged to the insulation, the error will be small (about 5 percent).

The analyses showed that the vent flow is sufficiently large that the heat conducted down the support tube is intercepted by the cold gas for the entire range of possible temperatures at the top of the support. Therefore, the heat input to the liquid is less than that coming through the insulation in the ullage area of the tank dome. It was possible to match T30, at the cooling coil, if the structure at the top of the support tube was assumed to be at about -100°F. Although this structure was not instrumented, this value appears

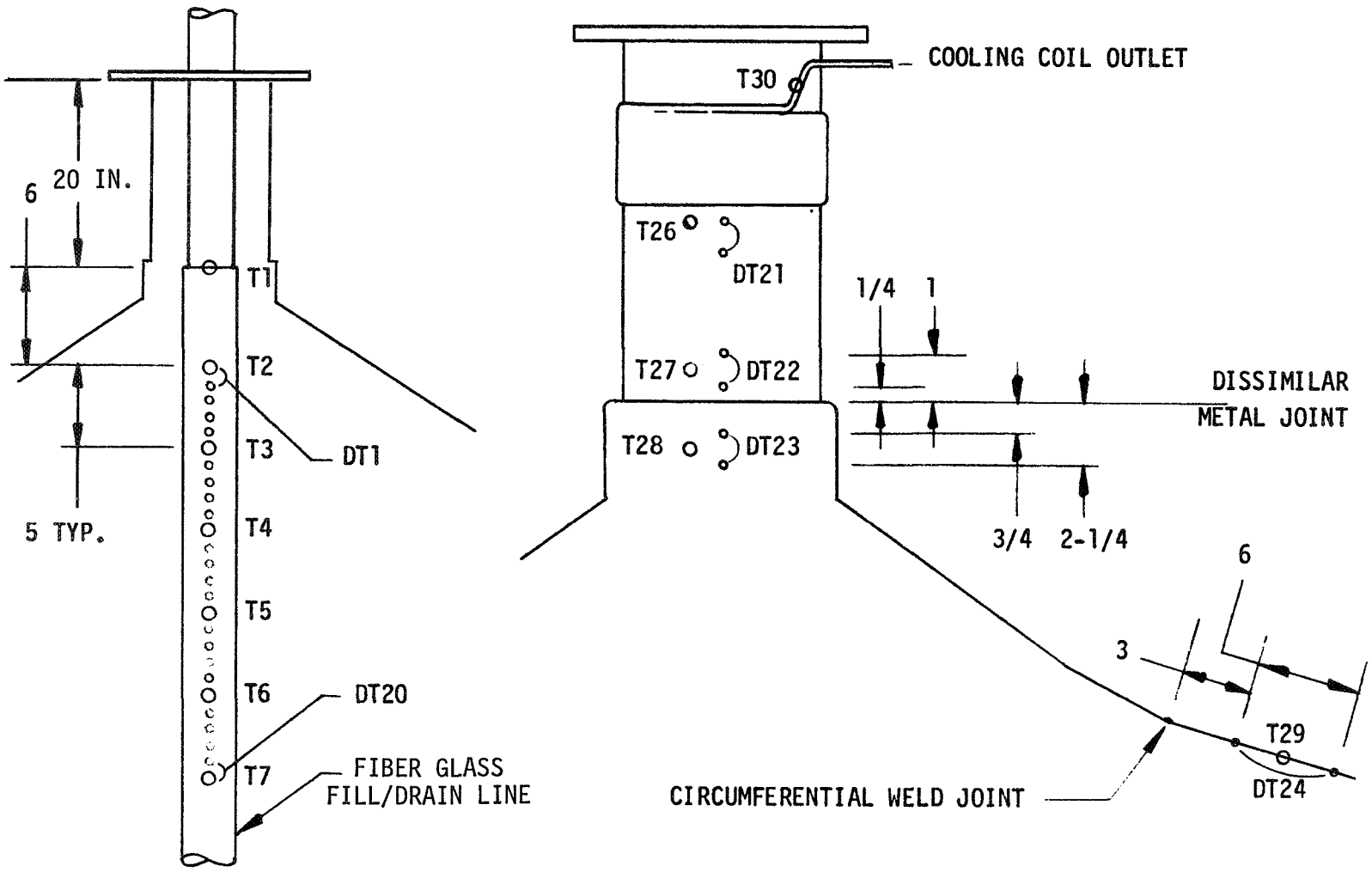

Figure 10-9. Thermocouple Locations

very reasonable. The tank proper is supported from a spider structure, connected about 10 ft away to the warm chamber wall.

Heat into the LH_2 at the tank wall-liquid interface was determined to be about 2.31 Btu/hr; less than the dome insulation heat input of about 3.73 Btu/hr (28.88 ft^2 x 0.129 Btu/ft^2). Therefore, the heat input chargeable to the insulation covering the wetted area (266.80 ft^2) is 37 - 2.31, which equals 34.69 Btu/hr or 0.13 Btu/ft^2hr. An upper limit charging all heat to wetted area insulation would be 0.138 Btu/ft^2hr (37/266.81).

10.2.8 MLI System Average Applied Conductivity

The value of 0.13 Btu/hr ft^2 corresponds to a conductivity of 1.53×10^{-5} Btu/hr-ft °R. It represents the characteristic average performance for an applied evacuated, 68-layer pair insulation system, including joints and fasteners. The corresponding conductivity-density parameter is 4.59×10^{-5} Btu/lb/ft^4/hr°R. This value is based upon the measured average insulation thickness of 0.69 in. and a density of 3 lb/ft^2. Weights of the 70 layers of 15-gage DAM and 68 layers of Dacron net B4A are 0.0012 and 0.0013 lb/ft^2 per sheet, respectively.

10.3 TEST 2 — MISSION SIMULATION

The insulation performance during all phases of a single flight vehicle mission from prelaunch LH_2 propellant loading to postlaunch evacuated equilibrium was measured during this test.

10.3.1 Test Procedure

The insulated tank was installed in the vacuum chamber without a purge bag as in Test 1. The chamber was pumped down to 1 psi and backfilled with helium, an operation repeated twice more before the tank was filled with LH_2. After two topping operations, tank ullage pressure was stabilized with the vent gas routed through a turbine flowmeter. This phase, ground hold, was followed by an additional topping and a rapid evacuation of the vacuum chamber, simulating a vehicle launch. At apparent MLI evacuated ($<10^{-5}$ torr) thermal equilibrium, the test was terminated. Table 10-5 lists the significant test events.

Table 10-5

MISSION SIMULATION TEST
SEQUENCE OF EVENTS

Time (Minutes)	Event
0 (10:44:00 AM 11/1/72)	Data system on
53	Initiate first fill
134	First topping
248	Second topping
265	Turbine meter on stream
525	Turbine meter off
552	Third topping
639.8	Open rapid-pumpdown valve
662	Boiloff flow through flowmeter
4,590	Terminate test

10.3.2 Results

The heat transfer characteristics of the helium-filled MLI layers during ground hold approximated that of the helium conductivity alone. Boiloff measurements yielded a corrected heating rate of 275 Btu/hr-wetted ft^2 (all boiloff charged to wetted area heating, see Section 10.4). Structural integrity of the MLI system design during launch decompression loading was demonstrated. Evacuated equilibrium was attained about 49 hours after the simulated launch. The MLI conductivity and heating rate at this time were found to be 2.33×10^{-5} Btu/hr-ft-°R and 0.195 Btu/hr-ft^2, respectively.

A detailed description of the data and results obtained for each test phase is presented in the following sections.

10.4 PRELAUNCH GROUND HOLD

This test phase was an evaluation of the net heat flux to the contained liquid and gas with the insulation system filled with helium gas at one atmosphere

pressure. The test period between 340 and 450 minutes was selected as the insulation thermal steady state. Figure 10-10 indicates that during this time, the tank ullage pressure was held within the band of 19.18 to 19.23 psi.

10.4.1 Test Environment

As expected, the temperature field on the vacuum chamber cold wall shroud surrounding the test tank was lower during the ground hold and subsequent evacuated test phases. The low thermal resistance with helium in the chamber resulted in a shroud temperature range of 10° to 25°F. Following evacuation at 640 minutes, the shroud reached a new equilibrium temperature of 54 to 60°F at 2,000 minutes.

The fill valve leakage was near zero throughout the test; no reading was indicated by the flowmeter across the valve.

10.4.2 Boiloff Mass Flow — Liquid Heating Rate

The test tank vent gas was routed through a turbine meter (F079) and a sonic nozzle for measurement. The output of the turbine meter, the primary measurement, was converted to scfm using a correction for both temperature and pressure:

$$\text{scfm} = \left(\frac{\text{F079}}{\text{OUTPUT}}\right) \times \frac{527.7}{14.696} \times \left(\frac{\text{ABSOLUTE PRESSURE FROM D515}}{\text{ABSOLUTE TEMP FROM D609}}\right)$$

This flowrate was then related to the net heat flux to the liquid using a standard density of 0.0052 lbm/ft^3 and a heat of vaporization of 190 Btu/lbm. Results are tabulated in Table 10-6. Note that the liquid boiloff rate decreases as the wetted area decreases.

The flowrate was also calculated from the sonic nozzle data for a few time points, checking the validity of the primary measurement. Computation based upon the instrument calibration curves supplied by MSFC yielded mass flows at 400, 425, and 450 minutes of 700, 670, and 630 scfm, respectively. The nozzle data for the period prior to 400 minutes was outside the range of calibration. It will be noted that the sonic nozzle flowrates are within 10 percent (lower) of those derived from the turbine flowmeter.

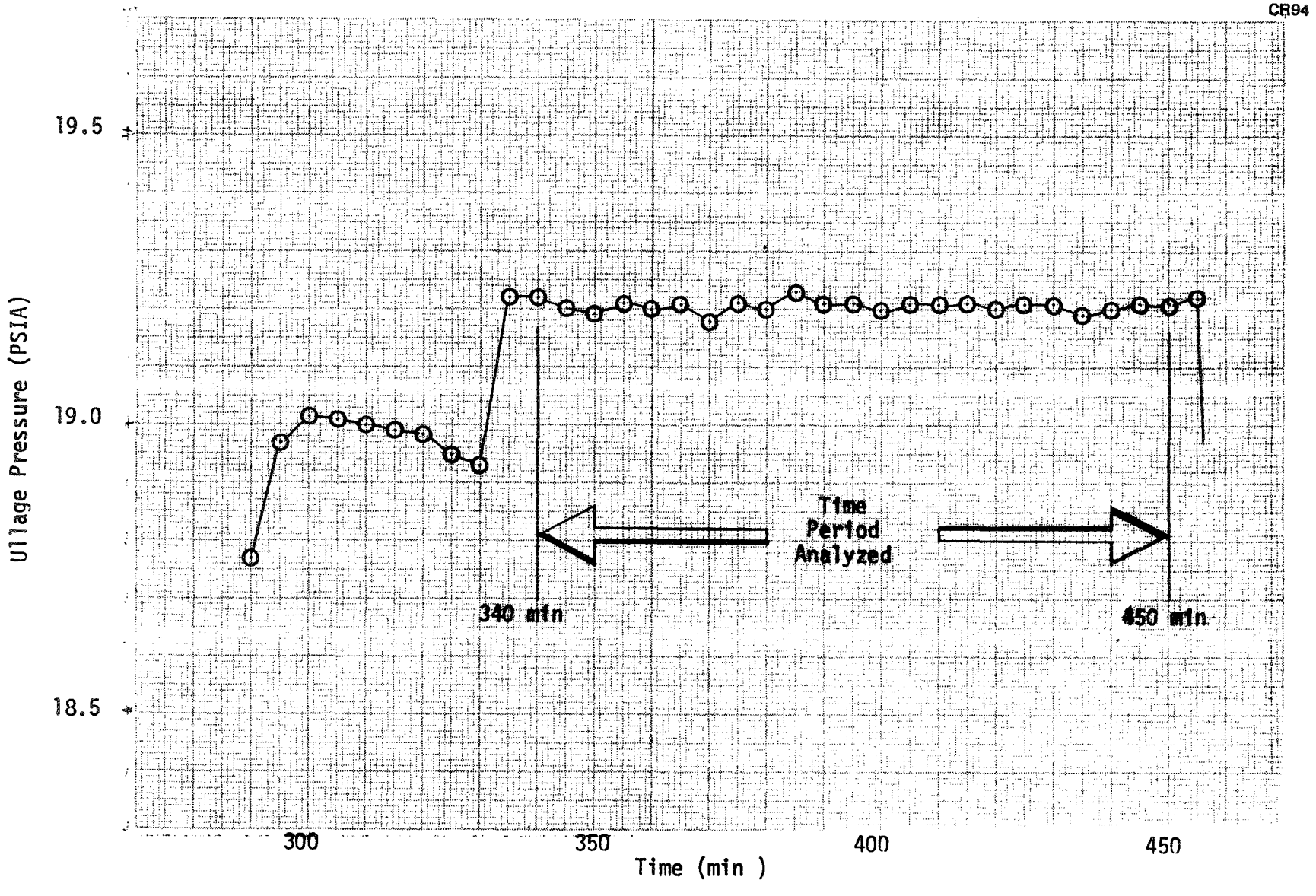

Figure 10-10. Tank Ullage Pressure During Ground Hold

Table 10-6

GROUND HOLD VENT FLOWRATE

Time (Minutes	Turbine Output (scfm)	Temperature (°F)	Pressure (psia)	Flowrate (scfm)	$\dot{Q}$ (Btu/hr)
340	435	-172.8	16.12	878	52,000
50	419	-171.9	16.07	840	49,800
60	389	-170.7	16.03	775	45,900
70	387	-168.8	16.06	767	45,500
80	396	-166.4	15.94	773	45,800
90	397	-164.8	15.91	769	45,600
400	389	-163.0	15.96	749	44,400
10	387	-161.1	15.87	739	43,800
20	395	-158.3	15.83	750	44,200
30	383	-155.9	15.78	714	42,400
40	374	-154.2	15.78	694	41,100
450	380	-151.7	15.72	696	41,300

10.4.3 Liquid Level and Wetted Surface Area

In order to calculate a net heat flux per unit area to the liquid, the wetted area must be known. The high ground hold heat load causes this area to change rapidly and must be accounted for in the calculations.

During the test, one of the two capacitance probes functioned. This unit, 35 in. in length, with its top 117.6 in. above the tank bottom, was completely or partially submerged four times while filling and refilling the tank. When exclusively in the ullage, its output was 2.4 in. and when covered with liquid, 13.9 in. A linear output was assumed, yielding the total liquid depth:

$$D = (117.6 - 35) + (3.05x - 7.3) \text{ in.}$$

where

x is the probe output and D is the liquid depth.

Although the above equation was used for the later evacuated-steady-state portion of the test sequence, it was necessary to estimate the liquid level for the prelaunch, ground hold, phase. The LH_2 top-off preceding this phase was terminated prematurely with the continuous sensor only partially covered. The level then dropped below this sensor at 317 minutes.

At the beginning of the period of interest (340 to 450 minutes), estimated depth was 79.1 in., based on an extrapolation of rate of recession shown by the level sensor prior to 317 minutes. Surface area and volume at this point are about 185.8 ft^2 and 315 ft^3, respectively. At the end of the period, the level was about 59.5 in. and wetted area was 141 ft^2 (428 lb LH_2 vaporized during the period).

10.4.4 MLI Thermal Performance

10.4.4.1 Measured Heating Rate

About 428 lb of hydrogen were vaporized during the steady-state period, 340 to 450 minutes. This was found to correspond to an insulation heat flux of 274 Btu/hr-ft^2 on the wetted tank wall. Computations are described in the following paragraphs.

The change in liquid volume in the tank can be expressed as:

$$\frac{dV}{dt} = -\frac{q}{\rho_L h_V} A$$

where

A = wetted area (ft^2)
V = liquid volume (ft^3)
ρ_L = liquid density (lbm/ft^3)

t = time (hr)

h_V = heat of vaporization (Btu/lbm)

q = insulation heat rate (Btu/hr-ft^2)

When the tank liquid level is low, in the cylindrical portion, the volume is linearly related to the wetted area:

$$V = aA + b$$

where

a = 2.14 ft

b = -82.4 ft^3

for the 105-in. tank.

The equation above can be integrated to yield

$$\frac{q}{a\rho_L h_V}\left(t_2 - t_1\right) = -\ln\left(\frac{V_2-b}{V_1-b}\right)$$

Substituting the test parameters (t_2, 450 minutes; t_1, 340 minutes; V_1, 315 ft^3; and V_2, 217 ft^3) yields a heat rate of 274 Btu/hr-ft^2.

10.4.4.2 Predicted Heating Rate

A theoretical analysis was accomplished to determine if the above heating rate was consistent with the observed MLI temperatures and heat transport due to the helium conductivity alone. A 3-D heat transfer computer code modeling the helium-filled MLI on the side of the tank was generated. The temperature-dependent properties of helium form a table within the program.

The experimental data indicated that the MLI thermocouples recorded constant temperatures (Figure 10-11) during the 340- to 450-minute steady-state period. For the boundary temperatures of -422° and -60°F, the resulting computed heat transfer through the sidewall helium layer, as a function of layer thickness, is shown in Figure 10-12.

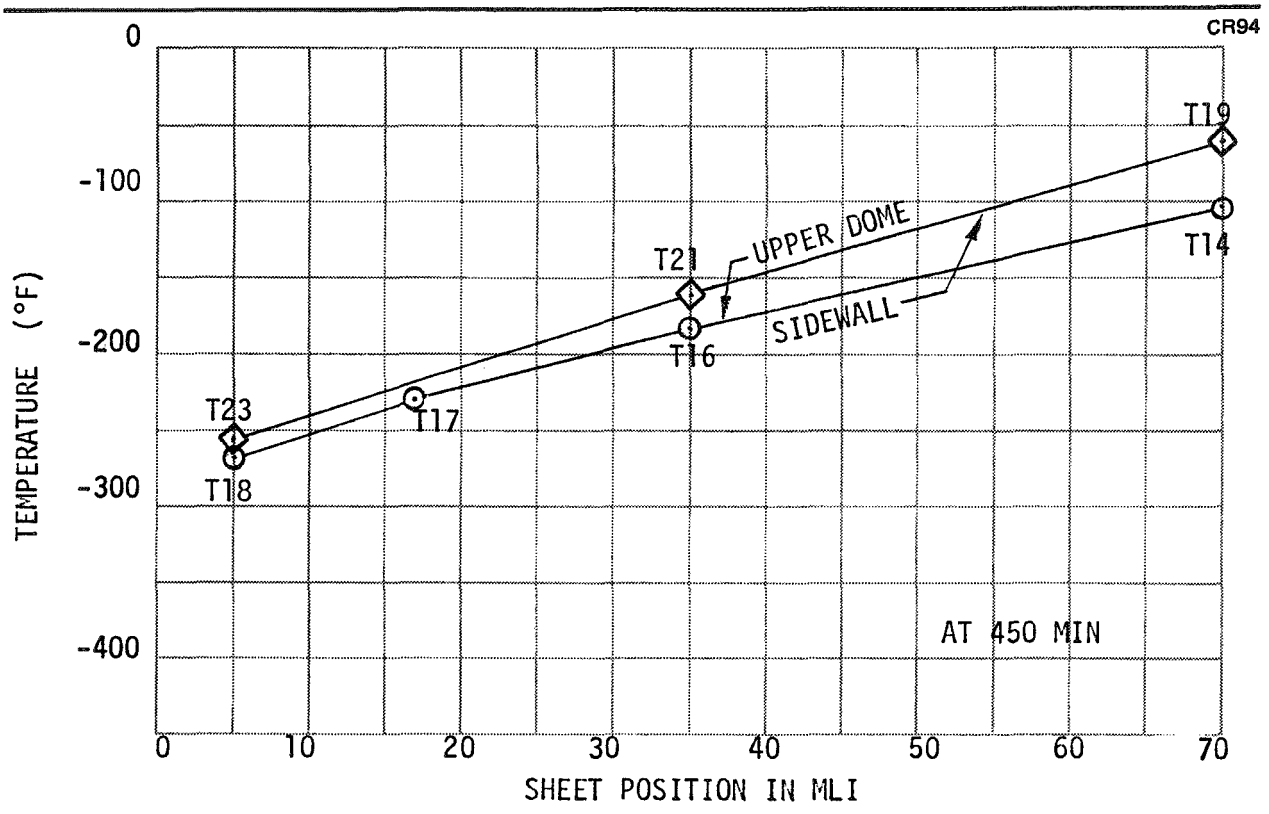

Figure 10-11. MLI Temperatures During Ground Hold

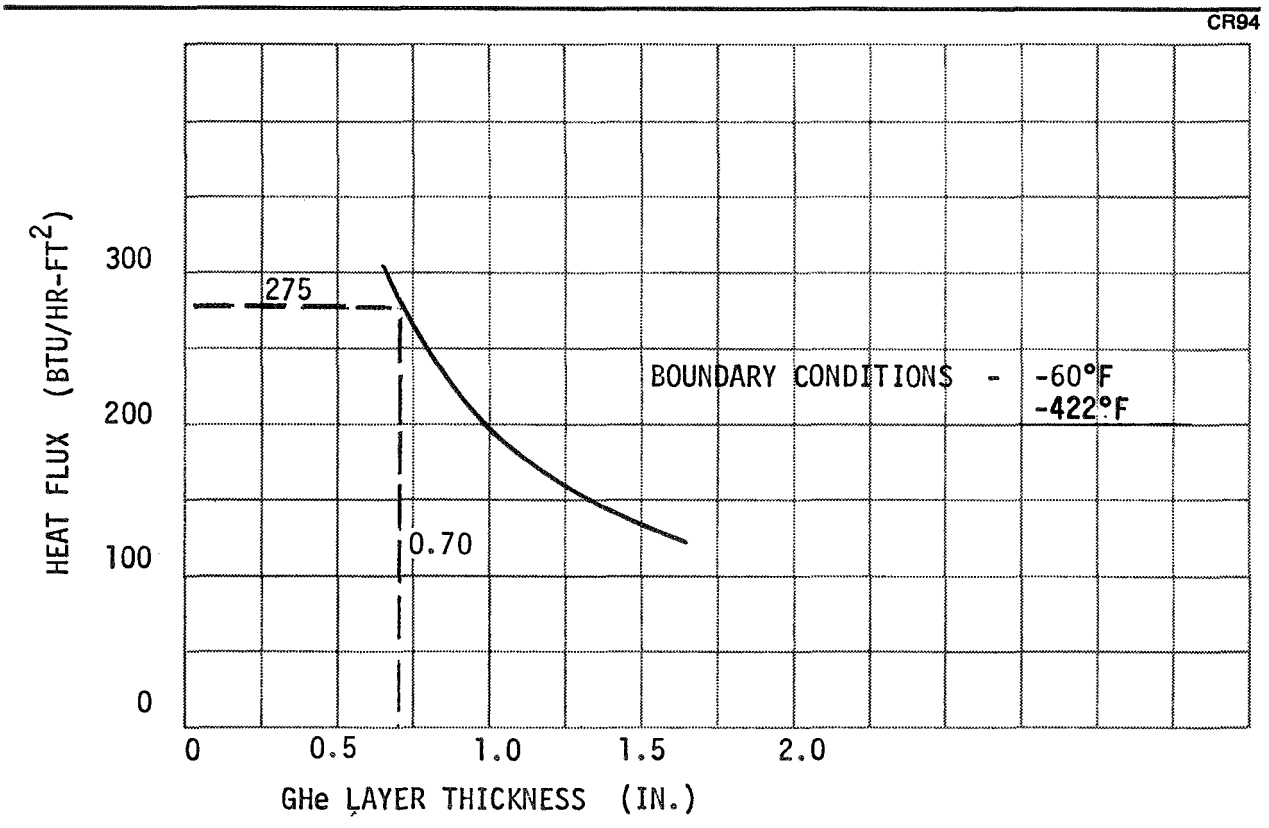

Figure 10-12. Computed Heat Transfer in GHe-Filled MLI - Sidewall

It can be seen that the measured heat flux correlates with a helium layer 0.7 in. thick. For comparison, the preinstallation insulation thickness was 0.69 in. However, a comparison of observed temperatures with the computed profile, Figure 10-13, yields a poorer correlation. Matching would require a higher heat flux with the insulation held away from the tank. Although the latter situation is probable (due to the tank's high circumferential weld beads) the higher heat flux is not. The upper limit on insulation heating results when all boiloff is attributed to wetted wall heating, as was done here. Also, both flowmeters indicated the same flow.

It was finally concluded that uneven spacing of the MLI layers may be the cause of the discrepancy. Future evaluation on smaller scale test panels is recommended. But, in the interim, for design purposes the use of helium conductivity alone for predicting prelaunch heat fluxes appears to be a valid approach.

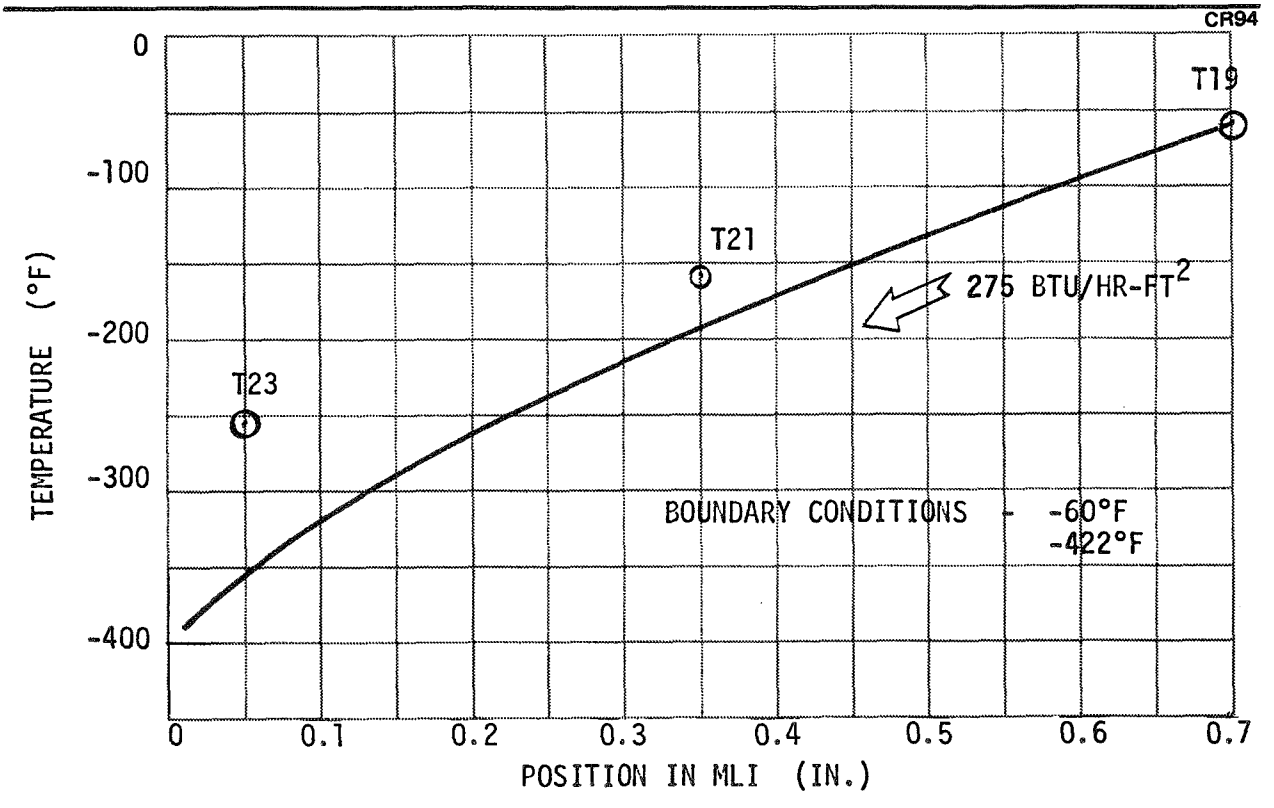

Figure 10-13. Computed Temperature Profile in GHe-Filled MLI

10. 4. 4. 3 Ullage Heating

Another portion of the heat passing through the insulation contributes to warming the gases that are generated by evaporating liquid before leaving the tank. This effect was assessed. However, computations must be viewed as questionable as no ullage temperature probes were present to measure the gas temperatures directly.

The best available measure of the ullage temperature is given by the seven thermocouples located on the fiber glass fill line running down the center of the tank (Figure 10-14). As T1 was positioned on the fill line within the support tube where the vent gas leaves the tank, it was assumed that T1 indicated the exiting gas temperature.

The net heat through the insulation on the dry portions of the tank wall was computed using the vent flowrate (turbine meter) and the increase in enthalpy as the gas moved through the ullage. Results are listed in Table 10-7. The enthalpy values used are those at 20 psia while the actual ullage pressure was 19. 2 psia. It is expected that in using the conditions at the higher pressure an error of less than 1 percent will be introduced.

The computation shows that as expected, the heat flux per unit area on the upper dome of the tank is different from that on the wetted portions due to the warmer tank wall. T29 on the surface of the upper dome had an output of -313°F at 450 minutes. Thermocouples T18, T17, T16, and T14 formed a temperature profile within the insulation near its top. The output of these probes rose at a uniform rate as the ullage temperature increased with a receding liquid level (Figure 10-14).

The computer code was again used to analyze the stagnant gaseous helium model for the insulation on the upper dome. An insulation thickness of 0. 69 in. was assumed. Figure 10-15 shows the results of the calculations with the tank wall temperature serving as the independent variable. The difference in enthalpy calculation, above, results in an average heat flux per unit area of 225 Btu/ft^2 on the dry portions of the tank wall. Figure 10-15 indicates that this heat flux would require a tank wall temperature of approximately -375°F. This is 62°F below that indicated by T29 (-313°F)

Table 10-7

HEATING RATE TO ULLAGE GAS

Time (Minutes)	T1 (°R)	$\dot{m}$ (lbm/hr)	Enthalpy at 20 psia (Btu/lbm)	$\dot{m}\Delta h$ (Btu/hr)
340	81	274	196	30,700
50	83	262	201	30,700
60	85	242	206	29,500
70	86	239	209	29,900
80	88	241	214	31,300
90	90	240	219	32,400
400	91	234	222	32,100
10	93	230	227	32,800
20	95	232	232	34,300
30	97	223	237	34,000
40	98	216	239	35,600
450	100	217	245	34,800

Enthalpy at 38°R = 84 Btu/lbm

or the temperature profile in the insulation. However, the insulation panels are compressed on the upper dome due to the weight of the sidewall insulation that they support. This can be expected to increase the heat flux in the dome area to a value greater than the average computed above. Although not computed, a higher dome heat flux should yield a better match with the observed temperatures.

10.5 LAUNCH SIMULATION

This test demonstrated the structural integrity of the MLI system under an imposed launch decompression loading environment. A steam ejector provided the capability of achieving the needed rapid evacuation of the helium within the chamber.

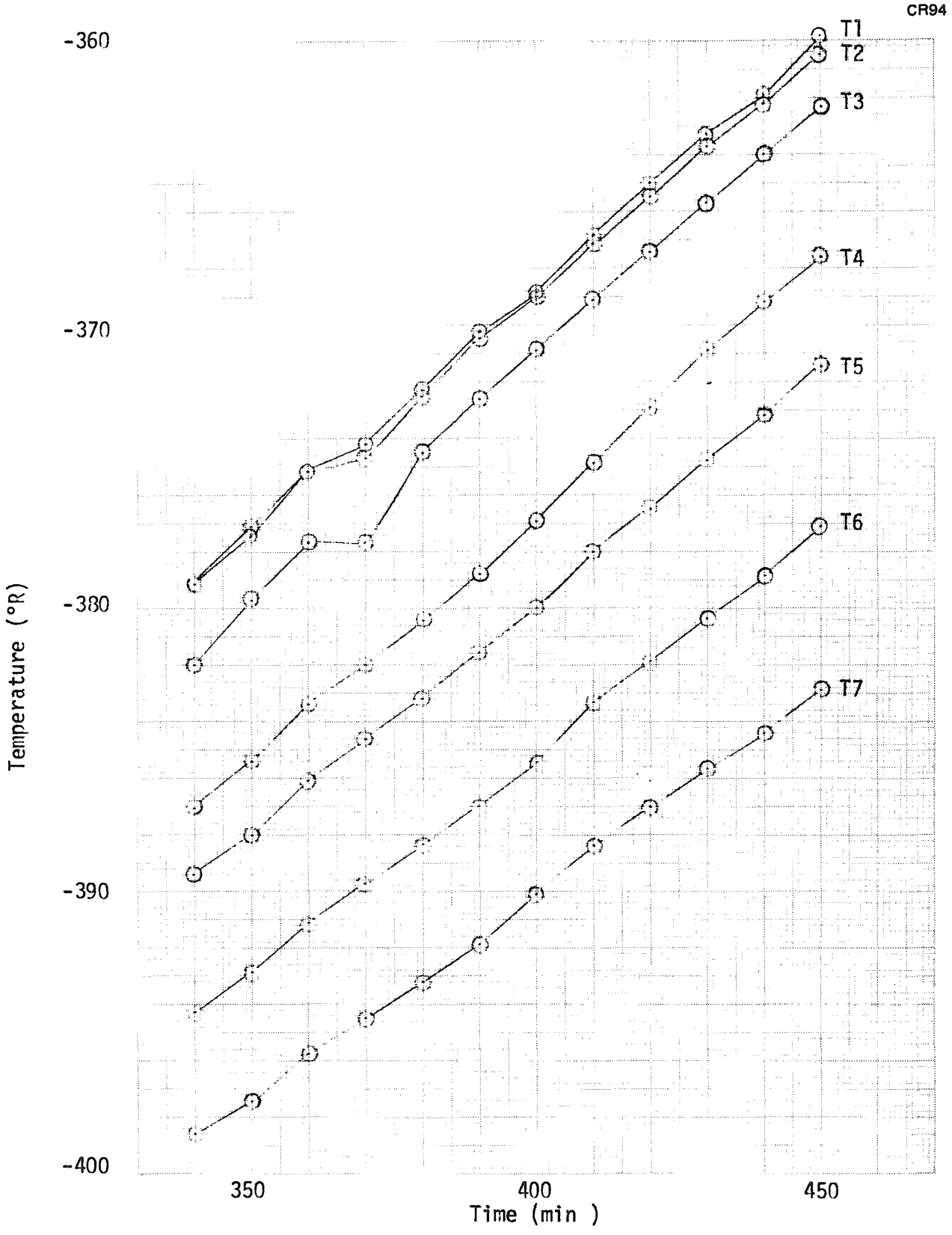

Figure 10-14. Fill Line Temperatures

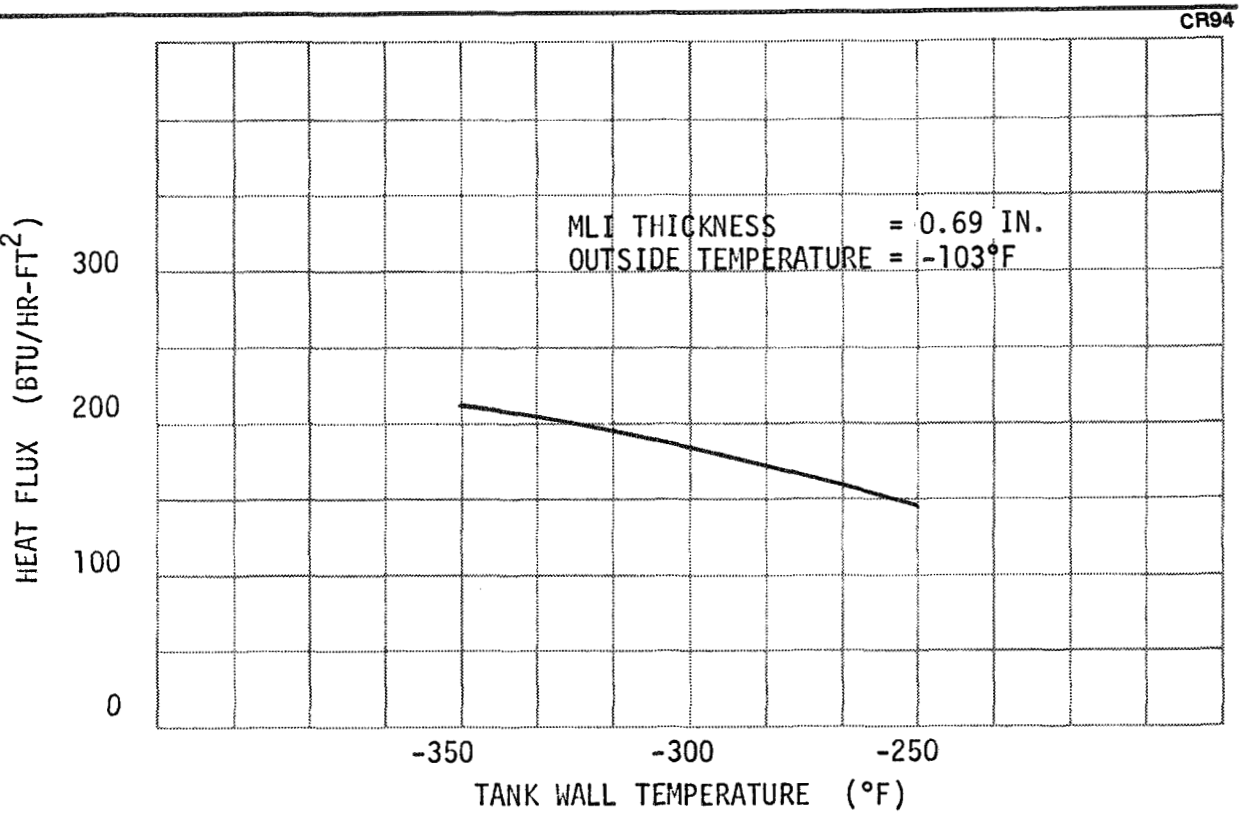

Figure 10-15. Computed Heat Transfer in GHe-Filled MLI - Top Dome

The rapid evacuation also provided a realistic postlaunch insulation configuration for the subsequent space equilibrium test. Evacuation loads might cause physical disarray of the MLI panels (open joints, etc.), inducing thermal degradation. Conversely, decompression has a tendency to fluff the insulation layers, suggesting a performance improvement.

Figure 10-16 shows the measured chamber pressure as it dropped quickly under the driving force of the steam ejector. A typical Saturn launch external pressure profile is superimposed. Note that a Saturn experiences a drop to 0. 1 torr in about 4 minutes while approximately 10 were required under test conditions. However, at higher pressures, the important areas for load simulation, the Saturn profile was exceeded.

After decompression, the insulation was viewed through a window in the vacuum chamber which included a vertical gore panel joint in its field of view. There were no observable changes in the insulation panels. Also, no significant changes in joints or the panels were found upon inspecting the tank after its removal from the chamber.

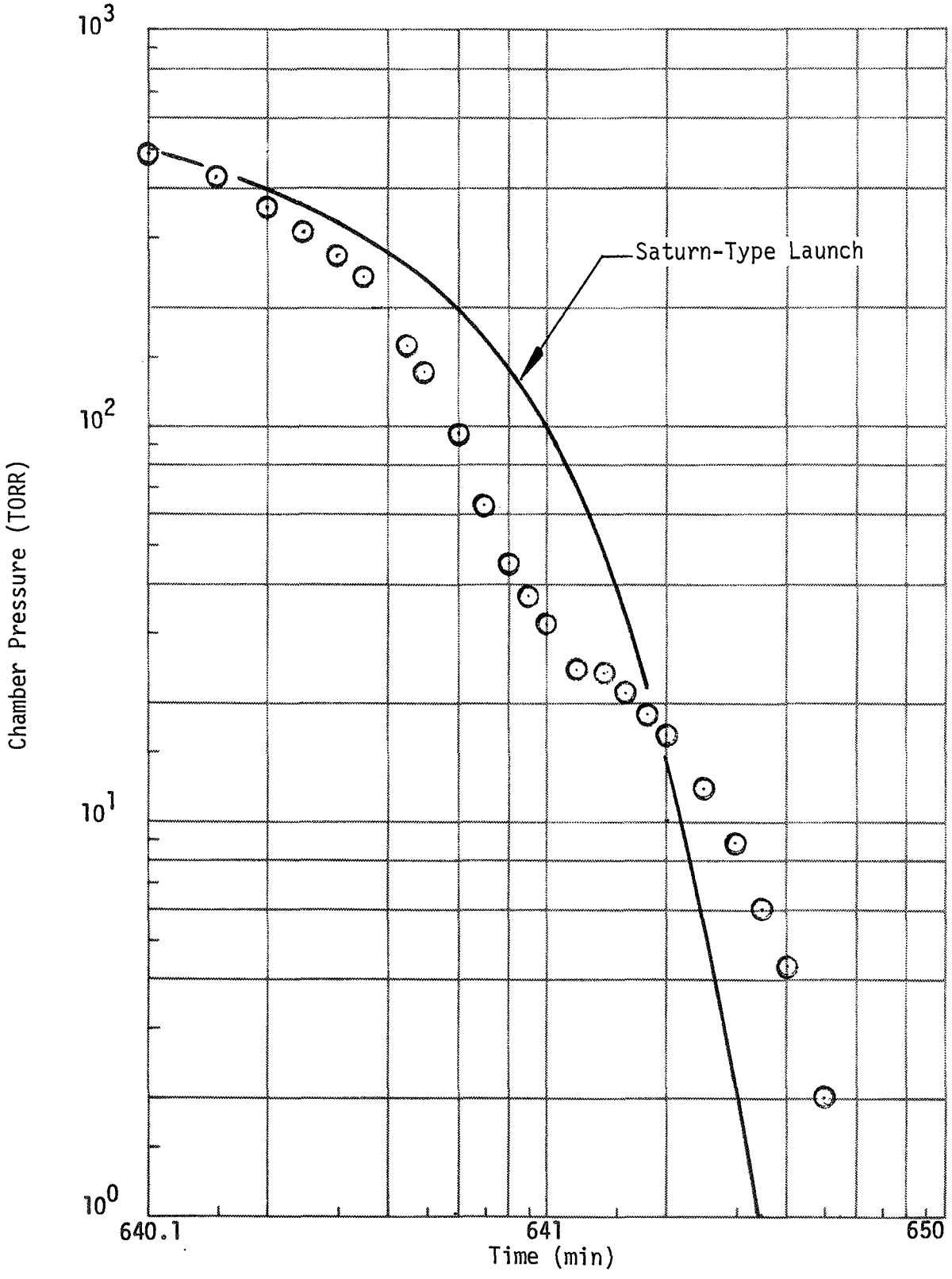

Figure 10-16. Chamber Pressure During Rapid Pumpdown

10.6 POSTLAUNCH THERMAL PERFORMANCE

This test yielded the thermal performance of the insulation system (time to equilibrium and evacuated heat transfer) after exposure to a typical vehicle launch environment. The as-applied heat transfer and conductivity were 0.195 Btu/hr-ft^2 and 2.33 x 10^{-5} Btu/hr-ft-°R, respectively. Temperatures within the insulation showed that equilibrium was reached after a period of about 49 hours.

The measured heat rate through the insulation system in this test, 50 Btu/hr, was found to be higher than in Test 1, 37 Btu/hr. The difference is believed to be at least partially due to the pressure of gas within the layers caused by degassing of absorbed water vapor. Mass spectrometer measurements made on MDAC IRAD tests appear to confirm this conclusion. A hot helium purge preconditioning process (before tank loading) may be required to quickly achieve the full performance capability of the MLI after launch. More experimentation in this area is recommended.

Application of these test results to space vehicle design should yield a conservative estimate of performance. The insulation, in an actual launch, would be subjected to acoustic loads, a factor not included here. Such loads are known to significantly fluff the insulation sheets, thereby improving thermal performance.

From the design standpoint, the MLI performance measured here should be considered as characteristic of a system which could be built and flown now without additional development. With development in the area of purge systems and improvements in joint design, a value less than that measured in Test 1 should be realistically attainable.

10.6.1 Test Environment

The postlaunch or evacuated portion of the mission simulation test followed the rapid chamber blowdown at 640 minutes and continued to test termination at 4,590 minutes (elapsed time: 66 hours). Fill valve leakage was near zero. The chamber cold wall temperatures gradually stabilized within the 54° to 60°F temperature band. Chamber pressure also met the steady-state acceptance criterion of less than 10^{-4} torr. Ullage pressure was controlled within a band of 0.02 psig throughout the test period.

10.6.2 Steady-State Insulation Temperatures

The response of the thermocouples within the MLI (Figure 10-17) indicated that steady-state conditions were achieved in the period after 3,600 minutes. Figure 10-18 shows the steady-state temperature profiles at both sidewall and dome locations.

Note that the steady-state temperature profiles exhibit the same characteristics observed in Test 1, a flatter curve with lower temperatures than the sidewall on corresponding MLI layers. As in Test 1, it was concluded that this is due to a higher layer density in the dome area and the influence of the more closely spaced dome joints. Also, dome area joints have a much smaller overlap (2-in. minimum) between the inner and outer MLI panels than the sidewall where about a 1-ft overlap occurs.

10.6.3 Ullage Pressure

Control of the ullage pressure was markedly improved during this test over that attained during Test 1. The total variation after chamber evacuation was within a band of 0.02 psi. For long periods on the order of 17 to 20 hr, the maximum deviations were 0.0085 to 0.005 psig. Also, there appeared to be no relationship between the ullage pressure and ambient temperature as was the case in Test 1.

The ullage pressure as measured by the primary sensor (Texas Instrument transducer, 14/20 psig, MSFC D679) is plotted in Figure 10-19. Ambient temperature is also shown for reference.

The test tank ullage pressure change of 0.085 to 0.005 psig introduces negligible error as long as average heat fluxes over a long period of time are sought. For example, the pressure change (ΔP) in the period 2,000 to 3,000 minutes (16.7 hr) is only 0.085 psi, or about 16 Btu, an error in calculated heat flux of less than 1 Btu/hr. In the period 3,600 to 4,450 minutes (steady-state region), maximum ΔP is 0.005 psi or an error of about 0.67 Btu/hr.

Insulation performance computations from boiloff measurements in the post-3,600-minute period should be conservatively high. Pressure was slowly decreasing throughout most of this time frame.

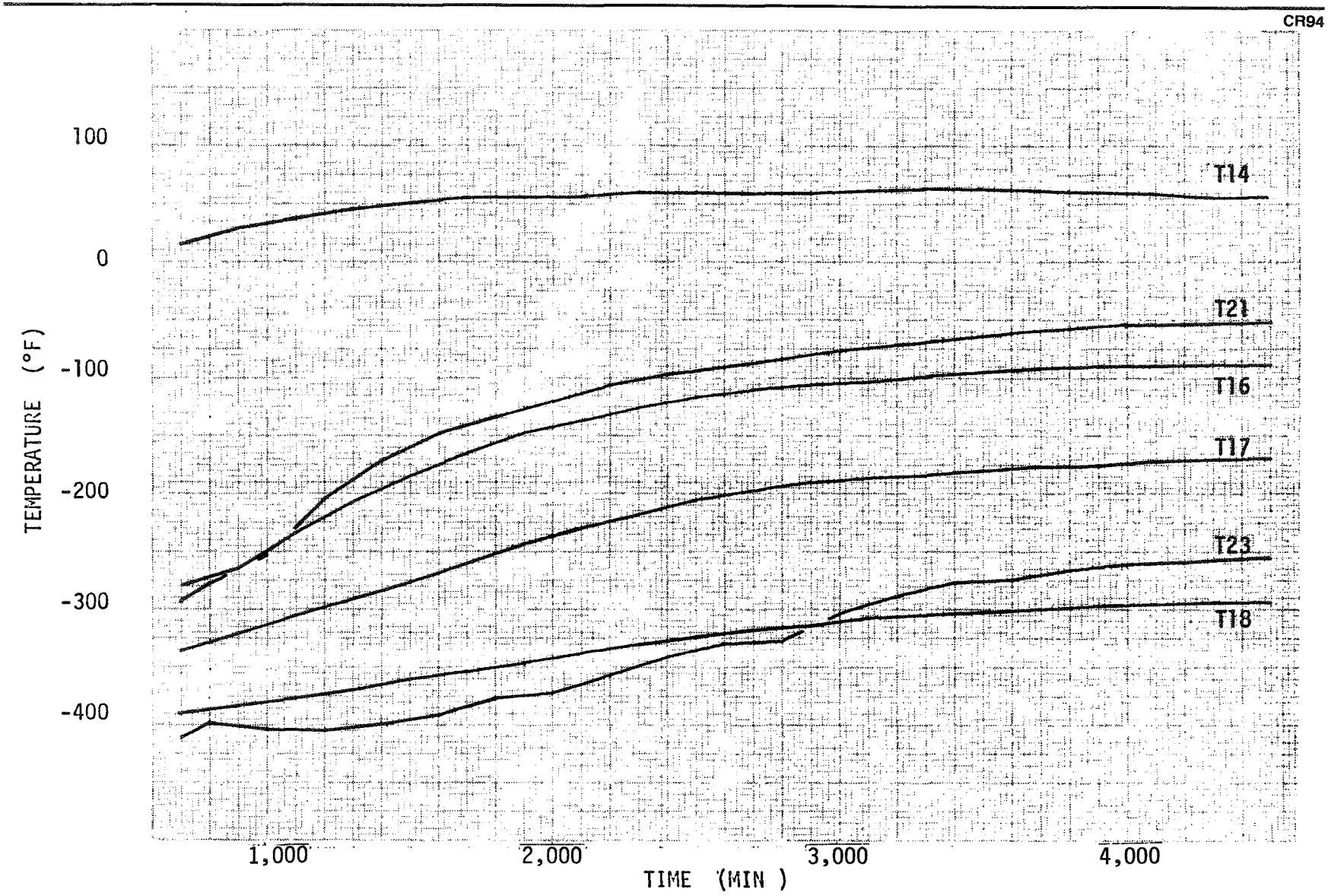

Figure 10-17. MLI Temperature Profiles

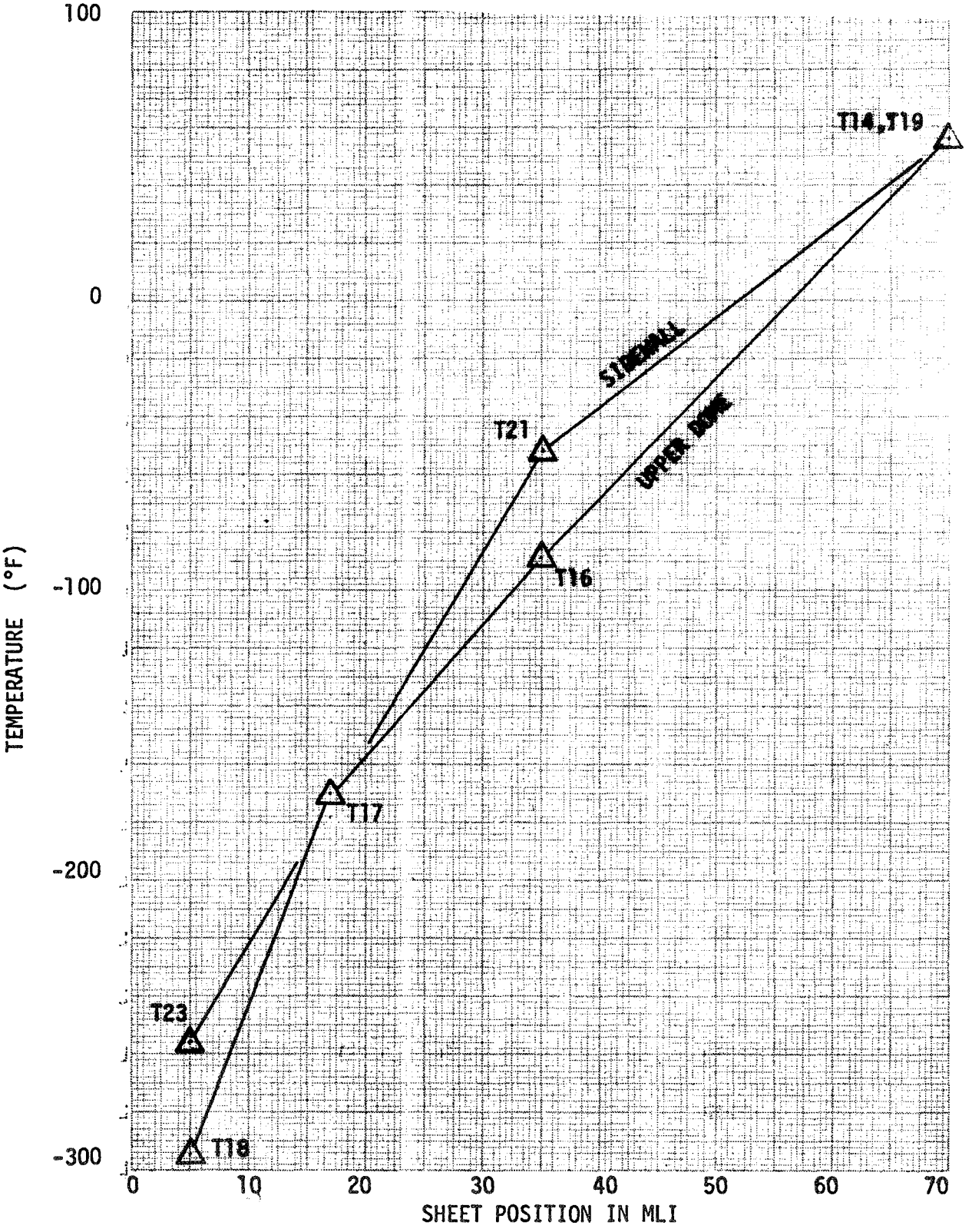

Figure 10-18. Steady-State MLI Temperature Profiles

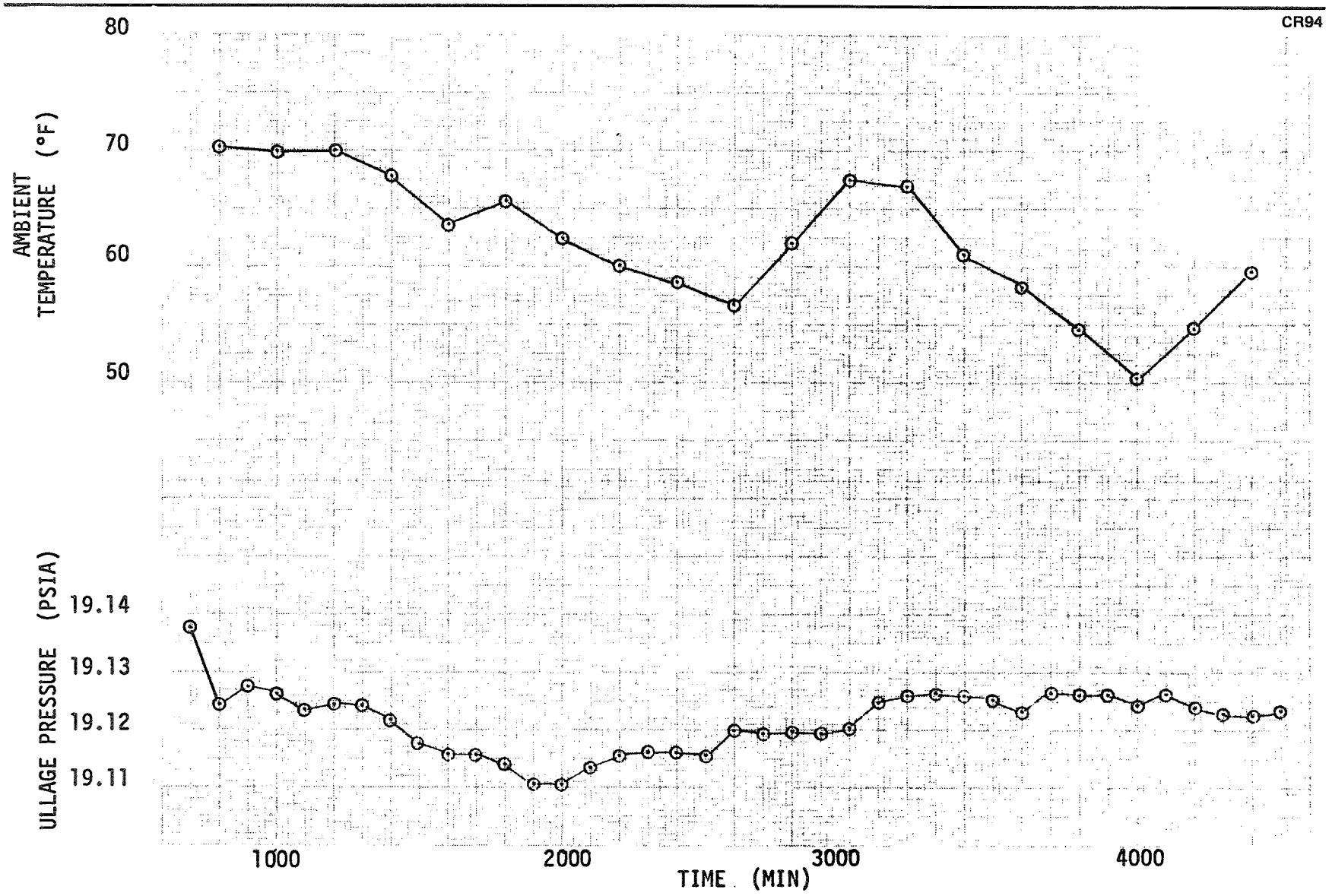

Figure 10-19. Tank Ullage Pressure and Ambient Temperature

10.6.4 Total Tank Heating Rate

The post-rapid-evacuation boiloff mass is plotted in Figure 10-20. Although the data are erratic, the expected general shape can be seen; a sharp reduction in heating rate to a low point, followed by a slow rise to an evacuated steady-state value. As evacuation occurred at 640 minutes, the low point was reached in about 10 to 13 hours.

The measured flowrate was augmented or diminished in value by the changes in liquid heat storage capacity induced by variations in tank ullage pressure. An attempt was made to correct the flowmeter data for these bulk heat capacity changes in the hope that the boiloff curve would be smoothed out. However, the result was not successful; the data scatter masked any evidence of the dip in net heat flux or a smooth steady-state value.

An integrated average technique was then used to obtain a steady-state heating rate since the pressure changes averaged over a long period of time introduced negligible error. The total measured boiloff mass for the steady-state period (3,594 to 4,403 minutes) was computed using quarter-hour increments then averaged over the entire period. A correction was applied to account for a zero shift. The result was a 50 Btu/hr total heating rate. A check was made using the backup flowmeter data and the same computational technique. This data yielded a 47 Btu/hr heating rate.

The amount of heat represented by the dip below the steady-state value, 158 Btu, was also computed by the same technique. This suggests a useful result for design in the absence of a verified computer program defining heat rate after launch. The heating rate may be approximated by a straight-line decline from the ground hold value to an evacuated value 5.5 hr (336 minutes) after launch.

10.6.5 Liquid Level and Wetted Surface Area

The continuous level sensor indicated a gradual and uniform lowering of the liquid level from 88 to 87.4 in. in the period 1,000 to 4,000 minutes during the evacuated test. The corresponding change in volume is 2.86 ft^3 and, in surface area, from 206.4 to 204.8 sq ft.

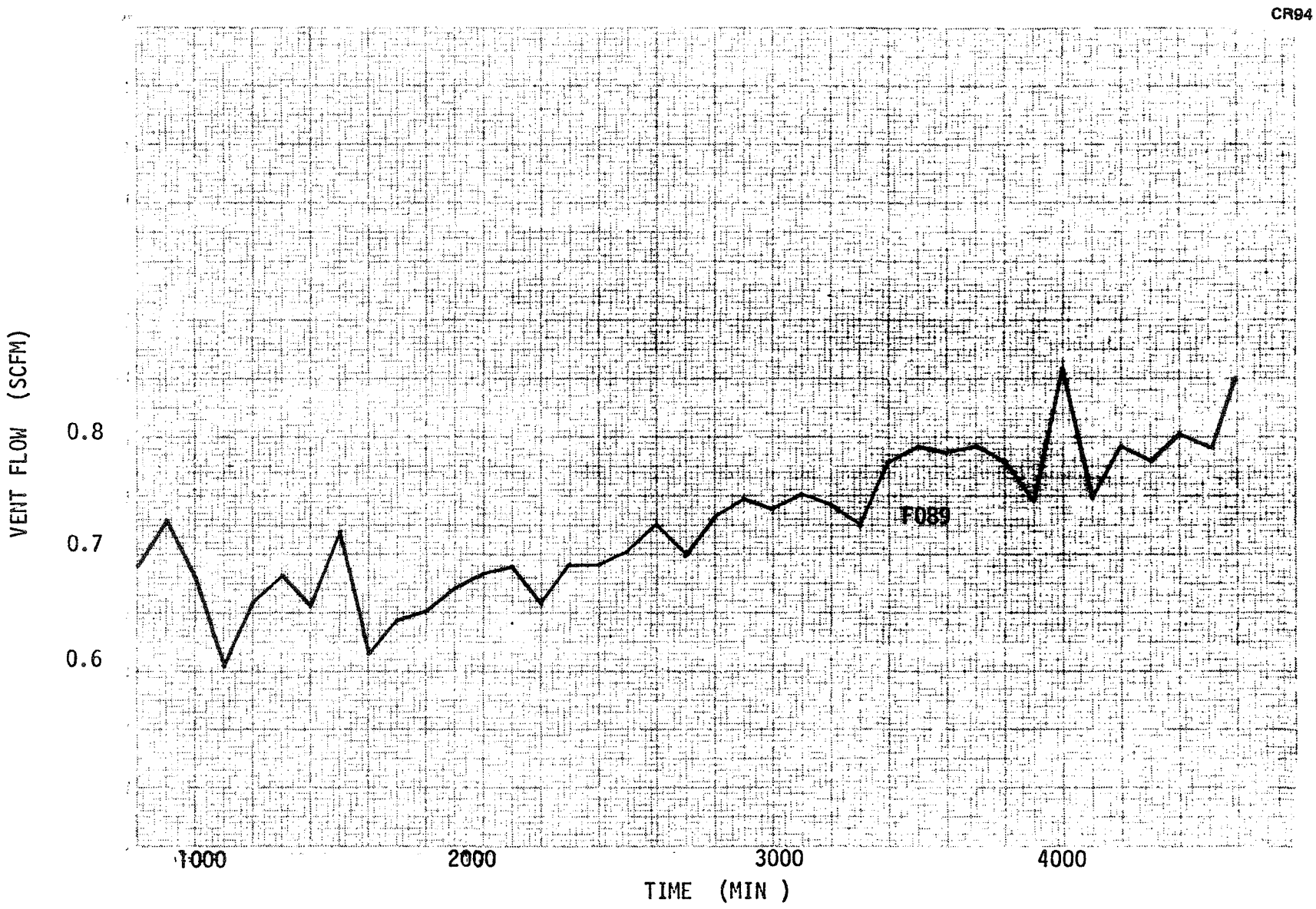

Figure 10-20. Primary Vent Flow Measurement

Note that the above liquid loss corresponds to a heat input of 47.6 Btu/hr (saturated liquid at 19.1 psig). This is an excellent correlation with the 50 and 47 Btu/hr rates computed from the boiloff flowmeter data.

10.6.6 Insulation Evacuated Steady State Performance

The tank support heat input was subtracted from the total tank heating rate to yield wetted area MLI thermal performance. The fill line heat short contribution was shown to be negligible in Test 1 and was therefore neglected. There was no fill valve leakage.

Heat flow into the liquid through the tank wall at the liquid-ullage interface was approximately 10 Btu/hr, or about 60.5 percent of the MLI heat transfer in the dry wall ullage area. This ratio of heat through the wall to heat drawn away by the vent gas was obtained from the results of Test 1 and parametric analyses of the tank support area. The computer code used in Test 1 to calculate support heating could not be applied here. The test liquid level was far below the range of applicability of the model.

The resulting MLI heating rate was 0.195 Btu/hr-ft^2 for the 50 Btu/hr total tank heating rate and wetted and dry surface areas of 204.95 and 84.8 ft^2, respectively. The latter figures correspond to areas at a liquid level of 87.4 in.

Any errors introduced by the support tube heating computation method are well within the uncertainties in the basic test data. If the support was neglected and all heat averaged over the entire tank, the MLI heat rate is 0.173 Btu/hr-ft^2. This, though, is low, as heat drawn out by vent gas is not included in MLI heat transfer. An upper limit of 0.244 Btu/hr-ft^2 results if the total heat is averaged over the wetted area alone. In this test, such a figure greatly underrates the MLI performance, as about 30 percent of the tank area was dry due to the low liquid level at the start of the test. The average (without support) is 0.209 ± 0.035 Btu/hr-ft or an error band of ±16 percent. Note that the derived MLI heat rate, 0.195 Btu/hr-ft^2, is on

the low side of this average as would be expected. Future testing should be accomplished at a liquid level which minimizes dry wall area and the change in dry wall area throughout the test.

The heat flux rate through the MLI in Test 2 was 50 percent higher than in Test 1. Some possible reasons for this increase are: (1) interstitial gas pressure higher than 10^{-4} Torr; and (2) increased heat leaks through joints due to rapid-evacuation-induced joint opening.

Conclusion 1, above, appears justified by the traces of thermocouples T14 through T23 in Tests 1 and 2 (Figures 10-3 and 10-17). In Test 2, Figure 10-17 shows the temperature gradient to be much less steep. This is a definite indication of entrapped gas and high interstitial gas pressures. This conclusion is further justified by the fact that in Test 1 the tank was warm and pre-evacuated prior to LH_2 loading, and optimum evacuation conditions existed. Therefore, a lower interstitial gas pressure would be expected in Test 1 than in Test 2.

Conclusion 2 is more difficult to substantiate. It is possible that joint performance degradation, caused by the rapid-evacuation structural loading, contributed to the increased heat transfer observed in Test 2. However, the joints were examined visually after Test 2, and no indication of damage or pull apart could be determined.

A better removal of interstitial gases should yield a significant gain in thermal performance from the values measured in Test 2. Therefore, the potential benefits to be gained by hot purging, prior to tank loading, should be investigated in future studies.

10.6.7 MLI System Applied Conductivity – Density

The MLI system conductivity was 2.33×10^{-5} Btu/hr-ft-°R, corresponding to a heat rate of 0.195 Btu/hr-ft^2, 57°F outside layer temperature, and 0.69-in. insulation thickness. Conductivity-density is 6.99×10^{-5} Btu lb/hr-ft^4-°R (ρ = 3.0 lb/ft^3).

Section 11
STUDY CONCLUSIONS

Many conclusions, both general and detailed, resulted from the work conducted under this contract. These have been discussed in the previous sections of this report together with the pertinent technical details. To provide a convenient reference, some of these conclusions have been extracted from the body of the report and are summarized below.

11.1 GENERAL

A practical, flightworthy, MLI system can be built for single-flight space vehicle application. The 15-gage DAM-B4A Dacron net composite and the MLI system application design defined in the study have been shown to satisfy the requirements for such an application.

Although the system may be applied directly to tanks containing cryogens at temperatures as low as about -300°F, further structural testing (dynamic) is needed for LH_2 applications. Also, the scope of the study precluded thermal optimization of the design. Significant performance improvements can be achieved with additional effort in the following areas: joint and penetration design, reflector perforation optimization, face sheet weight reduction, and purge preconditioning. Purge system design verification testing is also needed.

11.2 ITEMS PERTINENT TO FUTURE MLI DESIGN AND DEVELOPMENT

Additional information and substantiating data for the conclusions listed in the following subsections may be found in the report sections referenced in parentheses after the subsection heads.

11.2.1 Design Concept (Sections 2 and 4)

The modular design concept, assembling the MLI reflector-separator stack into a load-carrying package, offers two significant advantages: ease of

design for application to various vehicle geometries, and relative ease of fabrication and installation. The required MLI thickness on the tank should be applied in two panels, one on top of the other, with the outer offset from the inner to eliminate through joints. However, future test data on attachment, fastener, and stepped joint heat transfer may show that only one panel is necessary. Simple geometric shapes for panels should be used.

The MLI panels should be mounted on a substrate support when insulating piping penetrations. A fiberglas tube that goes over valves, expansion joints, etc. and presents a uniform surface for the insulation appears attractive. In the insulated area, straight pipe runs are most desirable. If this is not possible, the MLI design must allow for pipe movement resulting from tank chilling.

Panel joints must be positively closed on both inner and outer faces with the closure being essentially continuous on at least the outer face.

11.2.2 Manufacturing Methods (Section 3)

MLI composite stacks do not possess a minimum practical layup density. Any two stacks consisting of the same number of layers will exhibit a different thickness. But, average finished panel density can be predicted from stack compression tests.

MLI panel thickness measurements, needed to ensure that a finished panel possesses an acceptable density, are best accomplished with an electrical probe. The device designed and used during the study can be directly adapted to production inspection.

A hollow drill is the preferable method for forming holes in the MLI stack for assembly fastener insertions. Fastener spacing has an insignificant effect on finished panel density.

Panel assembly dimensional tolerance controls were built into the panel layup tooling. This approach should also be followed for future tooling designs.

Some panel assembly operations are adaptable to automation. In particular, automating the initial stacking of reflectors-separators from the "as received" rolls appears to offer significant cost reductions.

11.2.3 Composite Materials (Section 5)

The electrical resistance test technique defined in the study offers promise of fulfilling the need for an inexpensive and rapid method for screening new candidate MLI materials.

Fifteen-gage (0.15-mil) double-aluminized Mylar should be used for reflector materials.

There appears to be a requirement for hot purge preconditioning of the MLI before tank propellant loading can affect the choice of MLI composite materials. Single-aluminized Mylar curls at a relatively low temperature, 150°F.

Insufficient test data (evacuation and thermal performance characteristics) are available to select an optimum reflector perforation configuration.

The 15-gage DAM-B4A Dacron net composite is thermally superior to Superfloc, the next best material evaluated.

11.2.4 MLI System Component Thermal Performance (Section 6)

There is a significant lack of data on the heat transfer through typical full-size heat shorts (joints, fasteners, penetrations, etc.).

Composite heat transfer data (conductivity) obtained at LN_2 boundary temperatures yield a conservative design when applied to LH_2 tanks.

There appears to be no thermal performance degradation of MLI panels that have been stored in a GN_2 environment.

Density control of test samples on a cylindrical calorimeter is achievable with the method defined in the study.

In current MLI system design, heat shorts account for about 50 percent of the total system heat transfer.

11.2.5 Structural Considerations (Section 7)

The MLI panel design formulated in the study is structurally adequate (Saturn launch environment) for applications with temperatures as low as 300°F. Additional dynamic tests are needed for design verification at LH_2 temperature.

Mylar sheet, 0.25 mil thick (25 gage) is adequate to resist decompression-induced fastener tearout if the load (1 sq. foot panel area) is distributed over a 0.5-in.-diameter washer-type fastener head.

The panel fastener configuration, fasteners 12 in. on center, is adequate but not necessarily optimum.

It is appropriate to design Mylar MLI systems to just fit the tank while warm. The tank will shrink faster than the Mylar during chilldown.

11.2.6 Large-Tank Test Article Design (Section 8)

The design goal of the basic 105-in.-tank calorimeter used in the program was achieved: essentially complete isolation of the test MLI system from heat shorts to the external environment.

The externally closed fill line on the test tank must be connected to the ullage during test to ensure that the gas pressure in the line is equal to the ullage pressure. Otherwise, an oscillating liquid column that activates a heat pump will occur in the fill line.

To minimize the uncertainty band in test data, the ratio of dry-to-wetted wall area change during test should be minimized.

It is desirable to install heat flux gages (thermopiles) at various locations on the test tank or insulation. These units would provide: backup to the primary boiloff measurement, smooth heat flux data during simulated launch, and measurement of variations in heat flux over the tank surface.

Vent gas temperature measurements, not included on the study test article, should be provided for in future tests.

11.2.7 Large Tank Test Results (Section 10)

A higher heat flux can be expected if the tank is loaded under simulated vehicle prelaunch conditions (helium in MLI) than if the MLI has been evacuated before loading. Therefore, this situation must be considered when applying post-evacuated test data to vehicle design. A non-conservative design could result.

A design uncertainty factor of 2.0 for heat shorts, such as used in this study, is over conservative: 1.25 appears more appropriate.

Ground hold heat transfer can be expected to be essentially equal to heat transfer computed on the wetted tank area using only the conductivity of the interstitial GHe purge gas.

The high prelaunch heat transfer can be expected to drop to a value equal to the evacuated space performance in the period of about 100 minutes after launch (68 layers MLI).

Heat transfer in the MLI will be transient until about 50 hours after launch. Minimum heat flux to the tank (less than evacuated equilibrium) occurs at about 14.5 hours after launch (68 layers MLI).

Section 12

REFERENCES

1. Investigation of High Performance Insulation Application Problems. First Quarterly Report, Contract NAS8-21400, McDonnell Douglas Astronautics Company – West, Report No. DAC-63250, April 1969.

2. Investigation of High Performance Insulation Application Problems. Contract NAS8-21400, 2nd Quarterly Report, McDonnell Douglas Astronautics Company – West, Report No. MDC-G1152, July 1969.

3. Investigation of High Performance Insulation Application Problems. Contract NAS8-21400, 3rd Quarterly Report, McDonnell Douglas Astronautics Company – West, Report MDC-G1238, October 1969.

4. Investigation of High Performance Insulation Application Problems. 4th Quarterly Report, Contract NAS8-21400, McDonnell Douglas Astronautics Company – West, Report No. MDC-G0275, January 1970.

5. Ranking and Selection of Insulation Systems for MNV Application. Special Report No. 1, Contract NAS8-21400, McDonnell Douglas Astronautics Company – West, Report No. DAC-63264, July 1969.

6. Investigation of High Performance Insulation Application Problems. Interim Progress Report, Contract NAS8-21400, McDonnell Douglas Astronautics Company – West, Report No. MDC-G2135, February 1971.

7. Program For Testing A Multi-Layer Insulation System On A 105-Inch NASA Calorimeter. Special Report, Contract NAS8-21400, McDonnell Douglas Astronautics Company – West, Report No. MDC-G2969, May 1972.

8. Thermal Testing of Typical Vehicle Multilayer Insulation Panel Components, McDonnell Douglas Astronautics Company – West, Independent Research and Development Report MDC-G2153, March 1971.

9. Design of Purge Systems for Cryogenic Tank Multilayer Insulations, McDonnell Douglas Astronautics Company – West, Independent Research and Development Report MDC-G2154, March 1971.

10. Investigations Regarding Development of a High-Performance Insulation System, Contract NAS8-20758, Final Report, Lockheed Missiles and Space Company Report K-17-68-5, July 1968.

11. Singleton, Robert C., Arc Welded Fasteners, Nelson Stud Welding Company Paper, United-Carr Division of TRW Inc., Lorain, Ohio.

12. Crawford, R.F., and Hannah, R.G., Cyrogenic Insulation Research. Final Report, Contract NAS 8-11397, The Martin Co., CR-61162, January 23, 1967.

13. Arthur D. Little, Inc. Basic Investigation of Multi-Layer Insulation Systems. Contract NAS 3-4181 (ADL 65958-00-01), February 29, 1964.

14. Study of Thermal Conductivity Requirements, Contract NAS 8-21347, Lockheed Missiles and Space Company Report LMSC/HREC D148611-I, January 1969.

15. Cryogenic Insulation Development, Third Quarter Progress Report. Contract NAS8-18021, General Dynamics, Convair Division, 21 October 1968.

Appendix A
MLI COMPONENT MATERIALS PROCUREMENT DATA

A.1 RECOMMENDED MLI SYSTEM

The purchased components of the recommended MLI system, as installed on the 105-in.-tank calorimeter, were obtained from the vendors noted in Table A-1. Other miscellaneous items (grommets, nylon buttons, etc.) noted on the insulation assembly drawings of Section 8 were obtained from the Douglas Aircraft upholstery shop. Additional ordering data, were required, is denoted below.

A.1.1 Reflectors

The reflector material was Mylar, Type S, 15 gage (0.015 mil) thick, aluminized in both sides. A nominal emittance of 0.03 was specified, with no single reading to exceed 0.035 as measured on a Lion Emissometer, Model 25B.

A.1.2 Reflector Perforations

Reflectors were perforated by Perforated Specialties Co. to one of their standard configurations. This was pattern design number 9810 which has 0.055 inch holes arranged in a square pattern to yield a 2.38 percent open area with ten holes per square inch. Holes are about 0.319 inches on center.

A.1.3 Fasteners

The fastener was a modified Dennison "Swifttach" (double T configuration). These were injection molded to order in pure nylon with a shank 0.035 inch diameter (nominal) by 0.5 inch long. The manufacturer's part identification number is MD-.5.

A.1.4 Separator Net

The vendor's specifications for the separator net were used. These were: 40-denier polyester (Dacron) net; construction type A44, Patent 3, 071, 951; Style B4A; nominal 53 meshes per square inch, 6.6-mil thickness, 0.18 oz per square yard. The net was ordered scoured with a heat-set resinless finish.

Table A-1

MLI COMPONENT MATERIALS

Item	Vendor	Application	Weight
1. Mylar Double-Aluminized, 15-gage	National Metallizing Division Standard Packaging Co. Cranbury, N. J. 08512	MLI composite reflector	0.0012 lb/ft^2 per sheet
2. Mylar Perforations; Pattern 9810, 2.38 percent open area.	Perforated Specialties Co., Inc. 351 West 35th St. New York, N. Y.	Reflector perforations	
3. Net, Polyester (Dacron), Style B4A	Apex Mills, 49 West 37th St., New York, N. Y.	MLI composite separator	0.0013 lb/ft^2 per sheet
4. Net, Dacron, Style 15320 Scoured and Heat-Set Finish	Stern and Stern Textiles Hornell, N. Y.	Face sheet substrate	0.81 oz/yd^2
5. Tape, Heat-Sealable, Roll, Type GT400	G. T. Schjeldahl Co., Northfield, Minn.	Face sheet reinforcement	0.055 lb/ft^2
6. Fasteners, Swifttach, Double T	Dennison Manufactoring Co. Farmington, Mass. 01701	Panel assembly	
7. Cord, Tefglas, Type H-18	Holland Thread Co. Stroudsburg, Pa.	Joint closure lacing	
8. Tape, Pressure Sensitive, Polyester Film, Type 850	Minnesota Mining and Manufacturing Co.	Reflector contour dart closure	

A.1.5 Heat Sealable Tape

This tape for reinforcing face sheets has a 1.5-mil-thick polyester adhesive on both sides of a 5-mil Mylar substrate.

A.2 OTHER MLI COMPOSITE MATERIALS

Procurement data for the MLI reflector and separator materials evaluated during the study Phase I screen work (Section 5) are contained in Reference 10. For convenience, pertinent ordering data for the leading candidate materials are denoted below.

A.2.1 Separator Net, Dacron, Type B2A

This material was also supplied, as the B4A above, by Apex Mills. Suggested manufacturer's specifications were the same as the B4A except for mesh count, thickness, and weight. These are 198 meshes per inch, 6.7 mils and 0.31 oz per square yard, respectively.

A.2.2 Superfloc Film

Obtained from Dr. Karl Leonhard, Convair Division, General Dynamics Corporation, San Diego, California. The Mylar film substrate (15 gage) was supplied by MDAC per the above noted Mylar ordering data.

A.2.3 Tissuglas Paper Separator

Obtained from Pallflex Production Corporation, Kennedy Drive, Putnam, Connecticut. The material was ordered as Type 60G, 42-in. width with a nominal 0.0009-in. thickness.

A.2.4 Nylon Net Separator

Obtained from Sears, Roebuck and Co., Commercial Contract Division, Dept. 400, 5525 South Soto St., Vernon, California per the following: nylon net, catalog no. 36H 1012H, Color 27 (white), 1/16 x 3/32 in. hexagonal mesh.